Manufacturing of high precision bores

Proefschrift

ter verkrijging van de graad van doctor
aan de Technische Universiteit Delft,
op gezag van de Rector Magnificus prof. dr. ir. J.T. Fokkema,
voorzitter van het College voor Promoties,
in het openbaar te verdedigen

op dinsdag 13 juni 2006 om 10.00 uur

door
Ivett Viktória BANA
okleveles gépészmérnök, Universiteit Miskolc, Hongarije
geboren te Miskolc, Hongarije.

Dit proefschrift is goedgekeurd door de promotoren:
Prof. Dr.-Ing. habil B. Karpuschewski
Prof. Dr. habil J. Kundrák

Samenstelling promotie commissie:

Rector Magnificus	voorzitter
Prof. Dr.-Ing. habil B. Karpuschewski	Technische Universiteit Delft, promotor
Prof. Dr. habil J. Kundrák	Universiteit Miskolc, promotor
Prof. Dr.-Ing. P. H. Osanna	Technische Universiteit Wenen
Prof. Dr. I. Horváth	Technische Universiteit Delft
Prof. dr. ir. A. van Keulen	Technische Universiteit Delft
Dr. ir. A. M. Hoogstrate	Technische Universiteit Delft
Ir. D. Szepesi	Hembrug BV, Haarlem
Prof. dr. I. M. Richardson	Technische Universiteit Delft, reservelid

ISBN-10: 90-9020708-2
ISBN-13: 978-90-9020708-7

Copyright © 2006 by Viktória Bana
All rights reserved.

Printed in The Netherlands

This project was established between the Delft University of Technology (PMA) and the machine tool manufacturer Hembrug B.V. in Haarlem. The cooperation was supported by the Dutch Ministry of Economical Affairs (Project number: TSGE 1079) and the tool manufacturer Kennametal Inc.

“The Lord: I told you, man: fight, trust and be full of hope!”
Imre Madách: The Tragedy of Man

Acknowledgement

During the writing of my dissertation, I received support and help from several people, research institutes, companies and friends.

I would like to thank my supervisors, Prof. Dr.-Ing. habil Bernhard Karpuschewski and Prof. Dr. habil János Kundrák, for their support and encouragement during my research work.

I would also like to thank my colleagues at TU Delft, in particular, the Laboratory for Precision Manufacturing and Assembly, for their support. I especially want to thank my daily supervisor Dr. Ir. André M. Hoogstrate, and George Schrumpf from the technical staff. Dear my fellow researchers, I am glad to have met all of you. Csilla, I really appreciate all the help you gave me. You never let me down and I thank you very much for this.

I began my PhD work in Hungary, at the University of Miskolc, in the Department of Production Engineering. A significant part of the experimental results presented in this thesis was achieved there. Dr. József Pap and Dr. Károly Gyáni are gratefully acknowledged for their support and enduring patience. I am also grateful to the technical staff in the workshop.

Special acknowledgements go to the people at the Otto-von-Guericke University, the Institut für Fertigungstechnik und Qualitätssicherung in Magdeburg, and the Vienna University of Technology, Department for Interchangeable Manufacturing and Industrial Metrology. I would like to thank them for the support, time and energy they expended on me, during my research studies performed abroad.

I would like to express my appreciation to the people at the ZF Hungária Kft. in Hungary, and the Hembrug B.V. in Haarlem, Holland, who contributed to the fulfilment of my thesis.

I would like to record my gratitude to all my friends for encouraging and helping me. Thanks to Erin for her quick and accurate revising of my work. Dear Viktor, your support, encouragement and patience are always by my side. Thank you.

Dear Mummy, I would like to thank you for bringing me up in the greatest love and care. I deeply appreciate your support and understanding. Without you, I cannot be who I am.

As well, I must never forget to mention my loved ones who cannot be with me. Their love and support was always with me, even now. Thank you so very much.

Drága Édesanya, szeretném megköszönni, hogy a legnagyobb szeretetben és gondoskodással neveltél fel. Hálás vagyok a mindenkori megértésedért és támogatásodért. Nélküled nem lehetnék az, aki vagyok.

Delft, June 2006,

Viktória Bana

Summary

Traditional finishing, like grinding, particularly in the machining of hardened parts, requires the consumption of a significant amount of coolant. This is harmful for the environment. Besides this, more initiatives were taken in process planning to improve the process economy and flexibility. Reduction of machining cost and time is one of the most important factors in development of new technologies. In the 70s, preliminary research studies were done to develop hard turning process as new technology which can fulfill the same requirements as grinding. With the development of advanced machine tools and PCBN cutting tools, in the 90s the application of hard turning also became available for the industry.

It has been already proved that hard turning is capable technology in cutting of hardened steels however, there are few results regarding to bore manufacturing. Therefore, the replace ability of hard turning against grinding must be defined in high precision bores when the workpiece has different geometry (bore diameter, length to diameter ratio, wall thickness ratio). Moreover, as tolerances given for a workpiece are getting stricter, the transition range between hard turning and grinding must be determined. In some cases, it can be also worthy to utilize the advantages of these two processes to create a powerful combined technology. Therefore, a "set of rules" was developed to assist the selection of proper process at process planning.

The research work focussed on manufacturing of high precision bores, in the field of the automotive industry. The components, like gears and injection nozzles, are hardened to offer a longer lifetime, and better functional behaviour. The aim of this work was to select the proper process and process conditions in manufacturing high precision bores. The limit of hard turning was studied, and the transition range between hard turning and grinding was defined.

Process planning was done in two stages. In the first stage the process and setup is selected, based on workpiece properties and coarse process parameters, in the second stage the refined machining parameters are selected, based on selected experiments and empirical modelling. The machine tools, devices, cutting tools, etc, determine the coarse parameters. The machine tool stiffness is one determinant, and the selection of clamping devices must be done carefully. For instance, hard turning cannot be applied below a diameter of 2.4 mm, due to the lack of a standard turning tool. The refined parameters include the technological data that can be set.

To select the most suitable process, and define the transition range between hard turning and grinding, the workpiece properties were considered. With regard to the bore diameter, two groups were created. For diameters over 16 mm, the machine tools are generally dedicated for a general purpose. In diameters under 16 mm, the clamping and tooling systems are often special, higher revolutions and accuracy are required and therefore, they are proposed for certain operations.

In the case of gears, which are disc type parts, it was proved that hard turning is more advantageous with regard to the economy and surface quality than grinding, as it can guarantee a

tolerance of IT5-6. In order to maximize its economical benefits, process optimisation was elaborated. The modelling of the cutting process, based upon the process and product characteristics, speeds up the process optimisation significantly. Therefore, cutting forces and temperatures were studied, and the surface quality was investigated to optimise and control the process of the manufacturing of high precision bores. The investigated bore diameter varied between 35 and 80 mm, and the investigated length to diameter ratio range was 0.3 to 1.1.

In order to extend the limit of hard turning, the strictest requirements were taken; therefore the second part of this research was the machining of small bores. Injection nozzles possess small and long bores. Bore diameters were varied between 3 and 4 mm, while the length to diameter ratio of 2 to 4 was machined. Due to this, hard turning could not fulfil the prescribed requirements, and the application of a grinding process was needed. Rather than using a grinding only solution, a combination of hard turning and grinding was the most favourable. In this manner, roughing was done with hard turning, while grinding was applied as a finishing operation. To avoid non-productive times and clamping errors, the two processes were performed in the same machine tool. In this technology, the advantages of grinding and hard turning are combinable. The major amount of the allowance can be removed with hard turning, and a minor material removal grinding step can be used to reach the required quality. Due to the high value of the length to diameter ratio, the occurring tool bending and vibration are significant. Compared to hard turning, grinding can be performed with a near zero depth of cut (spark-out), leading to reduced grinding forces. The effect of cutting forces and cutting temperatures on the product characteristics was studied.

To describe the entire process, a set of models has been developed. This interconnects the input models with the output models through the process models. The specific investigations performed during the research work verified the sub-parts of the process models, which together established the predictive model, and made it possible to build up the “set of rules”.

Samenvatting

Bij traditionele nabewerkingmethoden, zoals slijpen, wordt, met name bij de bewerking van geharde werkstukken, gebruik gemaakt van significante hoeveelheden koelsmeermiddel. Dit is schadelijk voor het milieu. Daarnaast heeft de proces ontwikkeling zich gericht op het verlagen van de proceskosten en het vergroten van de flexibiliteit.

Een van de belangrijkste factoren bij de ontwikkeling van nieuwe technologieën is de reductie van de bewerkingskosten en –tijd. In de jaren 70 zijn de eerste onderzoeken uitgevoerd om het harddraaiproces te ontwikkelen als een nieuwe technologie die aan dezelfde eisen kan voldoen als slijpen. De ontwikkeling van geavanceerde verspaningsmachines en PCBN snijgereedschappen in de jaren 90 maakte harddraaien beschikbaar voor industriële toepassing.

Het is reeds bewezen dat harddraaien een geschikte technologie is voor het verspanen van gehard staal, er zijn echter weinig resultaten die het bewerken van gaten behandelen. Daarom moet de vervangbaarheid van slijpprocessen door harddraaien bij het bewerken van precisie gaten gedefinieerd worden in relatie tot de gat geometrie (gat diameter, lengte diameter verhouding, wanddikte verhouding). Tevens moet dit overgangsgebied van harddraaien naar slijpen worden gedefinieerd met betrekking tot de werkstuk toleranties. In sommige situaties kan het de moeite waard zijn om beide processen te combineren om zo een krachtige gecombineerde technologie te creëren. Daarom is een set vuistregels opgesteld om de keuze van het juiste proces in de werkvoorbereidingsfase te ondersteunen.

Het onderzoekswerk richtte zich op de productie van gaten met hoge nauwkeurigheid, zoals toegepast in de automobiel industrie. De onderdelen, zoals tandwielen en injectie nozzles, zijn gehard om de levensduur en de functionaliteit te verbeteren. Het doel was om het juiste proces en de juiste proces condities te selecteren voor het vervaardigen van hoognauwkeurige gaten. De limiet van harddraaien is bekeken en het overgangsgebied tussen harddraaien en slijpen is gedefinieerd.

De proces selectie is uitgevoerd in twee fasen. In de eerste fase zijn het proces en de opstelling geselecteerd, baserend op werkstuk eigenschappen en grove proces parameters, in de tweede fase zijn de verfijnde proces parameters bepaald, gebaseerd op experimenten en empirische modelvorming. De beschikbare gereedschapmachines, hulpmiddelen, gereedschappen etc. bepalen de grove parameters. De machine stijfheid is een factor en de selectie van spanmiddelen moet weloverwogen worden gedaan. Harddraaien kan bijvoorbeeld niet worden toegepast voor diameters kleine dan 2.4 mm vanwege het gebrek aan een geschikt draaigereedschap. De verfijnde parameters omvatten de technologische waarden die kunnen worden ingesteld.

Om het meest geschikte proces te kunnen selecteren en het overgangsgebied tussen harddraaien en slijpen te definiëren werden de eigenschappen van de werkstukken bekeken. Twee groepen werden gecreëerd betreffende de diameter van de gaten.

Voor diameters boven 16 mm zijn ‘general purpose’ machines gebruikt. Voor diameters kleiner dan 16 mm de opspanmiddelen en gereedschappen zijn vaak bijzonder en daarmee specifiek voor een bepaalde bewerking.

In het geval van tandwielen, wat schijfvormige producten zijn, is het aangetoond dat harddraaien voordeliger dan slijpen, wat betreft de kosten en oppervlaktekwaliteit, omdat een tolerantieklasse IT5-6 haalbaar is. Om de kostenvoordelen te maximaliseren is een uitgebreide procesoptimalisatie uitgevoerd. Deze optimalisatie wordt aanzienlijk versneld door modellering van het verspaningsproces baserend op de proces- en producteigenschappen. Daarom werden de verspaningskrachten en –temperaturen bestudeerd en de oppervlaktekwaliteit onderzocht om de vervaardiging van hoognauwkeurige gaten te optimaliseren en controleren. De onderzochte gatdiameter varieerde tussen 35 en 80 mm en de lengte-diameter verhouding van 0.3 tot 1.1.

Om de grenzen van harddraaien te verleggen zijn de meest strikte eisen gesteld, daarom betrof het tweede gedeelte van het onderzoek het bewerken van kleine gaten. Inspuit nozzles hebben kleine diepe gaten. De gatdiameters zijn gevarieerd tussen 3 en 4 mm, terwijl de lengte-diameter verhouding is gevarieerd van 2-4. Om deze reden kon harddraaien niet voldoen aan de eisen en was een slijpproces vereist. Een combinatie van harddraaien en slijpen was voordeliger dan het gebruik van een puur slijpproces. In dit gecombineerde proces wordt harddraaien gebruikt voor de voorbewerking en slijpen als nabewerking. Om spanfouten en non-productieve tijd te beperken werden beide processen uitgevoerd op dezelfde machine. Met deze techniek worden de voordelen van slijpen en harddraaien gecombineerd. Het grootste gedeelte van het te verwijderen materiaal wordt verwijderd met harddraaien en een slijpbewerking met minimale materiaalafname kan wordt gebruikt om de vereiste kwaliteit te halen. Door de grote lengte-diameter verhouding zijn de optredende krachten en de buiging van het gereedschap significant. Vergeleken met harddraaien is het bij slijpen wel mogelijk om de snedediepte nagenoeg tot nul te laten dalen (uitvonken), hierbij dalen de optredende krachten ook richting nul. De effecten van verspaningskrachten en – temperaturen op de producteigenschappen is bestudeerd.

Een set modellen is ontwikkeld om het hele proces te beschrijven, deze verbinden de input modellen met de output modellen via the proces modellen. De experimenten uitgevoerd tijdens het onderzoekswerk zijn gebruikt om de onderdelen van de procesmodellen te verifiëren. Samen vormen deze het predictieve model, tevens maakten de experimenten het mogelijk om enkele vuistregels vast te stellen (“set of rules”).

Contents

Acknowledgement v

Summary vii

Samenvatting ix

Contents xi

Nomenclature xv

1 Introduction 1

2 State of the art in bore machining 5
- 2.1 Product description 5
- 2.2 Hard turning 5
- 2.3 Internal grinding 7
- 2.4 Set of rules in process selection 9

3 State of the art in hard turning and grinding 11
- 3.1 Process characteristics 11
    - 3.1.1 Chip removal process 11
    - 3.1.2 Cutting forces 12
    - 3.1.3 Cutting temperature 14
    - 3.1.4 Tool wear 16
- 3.2 Product characteristics 17
    - 3.2.1 Size, form and positional accuracy 17
    - 3.2.2 Surface roughness 18
    - 3.2.3 Microstructure 19
    - 3.2.4 Microhardness 22
    - 3.2.5 Residual stress 23

4 Research goal and approach 25
- 4.1 Aim of the investigations 25
- 4.2 Approach 26
- 4.3 Structure of the thesis 27

5 Used experimental and measuring equipment 29
- 5.1 Machining of bores with diameters of 35-80 mm 29
  - 5.1.1 Machine tools 29
  - 5.1.2 Workpiece material 29
  - 5.1.3 Cutting tool 30
  - 5.1.4 Cutting force measurement 31
  - 5.1.5 Cutting temperature measurement 32
  - 5.1.6 Calorimetric measurement 33
- 5.2 Machining of bores with small diameter 34
  - 5.2.1 Machine tool 34
  - 5.2.2 Workpiece material 35
  - 5.2.3 Cutting tool 36
  - 5.2.4 Coolant 37
  - 5.2.5 Cutting force measurement 37
  - 5.2.6 Calorimetric measurement 39
- 5.3 Other measuring equipment 40
  - 5.3.1 Surface roughness and geometrical accuracy 40
  - 5.3.2 Metallographic and microscopic investigations 40

6 Set of models for machining of hardened bores 43
- 6.1 Model construction 43
- 6.2 Tool bending and machining errors caused by the force 45
- 6.3 Modelling of mechanical and thermal effects 47
  - 6.3.1 Cutting forces 47
  - 6.3.2 Cutting temperature 47
- 6.4 Modelling of micro and macro geometrical errors 48
  - 6.4.1 Empirical modelling of geometrical errors 48
  - 6.4.2 FEM analysis of thermal errors 51
- 6.5 Predict the change of surface integrity 56
- 6.6 Optimisation applied in hard turning 57

7 Machining of disc type parts 61
- 7.1 Experimental investigations 61
  - 7.1.1 Cutting forces 61
  - 7.1.2 Cutting temperature 63
  - 7.1.3 Surface roughness 63
  - 7.1.4 Macro geometrical accuracy 72

        7.1.5 Surface integrity 78
    7.2 Models to predict the performance of hard turning 83
        7.2.1 Model for determination of cutting forces 83
        7.2.2 Prediction of cutting temperature 84
        7.2.3 Modelling of surface roughness 86
        7.2.4 Modelling of macro geometrical accuracy 89
        7.2.5 Computer-based modelling of thermal distortion 89
        7.2.6 Modelling of the appearance of white layer 91
    7.3 Cycle time and material removal rate 92
    7.4 Optimal cutting data for machining of disc type parts 94

8 Machining of small bores 99
    8.1 Experimental investigations 99
        8.1.1 Cutting forces - machining a batch 99
        8.1.2 Surface roughness 105
        8.1.3 Macro geometrical accuracy 112
        8.1.4 Effect of l/d ratio on the machining result 115
        8.1.5 Surface layer properties 118
    8.2 Models to predict the performance of combined machining 121
        8.2.1 Empirical model for determination of cutting forces 121
        8.2.2 Modelling of surface roughness 121
        8.2.3 Effect of l/d ratio on the machining accuracy 123
        8.2.4 Thermal distortion in machining of small bores 125
    8.3 Cycle time and material removal rate 128

9 Determination of the transition range between hard turning and grinding 131

10 Conclusions and recommendations 137

References 139

About the author 149

Nomenclature

Symbol	Unit	Definition
a_e	mm	depth of cut
a_p	mm	depth of cut in cutting
A_{VB}	μm^2	area of flank wear land
A_w	mm^2/s	surface rate
b_s	mm	width of the grinding wheel
c	J/kgK	coefficient of specific heat
c_w	J/kgK	coefficient of specific heat of the workpiece
c_{wa}	J/kgK	coefficient of specific heat of the water
C	-	coefficient in the tool life equation
C_F, C_{Fp}, C_{Fc}, C_{Ff}	-	coefficient
C_{CYLpar}, C_{CYLt}, C_{RONt}	-	coefficient
C_{Ra}, C_{Rq}, C_{Rt}, C_{Rz}	-	coefficient
$C_{P'\alpha}$, C_{ϑ}	-	coefficient
CYLpar	μm	generatrix parallelism deviation
CYLt	μm	peak-to-valley cylindricity deviation
E	GPa	Young modulus
d	mm	workpiece inner diameter
d_e	mm	equivalent diameter of the workpiece
d_{eq}	mm	equivalent wheel diameter
d_{root}	mm	root circle diameter of the gear
d_s	mm	grinding wheel diameter
d_t	mm	tool shaft diameter
d_w	mm	workpiece diameter
dr_w	mm	maximum thermal radial expansion of the workpiece
dz_w	mm	maximum thermal longitudinal expansion of the workpiece
$d\vartheta$	°C	change of the temperature in the workpiece
f	mm/rev	feed per revolution
f_{optK}	mm/rev	optimal feed according the minimal machining cost
F_c	N	main cutting force
F_f	N	feed force

F_n	N	normal force
F'_n	N/mm	specific normal force
F_p	N	passive force during cutting
h	mm	undeformed chip thickness
h_{min}	mm	minimal undeformed chip thickness
G ratio	-	grinding ratio
i	-	number of strokes
I	m^4	moment of inertia
k_F, k_{Ra}, k_{Rq}, k_{Rt}, k_{Rz}	-	exponent
k_g	€/min	cost of the machine tool
K	€	machining cost
K_e	€	cost of a cutting tool edge
l	mm	length of the workpiece
l_c	mm	contact length between the tool and workpiece
l_g	mm	geometric contact length
l_s	mm	length of the tool
l_1	mm	additional length for approach and overtravel
L	m	length of cut
m	-	exponent of the tool life equation
m_w	kg	mass of the workpiece
m_{wa}	kg	mass of the water
n	1/min	number of revolutions per minute
M	Nm	moment
N	-	number of machined workpieces
P_c	kW	cutting power
P_α'	W/mm	power per unit length
P_α''	W/mm^2	power per unit area
q	W/m^2	heat flux at the workpiece-cutting tool interface
q	N/m	load intensity
q_s	-	speed ratio in grinding
Q_{calc}	J	amount of heat quantity calculated by the model
Q_{exp}	J	amount of heat quantity measured in the experiment

Q_w	mm^3/s	material removal rate
Q_w'	mm^3/mm s	specific material removal rate
r_β	mm	cutting edge radius
r_ε	mm	tool corner radius
r_w	mm	radius of the workpiece
Ra	µm	arithmetical mean deviation of the assessed profile
Ra_{th}	µm	theoretical arithmetical mean deviation of the profile
Ra_1	µm	modelled arithmetical mean deviation of the profile $Ra_1 = f(v_c, f, a_p)$
Ra_3	µm	modelled arithmetical mean deviation of the profile $Ra_3 = f(v_c, a_p, Ra_{th})$
Rku	-	kurtosis of the profile
Rp	µm	height of profile peak
Rq	µm	root-mean-square deviation of the profile
Rq_{th}	µm	theoretical root-mean-square deviation of the profile
Rq_1	µm	modelled root-mean-square deviation of the profile $Rq_1 = f(v_c, f, a_p)$
Rq_3	µm	modelled root-mean-square deviation of the profile $Rq_3 = f(v_c, a_p, Rq_{th})$
Rsk	-	skewness of the profile
Rt	µm	total height of the profile
Rt_1	µm	modelled total height of the profile $Rt_1 = f(v_c, f, a_p)$
Rv	µm	height of profile valley
Rz	µm	ten-point height of the profile
Rz_{th}	µm	theoretical ten-point height of the profile
Rz_1	µm	modelled ten-point height of the profile $Rz_1 = f(v_c, f, a_p)$
Rz_2	µm	modelled ten-point height of the profile $Rz_2 = f(v_c, f, a_p, VB)$
Rz_3	µm	modelled ten-point height of the profile $Rz_3 = f(v_c, a_p, Rz_{th})$
RONt	µm	peak-to-valley roundness deviation

S	-	contact surface between the tool and workpiece
S_1	-	workpiece surfaces
Sa	μm	arithmetical mean deviation of the surface
Sku	-	kurtosis of the surface
Sp	μm	surface peak
Sq	μm	root-mean square deviation of the surface
Ssk	-	skewness of the surface
St	μm	total height of the surface
Stp	%	surface bearing area ratio
Sv	μm	surface valley
SV_γ	μm	displacement of the cutting edge in the direction of rake face
t	s	time
t_c	min	cycle time
$t_{c,GR}$	min	cycle time in grinding
$t_{c,HT}$	min	cycle time in hard turning
t_{cs}	min	time of tool change
t_{sp}	min	spark-out time in grinding
T	min	tool life
T_{Kopt}	min	tool life according the minimum cost
x_F, x_{Fp}, x_{Fc}, x_{Ff}	-	exponent
x_{Ra}, x_{Rq}, x_{Rt}, x_{Rz}	-	exponent
x_{CYLpar}, x_{CYLt}, x_{RONt}	-	exponent
$x_{P'\alpha}$, x_ϑ	-	exponent
y	m	deflection of the beam
$y_{F,}$ y_{Fp}, y_{Fc}, y_{Ff}	-	exponent
y_{CYLpar}, y_{CYLt}, y_{RONt}	-	exponent
y_{Ra}, y_{Rq}, y_{Rt}, y_{Rz}	-	exponent
$y_{P'\alpha}$, y_ϑ	-	exponent
v_c	m/min	cutting speed
$v_{c,optK}$	m/min	optimal cutting speed according the minimal machining cost
v_{fax}	mm/min	oscillation speed (axial feed speed) in grinding
v_{fd}	mm/min	axial feed speed in dressing

v_{frad}	mm/min	radial feed speed
v_s	m/s	grinding wheel peripheral speed
v_w	m/min	workpiece peripheral speed
V	m^3	volume of the workpiece
V	N	shear force
VB	mm	width of flank wear land of the cutting tool
WT	-	wall thickness ratio of the gear
z_w	mm	coordinate of the workpiece
z_F, z_{Fp}, z_{Fc}, z_{Ff}	-	exponent
z_{CYLpar}, z_{CYLt}, z_{RONt}		exponent
z_{Ra}, z_{Rq}, z_{Rt}, z_{Rz}	-	exponent
$z_{P'\alpha}$, z_{ϑ}	-	exponent

α	W/m^2K	convection heat transfer coefficient
α_{exp}	1/K	coefficient of thermal expansion
γ	°	cutting tool rake angle
Δd_w	µm	deviation from the nominal bore diameter
Δl_{ov}	mm	overlap of cuts in grinding
λ	W/mK	thermal conductivity of the workpiece
κ_r	°	tool cutting edge angle
ϑ_0	°C	room temperature
ϑ_{amb}	°C	ambient temperature
ϑ_w	°C	temperature of the workpiece
$\vartheta_{w,st}$	°C	caloric average temperature
ϑ_{wa}^{fin}	°C	final temperature in the calorimeter
ϑ_{wa}^{st}	°C	starting temperature in the calorimeter
μ	-	friction coefficient
Θ	°C	average cutting temperature
Θ_{calc}	°C	modelled average cutting temperature
Θ_{real}	°C	measured average cutting temperature
ρ	kg/m^3	density

Abbreviations

CBN	cubic boron nitride
DL	dark layer
FEM	finite element method
GR	grinding
HRC	Rockwell hardness
HT	hard turning
HV	Vickers hardness
IPS	inverse problem solution
NC	numerical control
PCBN	polycrystalline cubic boron nitride
RML	mean line of the roughness profile
WL	white layer

1 Introduction

This thesis focuses on manufacturing of parts made from hardened steels. Due to the high loads and stresses that the parts have to bear, it is necessary to perform heat treatment, which increases the toughness and wear resistance of the material. In order to ensure a longer lifetime for components made from steel and increase their functional behaviour, the number of hardened surfaces is increased. Machining of hardened surfaces can nowadays be performed with defined cutting edges, e.g. turning, or with undefined cutting edges, e.g., grinding. Due to the high hardness (> 60 HRC) of the machined steel, tool material with high hardness is needed. In both situations CBN is the preferred tool material. However, the functionality of components made from hardened steel is becoming increasingly sophisticated. If the surfaces are not only hardened but also complex, (e.g. face, cone, sphere), grinding is not flexible enough. To machine more surfaces in one clamping, hard turning provides better possibilities for finishing of hardened steels.

The surfaces to be machined can be external and internal. Compared to external surfaces, the machining of internal surfaces is more complex. There is little data available in the technical literature, and the machining conditions are more complicated. It is difficult because it is not possible to observe the chip removal, as it occurs inside the bore. The heat-removal is more intricate as the machining system has less rigidity and the preparation of tool edge geometry must be done more carefully. This thesis will therefore focus on internal machining operations.

The bores can be classified according to their length and diameter and to length to diameter ratio. Traditional machine tools and tooling are generally developed for diameters greater than 16 mm. For diameters less than 16 mm, the requirements on the machine tools are higher. Higher revolutions are needed to keep the proper cutting speed, and higher machine tool accuracy is required for accomplishment of precision manufacturing. Machine tools for small sized parts become special machines as they are developed for specific machining processes or operations. Because of this, their application area is reduced.

To achieve competitive machining processes, cost reduction, improvement of productivity, and environmental protection are significant. Nowadays, development of machine tools and tools applied in machining make higher rigidity and better accuracy possible. Moreover, higher material removal rate and better surface quality can be ensured for the machined parts.

Proper selection of manufacturing processes mainly depends on the geometry of the part to be machined and the accuracy prescribed. In manufacturing of high precision bores, both hard turning and grinding can take place as a finishing process. In Figure 1.1, a comparison of grinding with hard turning is presented [KOC96]. Here, the criteria for process evaluation are economics, flexibility, ecology, and workpiece quality. With regard to the flexibility and ecological points of view, hard turning has a positive evaluation while grinding provides good quality. In hard turning, several research studies have already presented such surface quality which is comparable with grinding [TÖN00], [JAC02]. The cost of the turning tool is higher, however, hard turning results in a higher material removal rate. Therefore, as both processes have advantages and disadvantages, in some applications they can complement each other. For example, in combined or simultaneous processes, the advantages of both methods can be clearly seen.

		Hard turning	**Grinding**
Economical aspects	Process time	+/-*	+/-*
	Material removal rate	+	-
	Cost of acquisition	o/+**	o/-**
	Tool cost	-	+
Flexibility	Multi-face machining	+	-
	Profile machining	+	-/o
Ecological aspects	Power requirement	+	-
	Coolant	+	-
	Chip recycling	+	-
Quality	Workpiece quality	?	+
	Process reliability	?	+
	Surface integrity	?	+

Legend:
+ positive evaluation
- negative evaluation
o neutral
? valuation is not possible

Remarks:
*depending on the application a ratio of 1:10 up to 10:1 is possible
**special purpose machine or grinding center are often necessary

Figure 1.1: Comparison of grinding with hard turning [KOC96]

One of the largest application areas of hardened bores is the automotive industry. One application area is the transmission gears, where the bore of gears can be machined with hard turning or grinding. Hard turning can replace the finish grinding process as the diameter of the bore is generally greater than 16 mm, and the length to diameter ratio of the bore is in most cases lower than 1. The other application area chosen in this work is the fuel-injection engine, where the bore of fuel injection nozzle is machined with hard turning and grinding. Here, the difficulty is that the bore diameter is small, varying between 2…6 mm, while the length to diameter ratio can reach 5. As the diameter is small and the bore is long, the hard turning process itself cannot fulfil the requirements alone. Therefore, the combination of both hard turning and grinding processes is required.

This thesis aims to select the proper process(es) for manufacturing of high precision bores according to the diameter, the length to diameter ratio of bores, and the accuracy prescribed for the machined bores. In parts with given geometry and required accuracy, the question this thesis will explore is whether hard turning, grinding, or a combination of both processes can fulfil the requirements. Therefore, it will attempt to define the limit of hard turning and the transition range between hard turning and grinding.

2 State of the art in bore machining

2.1 Product description

The machine parts made from hardened steel are highly important components under significant load [TÖN00]. To achieve a longer lifetime and better functional properties, the steel machine parts, such as gears, bearings, and injection nozzles, are often hardened. The functional behaviour is determined by the surface quality, which is significantly influenced by the finishing process. Typical quality characteristics of the bores that must be ensured by the material removal process are summarized in Table 2.1. This table includes the quality characteristics regarding transmission gears and injection nozzles, which constitute the two objective workpieces of this research work.

	Transmission gears	**Injection nozzles**
Diameter tolerance	IT 5-6	IT 3-5
Length to diameter ratio	l/d ≤ 2	l/d ≥ 2
Allowance, diameter related	0.1-0.2 mm	
Hardness	≥ 60 HRC	
Roughness	Rz = 3-6 μm	Ra ≤ 0.2 μm
Out-of-roundness	≥ 4 μm	≤ 1 μm
Parallelism error	≥ 4 μm	≤ 1 μm

Table 2.1: Demands on high precision bores

2.2 Hard turning

The development of cutting processes is approaching high precision ranges. The improvement in machine tools accuracy and advanced tool materials have made it possible to finish high precision bores with the turning process. It is called hard turning because the hardness of the material to be machined is higher than 45 HRC [JOC01]. The advantages and disadvantages of hard turning are presented below [GUO02], [KNU00]:

Specific advantages:

- A higher material removal rate is possible, and therefore, it is more productive.
- Stiffness of the dedicated machine tools is adequate. In many cases, one machine is enough.
- It reduces the number of operations during machining, making it more flexible and economical.
- It can be done without coolant and is therefore an environment friendly process.

Specific disadvantages:

- If it is dry machining, higher friction occurs between the tool and workpiece. Therefore, the generated heat is also higher, which can cause thermal problems for the tool, machine and workpiece.

- Unlike grinding, it is single point cutting and the process stability can be problematic.
- The high passive force results in high mechanical load acting on the workpiece, cutting tool and machine.

With the development of PCBN and mixed ceramic cutting tool materials, hard turning has come to the forefront for machining hardened steel, ferrous powder metal, cast iron and heat resistant alloy [UES99]. PCBN is the second hardest cutting tool material, after diamond. Therefore workpiece material up to 70 HRC can be machined. Table 2.2 shows some typical mechanical and thermal properties of CBN versus other cutting tool materials according to Kennametal, Sandvik, Sumitomo and De Beers tool manufacturer companies.

	Tungsten carbide	**Mixed ceramic**	**CBN**	**Diamond**
Density (g/cm^3)	6.0-15.0	3.8-7.0	3.4-4.3	3.5-4.2
Hardness (HV 30)	1300-1700	1400-2400	3000-4500	4000-7000
Young's modulus (GPa)	430-630	300-400	580-680	680-890
Fracture toughness (MPam$^{1/2}$)	8-18	2-7	6.7	8.89
Thermal stability (°C)	800-1200	1300-1800	1500	600
Thermal conductivity (W/mK)	100	30-40	40-200	560
Thermal expansion coefficient (10^{-6}K^{-1})	5.0-7.5	7.4-9.0	3.6-4.9	0.8

Table 2.2: Properties of various cutting tool materials

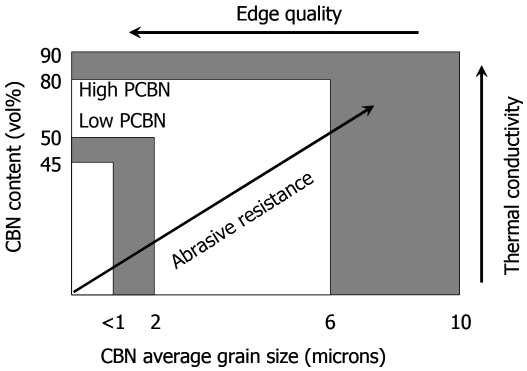

Figure 2.1: Effect of CBN content and grain size on PCBN tool properties [BAI02]

The attainable surface quality of the machined part is an important quality criterion for hard turning. It is determined by the feed rate and the cutting edge quality [FLE00]. Cutting edge quality is defined by the CBN grain size and binder combinations, while the CBN content influences the thermal conductivity of the cutting tool [LIU95], [UES99]. The effect of CBN content and grain size on PCBN tool properties is presented in Figure 2.1.

Precision hard turning provides tolerance IT5-7, where the attained roughness is in the range Rz = 2-4 µm [LIU96], [JOC01]. Under extreme machining conditions, high precision hard turning is realized where tolerance IT3-5 and roughness Rz ≤ 1.5 µm can be attained [MES05]. Here the conventional lathes are not accurate enough, but high precision lathes are capable of guaranteeing these strict tolerances. The accuracy demands on these machine tools are comparable with grinding machine tools with regard to the accuracy of the slides and spindle, and static, dynamic and thermal stiffness [TÖN00]. The attainable surface quality also strongly depends on the machining parameters. In high precision turning, the generally applied cutting speed varies between 100-200 m/min. The feed is in the range of f = 0.05-0.15 mm/rev and the depth of cut varies between 0.1-0.5 mm. In precision hard turning, the applied speed is between 150-220 m/min, the applied feed between 0.01-0.10 mm/rev, and depth of the cut between 0.02-0.3 mm [SHA93], [SOO00], [JOC01].

2.3 Internal grinding

Grinding is a material removal process in which chip removal is generated by a tool (usually a grinding wheel) with multiple geometrically non-defined cutting edges. The abrasion process has been used for hundreds of years, whether for sharpening axes or shaping swords in the middle ages. Grinding processes can be distinguished according to the workpiece geometry (e.g. surface, thread, profile etc.), to the grinding wheel position (e.g. external, internal etc.) or to the feed direction (e.g. plunge, through-feed, centreless etc.) [KÖN80], [KIN86], [MAL89]. Here, the focus is on internal grinding of high precision bores made from hardened steel. Therefore, only this segment of grinding is discussed.

Internal grinding is generally used as a finishing process, and therefore, the achievable surface roughness, parallelism error and out-of-roundness are of great importance [SAL80]. Grinding is much more complex than turning. Grinding and dressing strategies can vary widely, as can the combinations of machining parameters applied. Figure 2.2 presents an overall view of grinding technology, regarding input and process parameters, as well as the results of grinding. The kinematics of the most commonly used plunge and traverse grinding process are illustrated in Figure 2.3. The wheel rotates at 30000 rpm or higher, and the workpiece is held in a rotating chuck [KÖN80], [MAL89]. The geometrical conditions have highly unfavourable effects on the grinding process [JÜR80], as the bore's diameter (d_w), determines the diameter of the grinding wheel (d_s) applied, namely $d_w > d_s$. In practice, the wheel diameter to workpiece diameter ratio (d_s/d_w) is 0.6-0.9, and the wheel diameter to width of the grinding wheel ratio (d_s/b_s) is 0.7-0.5 [JÜR80], [KÖN80] [MAL89]. The contact length between workpiece and tool occurs along a rather long line, and therefore, grinding possesses high process robustness. An advantage of grinding is that it can be performed with near zero depth of cut. When the normal force is reduced to nearly zero [JÜR80], [BAL85], this is called "spark-out".

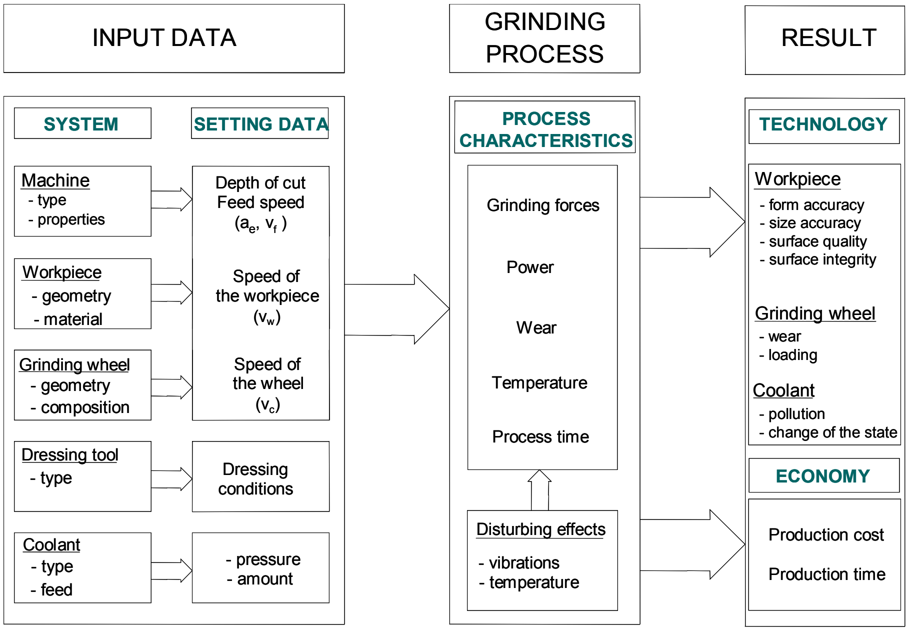
INPUT DATA
GRINDING PROCESS
RESULT
SYSTEM
SETTING DATA
Machine
- type
- properties
Workpiece
- geometry
- material
Grinding wheel
- geometry
- composition
Dressing tool
- type
Coolant
- type
- feed
Depth of cut
Feed speed
(a_e, v_f)
Speed of the workpiece
(v_w)
Speed of the wheel
(v_c)
Dressing conditions
- pressure
- amount
PROCESS CHARACTERISTICS
Grinding forces
Power
Wear
Temperature
Process time
Disturbing effects
- vibrations
- temperature
TECHNOLOGY
Workpiece
- form accuracy
- size accuracy
- surface quality
- surface integrity
Grinding wheel
- wear
- loading
Coolant
- pollution
- change of the state
ECONOMY
Production cost
Production time

Figure 2.2: Relation between input parameters and results in grinding [KÖN80]

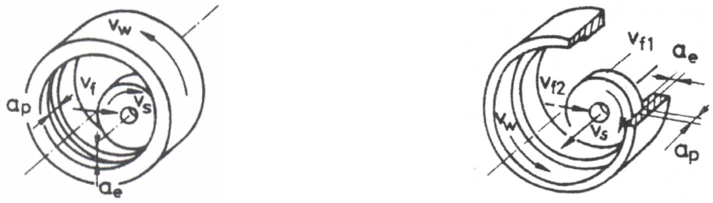
v_w
v_f
v_s
a_p
a_e
v_f1
a_e
v_f2
v_w
v_s
a_p

a.) plunge

b.) traverse

Figure 2.3: Kinematics of internal grinding [KÖN80]

Usage of a CBN vitrified bonded grinding wheel provided a large step forward in the automotive industry. For example, an automotive engine component manufacturer was able to eliminate a production bottleneck by switching to vitrified CBN wheels. Cycle time was reduced by 30% by eliminating 100 wheel changes [SUB88]. The performance of wheels containing superabrasives (diamond or CBN) is defined by the abrasive grain size, wheel hardness, concentration and bond type. The selection of proper wheel specification is a key input to the grinding system [MAL89].

In conventional grinding, the attainable size accuracy is IT5 or better. In grinding with superabrasives, typical Ra values for production grinding operations varies from 0.15 µm, although finishes below this value are also not uncommon [MAL89].

2.4 Set of rules in process selection

In the manufacturing chain, when machining bores made from hardened steel, the finishing takes place after the hardening process. The capabilities of hard turning and grinding processes must be investigated to select one of them as the most suitable finishing operation. Grinding is a typical finishing operation, but in the last decade hard cutting has replaced this abrasive process on the basis of research works performed in scientific areas. On the other hand, the industrial application of new techniques is often problematic as the following rule is followed: "Never change a running system" [KLO05]. Apart from the achievable surface quality, the process reliability, tool wear, material removal rate, economical and ecological aspects must be taken into account when selecting the machining process.

With respect to turning and grinding, several variations can be chosen for roughing and finishing operations. The possible combinations are given by Figure 2.4 below.

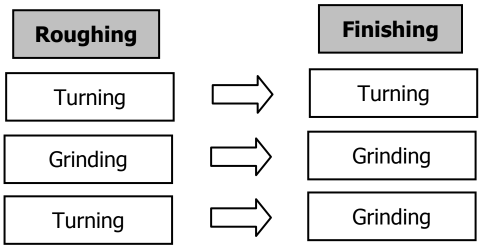

Figure 2.4: Options for process selection regarding turning and grinding processes

When using different operations for roughing and finishing, it is possible to utilize more the advantages of them effectively. Figure 2.5 summarizes the advantages and disadvantages of grinding and hard turning operations. In this case they are not competing technologies, but instead complete each other.

The roughing and finishing processes, regardless of whether they are the same or different processes, can either be performed in the same machine or in different ones. The different processes integrated into one machine tool offer the following advantages [ANK99], [JOH03], [MÜL03], [KLO05]:

- reduction of the number of machine tools;
- improvement of surface quality due to the reduction of the number of clampings;
- cost savings and time savings, as in some applications the combined process can be quicker than a single process;
- increase of flexibility;
- less time for dressing, as the grinding allowance is small and the wheel wear is less;
- due to the small grinding allowance, it is possible to grind without burning the surface.

	Hard turning	**Grinding**
Advantages:	- high flexibility - high removal rate - dry cutting – environmentally friendly process - high productivity - good surface finish	- high process robustness - high surface quality - damage in surface layer can be controlled (e.g. surface burning) - depth of cut can be near zero - lower tool cost
Disadvantages:	- mainly dry cutting – higher cutting temperature - process instability – single point cutting - damage in surface layer may appear (white layer) - higher tool cost - in machining of long workpieces, non-admissible machining errors may appear - if $h<h_{min,}$ the material removal cannot be accomplished	- coolant is required – harmful for the environment - chip recycling is rather complex - higher power consumption - less flexible - lower material removal rate - dressing

Figure 2.5: Advantages and disadvantages of hard turning and grinding

In many cases, the functional surfaces, even if they are complex, can be machined with hard turning. Grinding is only applied if the surface quality is the most important criterion [ANK99], [JOH04]. Due to the small grinding allowance, the application of minimal coolant is possible, and therefore, the cost of disposing of the coolant falls considerably. High flexibility can be reached, high accuracy can be ensured, and high process reliability can be guaranteed. In turning, under a given chip thickness, the material removal cannot be accomplished. However, in grinding, the depth of cut can be reduced to zero during spark-out [WEI98], [JOH03]. Moreover, the roughing process, namely hard turning, must ensure minimal and constant allowance for grinding [JOH04].

The selection of the most suitable finishing process must satisfy a very important criterion, namely: “The component has to fulfill its duty over a defined period of time under certain conditions” [KLO05]. Therefore, it is necessary to study the capability profiles of hard turning and grinding processes with the focus on the workpiece itself.

If both hard turning and grinding fulfill the requirements prescribed for the bore, the question becomes which is the more economical and/or ecological operation. In this case, the aim is to select the proper operation on the basis of economical improvement and therefore, the replacement of operations based on economic benefits. On the other hand, if the purpose is to achieve improved tolerances, the technological aspects come to the forefront. In the latter case, grinding is recommended. However, the combined machining processes also provide a proper solution, as hard turning is more economical and grinding guarantees the prescribed surface finish.

3 State of the art in hard turning and grinding

3.1 Process characteristics

3.1.1 Chip removal process

The chip formation mechanism of hardened steels is significantly different from traditional cutting and has a dominant effect on the generated surface quality [NAK88]. To reduce tool wear and form errors in cutting of hardened steels that are performed with a PCBN tool, low depth of cut and feed are applied, plastic deformation occurs in the subsurface layer of the workpiece [TÖN00]. For its explanation, several assumptions exist; one is the thermo-mechanical theory and the other is a hydrostatic theory. The thermo-dynamical theory explains the formability of the workpiece by heating up the chip formation zone [KÖN94]. The hydrostatic theory is based upon the fact that the formability of the material strongly depends on its stress state [TÖN93]. When the tool penetrates into the workpiece, high compressive stress develops in front of the cutting edge [KÖN93a], [FLE98]. This stress can be regarded as biaxial and plane compressive stress. The maximum of compressive stresses appears in the field of chamfer of the cutting tool [KÖN90]. In the cutting zone, the material behaviour of the workpiece and the thermo-mechanical mechanisms also depends on the cutting parameters [KÖN93a].

As a function of the cutting parameters and the workpiece's material properties, the cutting may lead to continuous or segmented chip formation. Generally, a continuous chip will occur if the chip thickness is lower than 20 μm [TÖN00]. If the chip thickness is lower than the minimum permissible value (h_{min}), the material of the workpiece will be ploughed and pressed between the flank face of the tool and the machined surface. This is due to the high pressure and temperature [KIS01]. The transformation from a continuous chip into a segmented chip can take place with the increase of the cutting speed. The transformation is also influenced by the hardness of the machined material [MAT86], [NGE99a]. The development of a saw-toothed chip is also proved by several experimental results [NAK88], [SHA93], [FLE98], [VYA99], [ELW00a], [SOO00]. It occurs if the shear deformation in the surface attains a value that the machined material cannot bear. According to Elbestawi, a saw-toothed chip develops if the cutting pressure exceeds 4000 MPa [ELB96]. This kind of chip formation is determined by the high negative rake angle, the brittleness of the material to be machined, and the high compressive stress occurred [ELW00b].

Unlike turning, a grinding tool has a multitude of geometrically undefined cutting points, which are irregularly distributed on the wheel surface. The contact between tool and workpiece occurs in a line, and both wheel and workpiece are rotating. The grinding process starts the chip removal with individual grains [CHE02]. The abrasive grain can be regarded as a defined cutting edge, whose rake angle can vary up to $\gamma = -80°$. From the point of view of cutting ability, the edge radius of the grain plays a significant role due to its dominant effect on the effective rake angle [BAL85]. Compared to conventional grinding wheels, the superabrasive wheel grains, like CBN, have a smaller edge radius due to its beneficial crystal structure. This leads to better chip removal in the cutting of hardened steels. The chip thickness (h) is very small compared to the grain size and is also much smaller than in the turning process.

Due to long service life, conventional grinding wheels have often been replaced by CBN. *G* ratio, which is a ratio of material removal and volumetric wheel wear during the same period of time, of 1200 up to 15000 can be achieved with CBN wheels [CHE02], [MEI05]. The performance of a CBN grinding wheel primarily depends on its composition [KÖN80]. A number defines the size of the abrasive grain. In Europe the average grain size is given by the manufacturers according to not only the FEPA standard but also the US-Mesh standard. For instance, grain size 10 (B1182) is regarded as very coarse, 100 (B151) as fine, and 500 (B46) as very fine [KAL95], [MEI05]. The concentration defining the volume of CBN strongly determines the material removal rate and tool life. The bond types, namely vitrified, resinoid, electroplated and sintered metal, hold together the wheel constituents [KIN86], [MAL89]. During grinding, the pressure occurred in the contact zone loads the grinding grains. If this pressure is too low, the wheel blunts and starts to build up pressure. Poor surface finish, dimensional error, and occasionally abrasive burning (thermal damage to the peripheral zone) are the consequences. If the pressure is above the level that would guarantee self-dressing, the wheel collapses. Due to this, proper selection of grinding wheel hardness must be chosen very carefully, and according to the grinding method and condition.

3.1.2 Cutting forces

Unlike traditional turning, the passive or back force is the highest in hard turning [KUN79], [NAK88], [KÖN93a], [TÖN95b], [EGA95], [CHO99a], [PAT00]. This is due to the fact that in hard turning, the chip formation takes place mainly on the corner radius of the cutting tool and the cutting is performed with a high negative rake angle [TÖN00]. The passive force to main cutting force ratio (F_p/F_c) also increases with the increase of the negative direction of the rake angle. This is a result of the segmented and saw-toothed chip formation [NAK88]. If hard turning is not performed with the generally applied low depth of cut ($a_p < 0.2$ mm), the main cutting force will become the main force constituent [LIU95].

The edge preparation of the PCBN tool also has an effect on the forces. With the increase of honing of the edge, both the passive force and the main cutting force become higher [THI99]. The investigations indicated that the tool geometry primarily influences the cutting forces and the technological data has only a secondary effect on it. Higher tool corner radius (r_ε) also results in higher cutting forces [TÖN00]. If the boron nitride content of the applied tool is less, the cutting forces reduce due to the lower heat conductivity of PCBN [NGE99b]. The extension of width of flank wear land generates higher forces, which in turn mainly increases the passive force [KUN79], [TÖN95b], [LIU95], [CHE00a], [POU01]. As a function of the increased width of flank wear land, the following cutting forces were measured under different technological data: F_p = 70-980 N, F_c = 60-300 N, F_f = 50-200 N.

According to certain publications, the variation of cutting speed has little impact on the cutting forces [KUN79], [CHO99b] when using relatively low cutting speed (v_c = 56-112 m/min). The investigations of several researchers proved [NGE99b], [TÖN00] that cutting force decreases when using a higher cutting speed range (v_c = 75-200 m/min). The higher energy put into the system generates a higher temperature in the cutting zone, and as a consequence, the strength of the workpiece material reduces. The increase of both the feed and depth of cut heightens the forces acting in hard turning [THI99], [TÖN00].

In machining of hardened steels, the resultant forces are strongly determined by the hardness of the workpiece material [NAK88], [NGE99b], [TÖN00]. Determination of grinding forces is important in order to estimate grinding power requirements and determine tool deflections, as it has high importance on the dimensional accuracy. In internal grinding, the normal force causes size and form errors in the workpiece [JÜR80]. Tool deflection can be critical in precision grinding [KAL95], which can be reduced by spark-out. During spark-out, the static normal force decreases exponentially, the surface finish and geometrical accuracy of the machined workpiece continuously improve and chip removal occurs at slower rates. However, spark-out time must be reduced to attain an economical process. Utilizing an open wheel structure keeps its surface clean and provides better wheel performance [CHE02]. Essentially, the cutting ability of the grinding wheel is improved, reducing grinding forces and temperatures, and avoiding grinding burn. Attaining the open wheel structure is mainly determined by the dressing method and parameters, however, the coolant type and its supply also influences it [KÖN80], [MAL89], [CHE02]. It was observed that the normal force is lower when using mineral or neat oil rather than machining with emulsion [JÜR80], [MON06]. This is due to the fact that the wheel wear is more intensive if an emulsion is applied.

During internal grinding, the forces are also influenced by the diameter of the grinding wheel applied [JÜR80]. From the point of view of wheel wear, it is more advantageous to use a grinding wheel with a bigger diameter, but it is necessary to reduce the contact length between the workpiece and the wheel, as it leads to lower grinding forces. In internal grinding of hardened steels, it is suggested that the wheel diameter to workpiece diameter ratio (d_s/d_w) should be lower than 0.8, as otherwise, the forces increase steeply. The grinding forces reduce as the wheel speed is increased [BAR89]. With the increase of the cross sectional area of the cut, the forces will increase as well [JÜR80]. Normal force depends on the plunge width, the speed of the workpiece, and the hardness of the wheel. The normal force between the workpiece and the tool changes proportionally to the plunge width, and alters slightly, depending on the specific material removal when applying a harder wheel.

3.1.3 Cutting temperature

Nearly all the energy input is transformed into thermal energy, which is distributed into the workpiece, grinding wheel, turning tool, chips, coolant and the environment. The mechanical and thermal effects generated during grinding and turning are shown in Figure 3.1 [TÖN92], [TÖN98]. In turning and grinding, the mechanical and thermal effects are comparable, but the geometric proportions differ by approximately one order of magnitude.

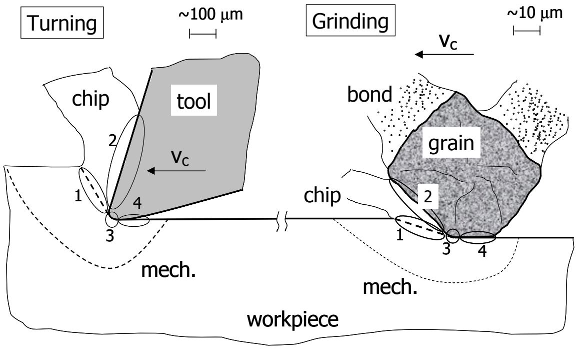

1 work of deformation, shearing zone
2 friction work, rake face
3 surface work, cutting edge
4 friction work, flank

Figure 3.1: Mechanical and thermal effects in cutting and grinding [TÖN98]

During machining processes, the cutting energy transforms almost completely into heat [BAL85]. Due to plastic deformation of the workpiece material and friction taking place in the chip-tool contact area, the temperature increases in the primary and secondary shearing zone [ABR96b]. The temperature developed in the contact area between the chip and tool is significantly higher than in the primary strain zone [NGE99b]. On the chip-tool contact boundary, there are three main heat sources: 1) plastic deformation in the chip contacting with the rake face; 2) friction occurring between tool and chip, and 3) sliding velocity of the chip on the rake face of the cutting tool. During cutting, the high temperature is caused by the high friction developing on the rake face [TÖN95a], [ABR96b]. This high temperature does not penetrate deeply into the workpiece [KÖN93a]. During cutting, the heat has an effect not only on the tool wear, but also on the surface integrity of the machined workpiece [TÖN95a], [NGE99b], [UED99]. Due to this high temperature, the tool wear becomes more intensive and tensile residual stress occurs in the surface layer. The thermocouple techniques are measuring methods spread in a wide range to determine the temperature of the cutting tool and the chip-tool interface [UED99], [KAR01]. However, the calibration at high temperature is difficult [LES97]. Contrary to this, the temperature measurement performed by the infrared thermometer is more advantageous [WAR90]. Measurement of cutting temperatures makes it possible to determine the temperature occurring on the tool-workpiece interface, and the thermal power beneath the workpiece's subsurface [SCH99], [TÖN00]. The thermal power per unit length (P_{α}') is defined as a physical parameter, which determines the maximum temperature in the subsurface of the workpiece and predicts the appearance of the white layers. If the cutting temperature exceeds the α-γ transition limit of the machined material, a rehardened layer will form out [KÖN93a], [TÖN95a], [BRI99]. With the increase of cutting time, the thermal power per unit length increases linearly, however the thermal power per unit area (P_{α}'') decreases. It is contradictory to the measurements, which indicate higher temperature with the increase of the width of flank wear land. Therefore, the correlation between the contact surface related power per unit area (P_{α}'') and the subsurface temperature is not possible. The temperature developed during cutting strongly depends on the heat conductivity of the cutting tool [ABR96b], [NGE99a]. Under the same technological data, about 52% of the generated heat is transmitted into the chip when using a cutting tool with 90% CBN content. But, it is only 41% when applying a cutting tool with 50% CBN content [NGE99b]. Among the technological data, the cutting speed and the feed have the primary and secondary effects on the developed temperature, while the depth of cut hardly influences it [ABR96b], [ABR97], [UED99]. With the increase of the cutting speed, the cutting temperature increases, but the heat penetration depth into the workpiece decreases, because the heat source moves faster [ABR96b], [NGE99b].

Specific energy in grinding is generally an order of magnitude higher than in conventional cutting due to the high negative rake angles presented by the abrasive grains [HOU04]. Heat dissipation is crucial in order to avoid thermal damage of the workpiece [TÖN92]. Heat partition varies in a wide range, depending on the grinding conditions [HOU04]. When grinding of hardened steels with aluminium oxide and CBN wheels, it was proved that heat partition was 30% to the wheel, 65% to the workpiece, and 5% to the chips in up-grinding of steel [JUY98]. The components, such as grinding wheel, workpiece, chips and coolant are subject to thermal loads. The excessive grinding temperatures cause thermal damage to the workpiece, including unfavourable tensile residual stresses, surface burn, cracks, appearance of the white layer, and softening of the surface layer [TOR78], [MAL89]. The increase in temperature of the workpiece surface largely depends on the amount of the energy generated by grinding that enters the workpiece [CHE02]. If the transitional temperature of the workpiece material is not exceeded, tensile residual stresses can be avoided.

Occasionally, the cutting fluid does not remarkably reduce the temperature in the grinding zone. This is due to its penetration ability in that region and the velocity of the cutting fluid jet [MAL89], [MON06]. Therefore, it must be ensured that the cutting fluid can perform its function in an optimised way. When choosing an adequate type of coolant and providing proper direction and velocity of the grinding fluid jet, the cutting fluids reduce friction and temperature in the cutting region. This also leads to a longer tool life, as the grinding wheel wear is reduced.

3.1.4 Tool wear

Tool wear has a significant effect on the economics, the cutting conditions, the machining accuracy, and the quality of the machined surface. The composition of tool material, tool geometry and its edge preparation has a significant effect on the wear mechanisms [KUN79], [TÖN95b], [CHO99b], [KIS01], [ZHO03]. A cutting tool with a lower CBN content indicates higher tool life [CHO03]. This can be explained by: 1) the protective layer which develops on the flank face of the cutting tool; and 2) the lower heat conductivity of the cutting tool which leads to the material becoming plastic in the shearing zone, which reduces the tool wear. When using a PCBN tool with lower heat conductivity, the cutting temperature is higher. This leads to the formation of a stable protective layer and results in a higher wear resistance.

For CBN tools, ceramic binder material is mainly applied, which has a higher hardness. Therefore, both abrasive and diffusion wear can be reduced [ZIM97]. The dominant wear mechanism of PCBN tools is the recrystallization of binder material generated by the heat [KÖN93b]. The lower the boron nitride content of the tool, and/or the smaller the grain size, the longer the tool life will be [KÖN93b], [EGA95], [CHO99b]. The wear of the PCBN tools is mainly abrasive. The wear first appears on the flank face and it has a significant effect on the tool life. However, crater wear was also observed [KUN79], [HOF98], [CHO99b], [KIS01], [POU01]. The wear of both the rake face and the flank face does not represent deep grooves. This indicates a good possibility to achieve suitable surface quality and size accuracy [TÖN00]. Generally, a chamfered tool is used to stabilize the brittleness of cutting edge [KÖN90], which reduces the wear intensity only in a smaller degree [KIS99].

To reduce PCBN tool wear, some tool manufacturers apply coatings (e.g. TiN, TiC, TiAlN etc.) on the cutting tools for the following reasons [POU01]:

a) to recognise the wear earlier in industrial applications;
b) to develop suitable tools for machining of both soft and hard materials;
c) to reduce the crater wear (diffusion wear); and
d) to reduce the friction force occurring on the rake face.

In comparing the wear characteristics of a coated tool and a non-coated tool, it is noted that the wear intensity is higher for the uncoated tool when using low cutting speed. However, in the case of the application of high cutting speeds, the tool life was the same for both cases. Due to the high cutting temperature, the coating wears off relatively quickly.

If the grinding wheel is dull, the grains do not cut the material, and instead ploughing and sliding effects occur [CHE02]. The tool wear mechanism is much more complex in grinding than in hard turning. The tool wear consists of the wear of the grains and the binder material. The wear of the wheel and its tool life are significantly determined by the material to be machined and the heat treatment of the workpiece [GYA93]. In internal grinding, the wheel wear receives greater attention because the arc of contact between the wheel and workpiece is longer in comparison with other grinding processes. This leads to remarkably radial wear [JÜR80]. The forces occurring during grinding significantly determine the wear of the CBN wheel. The softer wheel wears quicker, however, the grinding forces are lower here. Therefore, it is important to make a compromise between wheel wear and grinding forces. The tool wear is also influenced by the CBN concentration of the wheel [SUB88], as a higher CBN concentration results in higher *G* ratio. Generally, use of coarser abrasive grit sizes is an approach adopted to achieve longer wheel life [SUB88]. When machining with the optimal CBN grit size, it is possible to reach proper results in terms of long wheel life, low grinding power and good surface finish. But, it depends on the material removal rate, workpiece material, machine settings and coolant application. In the cylindrical grinding process, to use small CBN wheels economically, the influential factors determining the wheel wear are classified into two groups [TÖN89]. The first group contains the parameters, which have the most important effect on the grinding behaviour and wheel wear. These parameters are the specific material removal rate (Q'_w), and the cutting speed (v_c). The parameters that are classified in the second group have less effect on the wheel wear. These are the geometric contact length (l_g) and dressing parameters.

The wear intensity of the applied CBN wheel is also determined by the cooling liquid used [JÜR80]. When applying water, it forms a chemical reaction with the boron nitride. Compared to emulsion, the application of mineral oil generates a grinding ratio of about 10 times higher (G = 16000) than the emulsion when $Q'_w = 1\ mm^3/mm\ s$. At a two times higher specific material removal rate ($Q'_w = 2\ mm^3/mm\ s$), an increase of 30%, is achieved.

3.2 Product characteristics

3.2.1 Size, form and positional accuracy

Workpiece accuracy can be defined as the interference of deviation of size, surface roughness, geometrical deviations of form and position [OSA92]. The geometrical accuracy attained after finishing is dominant in the functional behaviour of the automotive parts [BOR01]. Form errors of the workpiece occur due to the thermal expansion of the workpiece and tool during machining [TÖN00]. This may lead to parallelism error and conicity of the machined bore. Turning lathes with high accuracy make it possible to compensate form errors caused by thermal effects by applying proper corrections in the NC control. Factors determining the geometrical accuracy of the machined parts are summarized in Figure 3.2.

Among these, the achievable accuracy is determined mainly by the accuracy of the machine tool, its control system, and the edge preparation of the cutting tool [KÖN94]. It is a fundamental prescription that the clamping forces should not cause deformation of the components. In many cases, it is not possible with mechanical clamping methods. However, it can be achieved by using magnetic chucks. During turning of hardened bores (100Cr6), the measured values of form and positional accuracy are all acceptable [KÖN94], [FLE00]. The values attained for both roundness and parallelism fulfilled the requirements. Moreover, they were one third of the prescribed values. When machining bores with a diameter of 120 mm, the out-of-roundness was 2.6 μm, and the parallelism error was 1 μm [FLE00].

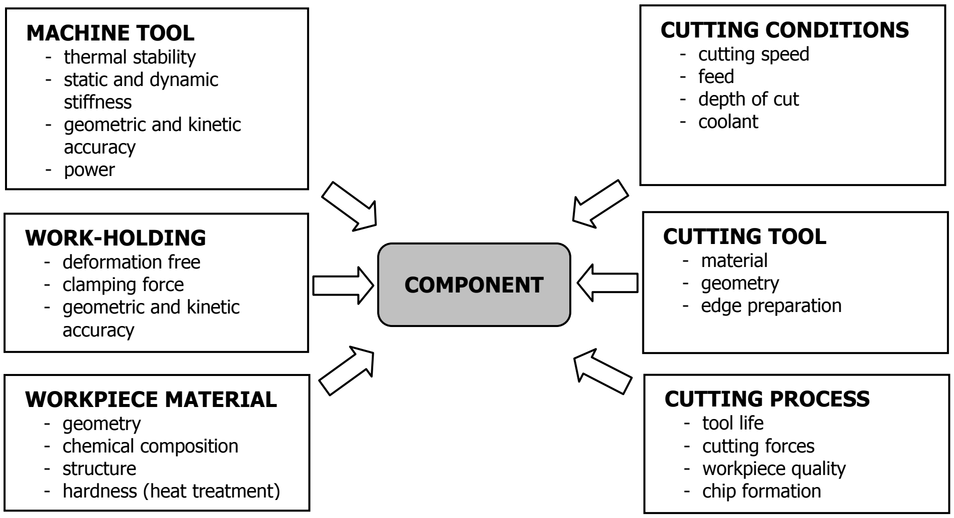
MACHINE TOOL
- thermal stability
- static and dynamic stiffness
- geometric and kinetic accuracy
- power
CUTTING CONDITIONS
- cutting speed
- feed
- depth of cut
- coolant
WORK-HOLDING
- deformation free
- clamping force
- geometric and kinetic accuracy
COMPONENT
CUTTING TOOL
- material
- geometry
- edge preparation
WORKPIECE MATERIAL
- geometry
- chemical composition
- structure
- hardness (heat treatment)
CUTTING PROCESS
- tool life
- cutting forces
- workpiece quality
- chip formation

Figure 3.2: Determining factors on the geometrical accuracy of the components after [FLE00]

3.2.2 Surface roughness

The main criterion of the workpiece's quality, especially for finishing, is the surface roughness [TÖN00]. Surface texture is generally the main factor limiting the tolerance, which can be achieved in machining [MAL89]. It is required to provide smoother surfaces for the machined parts in order to maintain tighter tolerances. The roughness of turned or ground surfaces can lead to an uncertainty in size measurement, as shown in Figure 3.3. The surface roughness requirements are often consequences of geometrical accuracy, which are strongly determined by grinding and turning conditions.

The ideal or theoretical surface roughness is always less than the actual value due to the material side flow, built-up-edge phenomena, tool wear, stiffness of the mechanical system consisting of machine tool, cutting tool and clamping device and vibrations. Determination of empirical models on the basis of experiments, giving relationship between machining parameters and roughness values, are suitable to predict the attainable surface roughness after grinding and turning [MAL89], [LUT98].

A hard turned surface indicates uniform smoothness and a roughness profile with regular geometry. The surface is more uniform because the scatter of roughness values is relatively low [ABR96a].

Using optimised technological parameters, surface roughness in the range of Rz = 2-4 μm can be realized [EGA95], [TÖN95a], [SHA98]. The arithmetic mean deviation of the assessed profile (Ra) can alter between 0.2 and 1.2 μm in hard turning [KUN85], [LIU96], [ELW00a], [FLE00], [KUN00], [KIS01] but under extreme conditions, a value of 31 nm could be attained [KNU00].

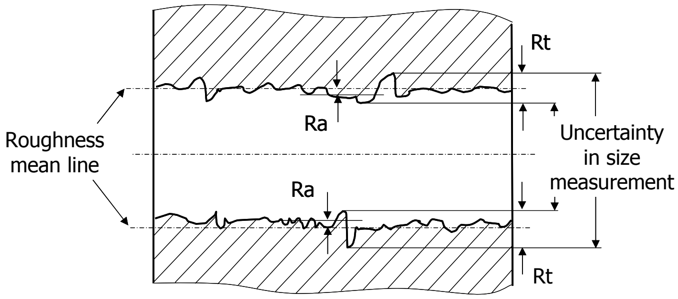

Figure 3.3: Relationship between roughness and tolerance based on [MAL89]

The cubic boron nitride content of the cutting tool and its worn state influence the surface roughness generated after cutting [FLE98], [KNU00]. A cutting tool with a lower CBN content, stronger binder material, and smaller grain size provides better surface roughness. With the increase of the tool corner radius (r_ε), and cutting edge radius (r_β), or by using a honed tool with chamfer, the roughness values reduce [FLE00], [KNU00].

Within the technological data, the increase of cutting speed results in the reduction of roughness characteristics for both turning and grinding [KUN82], [MAL89]. Many experiments, e.g. [LIU96], [ELW00a], [KUN00], [SOO00], confirm that a higher feed generates a higher surface roughness, but the depth of cut hardly influences it [AGH00]. In grinding, the speed ratio ($q_s = v_s/v_w$), spark-out time, and oscillation speed (v_{fa}) also influence the surface roughness [KÖN80], [MAL89]. When increasing the spark-out time, the grinding forces are continuously reducing, which results in a better surface finish. In addition to the grinding parameters, the dressing parameters also have an effect on the attainable surface roughness [JÜR80]. Finer dressing generally produces a smoother wheel surface. Therefore, the surface roughness of the ground workpiece is also smoother, and the dressing lead has a higher influence than the dressing depth [LIN73].

3.2.3 Microstructure

Due to the high temperature and frictional heat developing during cutting, phase transformations occur in the microstructure of the material. The structure of the machined surface may significantly differ from the initial state. In turning of hardened and alloyed steels, the material will be softened, as the softening temperature is exceeded, and so-called overtempered martensite will evolve [CHO99a]. If the austenizing temperature is attained, austenite will develop in the surface layer, and because of the cold bulk material or the applied cooling, untempered martensite will evolve. This is brittle, contains stresses, cracks easier, and reduces the fatigue life in principle. In the investigation of the microstructure of hard turned parts, it was proved that a white layer also appears, as in the case of grinding [CHO99a], [TÖN00], [BAR02], [GUO04].

The white layer is a result of microstructural alteration. It is called white layer because it resists standard etchants and appears white under an optical microscope, or featureless in a scanning electron microscope [TÖN00]. As it has very fine microstructure, the granular structure cannot be observed, and therefore, it will appear as a white colour. Furthermore, the white layer has a high hardness, often higher than the bulk. In cutting of case hardened steel, the hardness of the white layer was measured at approximately 1000 HV0.025. This is 20% higher than the hardness of the base material [TÖN95a]. An example of the developed white layer is presented in Figure 3.4 [RAM05].

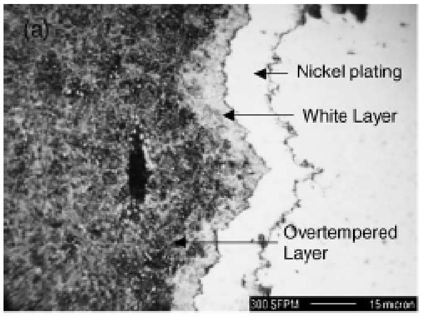

Workpiece material: 100 Cr6 (AISI 52100)
Cutting tool: PCBN, Kennametal KD050
Tool geometry: ANSI TNG-432
Cutting parameters in hard turning:
v_c = 91.4 m/min
a_p = 0.254 mm
f = 0.127 mm/rev
Coolant: -

Figure 3.4: Optical micrograph of the white layer [RAM05]

When the cutting temperature achieves the α-γ transition level, the martensite forming the microstructure of the material is metastable enough to turn into ferrite and cementite. However, there is not enough time for the solution of carbides. As a result, more retained austenite will be in the microstructure of the surface than in the bulk material [ABR96a], [CHO97], [BRI99].

The white layers consist of 2/3 part retained austenite, depending on the tool wear, but independently from the applied cutting tool [TÖN00]. Apart from the retained austenite, the microstructure of the white layer contains martensite, which has a tetragonal strained lattice and withstands the general etching mediums. After machining, no amorphous layer develops, as the conductivity of the machined workpieces does not reduce. The amorphous material is not conductive and therefore, it can be stated that the white layer has a crystal structure [BRI99].

Whether white layer appears or not, only the energy impact on the workpiece is relevant. Type and composition of the white layers only depend on the material transformations due to the time-temperature cycle.

Generally, the white layer is defined as a harmful phenomenon for the parts. However, TiN coatings applied on a tool can also appear as white layers, which are not regarded as damage on the part [BRI99]. The white layers are classified into two groups. When applying a special etching medium or using a longer etching time, some white layers remain white, while others indicate a fine-grained martensite structure. In the latter case, they are advantageous because the fine grain size and high hardness have a positive effect on the functional properties of the components. However, more detailed studies are necessary concerning the occurrence of white layers before its effect on the functional behaviour can be stated.

With respect to the generation of the white layer during hard turning, two conditions must be fulfilled [BRA95]: 1) the temperature in the contact zone between the workpiece and the tool must attain the austenizing level of the workpiece material; and 2) the cooling of the surface layer must occur in a very short time.

In hard turning, the contact time between the tool and the workpiece is very short, and often less than 0.1 ms. The contact time is significantly higher in grinding. It is often manifold of the contact time that occurs in cutting.

With the increase of tool wear, the friction between the tool and the workpiece increases, this causes further rise in temperature. Performed investigations proved [BRA95], [TÖN95b], [SOO00], [ELW00a] that the occurrence of the white layer and its thickness are influenced by the flank wear of the cutting tool. The technological data suggests that the applied cutting speed has a significant effect on it. The increase of flank wear determines the formation of the workpiece subsurface area according to the following [TÖN00]:

a) as a consequence of geometrical change of the flank face, the extended contact time causes the increase of frictional heat;
b) the plastic deformations lead to higher temperatures and help the austenization in the workpiece material.

Depending on the state and geometry of the applied tool, and the technological parameters, the rehardened zones can appear in "spots", or it can occur as white layers forming a continuous surface.

In cutting of hardened steels, the occurrence of the rehardened layers and its thickness are influenced by the tool wear, its geometry and the technological data [RAM99]. Under different machining conditions, the thickness of white layer may vary between 1 and 15 μm [TÖN95a], [CHO97], [AKC99], [WAN99], [SOO00], [RAM05]. Generally, with the increase of flank wear, the white layer thickness increases [BAR97], [BAR02]. However, in low cutting speeds, it is not obvious [CHO97]. If a sharp tool is applied [SOO00], a hardened layer will not occur, even when using a high cutting speed (v_c = 240 m/min). White layers were also observed when using a cutting tool with a chamfer [KIS01].

3.2.4 Microhardness

Determination of microhardness after finishing is necessary to describe and better understand metallographic processes, such as the generation of softened and rehardened martensitic layers.

Investigations of the microhardness in machining of hardened steels indicate different results [ELW00b]. Some research suggests that the microhardness hardly changes, while according to other studies, it significantly increases or decreases in the machined surface, especially as a function of the width of flank wear land. The investigations of several researchers proved [KUN85], [AGH00], [ELW00b] [TÖN00] that a hardened layer develops during hard turning. Compared to the hardened layer before machining, the increase in hardness is about 20-30 %, and its maximum value varies between 850 and 1400 HV, depending on the machined material. In the microhardness measurement of the ground specimen, grinding burn was found, accompanied by reaustenization of the workpiece material [MAL89]. In this case, white layer generally appeared. Without any burning, some softening can be observed due to tempering close to the surface [YOK77].

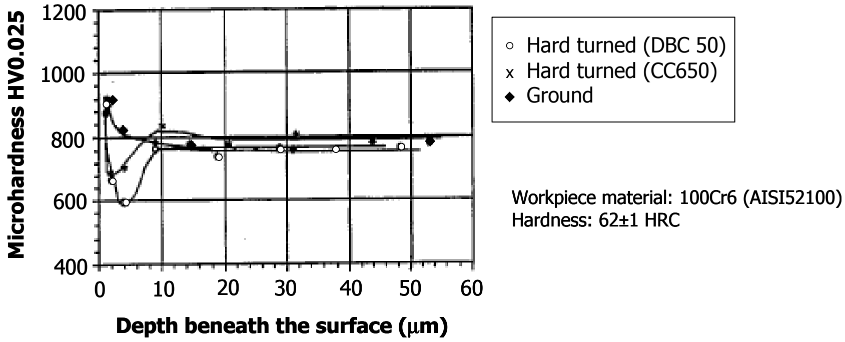

Figure 3.5: Microhardness variation after finish turning and grinding hardened bearing steel [ABR96a]

In the case of an application of low feed (f = 0.06 mm/rev), low depth of cut (a_p = 0.05 mm), and a high cutting speed (v_c = 200 m/min), material softening was observed when turning of hardened bearing steel, see Figure 3.5 [ABR96a]. The microhardness was significantly reduced up to depth of 5 μm measured from the surface level, and it increased gradually up to 10 μm. From here, it remained at a constant level. The ground specimen presented different hardness distribution, decreasing from 900 HV to the bulk hardness.

Taking into account the effects of tool wear in turning, the increase in hardness is higher when using a sharp tool, and its maximum value appears in deeper layers measured from the surface level [AGH00], [ELW00b]. Using a cubic boron nitride tool beyond the permissible width of flank wear land (VB = 0.4 mm), the microhardness reduces, and the material softens. The effect of the feed on microhardness was observed when the feed was varied and the other parameters were kept constant (v_c = 350 m/min, a_p = 0.2 mm). In higher feed (f = 0.2 mm/rev), the microhardness increased, while for low feed (f = 0.05 mm/rev), the material softened [ELW00b].

Among tool angles, the alteration of the rake angle has the most significant effect on the change of the microhardness [KUN79]. If the rake angle becomes more negative, from +5° up to -15°, the scale of the increase in hardness heightens, and its maximum value appears in the layers closer to the surface level [KUN79].

3.2.5 Residual stress

Among the alterations occurring in the surface and subsurface layers, the residual stress is also a significant factor that influences the fatigue life, namely the lifetime of the machined parts [BRI82]. The residual stress is defined as a stress, which occurs in an elastic body apart from external loads. Residual stresses during machining are generated by mechanical and thermal loads and phase transformations [ELW00b]. The mechanical load generated by cutting forces creates inhomogeneous and plastically deformed layers under the machined surface. In cutting with high speed, the yield stress of the workpiece reduces, resulting in significant changes in the residual stress [KIS01]. Measurement of the residual stress is mainly done by X-ray diffraction. This technique determines the alteration of distances between the atomic lattice planes.

The residual stress generated in the machined surface is influenced by the material, the preparation of the tool applied in finishing, the technological data, and the properties of the workpiece to be machined. The hardness of the steel is a significant determining factor, as with the increase of the hardness, the compressive residual stresses increases, and its maximum shifts towards the deeper area of the surface layer [MAT86].

Hard turning may result in the generation of tensile residual stresses, which within a few microns beneath the surface, transforms into compressive residual stresses [ABR96a]. In hard turning of tool steel D2 (62 HRC), the technological data indicate that the cutting speed mainly influences the residual stress [KIS01]. The increase of the feed heightens the maximum of the residual stress, and this maximum value appears in a longer distance measured from the surface level [KÖN90]. Using a higher depth of cut eliminates the disadvantageous tensile stress, even if a worn tool is applied.

Edge preparation, (e.g., chamfer or edge honing), and the rake angle of the cutting tool influences the residual stresses developing in cutting [MAT86], [JAC02]. Tool wear modifies the magnitude of the residual stresses, and its maximum value shifts to deeper layers measured from the machined surface level [KUN79], [KÖN90], [TÖN95b], [ELW00b].

Figure 3.6 compares the residual stress profiles in hard turned and superfinished to that in ground and superfinished surface [MAT99]. The profiles were measured in the circumferential direction of the bearing ring.

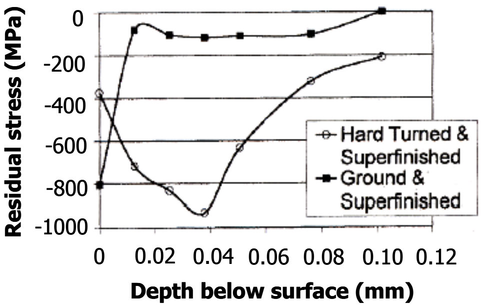

Figure 3.6: Residual stress profiles [MAT99]

After grinding and superfinishing, a high compressive residual stress arises close to the surface, which decreases quickly in the deeper layer measured from the machined surface. However, after hard turning and superfinishing, the reached residual stress is deeper. The residual stress was also measured after hard turning and grinding. Hard turning generated deep, compressive residual stresses. The superfinishing following hard turning and grinding altered the residual stresses only near the surface.

A high grinding temperature is generally undesirable because it introduces tensile residual stresses [CHE02]. In order to obtain compressive residual stresses, it is generally required to apply low removal rates. Unlike aluminium oxide, CBN grinding wheels induce compressive rather tensile residual stresses in grinding of hardened bearing steels. With an increase of the CBN concentration, the heat conductivity of the tool is higher, resulting in less heat, which shifts the residual stress to the compressive direction. In grinding, the produced residual stresses are influenced by the machining conditions (cutting speed, workpiece peripheral speed, depth of cut), topography of the grinding wheel (wear behaviour, dressing conditions), specification of the grinding wheel (structure, bond, hardness, type and size of grains), and the cooling conditions [BRI82], [MAL89].

4 Research goal and approach

4.1 Aim of the investigations

For the finishing of high precision bores in hardened steels, both grinding and hard turning are alternative processes. The most suitable manufacturing process must be chosen according to the geometry of the workpiece to be machined and the required tolerances prescribed for the bores. Previously, grinding was the only possible process for the finishing of hardened steels. Developments in machine tools and process technology opened possibilities with regard to hard turning as an alternative process for grinding operations. The advantages of hard turning, such as flexibility, economics and environmental friendliness, have caused a significant rise of the industrial relevance of hard turning in the last decade. Therefore, if the prescribed tolerances can be guaranteed with hard turning, it would be preferable over grinding as the finishing process. The general purpose of this work is to define an overall view for bore manufacturing, depending on the workpiece's geometry, the required accuracy, and surface quality. It aims to provide a "set of rules" for selection of the manufacturing process in the machining of high precision bores.

In summary, the main goal can be defined as follows:

The aim of this work is to select the proper process and process conditions for manufacturing of high precision bores in hardened steels. It will attempt to determine the limit of hard turning, and define the transition range between hard turning and grinding.

The selection of the process and the conditions will be done in two stages; the first stage is based on coarse parameters and the second stage on refined parameters. Coarse parameters are the limits that are determined by the available machine tools, cutting tools, devices etc. For example, hard turning cannot be used everywhere due to tooling limits regarding the bore diameter or length. In addition, the machine tool accuracy is of high importance, and the clamping devices should also be chosen carefully.

The refined parameters are the technological data that can be set. When the cutting parameters are optimised and well chosen, the limit of the given machining process can be extended. It is also possible for both processes (grinding and hard turning) to fulfil the requirements. However, grinding is not always economical and ecological.

To select the most suitable process, the workpiece properties, (e.g. material, hardness, bore diameter, length and accuracy etc.), must be taken into account. With regard to the bore diameter, the general machine tools are well suited for diameters over 16 mm. Machine tools and tooling suitable for diameters under 16 mm are mainly dedicated for a specific purpose. The improved tolerances demand better requirements. For instance, higher machine tool stiffness, higher revolutions, and a special clamping system are all required.

4.2 Approach

To establish the "set of rules", two typical application areas from the automotive industry were chosen; namely, gears and injection nozzles. The first part of the investigations deals with gears built into transmissions. They are generally disc type parts. In general, the diameter of the bore is more than 16 mm, and the length to diameter ratio is lower than 1. Firstly, it must be verified whether hard turning is a suitable process to guarantee the prescribed tolerances or if the application of the grinding process is required. Secondly, the process must be optimized to maximize the economical benefit. Modelling the cutting process, based upon the process and product characteristics, speeds up process optimisation significantly. Therefore, cutting forces and temperatures are studied and surface quality is investigated to optimize and control the process of the manufacturing of high precision bores. The investigated bore diameter varied between 35 and 80 mm, and the length to diameter ratio range was 0.3 to 1.1.

This research work was performed in the framework of a project established between the University of Miskolc, Department of Production Engineering and the ZF Hungária Kft by the support of the Hungarian Scientific Research Fund (Number of Agreement: T042962).

The second part of the investigations focuses on injection nozzles, which possess small and long bores. The bore diameter is less than 10 mm, while the length to diameter ratio can reach 5. Due to this, hard turning cannot likely fulfil the prescribed requirements, and the application of a grinding process may be needed. Rather than using a grinding only solution, it is also possible to combine hard turning and grinding in the most favourable way. In this manner, pre-machining is done with hard turning, while grinding is applied as a finishing operation. To avoid non-productive times and clamping errors, the two processes must be performed preferably in the same machine tool.

In the framework of a project established between the Delft University of Technology (PMA) and the machine tool manufacturer Hembrug B.V., a precision lathe – Slantbed Mikroturn 50 CNC – has been equipped with an additional high frequency grinding spindle. The cooperation was supported by the Dutch Ministry of Economical Affairs and the tool manufacturer Kennametal Inc.

It aimed to develop a combined technology for the machining of small bores with high quality. In this technology, the advantages of grinding and hard turning should be combined. The major amount of the allowance can be removed with hard turning, and a minor material removal grinding step can be used to reach the required quality. Due to the high value of the length to diameter ratio, the occurring cutting forces are a significant factor. Compared to hard turning, grinding can be performed with near zero depth of cut (spark-out), leading to reduced grinding forces. The effects of process characteristics (forces and heat) on the product characteristics were studied. The investigated bore diameters were in the range of 3 to 4 mm, while the length to diameter ratio was in the range of 2 to 4.

To describe the entire process, a set of models has been developed. This interconnects the input models with the output models through the process models. The specific investigations performed during the research work verify the sub-parts of the process models, which together establish the predictive model and makes it possible to build up the "set of rules".

4.3 Structure of the thesis

The applied experimental equipments, including machine tools, workpiece properties, cutting tools and measuring devices are summarized in Chapter 5.

In Chapter 6, the set of models for the manufacturing of hardened bores is presented. Regarding grinding and hard turning, the input models focus on the basic elements of the machining system, such as workpiece, machine, cutting tool, cutting parameters and stiffness of the machine-tool-device-workpiece system. To better understand the manufacturing process, FEM models and empirical models concerning cutting temperature, cutting forces, surface roughness, geometrical accuracy and surface layer properties were developed. The process models aid in finding the effect of input parameters on the process characteristics, and product characteristics as output parameters. They also help select the proper process for the manufacturing of high precision bores.

The experiments performed in manufacturing of disc type parts are presented in Chapter 7. Hard turning as a replacement for grinding can guarantee the required tolerances, and therefore, its performance must be improved. The models for prediction of performance of hard turning are demonstrated, and optimal cutting data are defined.

When machining small bores (d < 16 mm), a combination of hard turning and grinding was used as a new technology (Chapter 8). The performed investigations aim to predict the performance of combined machining, giving new alternatives for the manufacturing of diesel injection nozzles.

In Chapter 9, the limit of hard turning is discussed, and the determination of the transition range between hard turning and grinding is attempted. This means that in the manufacturing of high precision bores, the workpiece geometry, bore diameter, length to diameter ratio of the bore and prescribed tolerances determine the selection criteria. This leads to the question of whether to apply hard turning, grinding or a usable combination of both of them? This chapter attempts to answer this question.

Chapter 10 consists of the final conclusions and recommendations for future research work.

5 Used experimental and measuring equipment

5.1 Machining of bores with diameters of 35-80 mm

5.1.1 Machine tools

The experimental works in machining bores with diameters of 35-80 mm were mainly carried out at the University of Miskolc, Department of Production Engineering in cooperation with ZF Hungária Kft in Eger, Hungary. This firm is one of the production locations of ZF Friedrichshafen AG, which designs and produces transmissions for trucks and cars. The cutting temperature measurements in turning of hardened steels were performed at the Otto-von-Guericke University, Institute of Manufacturing Technology and Quality Management in Magdeburg, Germany. The specification of machine tools applied during this research work is summarized in Table 5.1.

	Turning lathes			**Grinding machine**
	PITTLER PVSL-2 (vertical)	**EEN 400** (horizontal)	**INDEX GU600-2** (horizontal)	**SI-4/A** (Berliner Werkzeugmaschinenfabrik)
Main drive power (kW)	28	17	45	9
Max. spindle speed (1/min)	3000	4000	6000	13000
Max. diameter of the workpiece (mm)	200	225	175	120
Max. workpiece length (mm)	depending on the chuck	1250	790	60

Table 5.1: Main specification of machine tools

5.1.2 Workpiece material

The workpieces used for the investigations have the same composition, but different geometrical features (Table 5.2). The material of the workpieces is case hardening steel, DIN 20MnCr5 (AISI 5120). Its chemical composition is summarized in Table 5.3.

Bore diameter d (mm)	**35**	**36**	**48**	**62**	**66**	**68**	**73**	**76**	**83**
Length of the bore l (mm)	35.10	38.45	27.35	40.80	28.35	29.10	46.80	24.20	33.80
Length to diameter ratio l/d (-)	1.00	1.06	0.57	0.66	0.43	0.43	0.64	0.32	0.40
Wall thickness ratio of the gear WT = d_{root}/d (-)	2.41	2.83	1.41	2.42	1.41	1.66	1.94	2.32	1.34

Table 5.2: Geometrical properties of the investigated gears

For a chosen gear (d = 62 mm), the hardness distribution measured after heat treatment is shown in Figure 5.1. In the case of the other investigated gears the measurements indicated similar results. Case hardened depth after heat treatment is 0.8 mm at HV550, and the required surface hardness is 61±2 HRC.

Element	C	Si	Mn	P	Cr	S	Mo	Ni	Cu	Al	Sn	Ti
%	0.15- 0.20	≤ 0.40	1.0- 1.3	≤ 0.025	1.0- 1.3	0.020- 0.035	≤ 0.12	≤ 0.30	≤ 0.30	0.02- 0.05	≤ 0.03	≤ 0.005

Table 5.3: Chemical composition of workpiece material 20MnCr5

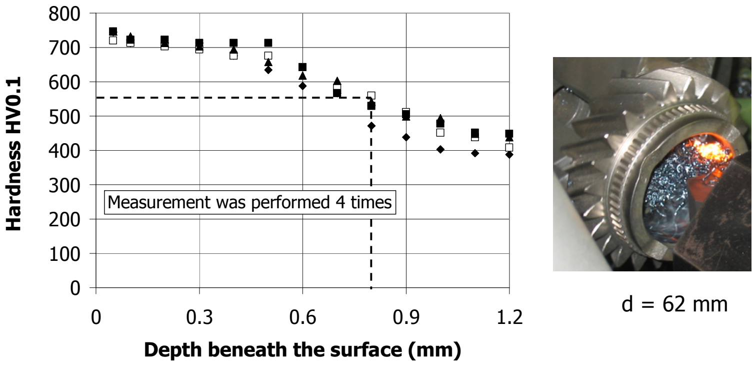

d = 62 mm

Figure 5.1: Hardness distribution of a gear measured within the bore after heat treatment

5.1.3 Cutting tool

For both turning and grinding, the applied cutting tool material was cubic boron nitride (CBN). The specification and geometry of the cutting tools are given in Table 5.4. The properties of CBN wheels used for internal grinding are summarized in Table 5.5.

Turning tools		
Specification	**Geometry**	**Tool holders**
GE Superabrasives D-CNMA 120408, BZN 8200 S202 (uncoated) 65% CBN, binder: ceramic, grain size: 2 μm	γ_n = -6°, α_n = 6°, κ_r = 95°, ε_r = 80°, r_ε = 0.8 mm chamfer: 0.2x20º	TIZIT S32U-PCLN L 12
Sandvik Coromant CNGA 120408 S01020 A7020 (coated)	γ_n = -6°, α_n = 6°, κ_r = 95°, ε_r = 80°, r_ε = 0.8 mm chamfer: 0.1x20º	CAPTO C5-PCLNL-17090-12
Sumitomo Carbide CNGA 120408 BNC80 (coated) 50-60% CBN, binder TiN based ceramic, grain size: 2-3 μm	γ_n = -6°, α_n = 6°, κ_r = 95°, ε_r = 80°, r_ε = 0.8 mm chamfer: -	

Table 5.4: PCBN cutting tools applied in hard turning

Grinding tools
Specification
CBN wheel 32x30x13 9A 80 K7 V22 BAYSTATE
CBN wheel 50x32x20 9A 80 K7 V22 BAYSTATE
CBN wheel 60x36x20 9A 80 K7 V22 BAYSTATE
CBN wheel 80x36x20 9A 80 K7 V22 BAYSTATE

Table 5.5: CBN wheels applied for grinding

5.1.4 Cutting force measurement

The cutting force measurement (Figure 5.2) was carried out with a Kistler three-component piezoelectric dynamometer – type 9257B, calibration range: F_x = -5kN ÷ +5kN, F_y = -5kN ÷ +5kN, F_z = -5kN ÷ +10kN, with a resonance of 3.5 kHz. The dynamometer was placed under the tool holder and connected to the Kistler charge amplifiers, type 5011 with a frequency limit of 200 kHz. For checking the measurement, a control oscilloscope, type Philips PM 3050, was used. Data acquisition was accomplished using a Spider8 measuring bridge with multiple channels. This is a measuring system for PCs for electronic measurement of mechanical variables such as force, acceleration, pressure etc. Catman 3.1, a Windows based software program was used to analyze the cutting forces on the desktop computer.

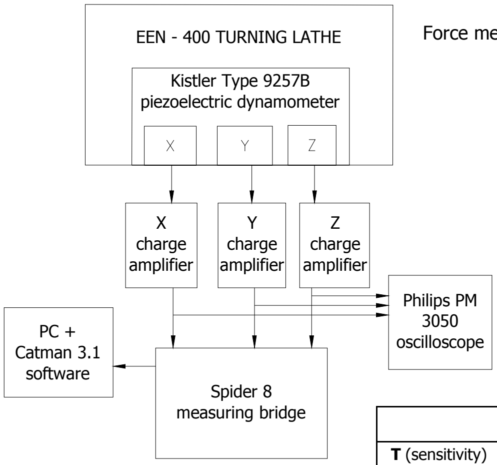
EEN - 400 TURNING LATHE
Kistler Type 9257B piezoelectric dynamometer
X
Y
Z
X charge amplifier
Y charge amplifier
Z charge amplifier
Philips PM 3050 oscilloscope
PC + Catman 3.1 software
Spider 8 measuring bridge

Force measurement set-up

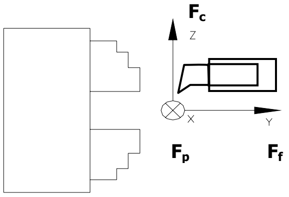

Cutting force directions

Characteristics of Kistler dynamometer

	X (F_p)	Y (F_f)	Z (F_z)	Unit
T (sensitivity)	7.84	7.9	3.78	pC/N
S (multiplicator)	5*10	5*10	5*10	N/V
LP (frequency of low pass filter)	3	3	3	kHz
TC (time constant)	100	100	100	s

Figure 5.2: Cutting force measurement set-up

5.1.5 Cutting temperature measurement

In cutting, several measurement techniques based on various physical principles have been developed [KAR01]. The measurement of the cutting temperature was performed with infrared methods. The advantage of this technique is that it operates precisely and reliably, and is definitely preferred when the target object is moving or would be damaged [WAR90]. However, it is more costly than systems based on direct contact devices, such as thermocouples and resistance probes. Furthermore, the infrared measurements are limited to exposed surfaces and cannot be used to directly measure temperatures in the interior of the chip [STE97].

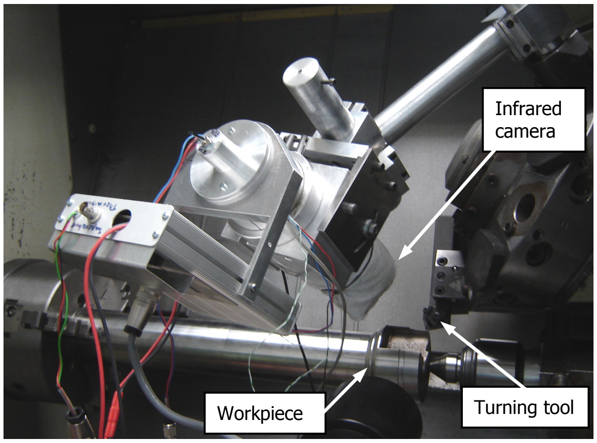

Figure 5.3: Set-up for cutting temperature measurement

The infrared camera used for the temperature measurement was developed by Frohmüller [FRO02]. The infrared camera includes the optical unit, the infrared detector, and the electronic input processor. The optical system determines the field of view, filters the unwanted wavelengths, and focuses the energy in the selected band onto the detector. The detector generates a corresponding analogue signal. The measured analogue signal is converted into digital, linearized, and compensated for different emissivity values. The output signal is received in voltage (V), from which the temperature values in degree Celsius are calculated with multiplicators. These multiplicators were determined according to the calibration method established by [FRO02]. The reproducibility of the instrument is ±0.25 °C. The set-up for cutting temperature measurement and the sketch of the workpiece are presented in Figure 5.3 and Figure 5.4. The diameter of the laser beam was 0.7 mm, and the distance between the measuring point and the instrument was 240 mm. The infrared camera was placed into the revolver head of the turning lathe with a clamping device specially designed for this measurement. Contrary to the advantages of this measurement technique, its disadvantage is that the temperature of the tool/workpiece contact zone cannot be measured directly, and the machining must be performed without coolant. This does not necessarily cause any problems as hard turning was carried out without coolant. However, during cutting the removed chip may cover the tool rake face, making it impossible to measure the cutting temperature. Therefore, the turning must be interrupted when measuring the cutting temperature (Figure 5.4b).

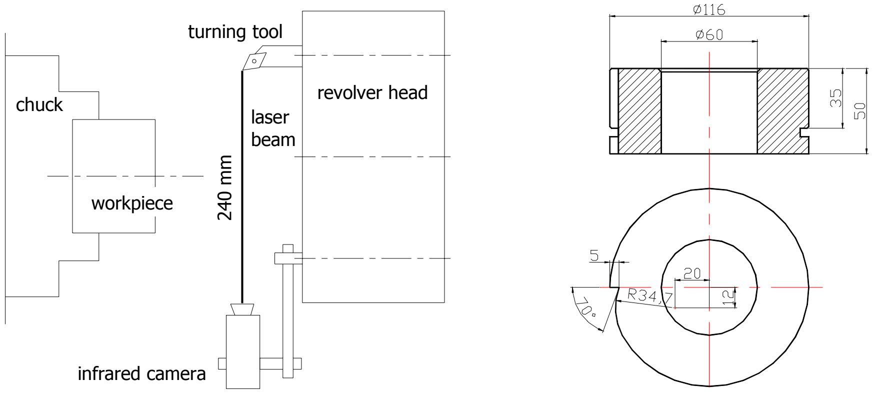

a) temperature measurement set-up

b) sketch of workpiece

Figure 5.4: Temperature measurement

5.1.6 Calorimetric measurement

This measurement is necessary to determine the thermal distortion in the manufacturing of bores. The determination of residual heat quantity (Q_{exp}) transmitted into the workpiece was carried out by calorimetric measurement. The applied calorimeter (Figure 5.5) was designed and built up by Sukaylo [SUK03] at the Otto-von-Guericke University in Magdeburg. In the calibration, the water placed into the calorimeter was warmed up (t = 30 s) and afterwards cooled down (t = 300 s) when the temperature was being measured. The electrical energy required for warming up the water and the temperature difference determines the thermal capacity of the calorimeter. After the turning of the bore, the workpiece was placed immediately into the calorimeter. After measuring the temperature rise in the workpiece, the residual heat quantity (Q_{exp}) can be calculated.

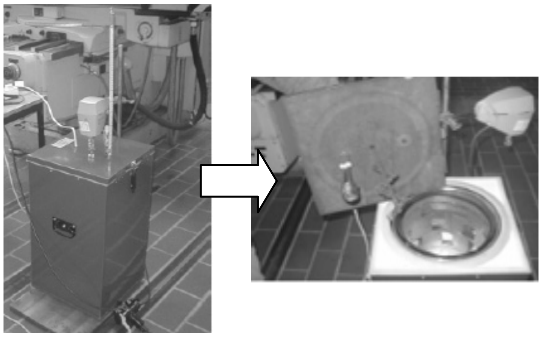

The calorimeter includes:

- vacuum vessel filled up with 20 litres of water
- glass stirring-rod to stir the water
- thermometer with accuracy ±0.001°C
- cartridge heater

Figure 5.5: Calorimetric measurement [SUK03]

5.2 Machining of bores with small diameter

5.2.1 Machine tool

Experimental investigations in machining of small bores were undertaken at the Delft University of Technology, Laboratory for Precision Manufacturing and Assembly. They were carried out on the Slantbed-Mikroturn 50 CNC hard turning machine, equipped with a high speed grinding spindle (Figure 5.6).

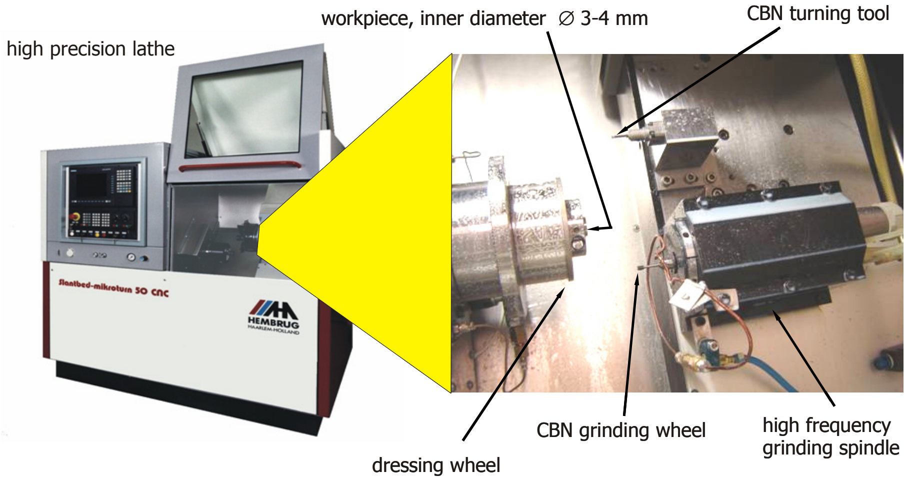
workpiece, inner diameter ∅ 3-4 mm
CBN turning tool
high precision lathe
Slantbed-mikroturn 50 CNC
HEMBRUG
HAARLEM-HOLLAND
CBN grinding wheel
high frequency grinding spindle
dressing wheel

Technical data Slantbed-Mikroturn 50 CNC	
Main drive power	7.5 kW
Hydrostatic main spindle speeds up to	10.000 1/min
Max. workpiece diameter for chucking applications	120 mm
Max. movement of z-slide	100 mm
Max. movement of x-slide	240 mm
Spindle run-out	≤ 0.1 µm
Repeatability hydrostatic x- and z-slides	± 0.1 µm
Rapid traverse at resolution 0.01µm	12 m/min
32-BIT CNC system, resolution	0.01 µm
Grinding spindle GMN HS 80c-120000/1.1	
Grinding spindle speeds up to	120000 1/min
Max. power	1.1 kW

Figure 5.6: Hembrug precision turning lathe with integrated inner diameter grinding

The steel machine frame is filled with concrete and supports the natural granite base. The granite base is the reference plane for the headstock and slide assembly. Between the granite base and the machine frame, a system of vibration dampers is mounted, which isolates the machine from floor vibrations above 7 Hz. Good chip removal and accessibility are provided by the 45° slantbed design. The main spindle is supported by two hydrostatic bearings; one combined axial/radial front bearing and one radial rear bearing. The hydrostatic bearings have air labyrinth sealing rings to prevent dust from penetrating the bearings from the outside, and hydraulic oil leakage from the bearings on the inside. The main spindle with standardized spindle nose provides the possibility of using various workpiece holding devices, such as pneumatic collets or three jaws chucks, electric permanent magnetic chucks, vacuum chucks or other clamping fixtures.

5.2.2 Workpiece material

In machining small bores, two different workpiece materials were used: DIN 16MnCr5 (AISI 5115) case hardening steel and DIN 100Cr6 (AISI 52100) bearing steel. The chemical compositions of the materials are given in Table 5.6 for 16MnCr5 and Table 5.7 for 100Cr6.

Element	**C**	**Si**	**Mn**	**P**	**Cr**	**S**	**Al**	**Cu**	**Mo**	**Ni**
%	0.14-0.19	0.15-0.40	1.00-1.30	≤ 0.035	0.80-1.10	≤ 0.035	≤ 0.015	≤ 0.30	≤ 0.12	≤ 0.30

Table 5.6: Chemical composition of workpiece material 16MnCr5

Element	**C**	**Si**	**Mn**	**P**	**Cr**	**S**	**Ni**	**V**	**W**	**Cu**	**Mo**
%	0.95-1.10	0.17-0.37	0.25-0.45	≤ 0.027	1.35-1.65	≤ 0.020	≤ 0.30	≤ 0.05	≤ 0.15	≤ 0.25	≤ 0.10

Table 5.7: Chemical composition of workpiece material 100Cr6

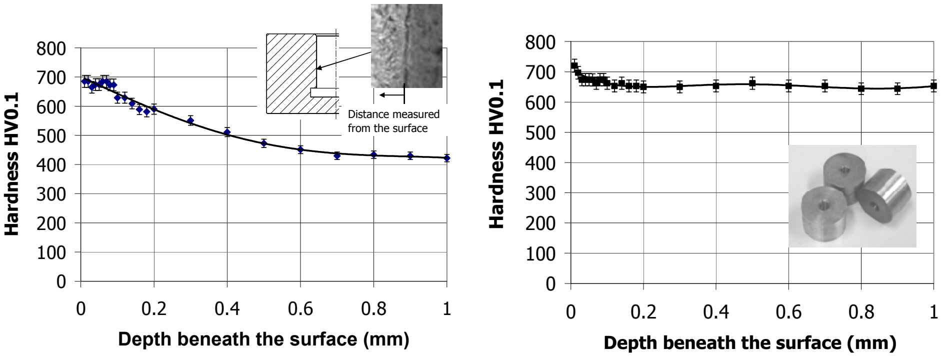

a) 16MnCr6 b) 100Cr6

Figure 5.7: Hardness distribution of two workpieces measured within the bore after heat treatment

The machined bore diameters varied between 3 and 4 mm, while the length to diameter ratio (l/d) was up to 4. The external diameter is 20 mm, the wall thickness ratio of the workpiece (WT) is at a minimum of 5, and therefore, the workpiece is "rigid" enough. Required workpiece hardness for both steels is 60±2 HRC. Figure 5.7 indicates the measured microhardness distribution after heat treatment.

5.2.3 Cutting tool

The turning of small bores was carried out with a Kennametal micro machining tooling system (Figure 5.8), which provides quick and accurate setups. In manufacturing of bores with diameter 3-4 mm, it was not possible to use inserted boring bars, the PCBN tool material is soldered on the tip of the boring bar. Figure 5.8 also summarizes the mechanical and physical properties of the PCBN cutting tool material, the tool geometry, and the measured values of the cutting tool corner radius (r_ε). The boring bar is made of tungsten carbide, as in machining of small and long bores, the tool deflection must be taken into account.

Kennametal PCBN MKTB KB5625
γ_n = 0°, α_n = 10°, κ_r = 95°, r_ε=0.2 mm
CBN content: 65%
binder: TiN-AlN
grain size: 2 μm
Tool holder: KM16 MKSM

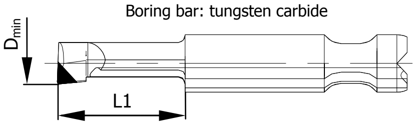

	Dmin (mm)	L1 (mm)
MKTB238012R	2.38	12.70
MKTB31709R	3.17	15.87
MKTB39622R	3.96	22.22

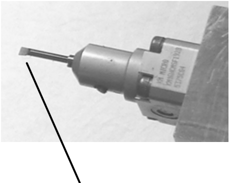

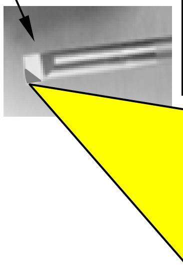

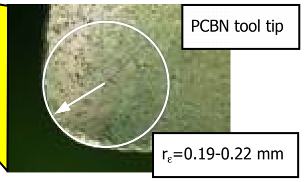

Mechanical and physical properties of CBN	
Density (g/cm^3)	4.28
Knoop hardness (GPa)	27.5
Young modulus (GPa)	587
Compressive strength (GPa)	3.55
Fracture toughness (MPa/m$^{1/2}$)	3.7
Trav. rupture strength (MPa)	225
Thermal conductivity (W/mK)	44
Thermal expansion (10^{-6}K^{-1})	4.7

Figure 5.8: Tooling for hard turning of small bores

In the grinding of small and long bores, the tool clamping system, the quill material, geometry and the wheel properties (type of material, hardness, grit size, concentration and binder material) are significant factors and must be chosen carefully. The applied grinding arbour is made from tungsten carbide, allowing maximum rigidity and minimal deflection. It was designed according to the diameter and length of the bore to be ground (Figure 5.9). The mechanical and physical properties of the tungsten carbide quill material and the tool geometry are given. Shorter (6 mm) and longer (18 mm) grinding tools were applied to study the effect of tool deflection on the machining results.

Figure 5.9 presents the specification of the CBN grinding wheels produced by Meister Abrasives. They differ in wheel hardness, mesh size, concentration, and binder material.

Before carrying out the experiments, the wheel was glued onto the quill with two components Epoxy adhesive. To remove the used wheel, the grinding tool must be placed into a furnace and heated up to 320 °C, with a holding time of half an hour.

Specification of the CBN grinding wheels:
Meister Abrasives
CB111-230-P-7-260-150-V55-32
CB111-325-P-7-260-150-V55-32
CB5-500-Q-8-255-200-V55-32
CB5-500-Q-10-195-200-V55-31

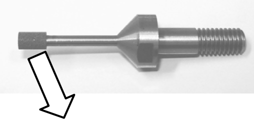

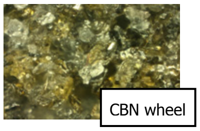

Mechanical and physical properties of the tungsten carbide quill material	
Density (g/cm^3)	14.45
Hardness (HV30)	1570
Young modulus (GPa)	590
Compressive strength (GPa)	5.5
Bending strength (GPa)	>4
Grain size (μm)	<1

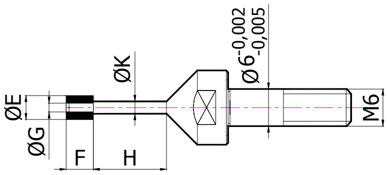

	H (mm)	F (mm)	∅K (mm)	∅G (mm)
A type	6	5	2	1.5
B type	18	5	2	1.5
C type	6	5	2.5	2
D type	18	5	2.5	2

Figure 5.9: Grinding tool specification

5.2.4 Coolant

Cimperial XE 04/04 water soluble metalworking fluid was applied as the coolant for grinding. It is a type of emulsion dedicated for heavy duty machining and grinding, and provides a high level of lubrication, high quality finish and excellent stability. Cleanliness is a very important criterion in the effectiveness and performance of metal working fluids. A Cimcool 50F system cleaner, specially designed to clean machines and fluid transport system, was used for cleaning the entire system.

5.2.5 Cutting force measurement

Cutting forces were measured in both the turning and grinding processes. According to space limitations, the Kistler piezoelectric dynamometer cannot be applied. The cutting force measurement was carried out with a pressure difference sensor connected to the main spindle (Figure 5.10). The machine operates with hydrostatic bearings, and the main spindle is supported by pressurized oil. When an external force acts on the main spindle, the radial bearing compensates the additional load. To compensate for this, the oil pressure on one side of the bearing is increased. The acting cutting force can be defined from the measurement of pressure difference (Figure 5.11a). The disadvantage of this measurement technique is that the cutting force can be monitored only in one direction. This is unlike the three components in the piezoelectric dynamometer, where all forces acting during cutting can be measured simultaneously.

The company GE Sensing produces the differential pressure sensor, Druck PMP 4000 series with model number PMP 4170. Its output voltage is ±5V, pressure range 2 bar, and accuracy ±0.04%. A power supply of 24V and 75mA was used in force measurement. The data processing and evaluation of the measured values were carried out with the LabVIEW program.

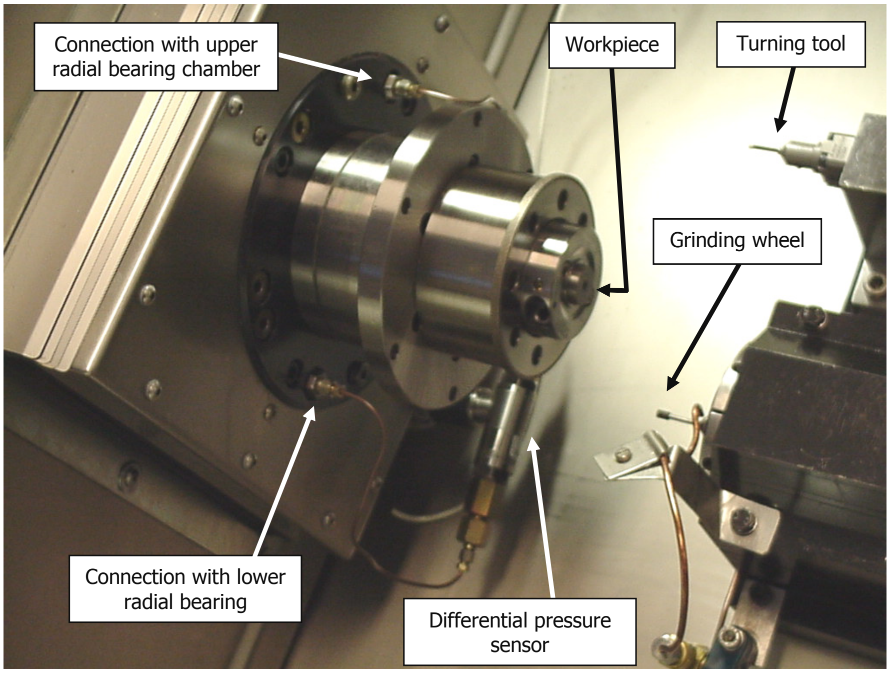
Connection with upper radial bearing chamber
Workpiece
Turning tool
Grinding wheel
Connection with lower radial bearing
Differential pressure sensor

Figure 5.10: Differential pressure sensor implemented into the machine

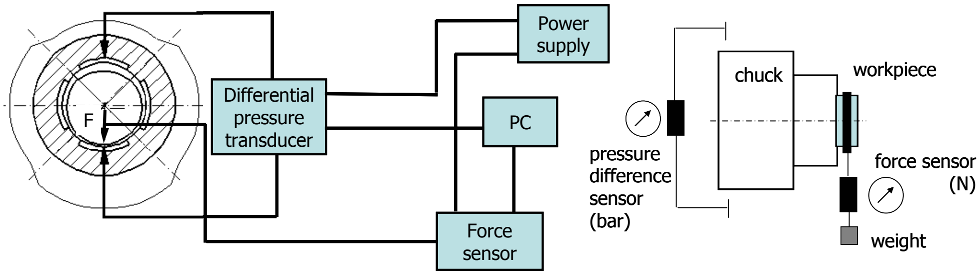
F
Differential pressure transducer
Power supply
PC
Force sensor
chuck
workpiece
pressure difference sensor (bar)
force sensor (N)
weight

a) pressure measurement on the hydrostatic bearing b) calibration set-up

Figure 5.11: Drawings of test set-up for force measurement

An additional force sensor (type: KAP-E from AST GmbH), operating with strain gauges for determination of forces, was applied to convert the pressure sensor output to actual cutting forces (Figure 5.11a). This force sensor has a range of ±10V and the forces can be measured up to 500 N. In the static calibration set-up when the main spindle does not rotate, both sensors (Figure 5.11b) were implemented into the machine. Different weights were used to cause different forces, while data were collected from both sensors simultaneously. The calibration was repeated several times, which lead to similar results. On the basis of this calibration, the increase of 1 bar pressure difference means that the cutting force is 98 N.

5.2.6 Calorimetric measurement

In the cutting of small bores, the measurement of residual heat quantity (Q_{exp}) transmitted into the workpiece was performed in a thermally insulated vacuum exicator (Figure 5.12). During cutting, the temperature rise in a workpiece with small bores is relatively low. Therefore, the vacuum ambient is more suitable for the determination of the residual heat quantity than water.

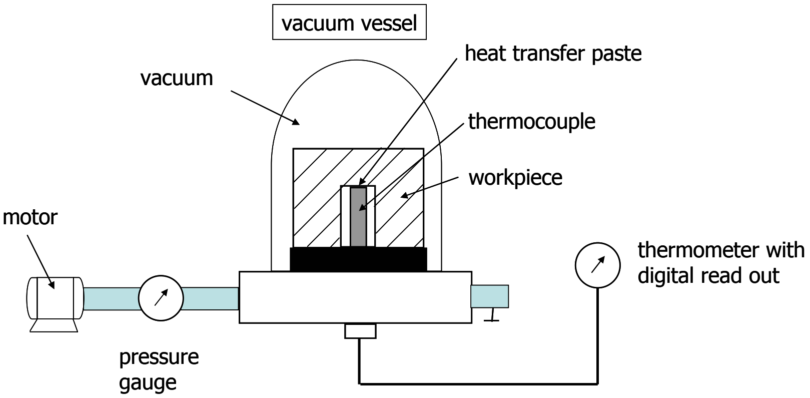

Figure 5.12: Set-up for measurement of residual heat quantity transmitted into the workpiece during cutting

In the vacuum, among the three modes of heat transfer (convection, conduction, and radiation), only radiation is operative. This is because there is no medium, like air or water, to convect or to conduct heat away from the object. As the temperature of a body increases, radiative energy is proportional to T^4, where ‘T’ is the temperature expressed in Kelvin. The energy lost by radiation occurs very slowly [GRO99].

Immediately after turning, the workpiece was put into the vacuum vessel and placed onto a thermocouple (Mineral Insulated, type K, IEC 584). Unclamping the workpiece, placing it into the vacuum vessel and creating the vacuum takes 10 sec. The absolute pressure of the vacuum is 10 kPa. During this time, the heat loss is only 1-2 %, due to the fact that heat conduction is stronger in the metal than the thermal convection between the workpiece and the ambient air. The contact performance between workpiece and thermocouple was improved by application of heat transfer paste. The temperature difference that arose during hard turning was directly measured with a thermometer with an accuracy of ±0.01 °C. In carrying out the calorimetric measurement, the initial temperature of the workpiece was 21.7 °C.

5.3 Other measuring equipment

5.3.1 Surface roughness and geometrical accuracy

Surface roughness measurements of the machined bores were performed with a Rank Taylor Hobson type Form Talysurf Series 120L stylus instrument (Figure 5.13a). The inductive gauge has a resolution of 16 nm. A Taylor Hobson type Talyrond 250 measuring machine (Figure 5.13b) was applied to measure roundness, cylindricity, parallelism, and straightness of the internal surface using a Gauss filter.

Size accuracy of small bores was measured with Mitutoyo Mini-Holtest 368-003. The measuring device can be used to measure the diameter of the bore in the range of 3-4 mm, graduation: 0.001 mm.

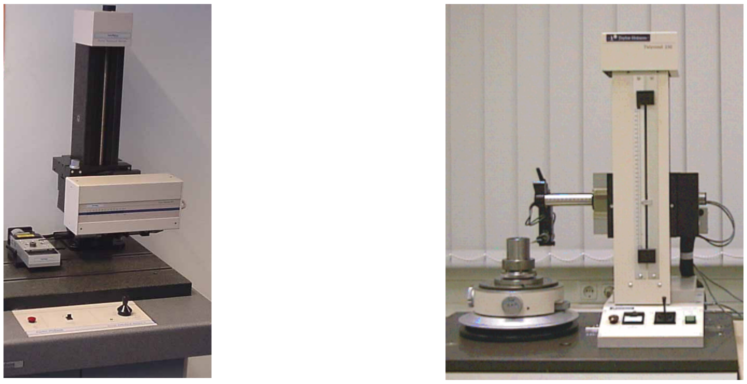

a) Talysurf Series 120L

b) Talyrond 250

Figure 5.13: Devices for measurement of (a) surface roughness, and (b) geometrical accuracy

5.3.2 Metallographic and microscopic investigations

In order to monitor the hardness of the non-machined workpieces (HRC) and analyze the microhardness of surface layer (HV), a Buehler Omnimet microhardness tester 886000 was applied after machining. The specimens were prepared with careful grinding in a number of rounds and then polished. The determination of Vickers microhardness was done with a 100 g load, for 10 s. In the metallographic investigation, the samples were coated with a Nickel supporting layer to protect the edges from any damage and etched using a Nital solution (3% nitric acid in methanol). A study of metallographic alterations was performed with an Olympus BX60M research microscope, with a magnification of 1000x. Both the microhardness tester and research microscope are fully motorized, equipped with high-resolution digital cameras, and connected to a PC, see Figure 5.14.

a) Buehler Omnimet 886000 b) Olympus BX60M

Figure 5.14: Applied (a) microhardness tester, and (b) research microscope

Microstructural investigation regarding the white layer was carried out with X-ray diffraction to reveal its composition. The martensite and retained austenite content of the white layer was measured with D8 ADVANCE (BRUKER AXS) X-ray diffraction. The measuring parameters were: applied ray: COKα, λ = 0.179024 nm; beam voltage: 40 kV; electron stream: 40 mA; aperture on primary side: Monocap ∅1 mm, secundary side: antiscattering 1 mm, detector aperture 0.2mm; measured angle interval: 2Θ = 45-130°; step: $\Delta(2\Theta)$ = 0.1°; collecting time: 60 s.

The monitoring of tool wear and measurement of surface features were achieved with a Keyence VHX-100 digital microscope using a VH-Z450 high range zoom lens (magnification: 450x-3000x). The high-resolution lens and optical edge enhancement function ensure higher reproduction than a conventional microscope. To ensure sharp 3D images, high quality depth composition is available, which provides an accurate representation of the target surface.

6 Set of models for machining of hardened bores

6.1 Model construction

From the point of view of industrial relevance, and because high quality parts with tight tolerances are needed, accurate predictions of results of the manufacturing process are required [LUT98]. The predictions should include both the technical aspects (geometrical accuracy, surface roughness, surface layer properties) and the commercial aspects (machining cost and time) of the machining performance.

To improve the reliability, stability and performance of the manufacturing process in machining of high precision bores, a predictive process modelling approach has been developed. To explain the entire process, a set of models has been established, which interconnects the input models with the output models through the process models (Figure 6.1). The specific investigations performed during the research work validate the intermediate process modelling steps, which together establish the predictive modelling approach.

The input model can be divided into two categories: a) the replacement of grinding with hard turning; and b) a combination of hard turning with grinding. In hard turning, the workpiece properties, the cutting tool characteristics, the cutting parameters, and the stiffness of the machine-tool-device-workpiece system can be regarded as input parameters. Furthermore, when hard turning and grinding are combined, the grinding and dressing conditions must be added to conditions of hard turning. Grinding is more complex than hard turning, as different grinding strategies can be applied in internal grinding, and the variability of the grinding and dressing parameters is large. Grinding wheel conditioning (method and dressing wheel properties), wheel type, and amount and pressure of the applied coolant also influence the machining results.

The process model includes different techniques for predictive modelling, such as empirical models and finite element method models. The empirical models provide an accurate prediction of the machining results such as cutting forces, cutting temperatures, geometrical accuracy, surface roughness and surface layer properties. The performed experimental investigations make the establishment of the empirical models possible. These empirical models as constraints are built into the optimisation process, which improves the performance of the bore manufacturing. Computer aided modelling (FEM) was applied to determine the thermal distortion in the workpiece during cutting. On the basis of the results of the FEM modelling and the cutting force measurement, the machining error caused by the heat and the force can be defined in bore machining.

The output models include both the process characteristics (tool wear, cutting forces, cutting temperatures and material removal rate), and the product characteristics (geometrical accuracy, surface roughness and surface integrity). Effects of the individual process characteristics on each other, and on the product characteristics, are given.

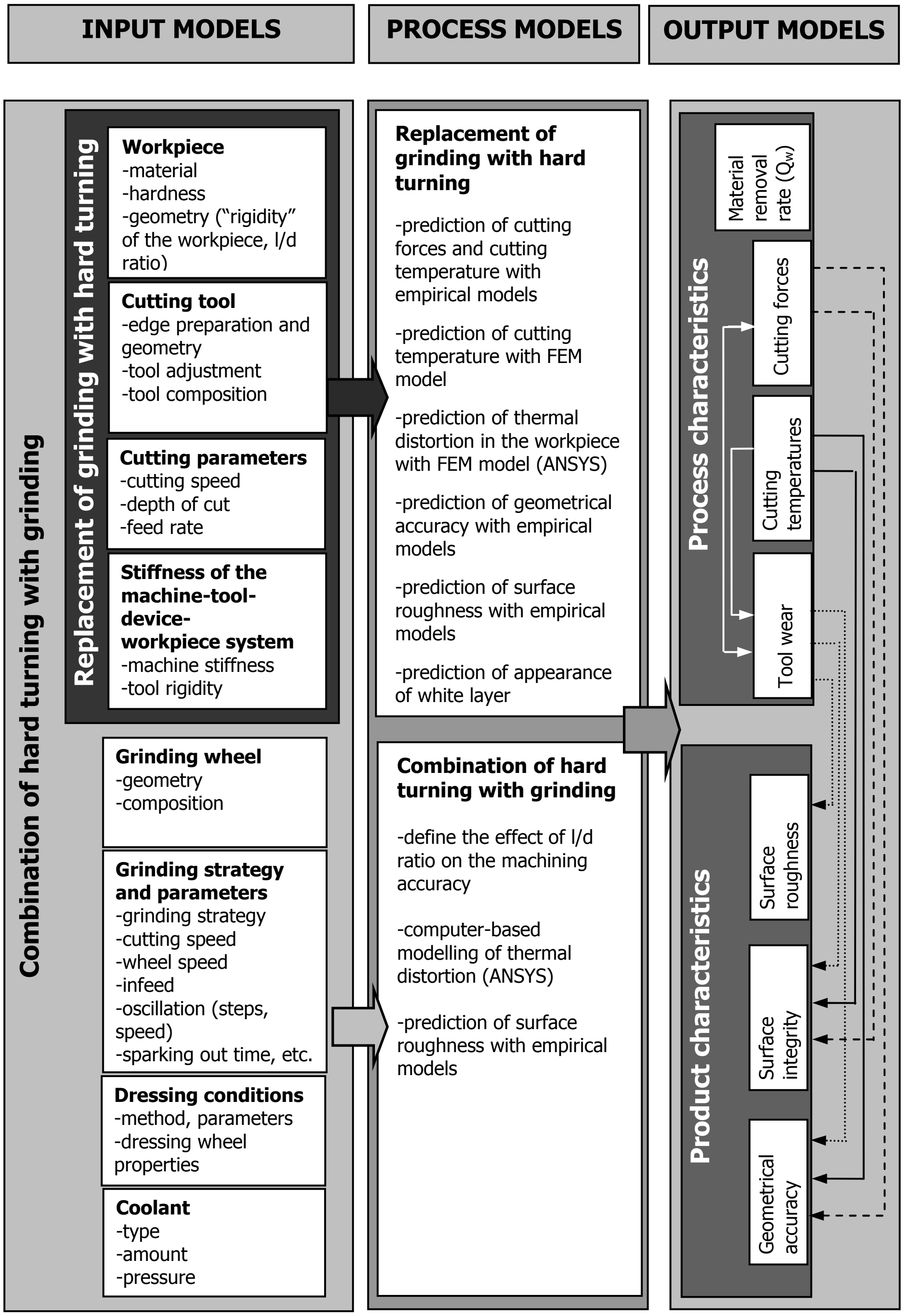
INPUT MODELS
PROCESS MODELS
OUTPUT MODELS
Combination of hard turning with grinding
Replacement of grinding with hard turning
Workpiece
-material
-hardness
-geometry ("rigidity" of the workpiece, l/d ratio)
Cutting tool
-edge preparation and geometry
-tool adjustment
-tool composition
Cutting parameters
-cutting speed
-depth of cut
-feed rate
Stiffness of the machine-tool-device-workpiece system
-machine stiffness
-tool rigidity
Grinding wheel
-geometry
-composition
Grinding strategy and parameters
-grinding strategy
-cutting speed
-wheel speed
-infeed
-oscillation (steps, speed)
-sparking out time, etc.
Dressing conditions
-method, parameters
-dressing wheel properties
Coolant
-type
-amount
-pressure
Replacement of grinding with hard turning
-prediction of cutting forces and cutting temperature with empirical models
-prediction of cutting temperature with FEM model
-prediction of thermal distortion in the workpiece with FEM model (ANSYS)
-prediction of geometrical accuracy with empirical models
-prediction of surface roughness with empirical models
-prediction of appearance of white layer
Combination of hard turning with grinding
-define the effect of l/d ratio on the machining accuracy
-computer-based modelling of thermal distortion (ANSYS)
-prediction of surface roughness with empirical models
Process characteristics
Material removal rate (Q_w)
Cutting forces
Cutting temperatures
Tool wear
Product characteristics
Surface roughness
Surface integrity
Geometrical accuracy

Figure 6.1: Set of models for manufacturing of high precision bores

6.2 Tool bending and machining errors caused by the force

The purpose of this calculation is to determine the maximum deflection of the grinding and turning tools, which are under concentrated and distributed loads during machining. The tool deflection may cause machining errors, and as its consequence, size errors will occur in the machined parts. The cutting tools are regarded as a cantilever beam in the calculation.

The deflection function, y(x), could be found from the basic differential equation of the deflection curve of a beam, if the bending moment function M(x) is known [SHI86]:

$$\frac{M(x)}{EI} = \frac{d^2y}{dx^2} \qquad (6.1).$$

This equation includes the applied moment (M), the modulus of elasticity (E), the moment of inertia (I), and the deflection of the beam (y). Shear force (V) and bending moment are related as:

$$V = \frac{dM}{dx} \qquad (6.2).$$

If the bending is caused by a distributed load, the relation between shear force and bending moment is:

$$\frac{dV}{dx} = \frac{d^2M}{dx^2} = q \qquad (6.3)$$

where q is the load intensity.

According to Equations 6.1-6.3, the following equations are yielded:

$$\frac{V}{EI} = \frac{d^3y}{dx^3} \qquad (6.4)$$

$$\frac{q}{EI} = \frac{d^4y}{dx^4} \qquad (6.5).$$

The following assumptions are made in the calculation:

1) The material of the beam is linear-elastic, with elasticity modulus E;
2) All loads are lateral and acting in the same plane. All deflections occur in this plane of bending;
3) Deflections are small compared to the length of the beam. In this case, equilibrium equations are applied to the non-deformed beam axis, and it is assumed that the curvature of the deformed beam (ρ) is equal to the second derivate of the deflection function.

On the basis of the mechanical design described above, the deflection due to bending is calculated for the grinding quill and the turning tool. The grinding tool can be regarded as a cantilever beam with intermediate load (Figure 6.2). The turning tool is a cantilever beam with end load, presented in Figure 6.3. According to the tool bending, the size errors caused by the forces can be determined, see Figure 6.2 and 6.3.

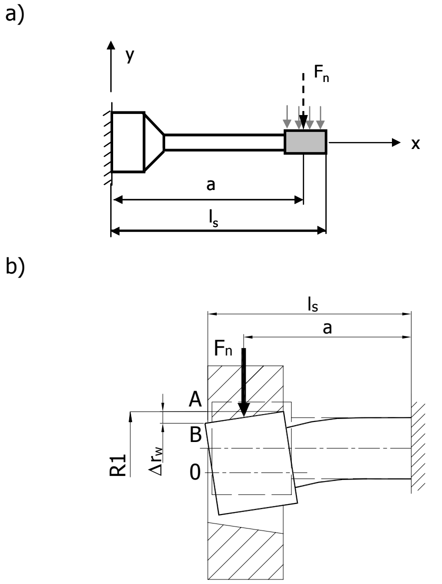

Maximum deflection of the grinding tool:

$$y_{max} = \frac{F_n \cdot a^2}{6EI}(a - 3l_s)$$

Assumptions:

- the workpiece is rigid enough

$$\Delta d_w = 2 \cdot \Delta r_w = 2(\overrightarrow{OA} - \overrightarrow{OB}) = 2(R1 - \overrightarrow{OB})$$

$$\overrightarrow{OB} = (R1 + \frac{F_n \cdot a^2}{6EI}(a - 3l_s))$$

Figure 6.2: (a) Grinding tool deflection; and (b) mechanical distortion in the workpiece

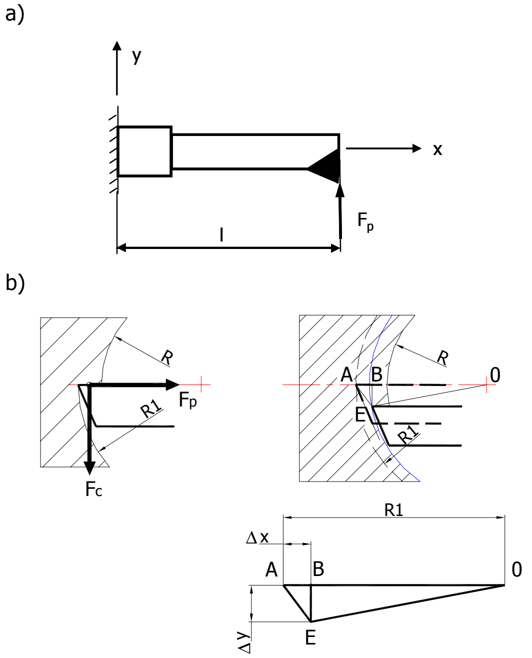

Maximum deflection of the turning tool:

$$y_{max} = -\frac{F_p \cdot l^3}{3EI}$$

$$\Delta d_w = 2(\overrightarrow{OA} - \overrightarrow{OE}) = 2(R1 - \overrightarrow{OE})$$

$$\overrightarrow{OE} = \sqrt{(R1 - \Delta x)^2 + \Delta y^2}$$

$$\Delta x = \frac{F_p \cdot l_s^3}{3EI}$$

$$\Delta y = \frac{F_c \cdot l_s^3}{3EI}$$

Assumptions:

- the workpiece is rigid enough
- the feed force (F_f) is relatively low, and can therefore be neglected

Figure 6.3: (a) Turning tool deflection; and (b) mechanical distortion in the workpiece

6.3 Modelling of mechanical and thermal effects

6.3.1 Cutting forces

One of the modelling approaches in the prediction of process characteristics is the empirical modelling [LUT98]. It is simple to apply in practice, however, experimental investigations are necessary, as a model is only valid for a certain tool-work material combination. The power-law form of the equation for predicting process characteristics (forces, temperature, tool life) is commonly applied in the machining processes [TAY07], [COL91]. In the case of manufacturing of high precision bores, it is attempted to generate a predictive empirical model for cutting forces, which was performed in MATLAB 6.5.1. In order to generate a relationship between the cutting force and the cutting data, regression analysis using least square method was applied. In this modelling, it can be analyzed how a single dependent variable is affected by the values of numerous independent variables. The coefficient of determination (R-squared value) was also defined, which indicates how closely the estimated values are to the measured data. The approximation is most reliable when the R-squared value is at or near 1.

To establish the empirical models, experimental investigations were performed. During the experiments, the cutting data (v_c, f, a_p) were varied, and the width of flank wear land (VB) was also considered. According to this, the power-law form of equation for modelling of the cutting force is:

$$F_i = C_F \cdot v_c^{z_F} \cdot f^{y_F} \cdot a_p^{x_F} \cdot VB(L)^{k_F} \qquad i = c, p, f \qquad (6.6)$$

where C_F is the coefficient of the cutting force equation, and x_F, y_F, z_F, k_F are the exponents of that. This equation can be determined and applied for all force components occurring during cutting.

6.3.2 Cutting temperature

Cutting temperature modelling was performed with finite element method software. Third Wave AdvantEdge is a tool for engineers to design, setup, improve and optimise machining processes. With this tool, it is possible to determine machining parameters and tooling configurations that can reduce cutting forces, temperatures and part distortion. This reduces the need for online testing, which costs money and valuable production time. However, the finite element model typically over predicts the process characteristics, due to the assumptions made. Therefore, the material models must be validated according to a given set of conditions.

Typical approaches for numerical modelling of metal cutting are the Lagrangian and Eulerian techniques. A Lagrangian finite element-based machining model is applied in this software. AdvantEdge [THI01], is an explicit dynamic, thermo-mechanically coupled finite element model specialized for metal cutting. Features necessary to model metal cutting accurately include adaptive re-meshing capabilities for resolution of multiple length scales. These include the cutting edge radius, the secondary shear zone and chip load, multiple body deformable contact for tool-workpiece interaction, and transient thermal analysis.

The software has three main components, all contained in one software package. The first component is a user interface, in which the simulation set-up can be compiled. Setup includes defining material conditions, tool geometries and machining parameters. The material model contains deformation hardening, thermal softening and rate sensitivity, tightly coupled with a transient heat conduction analysis, which is appropriate for finite deformations. The second component is the AdvantEdge Engine. It performs all the calculations from the set-up inputs. The third component is the simulation results viewer [THI01]. Here, the user can extract the necessary results, including cutting forces, cutting temperatures, steady state results etc.

Besides the FEM modelling, similarly to the modelling of cutting forces, prediction of cutting temperature was also accomplished with empirical models, on the basis of the performed experiments. Empirical model of cutting temperature Θ is found to be:

$$\Theta = C_{\vartheta} \cdot v_c^{z\vartheta} \cdot f^{y\vartheta} \cdot VB^{x\vartheta} \tag{6.7}$$

where C_{ϑ} is the coefficient of the cutting temperature equation and x_{ϑ}, y_{ϑ}, z_{ϑ} are the exponents of that.

6.4 Modelling of micro and macro geometrical errors

6.4.1 Empirical modelling of geometrical errors

In manufacturing, the ready products are mainly qualified with the maximum values of surface roughness and the geometrical accuracy. Generally, with regard to surface roughness, the arithmetical mean deviation of the assessed profile (Ra) and the ten-point height of the profile (Rz) are prescribed. The geometrical accuracy, including size errors, form errors, and positional errors, has a large significance in precision machining, as the tolerances are generally strict.

In industrial applications, prediction of micro and macro geometry errors is important, as they significantly influence the functional behaviour of the produced parts. Theoretical surface roughness can be easily defined with cutting tool geometry and cutting kinematics, without performing any experiments [LES78]. However, it does not provide exact results, as other cutting conditions are not taken into account. To reveal or compare the difference between the theoretical and the real roughness values, experimental investigations need to be done. Moreover, empirical modelling of micro and macro geometry errors assist in predicting the attainable geometrical accuracy, as a function of the technological data such as cutting speed, feed, depth of cut, length of cut. It can be built in the optimisation model as one of the constraints regarding the surface quality.

To determine the theoretical surface roughness values (Ra, Rq, Rt or Rz), the parameters of the cutting tool geometry and the applied feed are necessary (Figure 6.4).

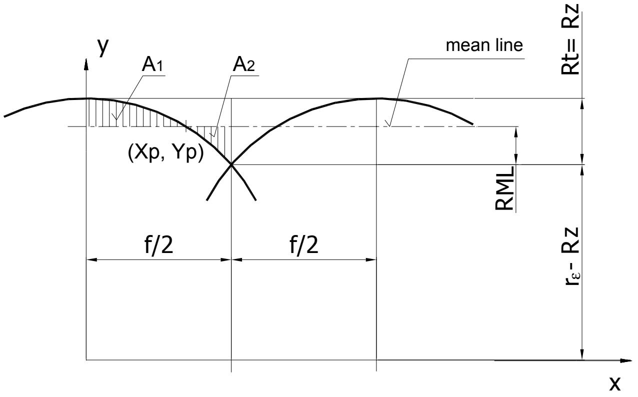

Figure 6.4: Determination of theoretical roughness

In hard turning, the applied PCBN tool possesses a corner radius, and therefore, r_ε must be taken into account. Among the cutting kinematics, the feed plays a significant role. According to Figure 6.4, the total height and/or ten-point-height of the profile are formulated in Equation 6.8:

$$Rt = Rz = r_\varepsilon - \sqrt{r_\varepsilon^2 - \frac{f^2}{4}} \tag{6.8}.$$

To define the Ra theoretical roughness, the mean line of the roughness profile must first be described. Namely, the coordinates of point x_p and y_p are needed, which are given by Equations 6.9 – 6.13:

$$\frac{f}{2}\left(RML + r_\varepsilon - Rz\right) = \int_{x=0}^{x=f/2} \sqrt{(r_\varepsilon^2 - x^2)}\,dx \tag{6.9}$$

$$y_P = RML + r_\varepsilon - Rz \tag{6.10}$$

$$x_P = \sqrt{r_\varepsilon^2 - y_P^2} \tag{6.11}$$

$$y_P = \frac{r_\varepsilon^2}{f} \arcsin\frac{f}{2r_\varepsilon} + \frac{1}{4}\sqrt{4{r_\varepsilon}^2 - f^2} \tag{6.12}$$

$$x_P = \sqrt{r_\varepsilon^2 - \left(\frac{r_\varepsilon^2}{f} \arcsin\frac{f}{2r_\varepsilon} + \frac{1}{4}\sqrt{4r_\varepsilon^2 - f^2}\right)^2} \tag{6.13}.$$

The mean line divides the search area signed with A_1 and A_2 (Figure 6.4), where $A = A_1 = A_2$ is valid. In this case, Ra can be formulated with Equation 6.14:

$$Ra \cdot \frac{f}{2} = 2A \quad \rightarrow \quad Ra = \frac{4}{f} \cdot A \tag{6.14}$$

where A can be calculated with Equation 6.15:

$$A = \int_{x=0}^{x=x_P} \sqrt{(r_\varepsilon^2 - x^2)}dx - x_P \cdot y_P \tag{6.15}.$$

After the integration, A is

$$A = \frac{1}{2}\left(x_P \sqrt{r_\varepsilon^2 - x_P^2} + r_\varepsilon^2 \arcsin\frac{x_P}{r_\varepsilon} \right) - x_P \cdot y_P \tag{6.16}$$

and Ra equals to

$$Ra = \frac{4}{f}(0.5 \cdot (x_P \sqrt{r_\varepsilon^2 - x_P^2} + r_\varepsilon^2 \arcsin\frac{x_P}{r_\varepsilon}) - x_P \cdot y_P) \tag{6.17}.$$

The root-mean-square deviation of the profile can also be defined on the basis of Figure 6.4:

$$Rq = \sqrt{\int_{x=0}^{x=f/2} (\sqrt{r_\varepsilon^2 - x^2} - y_P)^2 dx} \tag{6.18}$$

$$Rq = \sqrt{r_\varepsilon^2 - \frac{f^2}{12} - y_P^2} \tag{6.19}.$$

The definition of empirical models regarding the macro and micro geometrical accuracy was performed with the same method as was prescribed in predictive modelling of cutting forces (see, Chapter 6.3.1). During the performed investigation, the effect of cutting data (v_c, f, a_p), and the width of flank wear land was considered. The empirical model for surface roughness (Ra, Rq, Rz, Rt) are formulated below:

$$Ra = C_{Ra} \cdot v_c^{z_{Ra}} \cdot f^{y_{Ra}} \cdot a_p^{x_{Ra}} \cdot VB(L)^{k_{Ra}} \tag{6.20}$$

$$Rq = C_{Rq} \cdot v_c^{z_{Rq}} \cdot f^{y_{Rq}} \cdot a_p^{x_{Rq}} \cdot VB(L)^{k_{Rq}} \tag{6.21}$$

$$Rz = C_{Rz} \cdot v_c^{z_{Rz}} \cdot f^{y_{Rz}} \cdot a_p^{x_{Rz}} \cdot VB(L)^{k_{Rz}} \tag{6.22}$$

$$Rt = C_{Rt} \cdot v_c^{z_{Rt}} \cdot f^{y_{Rt}} \cdot a_p^{x_{Rt}} \cdot VB(L)^{k_{Rt}} \tag{6.23}$$

where C_{Ra}, C_{Rq}, C_{Rz}, C_{Rt} are the coefficients of the surface roughness equations, and x_{Ra}, y_{Ra}, z_{Ra}, k_{Ra}, x_{Rq}, y_{Rq}, z_{Rq}, k_{Rq}, x_{Rz}, y_{Rz}, z_{Rz}, k_{Rz}, x_{Rt}, y_{Rt}, z_{Rt}, k_{Rt} are the exponents of that.

Regarding the macro geometrical accuracy, three factors, including cutting speed, length of cut and wall thickness ratio of the gear body (WT), were taken into account in turning. As the gears are disc type parts and sometimes possess thin wall thickness, the effect of "workpiece rigidity" must be taken into account on the accuracy. In the macro geometrical accuracy of the bore, the out-of-roundness (RONt), the cylindricity error (CYLt), and the parallelism error of the bore generatrices

(CYLpar) are prescribed. Abbreviations are given according to ISO/TS 12181-1: 2003. They can be formulated as:

$$\mathrm{RONt} = C_{\mathrm{RONt}} \cdot v_c^{z_{\mathrm{RONt}}} \cdot \mathrm{WT}^{y_{\mathrm{RONt}}} \cdot L^{x_{\mathrm{RONt}}} \tag{6.24}$$

$$\mathrm{CYLt} = C_{\mathrm{CYLt}} \cdot v_c^{z_{\mathrm{CYLt}}} \cdot \mathrm{WT}^{y_{\mathrm{CYLt}}} \cdot L^{x_{\mathrm{CYLt}}} \tag{6.25}$$

$$\mathrm{CYLpar} = C_{\mathrm{CYLpar}} \cdot v_c^{z_{\mathrm{CYLpar}}} \cdot \mathrm{WT}^{y_{\mathrm{CYLpar}}} \cdot L^{x_{\mathrm{CYLpar}}} \tag{6.26}$$

where C_{RONt}, C_{CYLt}, C_{CYLpar} are the coefficients of the macro geometrical accuracy equations, and x_{RONt}, y_{RONt}, z_{RONt}, x_{CYLt}, y_{CYLt}, z_{CYLt}, x_{CYLpar}, y_{CYLpar}, z_{CYLpar} are the exponents of that.

6.4.2 FEM analysis of thermal errors

In order to improve the efficiency of hard turning and create proper surface quality, a study on workpiece thermal distortion was accomplished. The heat expansion causes form and size errors for the workpiece, which can be predicted with finite element methods.

Since the mid-90's, due to constantly improving computer hard- and software complex finite element simulations and model computations have become possible that can take all necessary influence parameters into consideration [BÄH98]. Because of this progress, the thermo-elastic deformation of a workpiece can be calculated as a result of mechanical and thermal influences with the help of the finite element method. Using such a process control, it is possible that the geometrical workpiece deviations caused by the heat can be reduced by process design and parameter selection, or by correcting the tool path during hard cutting [BÄH98].

A finite element method based computer model was developed for the simulation of thermal deformation in turning [SUK03]. A new inverse problem solution (IPS) technique [SUK04] was applied to obtain the heat induced in the cutting process and the heat transfer from the workpiece to the air. The sketch of the combined computational and experimental approach for finding thermal distortions in turning is presented in Figure 6.5.

According to Figure 6.5, the elaboration steps are as follows:

1) Measurement of the heat quantity transmitted into the workpiece with experimental investigation;
2) Determination of the thermal flux at the workpiece-tool interface by FEM model (ANSYS 8.1);
3) Modelling of the change in workpiece temperature and size error, caused by the heat with FEM (ANSYS 8.1).

Both gears and injection nozzles are axis-symmetric, and therefore, the workpieces can be modelled with half of the object for heat transfer analysis. In the gear model, the selected bore diameter is 48 mm (Figure 6.6), and it is 4 mm in the case of the injection nozzle (Figure 6.7). The selected workpiece diameters aim to compare the thermal effects in disc type parts, with bigger diameters versus small and long bores.

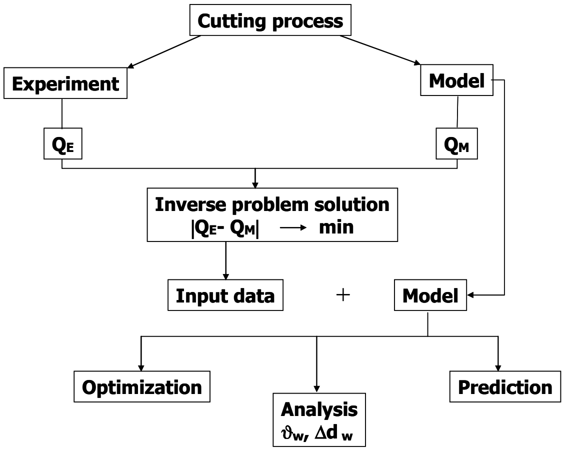
Cutting process
Experiment
Model
QE
QM
Inverse problem solution
|QE- QM| ⟶ min
Input data
+
Model
Optimization
Analysis
ϑw, Δd w
Prediction

Figure 6.5: Process model flow chart for finding thermal properties [SUK04]

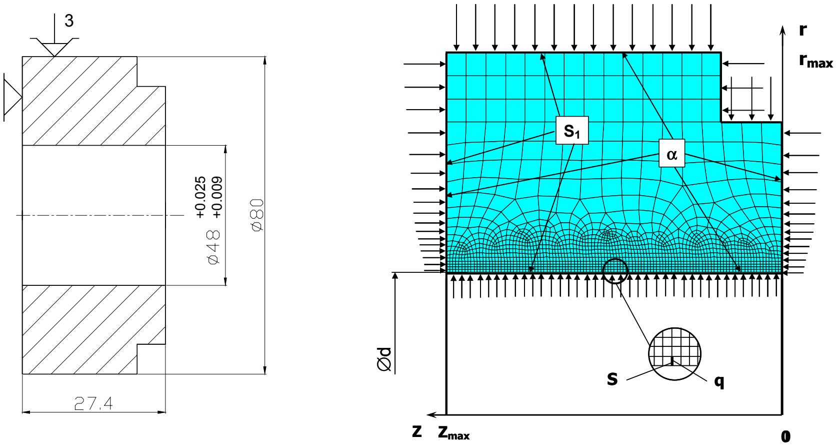
3
+0.025
+0.009
⌀48
⌀80
27.4
r
rmax
S1
α
⌀d
S
q
Z
Zmax
0

Figure 6.6: Sketch of the gear and physical model of heat transfer in hard turning

The geometrical model of the workpiece consists of plane surfaces and cylindrical surfaces (S_1), see Figures 6.6 and 6.7. On these surfaces, heat transfer that occurs can be described with the heat transfer coefficient (α). This coefficient changes as a function of the relative speed, and therefore, it is constant on the cylindrical surfaces, but different on the sides. Also, in two cylindrical surfaces with different diameters, the cutting speed is different, thus the heat transfer coefficient is different. The workpieces were clamped into a chuck during cutting. It means heat transfer also occurs in the chuck, which was taken into account during the simulation.

On the working cutting edge, there is a moving heat source with heat flux (q), which acts on the contact length (S) between the cutting tool and workpiece.

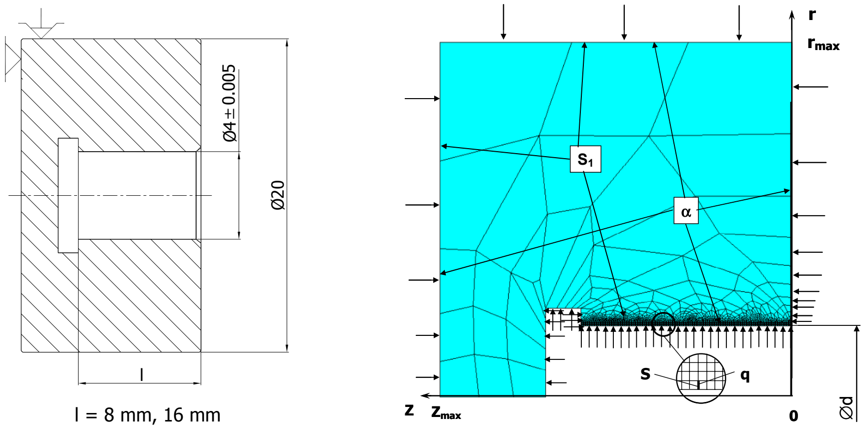

Figure 6.7: Injection nozzle and physical model of it for hard turning

For the physical model of the cutting process, the following statements and simplifications are made:

1) The spatial geometrical model of the workpiece and the model of the cutting process are reduced to a two-dimensional axis-symmetric model;
2) The heat generated during hard turning can be regarded as a ring-shaped heat source spread along the circumference of the workpiece uniformly, due to the high circumferential speed of the workpiece and low feed rate of the cutting tool [NIC80];
3) The heat transfer coefficient (α) is valid on the workpiece-air boundary surface (S_1). The heat transfer coefficient depends on the cutting speed and the temperature change. On the faces the calculation is performed with average cutting speed, because the temperature change is not considerable, and therefore, an average heat transfer coefficient can be applied.

The thermal state of the workpiece is given by the two-dimensional heat conduction equation [SUK03]:

$$c\rho\frac{\partial\vartheta_w}{\partial t}=\frac{1}{r_w}\frac{\partial}{\partial r_w}\left[r_w\lambda\frac{\partial\vartheta_w}{\partial r_w}\right]+\frac{\partial}{\partial z_w}\left[\lambda\frac{\partial\vartheta_w}{\partial z_w}\right] \tag{6.27}$$

where c is the coefficient of specific heat, ρ the density, t the time, r_w the radius of the workpiece, ϑ_w the temperature of the workpiece, λ the thermal conductivity of the workpiece, and z_w the coordinate of the workpiece. In Equation 6.27, the following boundary conditions and functions are valid:

$$t \geq 0; \quad 0 < r_w < r_{w\,max}; \quad 0 < z_w < z_{w\,max} \tag{6.28}$$

$$c = c(r_w, z_w, t, \vartheta_w); \quad \rho = \rho(r_w, z_w, t, \vartheta_w); \quad \lambda = \lambda(r_w, z_w, t, \vartheta_w) \tag{6.29}$$

Applied initial condition is:

$$\vartheta_w(r_w, z_w, 0) = \vartheta_0 \qquad (6.30)$$

where ϑ_0 is the room temperature.

Boundary conditions used:

At the contact surface (S) between cutting tool and workpiece, heat generation occurs. The heat flux (q) can be given by Equation 6.31:

$$-\lambda \frac{\partial \vartheta_w(r_w, z_w, t)}{\partial z_w} = q \qquad (6.31).$$

As the cutting tool is moving along in the bore, the contact surface depends on the place and the time:

$$S = S(r_w, z_w, t) \qquad (6.32).$$

At the surfaces S_1, heat transfer occurs from the workpiece to the ambient, which can be described for the cylindrical surfaces with Equation 6.33:

$$-\lambda \frac{\partial \vartheta_w(r_{w\max}, z_w, t)}{\partial r_w} = \alpha\left[\vartheta_w(r_{w\max}, z_w, t) - \vartheta_{amb}\right] \qquad (6.33)$$

where ϑ_{amb} is the ambient temperature.

The heat transfer can be determined for the plane surfaces with Equations 6.34 and 6.35:

$$-\lambda \frac{\partial \vartheta_w(r_w, 0, t)}{\partial z_w} = \alpha\left[\vartheta_w(r_w, 0, t) - \vartheta_{amb}\right] \qquad (6.34)$$

$$-\lambda \frac{\partial \vartheta_w(r_w, z_{w\max}, t)}{\partial z_w} = \alpha\left[\vartheta_w(r_w, z_{w\max}, t) - \vartheta_{amb}\right] \qquad (6.35).$$

The thermal deformation of the workpiece can be formulated in the radial direction with Equation 6.36, and in the longitudinal direction with Equation 6.37:

$$dr_w = \alpha_{exp}(\vartheta) \cdot r_w \cdot d\vartheta \qquad (6.36)$$

$$dz_w = \alpha_{exp}(\vartheta) \cdot z_w \cdot d\vartheta \qquad (6.37)$$

where dr_w is the thermal radial expansion of the workpiece, dz_w the thermal longitudinal expansion of the workpiece, and α_{exp} the coefficient of thermal expansion.

To predict the temperature alteration and the geometrical errors caused by the heat during hard turning, ANSYS 8.1 finite element software was used. The input data, which are necessary to perform the modelling, are summarized below.

From the literature concerning to the workpiece, the following parameters are needed:

- density (ρ),
- coefficient of thermal conductivity (λ),
- coefficient of specific heat (c),
- coefficient of thermal expansion (α_{exp}),
- Young modulus (E),
- Poisson-coefficient (ν).

The convection heat transfer coefficient can be calculated on the basis of the Reznikov-model [REZ81] with Equation 6.38 as:

$$\alpha = 6.85 \cdot 10^{-4} \frac{v_c^{0.65}}{d_e^{0.35}} \qquad (6.38).$$

From the experiments – on the basis of calorimetric method – it is required to measure the residual heat quantity transmitted into the workpiece (Q_E). This is necessary because it provides the determination of the heat flux (q) at the workpiece-tool interface, by means of the inverse problem solution (IPS) technique, see Figure 6.8.

EXPERIMENT	**FEM MODEL**
1. Hard turning of the workpiece	1. Modelling of warming-up of the workpiece with randomly chosen heat flux
2. Place the workpiece in a calorimeter	2. Modelling of temperature compensation in the workpiece without convection
3. Determination of the residual heat quantity transmitted into the workpiece (Q_{exp})	3. Calculation of the residual heat quantity (Q_{calc})
$Q_{exp} = (\vartheta_{wa}^{fin} - \vartheta_{wa}^{st}) \cdot c_{wa} \cdot m_{wa}$	$Q_{calc} = (\vartheta_{w,st} - \vartheta_0) \cdot c_w \cdot m_w$

$$\mathbf{Q_{exp} \cong Q_{calc}}$$

Figure 6.8: Determination of the heat flux [SUK03]

By means of the finite element software the heat flux is searched and determined, where $Q_{exp} \cong Q_{calc}$. At this point, the amount of heat transferred to the workpiece in the simulation model is equal to the amount of heat measured by the calorimetric method.

The simulation steps are presented in Table 6.1. During the modelling, time intervals must be defined to determine the temperature distribution in the workpiece at different times, as it is a transient process. The temperature and thermal distortion were determined in each cutting pass; and the transient analysis was continually repeated by adding a given time interval to the actual time. In the meshing, the face of the element, where the heat source acts with a heat flux (q), was equal to the contact length. This meant that the meshing was generated according to the actual feed and the depth of cut applied during turning.

Steps of modelling	**Results**
1. Generation of workpiece geometry	Geometry model
2. Selection of thermal element type, material properties, and meshing	Meshed model for thermal calculation
3. Definition of conditions (convection, conduction, heat flux)	Thermal finite element model
4. Calculation of temperatures	Temperature distribution in the workpiece
5. Change of element type which suits mechanical analysis	Meshed model for calculation of deformation
6. Definition of constraints (temperature distribution, fixing points)	Mechanical finite element model
7. Calculation of deformation	Thermo-elastic deformation of the workpiece

Table 6.1: Simulation steps in modelling workpiece deformation

6.5 Predict the change of surface integrity

During machining, the surface layer of the machined part is influenced by the thermo-mechanical material removal mechanisms. White layers have already been observed in many material removal processes, such as turning, grinding, reaming, milling, drilling and electrical discharge machining [BRI99]. White layer formation is mainly a thermal process involving phase transformation of the steel, and probably activated by plastic strain [REC03]. Currently, the microstructural evolution during white layer formation is not fully explained. In hard turning of hypereutectoid steel, such as 16MnCr5, and when the heating rate is high ($2.1 \cdot 10^6$ °C/s), it can be stated that due to its high carbon concentration, martensite may transform without diffusion to austenite. This is reverse martensitic transformation [REC03]. However, after passing the tool, to the generation of the white layer, the cooling of the surface layer must take place in very short time.

According to the research work performed by Schmidt [SCH99], it is proved that if the power per unit length (P'_α) achieves 150 W/mm, it causes the appearance of the white layer in cutting of hardened steels, which can decrease the lifetime of the parts. The power per unit length is defined as a quotient of the cutting power, and the contact length between tool and workpiece and can be formulated by:

$$P'_\alpha = \frac{P_\alpha}{l_c} = \frac{\mu \cdot \sqrt{F_p{}^2 + F_f^2} \cdot v_c}{l_c} \tag{6.39}$$

where P_α is the power, l_c the contact length between cutting tool and workpiece, F_p the passive force, F_f the feed force, μ the friction coefficient, and v_c the cutting speed.

On the basis of Schmidt's model [SCH99], the investigations performed in turning of high precision bores aim to reveal under what kind of technological data the generation of white layer can take place. It attempts to predict the appearance of the white layer as a function of the cutting data.
To calculate the cutting power, the cutting forces occurring during machining need to be measured. In the present workpiece-tool pair, the friction coefficient (μ) was 0.26, according to Schmidt's model [SCH99]. The contact length between tool and workpiece is defined by the cutting tool geometry and the depth of cut applied (Figure 6.9).

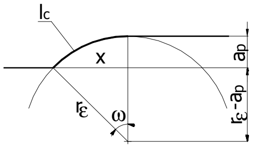

$$x = \sqrt{a_p(2r_\varepsilon - a_p)}; \qquad tg\varpi = \frac{x}{r_\varepsilon - a_p}$$

$$l_c = r_\varepsilon \mathrm{arc}\omega$$

Figure 6.9: Determination of contact length (l_c) between cutting tool and workpiece

The empirical model to predict the appearance of white layer, according to the experimental work can be given as:

$$P'_\alpha = C_{P'_\alpha} \cdot v_c^{z_{P'_\alpha}} \cdot f^{y_{P'_\alpha}} \cdot a_p^{x_{P'_\alpha}} \tag{6.40}$$

where $C_{P'\alpha}$ is the coefficient of this equation, and $x_{P'\alpha}$, $y_{P'\alpha}$, $z_{P'\alpha}$ are the exponents of that.

6.6 Optimisation applied in hard turning

To improve the effectiveness of the cutting process, it is necessary to study the technological factors of the process from an economical point of view [BAL85]. The selection of the cutting factors is closely related to the economical characteristics, such as productivity and production cost.
In the general method for optimisation of applied technological data, the concrete constraints are defined [HOR79], the depth of cut is regarded as a constant parameter, and the feed and the cutting speed are the only unknown quantities among the cutting data. The constraints of the optimisation model include tool life, cutting power, cutting temperature, cutting forces, tool wear and surface roughness. In this case, the aim is to extend it with other characteristics of the surface quality such as geometrical accuracy and microstructural change in the surface layer. The determination of the optimal cutting data, belonging to the minimum production cost, is attempted.

Firstly, the cutting parameters, which fulfil the best the objective function according to the constraints, are defined. Secondly, the tool life is determined. Together, these define the optimum cutting data.

The objective function is the minimum production cost:

$$K = \min\left[\frac{k_g}{n}\left(1 + \frac{t_{cs} + K_e / k_g}{T}\right)\right] \quad (6.41)$$

where k_g is the cost of the machine per minute, n the revolution, t_{cs} the time of tool change, K_e the cost of the cutting tool edge, and T the tool life.

The revolution and the cutting speed can be computed by the expression:

$$n = \frac{1000 \cdot v_c}{d\pi} \qquad \text{and} \qquad v_c = \frac{C}{T^m} \quad (6.42)$$

where C is the coefficient of the tool life equation, and m is the exponent of that.
The production cost function has a minimum, if:

$$\frac{\partial K}{\partial T} = 0 \quad (6.43).$$

The tool life belonging to the minimum cost is:

$$T_{Kopt} = \left(\frac{1}{m} - 1\right)\left(t_{cs} + \frac{K_e}{k_g}\right) \quad (6.44).$$

To set up the constraints, which affect the selection of the optimal cutting data, the necessary descriptive equations are listed in Equations 6.45-6.53.

1. Cutting speed

$$v_c = \frac{d \cdot \pi \cdot n}{1000} \quad (6.45)$$

2. Cutting power

$$P_c = \frac{F_c \cdot v_c}{60} \quad (6.46)$$

3. Cutting forces

$$F_p = C_{Fp} \cdot v_c^{z_{Fp}} \cdot f^{y_{Fp}} \cdot a_p^{x_{Fp}} \quad (6.47)$$

$$F_c = C_{Fc} \cdot v_c^{z_{Fc}} \cdot f^{y_{Fc}} \cdot a_p^{x_{Fc}} \quad (6.48)$$

$$F_f = C_{Ff} \cdot v_c^{z_{Ff}} \cdot f^{y_{Ff}} \cdot a_p^{x_{Ff}} \quad (6.49)$$

4. Tool life

$$C = T^{m} \cdot v_c \tag{6.50}$$

5. Admissible surface roughness of the machined workpiece

$$Rz = C_{Rz} \cdot v_c^{z_{Rz}} \cdot f^{y_{Rz}} \cdot a_p^{X_{Rz}} \tag{6.51}$$

6. Admissible geometrical accuracy of the cut part

$$RONt = C_{RONt} \cdot v_c^{zRONt} \cdot WT^{yRONt} \cdot L^{XRONt} \tag{6.52}$$

where RONt is the peak-to-valley roundness deviation, WT the wall thickness ratio of the gear body, and L the length of cut.

7. Description of the microstructural change – elimination of white layer

$$P'_{\alpha} = C_{P'_{\alpha}} \cdot v_c^{z_{P'_{\alpha}}} \cdot f^{y_{P'_{\alpha}}} \cdot a_p^{x_{P'_{\alpha}}} \tag{6.53}$$

where P'_{α} is the heat power per unit length, which defines the appearance of white layer.

The constraints related to the machine features, the process and the product characteristics are listed below. The equations are formulated and/or rewritten as a function of feed (f), or revolution (n), or the product of those (f·n).

1. Adjustable minimum feed regarding the machine tool

$$f \rightarrow f \geq f_{min} \tag{6.54}$$

2. Adjustable maximum feed regarding the machine tool

$$f \rightarrow f \leq f_{max} \tag{6.55}$$

3. Adjustable minimum revolution regarding the machine tool

$$n \rightarrow n \geq n_{min} \tag{6.56}$$

4. Adjustable maximum revolution regarding the machine tool

$$n \rightarrow n \leq n_{max} \tag{6.57}$$

5. Minimum chip thickness

$$\bar{h}_{min} = f\sqrt{\frac{a_p}{2 \cdot r_{\varepsilon}}} \rightarrow f \geq \frac{\bar{h}_{min}}{\sqrt{\frac{a_p}{2 \cdot r_{\varepsilon}}}} \tag{6.58}$$

6. Maximum cutting power

$$P_c = \frac{F_c \cdot v_c}{60} \leq P_{c\,max} \tag{6.59}$$

If Equations 6.45 and 6.48 are substituted in Equation 6.59, and expressed in terms of the feed and the revolution, the next inequality can be formulated

$$f^{y_{F_c}} \cdot n^{z_{F_c}+1} \leq \frac{60 \cdot P_c}{C_{F_c} \cdot \left(\frac{d\pi}{10^3}\right)^{z_{F_c}+1} \cdot a_p^{x_{F_c}}}$$

7. Maximum surface roughness

$$\begin{gathered} Rz = C_{Rz} \cdot v_c^{z_{Rz}} \cdot f^{y_{Rz}} \cdot a_p^{X_{Rz}} \rightarrow \\ f^{y_{Rz}} \cdot n^{z_{Rz}} \leq \frac{Rz}{C_{Rz} \cdot \left(\frac{d\pi}{10^3}\right)^{z_{Rz}} \cdot a_p^{x_{Rz}}} \end{gathered} \tag{6.60}$$

8. Maximum geometrical accuracy – admissible out-of-roundness

$$\begin{gathered} RONt = C_{RONt} \cdot v_c^{z_{RONt}} \cdot WT^{y_{RONt}} \cdot L^{X_{RONt}} \rightarrow \\ \left(\frac{1}{f}\right)^{x_{RONt}} \cdot n^{z_{RONt}} \leq \frac{RONt}{C_{RONt} \cdot \left(\frac{d\pi}{10^3}\right)^{z_{RONt}} \cdot WT^{y_{RONt}} \cdot \left(\frac{d\pi l}{10^3} \cdot N\right)^{x_{RONt}}} \end{gathered} \tag{6.61}$$

9. Prevention of the white layer

$$\begin{gathered} P_\alpha^{'} = C_{P_\alpha^{'}} \cdot v_c^{z_{P_\alpha^{'}}} \cdot f^{y_{P_\alpha^{'}}} \cdot a_p^{x_{P_\alpha^{'}}} \rightarrow \\ f^{y_{P_\alpha^{'}}} \cdot n^{z_{P_\alpha^{'}}} \leq \frac{P_\alpha^{'}}{C_{P_\alpha^{'}} \cdot \left(\frac{d\pi}{10^3}\right)^{z_{P_\alpha^{'}}} \cdot a_p^{x_{P_\alpha^{'}}}} \end{gathered} \tag{6.62}$$

After making a list of constraints, the inequalities can be plotted in a log n-log f plane. These linear functions will define the area, where the optimal cutting data can be found and indicate the optimum point.

7 Machining of disc type parts

Disc type parts, like gears, possess short bores, where the length to diameter ratio is typically lower than 1. However, the wall thickness ratio of the gear can vary in a wide range (WT = 1.34-2.83). This means that the clamping force applied during machining influences the attainable geometrical accuracy due to the workpiece "rigidity". If the tool is rigid enough, that is, that the tool length to diameter is lower than 1.5, the tool bending is negligible, so it cannot cause significant geometrical error. However, the effect of the cutting temperature and heat on the machining accuracy must be taken into account, as hard turning is done without coolant.

It is the goal of Chapter 7 to predict the performance of hard turning, and reveal the interconnections between the process and product characteristics. Determination of hard turning characteristics with FEM and empirical models provide an easy and useful prediction of cutting forces, cutting temperature and surface quality in the practice. The performed experimental investigations make the establishment of the empirical models possible. These empirical models, as constraints, are built into the optimisation process, which improves the performance of the bore manufacturing. For the prediction of the appearance of white layer the cutting power must be known, which can be calculated from the occurring cutting forces. Therefore, the determination of cutting forces is necessary with experimental investigations. In addition to the investigation of attainable surface quality in hard turning, the economical points of view, namely the material removal rate and the cycle time, must be compared between hard turning and grinding. These together clearly define whether or not grinding can be replaced by hard turning in machining of disc type parts.

7.1 Experimental investigations

7.1.1 Cutting forces

In the force measurements, a gear with a bore diameter of 48 mm was selected, and the cutting data were varied (v_c, a_p, f), but the width of flank wear land (VB) was kept constant. As the chip formation occurs on the tool radius in hard turning, and a cutting tool with a negative rake angle is applied, the passive force was determined to be the highest cutting force component. It exceeds 270 N, while the values of the other two force components remain always lower than F_p (Figures 7.1 and 7.2). The passive force is at least 1.3 times higher than the main cutting force, while the maximum is 2.1 times higher. All three force components are influenced mainly by the depth of cut and the feed; the cutting speed has less influence on them. The increase in the chip cross sectional area of cut heightens the forces, but the cutting speed decreases them, as the cutting temperature is in direct proportion to the speed. The generated heat amount is high enough to plasticize the workpiece material, and thus, a lower cutting force develops. Figure 7.1 presents the relationship between the measured cutting forces, and the applied feed and cutting speed. The passive force and the main cutting force increase with the feed, however, the feed force is hardly influenced by it.

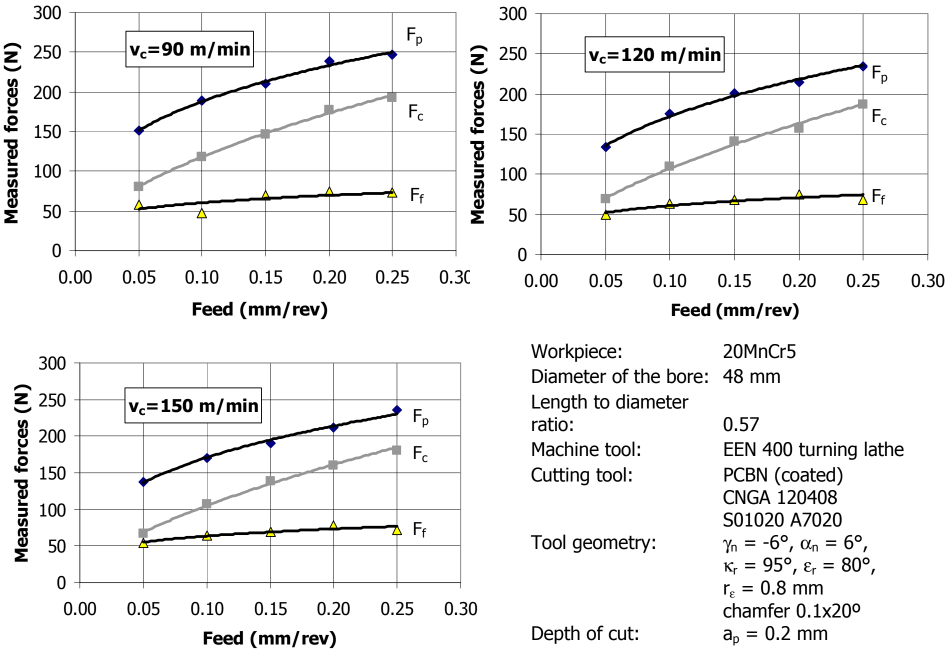

Workpiece:	20MnCr5
Diameter of the bore:	48 mm
Length to diameter ratio:	0.57
Machine tool:	EEN 400 turning lathe
Cutting tool:	PCBN (coated) CNGA 120408 S01020 A7020
Tool geometry:	$\gamma_n = -6°$, $\alpha_n = 6°$, $\kappa_r = 95°$, $\varepsilon_r = 80°$, $r_\varepsilon = 0.8$ mm chamfer 0.1x20°
Depth of cut:	$a_p = 0.2$ mm
Tool wear:	VB = 0.1 mm

Figure 7.1: Cutting forces as a function of the cutting speed and the feed in hard turning

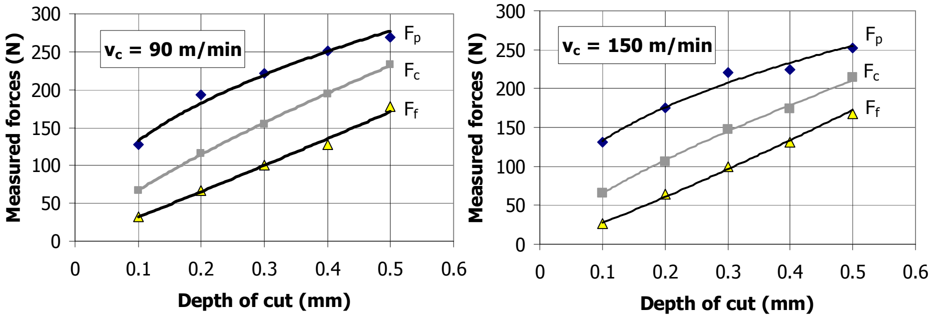

Workpiece:	20MnCr5
Diameter of the bore:	48 mm
Length to diameter ratio:	0.57
Machine tool:	EEN 400 turning lathe
Cutting tool:	PCBN (coated) CNGA 120408 S01020 A7020
Tool geometry:	$\gamma_n = -6°$, $\alpha_n = 6°$, $\kappa_r = 95°$, $\varepsilon_r = 80°$, $r_\varepsilon = 0.8$ mm chamfer 0.1x20°
Feed:	f = 0.1 mm/rev
Tool wear:	VB = 0.1 mm

Figure 7.2: Measured cutting forces as a function of the depth of cut in hard turning

With regard to the relation of cutting forces and depth of cut, all force components increase parallel to each other, if the depth of cut increases (Figure 7.2). The cutting speed also has a lower influence on the cutting forces.

7.1.2 Cutting temperature

In the cutting temperature measurement, the effect of the cutting speed, feed and the width of flank wear land were studied. As hard turning was performed without coolant, high temperatures developed, exceeding 1000 ºC. In the applied cutting speed range (v_c = 90-180 m/min), higher cutting speeds generated higher temperatures, and the same phenomena can be observed when the width of flank wear land increases (Figure 7.3). The measured temperature values are relatively close to each other, when a cutting tool with VB = 0.05 and 0.2 mm was used (Figure 7.3 left). Further extension of the width of flank wear land (VB = 0.4 mm) remarkably increases the cutting temperature. According to the measured values, it can be stated that with the increase of the feed, the cutting temperature decreases (Figure 7.3 right). These results are in direct contrast to experiments where an adverse phenomenon was found [ABR97], [LES97].

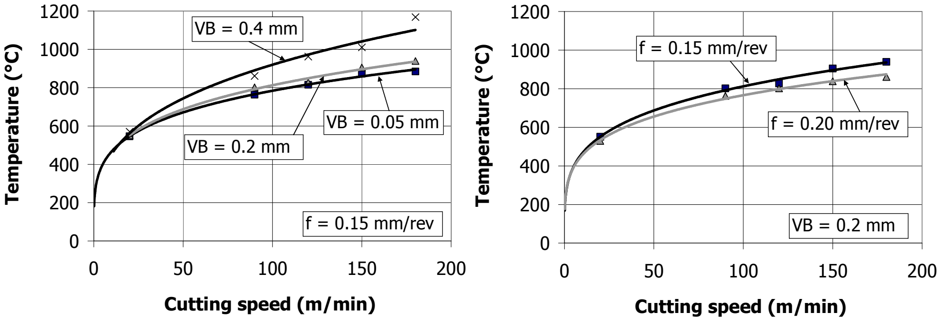

Workpiece: 20MnCr5
Machine tool: INDEX GU 600-2 turning lathe
Depth of cut: a_p = 0.2 mm

Temperature measurement: infrared camera

Cutting tool: PCBN (uncoated)
D-CNMA 120408
BZN 8200 S202
Tool geometry: $\gamma_n = -6°$, $\alpha_n = 6°$, $\kappa_r = 95°$,
$\varepsilon_r = 80°$, $r_\varepsilon = 0.8$ mm
chamfer 0.2x20º

Figure 7.3: Effect of the feed, the cutting speed, and the width of flank wear land on the cutting temperature in hard turning

7.1.3 Surface roughness

The study of surface roughness in bore manufacturing of gears aims to investigate the roughness parameters, according to the bore diameter (diameter range: 35-83 mm), and the width of flank wear land. In choosing a certain diameter value (d = 48 mm), the effect of the cutting data on the surface roughness was examined. Moreover, in the case of two diameters (d = 48, 83 mm), the two-dimensional and three-dimensional surface roughness characteristics were compared after hard turning and grinding, to qualify the performance of hard turning with respect to grinding. Considering grinding, the machining parameters were chosen according to the industrial recommendation applied at ZF Hungária Kft, in which grinding parameters fulfilled the requirements regarding the prescribed surface quality.

In bores with different diameters, the surface roughness investigations were divided into two groups, according to the prescribed ten-point-height of the profile. In the first group, it is Rz = 3 μm, and Rz = 5 μm for the second group. The workpieces were manufactured in a batch, however, the quantity and geometry of the machined gears were different. Therefore, the measured values of both the ten-point height of the profile and the width of flank wear land are plotted against the length of cut.

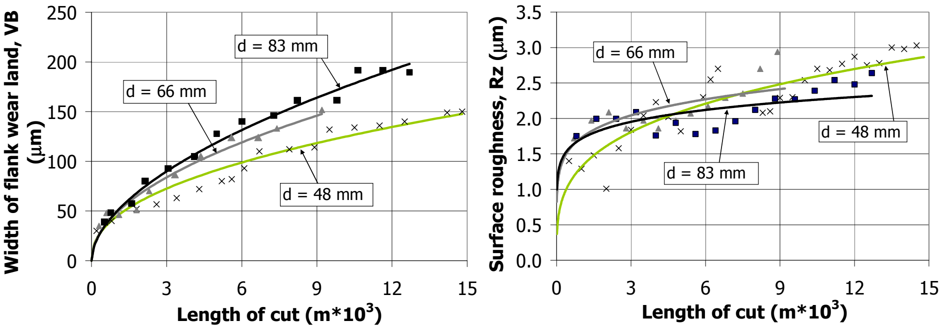

a) width of flank wear land (VB)

b) surface roughness (Rz)

Workpiece:	20MnCr5	Tool geometry:	γ_n = -6°, α_n = 6°, κ_r = 95°, ε_r = 80°, r_ε = 0.8 mm chamfer 0.1x20º
Machine tool:	PITTLER PVSL-2 hard turning lathe		
Cutting tool:	PCBN (coated) CNGA 120408 S01020 A7020	Depth of cut:	a_p = 0.1 mm
		Feed:	f = 0.08 mm/rev
		Cutting speed:	v_c = 200 m/min

Figure 7.4: Measured VB and Rz plotted against the length of cut, when the prescribed surface roughness is Rz = 3 μm

In the first group, gears with bore diameters of 48, 66, and 83 mm were selected. Figure 7.4 compares the extension of the width of flank wear land (Figure 7.4a) and the ten-point height of the profile (Figure 7.4b), as a function of the length of cut. The slope of the tool wear curve increases with the increase of the bore diameter. Nevertheless, the width of flank wear land does not exceed 0.2 mm during finish hard turning. The formation of surface roughness is already unclear. At first, it is lower for a diameter of 48 mm, but it increases more steeply with the length of cut. In each case, the surface roughness remains below the prescribed roughness value (Rz = 3 μm).

Figure 7.5 indicates the measured results, when the prescribed ten-point height of the profile is 5 μm. In this case, bore diameters of 35, 62 and 76 mm were investigated. The width of flank wear land is the highest for a diameter of 62 mm, whereas with diameters of 35 and 76 mm, the curves possess similar characteristics (Figure 7.5a).

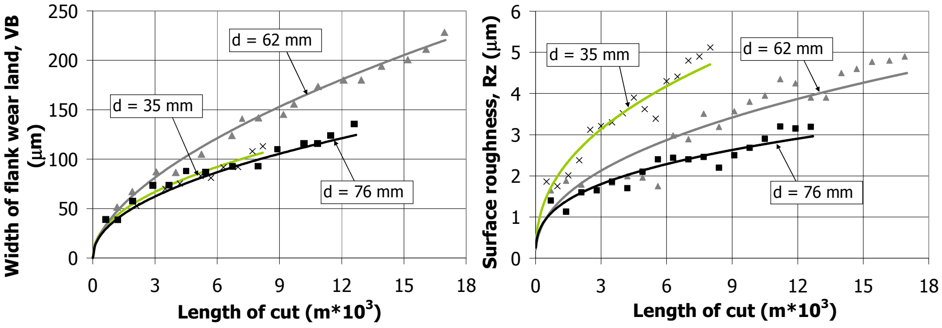

a) width of flank wear land (VB)

b) surface roughness (Rz)

Workpiece:	20MnCr5	Tool geometry:	γ_n = -6°, α_n = 6°, κ_r = 95°, ε_r = 80°, r_ε = 0.8 mm chamfer 0.1x20°
Machine tool:	PITTLER PVSL-2 hard turning lathe		
Cutting tool:	PCBN (coated) CNGA 120408 S01020 A7020	Depth of cut:	a_p = 0.1 mm
		Feed:	f = 0.08 mm/rev
		Cutting speed:	v_c = 180 m/min

Figure 7.5: Measured VB and Rz plotted against the length of cut, when the prescribed surface roughness is Rz = 5 μm

The surface roughness values will increase if the bore diameter decreases. This may be caused by the different chip formation kinematics, with the reduction of the bore diameter. If the bore diameter is smaller, the chip formation becomes increasingly difficult, the heat distribution is less efficient, and a higher tool vibration can arise.

In the case of a diameter of 83 mm, the extension of width of flank wear land is presented in Figure 7.6. The good micro geometry of the surface cut with a PCBN tool can be explained by the large number of microedges found on the worn flank of the tool, which polish the machined surface when cutting. Therefore, these surfaces obtain good micro geometry in cutting. Experiments undertaken earlier also showed that the favourable micro geometry is created after the degressive wear of the tool, and it remains constant in the stage of the linear wear [KUN00].

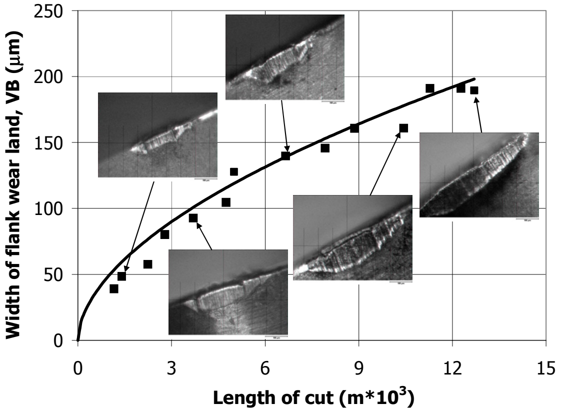

Workpiece: 20MnCr5
Machine tool: PITTLER PVSL-2 hard turning lathe
Diameter of the bore: 83 mm
Cutting tool: PCBN (coated) CNGA 120408 S01020 A7020
Tool geometry: γ_n = -6°, α_n = 6°, κ_r = 95°, ε_r = 80°, r_ε = 0.8 mm chamfer 0.1x20º
Depth of cut: a_p = 0.1 mm
Feed: f = 0.08 mm/rev
Cutting speed: v_c = 200 m/min

Figure 7.6: Typical tool wear characteristic as a function of the length of cut

In studying the effect of cutting data, a bore diameter of 48 mm was selected. The measured roughness values (Rz, Ra, Rq) present the significant effect of the cutting speed and feed on the surface quality (Figures 7.7, 7.8, and 7.9). The depth of cut has less influence on the measured results, and has no clear trend. The ten-point height of the profile remarkably increases with the feed, when a cutting speed of 90 m/min is applied (Figure 7.7a). A depth of cut of 0.25 mm generates the highest roughness values, whereas at a value of 0.2 mm, the measuring numbers of the ten-point height of the profile are the lowest.

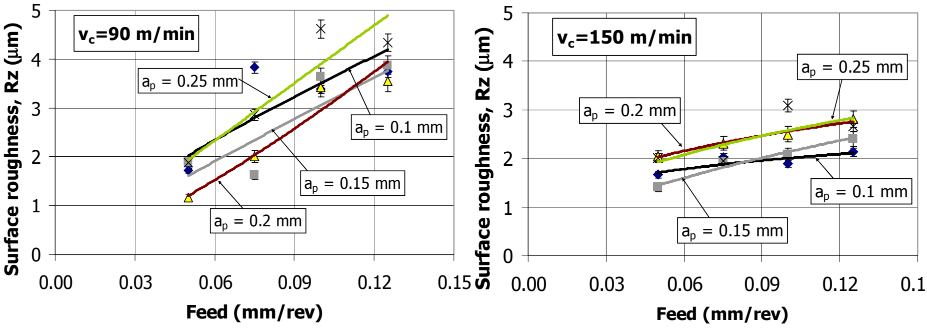

a) v_c = 90 m/min

b) v_c = 150 m/min

Workpiece: 20MnCr5
Diameter of the bore: 48 mm
Length to diameter ratio: 0.57
Machine tool: EEN 400 turning lathe

Cutting tool: PCBN (coated) CNGA 120408 S01020 A7020
Tool geometry: γ_n = -6°, α_n = 6°, κ_r = 95°, ε_r = 80°, r_ε = 0.8 mm chamfer 0.1x20º
Tool wear: VB = 0.1 mm

Figure 7.7: Effect of cutting data in turning on the ten-point height of the profile (Rz)

The slope of the roughness curves decreases with a cutting speed of 150 m/min, and the depth of cut has a more definite trend (Figure 7.7b). With a higher depth of cut, a higher surface roughness will arise. The same phenomena can be observed in the case of the arithmetical mean deviation of the assessed profile (Ra), and the root-mean-square deviation of the profile (Rq), see Figures 7.8 and 7.9.

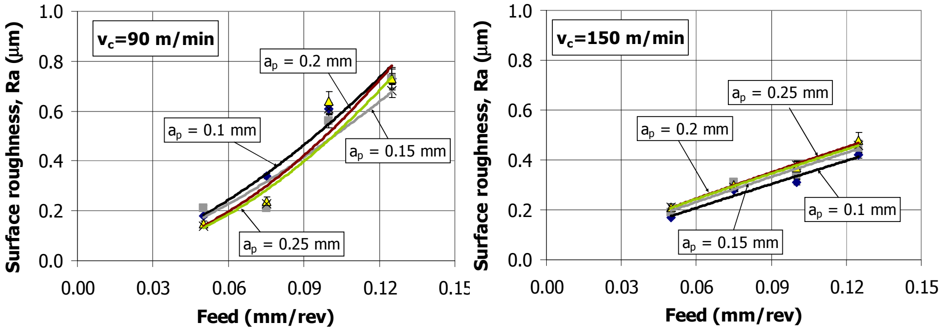

a) v_c = 90 m/min

b) v_c = 150 m/min

Workpiece: 20MnCr5
Diameter of the bore: 48 mm
Length to diameter ratio: 0.57
Machine tool: EEN 400 turning lathe

Cutting tool: PCBN (coated)
CNGA 120408 S01020 A7020
Tool geometry: $\gamma_n = -6°$, $\alpha_n = 6°$, $\kappa_r = 95°$,
$\varepsilon_r = 80°$, $r_\varepsilon = 0.8$ mm
chamfer 0.1x20º
Tool wear: VB = 0.1 mm

Figure 7.8: Effect of cutting data in turning on the arithmetical mean deviation of the profile (Ra)

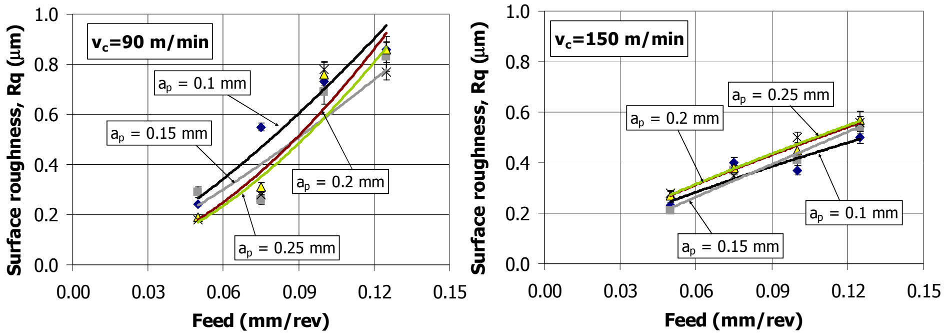

a) v_c = 90 m/min

b) v_c = 150 m/min

Workpiece: 20MnCr5
Diameter of the bore: 48 mm
Length to diameter ratio: 0.57
Machine tool: EEN 400 turning lathe

Cutting tool: PCBN (coated)
CNGA 120408 S01020 A7020
Tool geometry: $\gamma_n = -6°$, $\alpha_n = 6°$, $\kappa_r = 95°$,
$\varepsilon_r = 80°$, $r_\varepsilon = 0.8$ mm
chamfer 0.1x20º
Tool wear: VB = 0.1 mm

Figure 7.9: Effect of cutting data in turning on the root-mean-square deviation of the profile (Rq)

The measured roughness values can be explained by the process characteristics. If the cutting speed is higher, the cutting temperature will be increased resulting in lower cutting forces, which generates lower roughness values. However, both the depth of cut and feed enhance the cutting force, which generates higher surface roughness. The data indicates that when applying v_c = 90 m/min, the optimal cutting temperature may be not attained, and thus, the roughness values fluctuate, in addition to different depths of cut.

The main criterion in workpiece qualification, especially in the finishing process, is the surface quality. This includes the surface topography, which remarkably defines the functional characteristics of the workpiece [PAL92], [PAW97]. The hardened bore of gears can be finished with both grinding and turning. In the experiments, to perform the comparison, bores with diameters of 48 and 83 mm were selected. The prescribed roughness for the bores was Rz = 3 μm. On the basis of the experimental results (Figures 7.10 and 7.11), it can be stated that the ten-point height of the profile can be ensured in both processes. In the machining of a bore with a diameter of 48 mm, the Rz values are lower after hard turning (Figure 7.10), while they are the same in the manufacturing of a bore with a diameter of 83 mm (Figure 7.11). The Ra values are consistently better in grinding.

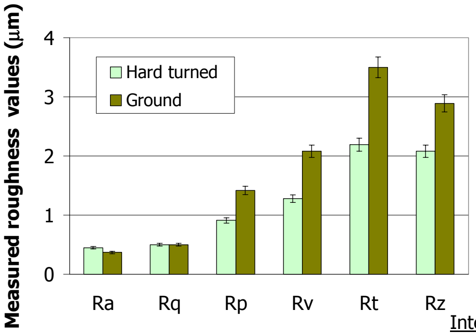

Hard turning:
Machine tool: PITTLER PVSL-2 hard turning lathe
Cutting tool: PCBN (coated)
CNGA 120408 BNC80
Tool geometry: $\gamma_n = -6°$, $\alpha_n = 6°$, $\kappa_r = 95°$, $\varepsilon_r = 80°$, $r_\varepsilon = 0.8$ mm
Tool wear: VB = 0.15 mm
Depth of cut: $a_p = 0.1$ mm
Feed: f = 0.1 mm/rev
Cutting speed: $v_c = 200$ m/min

Workpiece;
Material: 20MnCr5
Diameter of the bore: 48 mm
Length to diameter ratio: 0.57

Internal traverse grinding:
Machine tool: SI-4/A internal grinder
Grinding wheel: CBN wheel 32x30x13 9A 80 K7 V22
Wheel speed: $v_c = 25$ m/s
Speed ratio: q = 80
Workpiece speed: $v_w = 18$ m/min
Depth of cut: $a_e = 0.02$ mm/double stroke
Traverse speed: $v_f = 2.2$ m/min
Spark-out: 8 double stroke
Coolant: half synthetic, Q = 50 l/min

Figure 7.10: Comparison of surface roughness for a diameter of 48 mm

The experiments also proved that turning gives a surface micro geometry standing, close to the periodic one, with smaller wavelengths, while grinding creates a surface with irregular grooves and "pits" [PAL92]. The experiments performed previously have indicated [PAW97] that the amplitude parameters, mainly Rt, are suitable for monitoring the wear of cylindrical surfaces in the engine life. However, other researchers found [STO83] that the prediction of the Rq parameter is suitable for observing the functional wear. With regard to the measured Rq values, they are similar to each other with a diameter of 48 mm, while for a bigger diameter, the values are even lower after hard turning.

Among the roughness characteristics connected to the form of irregularities, the bearing length ratio (tp) indicates different features after hard turning and grinding (Figure 7.12). From a tribological point of view, a smoother surface, meaning a lower root-mean-square deviation value, and advantageous bearing length curves, ensure proper wear resistance and functional behaviour for the surfaces [VAL96].

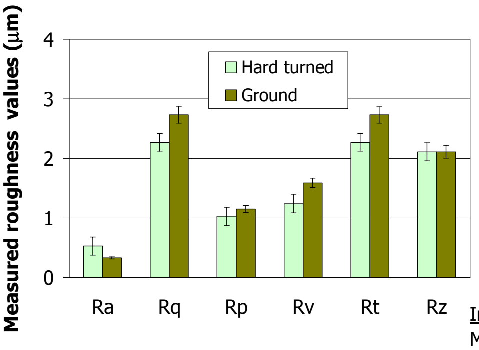

Hard turning:
Machine tool: PITTLER PVSL-2 hard turning lathe
Cutting tool: PCBN (coated)
CNGA 120408 BNC80
Tool geometry: γ_n = -6°, α_n = 6°, κ_r = 95°, ε_r = 80°, r_ε = 0.8 mm
Tool wear: VB = 0.15 mm
Depth of cut: a_p = 0.1 mm
Feed: f = 0.08 mm/rev
Cutting speed: v_c = 180 m/min

Internal traverse grinding:
Machine tool: SI-4/A internal grinder
Grinding wheel: CBN wheel 80x36x20 9A 80 K7 V22
Wheel speed: v_c = 43 m/s
Speed ratio: q = 80
Workpiece speed: v_w = 32.25 m/min
Depth of cut: a_e = 0.02 mm/double stroke
Traverse speed: v_f = 2.2 m/min
Spark-out: 10 double stroke
Coolant: half synthetic, Q = 50 l/min

Workpiece:
Material: 20MnCr5
Diameter of the bore: 83 mm
Length to diameter ratio: 0.40

Figure 7.11: Comparison of surface roughness for a diameter of 83 mm

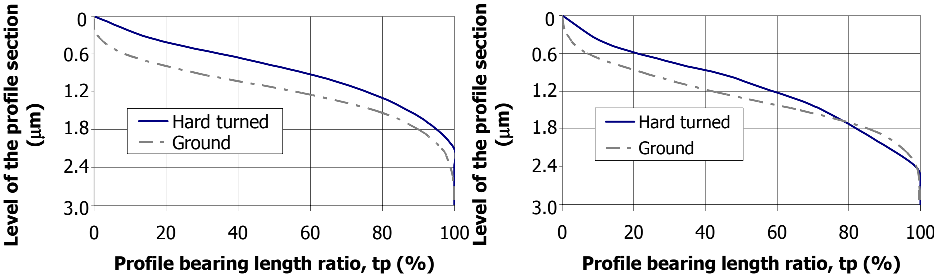

a) d = 48 mm

b) d = 83 mm

Figure 7.12: Comparison of the bearing length curves (applied cutting data in Figure 7.11)

The skewness of the profile, which characterises the symmetry of the material disposition of the profile, is approximately the same, and the value is negative for both processes (Figure 7.13). If the profile is symmetric, the Rsk value is zero. If the surface has more valleys than peaks, the skewness is negative, which results in a better fluid retention property, regarding the functional behaviour of the component [STO84].

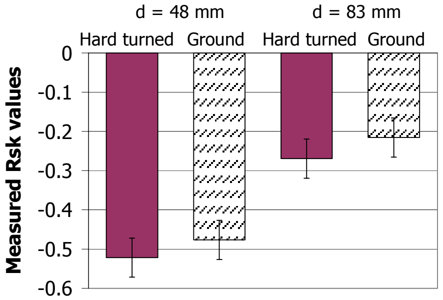

Hard turning:
Tool wear: VB = 0.15 mm
Depth of cut: a_p = 0.1 mm
Feed: f = 0.08, 0.1 mm/rev
Cutting speed: v_c = 180, 200 m/min

Internal traverse grinding:
Wheel speed: v_c = 25, 43 m/s
Speed ratio: q = 80
Workpiece speed: v_w = 18, 32.25 m/min
Depth of cut: a_e = 0.02 mm/double stroke
Traverse speed: v_f = 2.2 m/min
Spark-out: 8-10 double stroke
Coolant: half synthetic, Q = 50 l/min

Workpiece:
Material: 20MnCr5
Diameter of the bore: 48, 83 mm

Figure 7.13: Skewness of the profile (Rsk) after hard turning and grinding

Figures 7.14 and 7.15 present the diverse topographical features of both grinding and hard turning processes. Unlike grinding, hard turning generates regularly repeated surface elements.

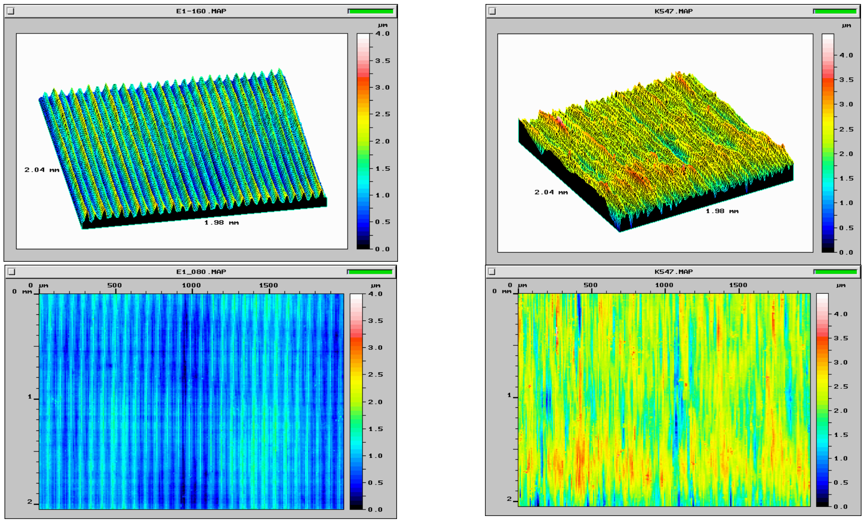

a) hard turned b) ground

Figure 7.14: Comparison of topography of hard turned and ground surfaces (d = 48 mm)

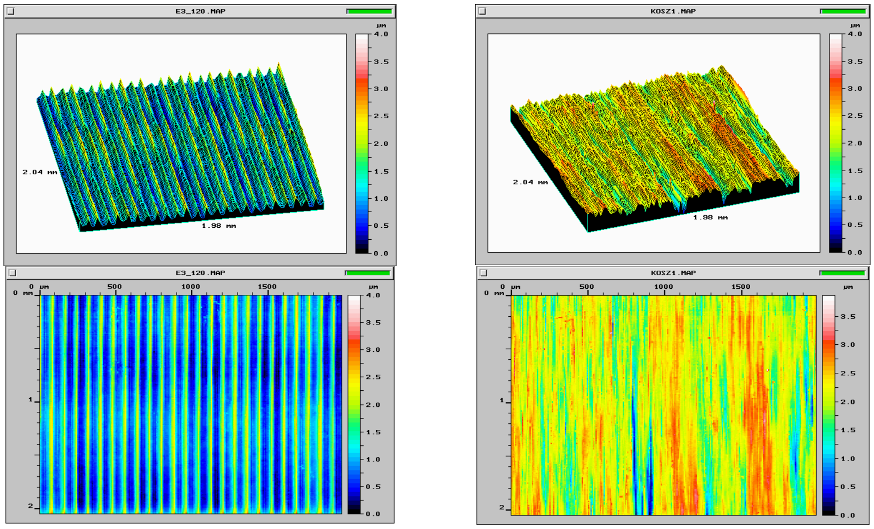

a) hard turned b) ground

Figure 7.15: Comparison of topography of hard turned and ground surfaces (d = 83 mm)

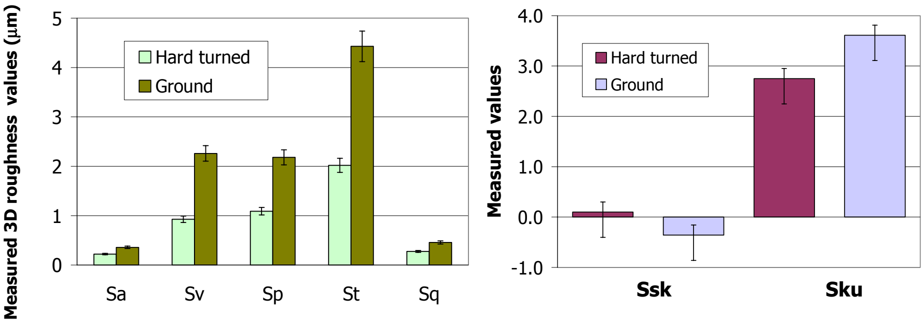

Workpiece:
Material: 20MnCr5
Diameter of the bore: 48 mm

Hard turning:
Machine tool: PITTLER PVSL-2 hard turning lathe
Cutting tool: PCBN (coated)
CNGA 120408 BNC80
Tool geometry: $\gamma_n = -6°$, $\alpha_n = 6°$, $\kappa_r = 95°$,
$\varepsilon_r = 80°$, $r_\varepsilon = 0.8$ mm
Tool wear: VB = 0.15 mm
Depth of cut: $a_p = 0.1$ mm
Feed: f = 0.1 mm/rev
Cutting speed: $v_c = 200$ m/min

Internal traverse grinding:
Machine tool: SI-4/A internal grinder
Grinding wheel: CBN wheel 32x30x13 9A 80 K7 V22
Wheel speed: $v_c = 25$ m/s
Speed ratio: q = 80
Workpiece speed: $v_w = 18$ m/min
Depth of cut: $a_e = 0.02$ mm/double stroke
Traverse speed: $v_f = 2.2$ m/min
Spark-out: 8 double stroke
Coolant: half synthetic, Q = 50 l/min

Figure 7.16: Comparison of 3D roughness values

In the 90s, elementary studies and research results [DON94a], [DON94b] that were published made it possible to characterize the surface micro geometry in three dimensions. These are the first initiatives for the standardisation of 3D parameters. The extension of the two-dimensional roughness characteristics for three-dimensional ones makes it possible to explore and evaluate the micro geometrical conditions more completely. Furthermore, it is also suitable for revealing and numerically characterising such properties, which cannot be determined from the profile section.

Figure 7.16 presents an example of 3D roughness measurement, for a diameter of 48 mm. In contrast to the measurements performed in 2D, where the Ra value was higher for hard turning than for grinding, the spatial measurement Sa is 0.36 μm in the ground surface, while it is 0.22 μm for the hard turned part. In the two-dimensional investigations, the root-mean-square deviation of the profile (Rq) is approximately the same for both processes, while in the three-dimensional analysis of the machined surface, the root-mean-square deviation of the surface (Sq) is diverse. Similarly to Sa, the Sq measures the deviation of surface points from the root-mean-square of the surface, but it is more sensitive to the large surface peak heights and/or valley depths. The skewness of surface height distribution (Ssk) numerically provides the skewness of the distribution of the surface departure density, calculated from the root-mean-square of the surface whose equivalent in two-dimensions is the Rsk (Figure 7.16). The measured Ssk values are near zero, thus, the graph of height distribution of the certain surface points is symmetrical. The Sku parameter characterises the kurtosis of the height distribution in the surface topography. As this parameter also accurately decribes the form of irregularities, it can therefore be applied as a functional parameter [DON94b]. In hard turning, Sku = 2.75 was measured, which was 3.61 for grinding.

7.1.4 Macro geometrical accuracy

As hard turning can be characterized by high cutting forces, and a significant amount of heat can arise, the macro geometrical accuracy is influenced by them. In the workpiece clamping, the applied force may affect the machining results, and therefore, the workpiece "rigidity" must be taken into account. In this case, it is characterised by the wall thickness ratio of the gear (WT), which is the quotient of the root circle diameter of the gear (d_{root}), and the bore diameter (d).

In studying the macro geometrical accuracy, the effect of the length of cut, the cutting speed and the workpiece "rigidity" was investigated. Bores with diameters of 36, 73, and 83 mm were selected, according to the wall thickness ratio of the gear body. The minimum wall thickness ratio is 1.34, and the maximum is 2.83. For comparison, see Table 5.2 in Chapter 5.1.

With regard to the attainable macro geometrical accuracy after turning and grinding, bore diameters of 76 mm (WT = 2.32), and 68 mm (WT = 1.66) were selected. In addition to the different workpiece "rigidities", the tolerances prescribed for the bores were also diverse, consisting of IT5 and IT6.

Figure 7.17 indicates the measured form and positional accuracy results in a relationship with the length of cut for a diameter of 36 mm, and is presented for a diameter of 73 mm in Figure 7.18. It is evident that the out-of-roundness and cylindricity error of the larger diameter, which has a lower WT value, are higher. The WT has no remarkable influence on the parallelism error of the generatrices, as it hardly changes. Figure 7.19 reflects the macro geometrical errors, arising from the deformation of the workpiece. With the decrease of the wall thickness, the out-of-roundness and the cylindricity error increase. The form errors increase in absolute meaning, while its scattering also significantly rises, especially in gears with diameters of 83 mm.

For the gear with a WT = 2.83, which can be regarded as quite rigid, the out-of-roundness of 0.006 mm prescribed for quality IT6, can be kept securely. For the gear with WT = 1.34, the prescribed value (0.006 mm) cannot be guaranteed. Evidently, the reason for this is the clamping system. Therefore, the clamping force and/or method must be modified.

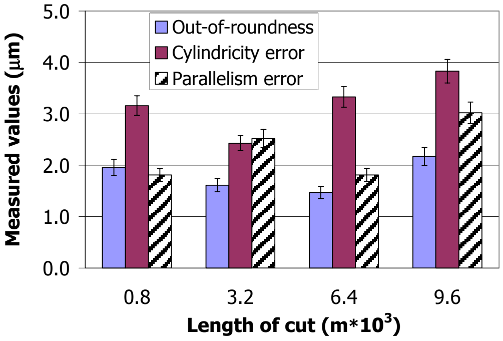

Hard turning:
Workpiece: 20MnCr5
Diameter of the bore: 36 mm
Length to diameter ratio: 1.06
Wall thickness ratio: WT = 2.83
Machine tool: PITTLER PVSL-2 hard turning lathe
Cutting tool: PCBN (coated) CNGA 120408 BNC80
Tool geometry: γ_n = -6°, α_n = 6°, κ_r = 95°, ε_r = 80°, r_ε = 0.8 mm
Depth of cut: a_p = 0.08 mm
Feed: f = 0.10 mm/rev
Cutting speed: v_c = 164 m/min

Figure 7.17: Measurement results of geometrical accuracy for d = 36 mm

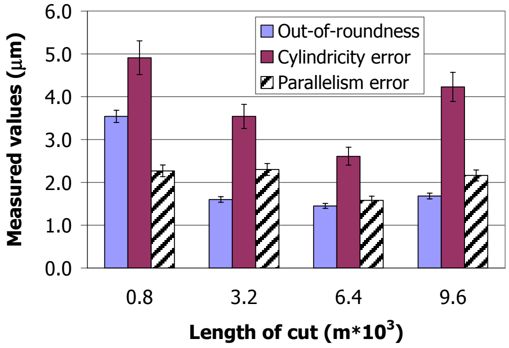

Hard turning:
Workpiece: 20MnCr5
Diameter of the bore: 73 mm
Length to diameter ratio: 0.64
Wall thickness ratio: WT = 1.94
Machine tool: PITTLER PVSL-2 hard turning lathe
Cutting tool: PCBN (coated) CNGA 120408 BNC80
Tool geometry: γ_n = -6°, α_n = 6°, κ_r = 95°, ε_r = 80°, r_ε = 0.8 mm
Depth of cut: a_p = 0.08 mm
Feed: f = 0.07 mm/rev
Cutting speed: v_c = 206 m/min

Figure 7.18: Measurement results of geometrical accuracy for d = 73 mm

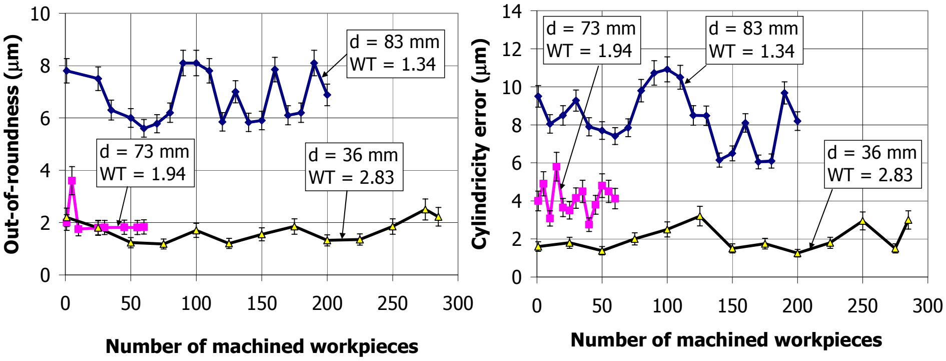

a) out-of-roundness

b) cylindricity error

Workpiece: 20MnCr5
Machine tool: PITTLER PVSL-2 hard turning lathe
Cutting tool: PCBN (coated) CNGA 120408 BNC80

Tool geometry: $\gamma_n = -6°$, $\alpha_n = 6°$, $\kappa_r = 95°$, $\varepsilon_r = 80°$, $r_\varepsilon = 0.8$ mm chamfer 0.1x20°
Depth of cut: $a_p = 0.08\text{-}0.1$ mm
Feed: $f = 0.07\text{-}0.1$ mm/rev
Cutting speed: $v_c = 164\text{-}206$ m/min

Figure 7.19: Comparison of the macro geometrical errors in hard turning

Replacement of grinding with hard turning is only possible if the macro geometrical errors also fulfil the requirements. Firstly, a gear with a diameter of 76 mm and WT = 2.32 was selected. In this case, the prescribed accuracy is IT5. The measuring results are presented in Figures 7.20 and Figure 7.22. Although the out-of-roundness is higher in hard turning, both processes satisfy the quality prescribed for IT5. The diagrams for out-of-roundness apply to the plane signed with C. This is because according to experience, the highest out-of-roundness always appears here. This can be explained by the deforming effect of the three-jaw chuck. The feature of the out-of-roundness is a three-lobe form for both processes.

The cylindricity error, like the out-of-roundness, is higher for hard turning. The reason for this is the higher clamping force, and the single point cutting tool removing the material. The parallelism is better in hard turning, however, on the entrance side, the diameter is smaller due to the insufficient conduction of the intensive heat. In grinding, the bore is conical. At the entering place of the tool, the diameter is larger.

With regard to the other gear (d = 68 mm), the prescribed tolerance is IT6, and the wall thickness ratio is lower, WT = 1.66. In comparison with the previous results, the out-of-roundness is much higher, and due to the three-jaw chuck, a three-lobe form can be observed, which appears here more remarkably than before (Figures 7.21 and 7.23).

HARD TURNING

Workpiece: 20MnCr5
Diameter of the bore: d = 76 mm
Length to diameter ratio: l/d = 0.32
Wall thickness ratio: WT = 2.32

GRINDING

Machine tool:
PITTLER PVSL-2
hard turning lathe
Cutting tool:
PCBN (coated)
CNGA 120408 BNC80
Tool geometry:
$\gamma_n = -6°$, $\alpha_n = 6°$, $\kappa_r = 95°$,
$\varepsilon_r = 80°$, $r_\varepsilon = 0.8$ mm
Depth of cut:
$a_p = 0.08$ mm
Feed:
f = 0.08 mm/rev
Cutting speed:
$v_c = 215$ m/min

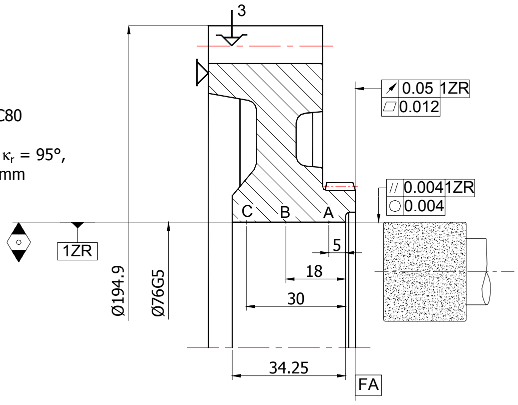

Machine tool:
SI-4/A internal grinder
Grinding wheel:
CBN wheel
60x36x20 9A 80 K7 V22
Wheel speed:
$v_c = 42$ m/s
Speed ratio:
q = 80
Workpiece speed:
$v_w = 31$ m/min
Depth of cut:
$a_e = 0.02$ mm/double st.
Traverse speed:
$v_f = 2.2$ m/min
Spark-out:
8 double stroke
Coolant:
half synthetic, Q = 50 l/min

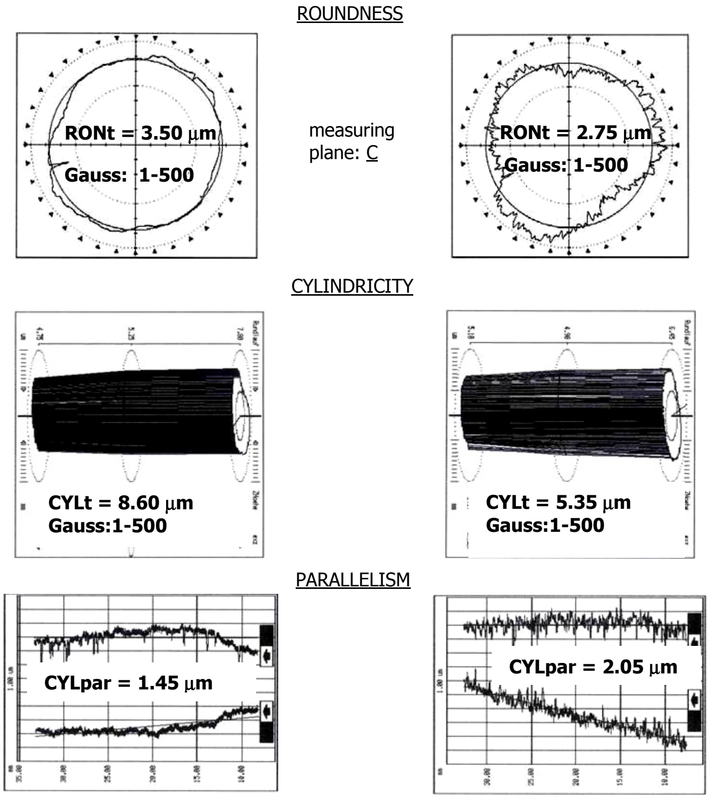

Figure 7.20: Measuring diagrams of the hard turned and ground profiles, d = 76mm, WT = 2.32

HARD TURNING

Workpiece: 20MnCr5
Diameter of the bore: d = 68 mm
Length to diameter ratio: l/d = 0.43
Wall thickness ratio: WT = 1.66

GRINDING

Machine tool:
PITTLER PVSL-2
hard turning lathe
Cutting tool:
PCBN (coated)
CNGA 120408 BNC80

Tool geometry:
γ_n = -6°, α_n = 6°, κ_r = 95°,
ε_r = 80°, r_ε = 0.8 mm
Depth of cut:
a_p = 0.08 mm
Feed:
f = 0.07 mm/rev
Cutting speed:
v_c = 228 m/min

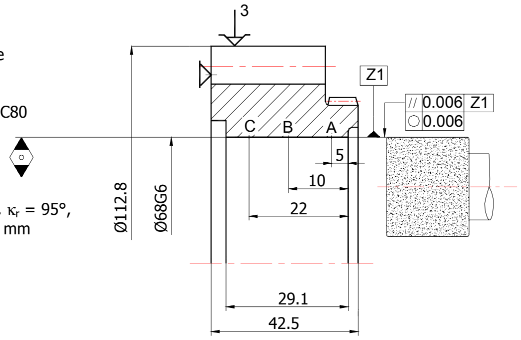

Machine tool:
SI-4/A internal grinder
Grinding wheel:
CBN wheel
50x32x20 9A 80 K7 V22
Wheel speed:
v_c = 46.7 m/s
Speed ratio:
q = 80
Workpiece speed:
v_w = 35.2 m/min
Depth of cut:
a_e = 0.02 mm/double st.
Traverse speed:
v_f = 2.2 m/min
Spark-out:
10 double stroke
Coolant:
half synthetic, Q = 50 l/min

ROUNDNESS

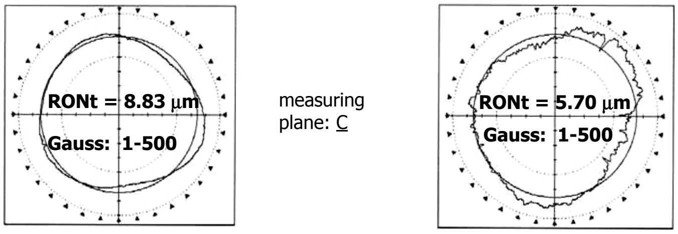

measuring
plane: C

CYLINDRICITY

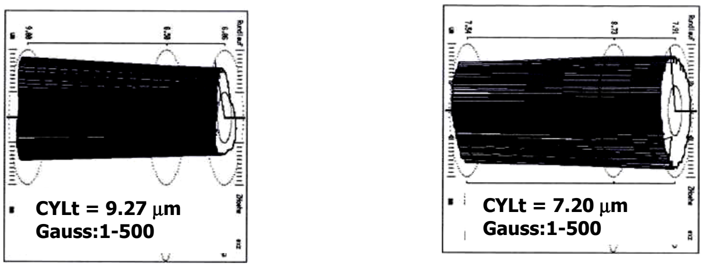

PARALLELISM

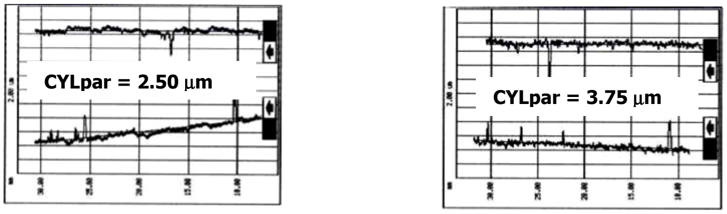

Figure 7.21: Measuring diagrams of the hard turned and ground profiles, d = 68mm, WT = 1.66

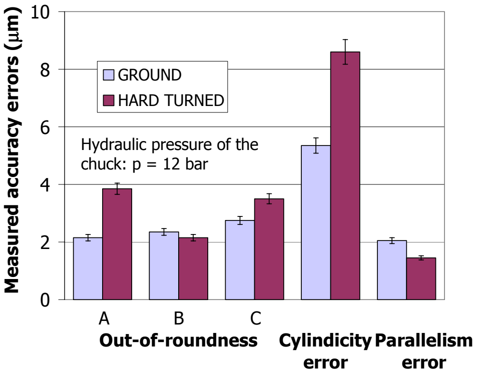

Hydraulic pressure of the chuck: p = 12 bar

Workpiece:
Material: 20MnCr5
Diameter of the bore: 76 mm
Length to diameter ratio: 0.32
Wall thickness ratio: 2.32

Hard turning:
Machine tool: PITTLER PVSL-2 hard turning lathe
Cutting tool: PCBN (coated)
CNGA 120408 BNC80
Tool geometry: $\gamma_n = -6°$, $\alpha_n = 6°$, $\kappa_r = 95°$, $\varepsilon_r = 80°$, $r_\varepsilon = 0.8$ mm
Tool wear: VB = 0.15 mm
Depth of cut: $a_p = 0.08$ mm
Feed: f = 0.08 mm/rev
Cutting speed: $v_c = 215$ m/min

Internal traverse grinding:
Machine tool: SI-4/A internal grinder
Grinding wheel: CBN wheel 60x36x20 9A 80 K7 V22
Wheel speed: $v_c = 42$ m/s
Speed ratio: q = 80
Workpiece speed: $v_w = 31$ m/min
Depth of cut: $a_e = 0.02$ mm/double stroke
Traverse speed: $v_f = 2.2$ m/min
Spark-out: 8 double stroke
Coolant: half synthetic, Q = 50 l/min

Figure 7.22: Comparison of macro geometrical errors, d = 76mm, WT = 2.32

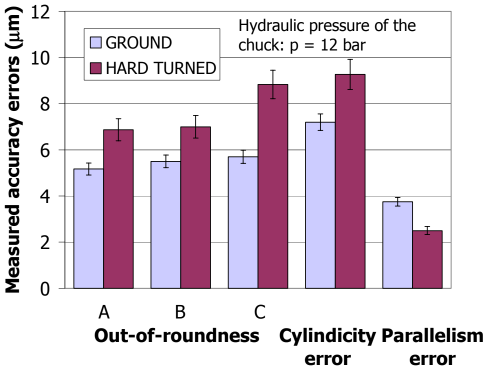

Hydraulic pressure of the chuck: p = 12 bar

Workpiece:
Material: 20MnCr5
Diameter of the bore: 68 mm
Length to diameter ratio: 0.43
Wall thickness ratio: 1.66

Hard turning:
Machine tool: PITTLER PVSL-2 hard turning lathe
Cutting tool: PCBN (coated)
CNGA 120408 BNC80
Tool geometry: $\gamma_n = -6°$, $\alpha_n = 6°$, $\kappa_r = 95°$, $\varepsilon_r = 80°$, $r_\varepsilon = 0.8$ mm
Tool wear: VB = 0.15 mm
Depth of cut: $a_p = 0.08$ mm
Feed: f = 0.07 mm/rev
Cutting speed: $v_c = 228$ m/min

Internal traverse grinding:
Machine tool: SI-4/A internal grinder
Grinding wheel: CBN wheel 60x36x20 9A 80 K7 V22
Wheel speed: $v_c = 46.7$ m/s
Speed ratio: q = 80
Workpiece speed: $v_w = 35.2$ m/min
Depth of cut: $a_e = 0.02$ mm/double stroke
Traverse speed: $v_f = 2.2$ m/min
Spark-out: 10 double stroke
Coolant: half synthetic, Q = 50 l/min

Figure 7.23: Comparison of macro geometrical errors, d = 68mm, WT = 1.66

The high out-of-roundness can easily be explained by the inadequacy of the clamping device. With such a small wall thickness, it is not allowed to clamp with concentrated force. The cylindricity error is higher in hard turning. In both cases, the bore is conical. In hard turning, the conicity is caused by the heat. The parallelism of the generatrices can be ensured for both processes, however, in grinding, it is higher than in hard turning.

The most critical element in the accuracy of hard turning is the generation of the out-of-roundness. If the workpiece is rigid enough, $WT \geq 1.90$, the out-of-roundness belonging to the quality IT5 can still be fulfilled. However, in lower rigidities, $WT < 1.70$, even the limit belonging to IT6 cannot be ensured. This is due to the high concentrated clamping force, which comes from the clamping mechanism with an uncontrollable pressure of 12 bars. The problem can be avoided with the application of a magnetic or vacuum chuck. The typical three-lobe form of the bores would disappear.

7.1.5 Surface integrity

With regard to the integrity of the machined surface, microhardness measurements were performed, and the appearance of the white layer in relation to the cutting data was examined.

Microhardness measurements were carried out for bore diameters of 48 mm and 62 mm after turning, and a hardness comparison between the turned and the ground surface was accomplished with a diameter of 83 mm.

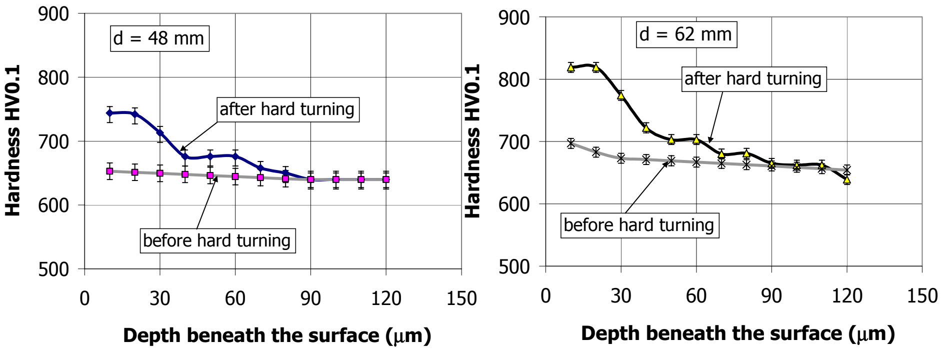

a) d = 48 mm

b) d = 62 mm

Workpiece: 20MnCr5
Diameter of the bore: 48 mm
Machine tool: PITTLER PVSL-2 hard turning lathe
Cutting tool: PCBN (coated)
CNGA 120408 BNC80

Tool geometry: $\gamma_n = -6°$, $\alpha_n = 6°$, $\kappa_r = 95°$,
$\varepsilon_r = 80°$, $r_\varepsilon = 0.8$ mm
Tool wear: VB = 0.15 mm
Depth of cut: $a_p = 0.1$ mm
Feed: f = 0.1 mm/rev
Cutting speed: $v_c = 200$ m/min

Figure 7.24: Microhardness of the hard turned bores with different diameters

The microhardness curve indicates a diverse feature after hard turning, compared to hardness distribution before cutting (Figure 7.24). After turning, close to the surface, the measured microhardness values are higher, and the hardness curve decreases into the depth beneath the surface, achieving the hardness value of the bulk.

In comparing the microhardness after grinding and hard turning, it was found that the hardness of the ground surface barely changes (Figure 7.25). The microhardness curves measured after heat treatment already do not include the hardness values of the removed material. It means that the hardness values of the allowance (0.3 mm) were removed from the plotted curves.

The reasons for the significant change in microhardness after hard turning can be varied. In hard turning, high temperatures and high pressures may develop, which have a common effect on the surface integrity. If the austenization level of the machined steel is attained due to the heat, phase transformation occurs, and because of the quick cooling, a fine martensitic structure with a higher hardness may develop [CHO97], [TIS00]. Likewise, part of the retained austenite content of the steel may transform into martensite, which can also result in higher hardness [TIS00]. Due to deformation, both the retained austenite and the martensite can harden [LEE99], [PET04]. Moreover, the temperature of $\gamma \rightarrow \alpha$ phase transformation is influenced by the pressure, and decreases gradually with the enhancement of the pressure [KOM95]. However, in order to determine the exact explanation of the change in microhardness, more investigations and studies are required.

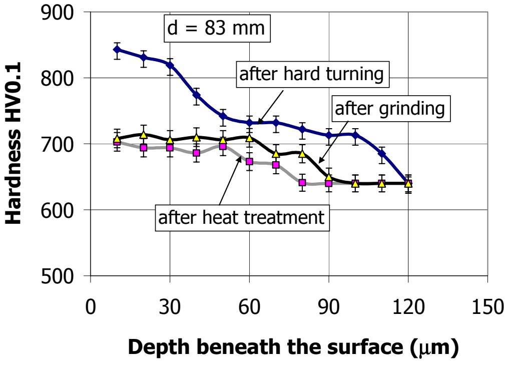

Workpiece:
Material: 20MnCr5
Diameter of the bore: 83 mm
Length to diameter ratio: 0.40

Hard turning:
Machine tool: PITTLER PVSL-2 hard turning lathe
Cutting tool: PCBN (coated) CNGA 120408 S01020 A7020
Tool geometry: $\gamma_n = -6°$, $\alpha_n = 6°$, $\kappa_r = 95°$, $\varepsilon_r = 80°$, $r_\varepsilon = 0.8$ mm
Tool wear: VB = 0.15 mm
Depth of cut: $a_p = 0.1$ mm
Feed: f = 0.08 mm/rev
Cutting speed: $v_c = 200$ m/min

Internal traverse grinding:
Machine tool: SI-4/A internal grinder
Grinding wheel: CBN wheel 80x36x20 9A 80 K7 V22
Wheel speed: $v_c = 43$ m/s
Speed ratio: q = 80
Workpiece speed: $v_w = 32.25$ m/min
Depth of cut: $a_e = 0.02$ mm/double stroke
Traverse speed: $v_f = 2.2$ m/min
Spark-out: 10 double stroke
Coolant: half synthetic, Q = 50 l/min

Figure 7.25: Comparison of microhardness after hard turning and grinding

The white layer investigation was carried out on the same machined surfaces, where the cutting force measurement was done. The effect of cutting data on the microstructural change was studied to reveal the relationship between the cutting speed, feed, depth of cut, and appearance of the white layer. In this case, it is possible to avoid the development of the white layer with the selection of the proper machining parameters. According to Equation 6.39 (Chapter 6.5), the power per unit length can be calculated on the basis of the cutting force measured in hard turning. As previously mentioned, the white layer will develop if the P'_α exceeds 150 W/mm [SCH99].

In applying a lower cutting speed (v_c = 90 m/min), the microstructural investigations proved that no white layer exists in the machined surface (Figure 7.26 and Figure 7.27). With the increase of the cutting speed (v_c = 120 m/min), the appearance of this layer can be observed, except when using a feed of 0.05 mm/rev (Figure 7.28 and Figure 7.29). On the other hand, the white layer is not continuous in each case, and its thickness also varies between 1 and 3 μm. With regard to the depth of cut and feed, they have no clear effect on the white layer thickness (Figure 7.30).

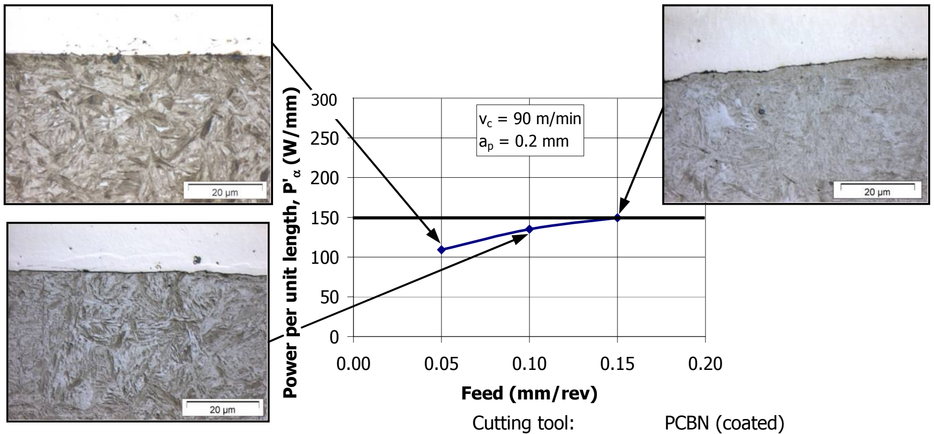

Workpiece:	20MnCr5	Cutting tool:	PCBN (coated) CNGA 120408 S01020 A7020
Diameter of the bore:	48 mm	Tool geometry:	γ_n = -6°, α_n = 6°, κ_r = 95°, ε_r = 80°, r_ε = 0.8 mm chamfer 0.1x20°
Length to diameter ratio:	0.57		
Machine tool:	EEN 400 turning lathe	Tool wear:	VB = 0.1 mm

Figure 7.26: White layer investigation, v_c = 90 m/min, a_p = 0.2 mm

The detected diffractograms indicate that the α-phase of the white layer is martensite, which has a deformed tetragonal lattice structure, caused by high dislocation density. In addition to the martensite, retained austenite can be found, in quantities varying between 5 and 25%. Figure 7.31 presents the relationship between the retained austenite content of the white layer, and the feed or the depth of cut. The increase of both the feed and the depth of cut reduces the retained autenite content. It is likely that the quantity of retained austenite can be modified by the white layer thickness and the austenite grain size developped during heating. More studies are required in order to obtain an exact explanation of this.

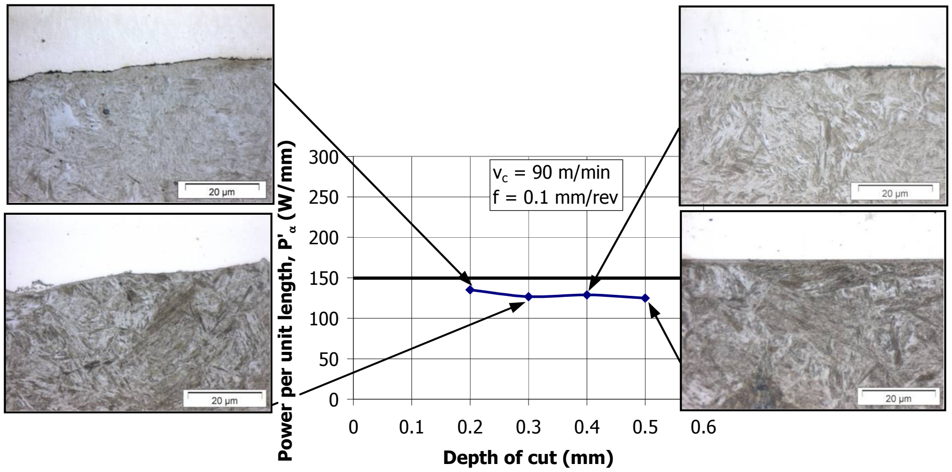

Workpiece:	20MnCr5	Cutting tool:	PCBN (coated) CNGA 120408 S01020 A7020
Diameter of the bore:	48 mm		
Length to diameter ratio:	0.57	Tool geometry:	γ_n = -6°, α_n = 6°, κ_r = 95°, ε_r = 80°, r_ε = 0.8 mm chamfer 0.1x20º
Machine tool:	EEN 400 turning lathe	Tool wear:	VB = 0.1 mm

Figure 7.27: White layer investigation, v_c = 90 m/min, f = 0.1 mm/rev

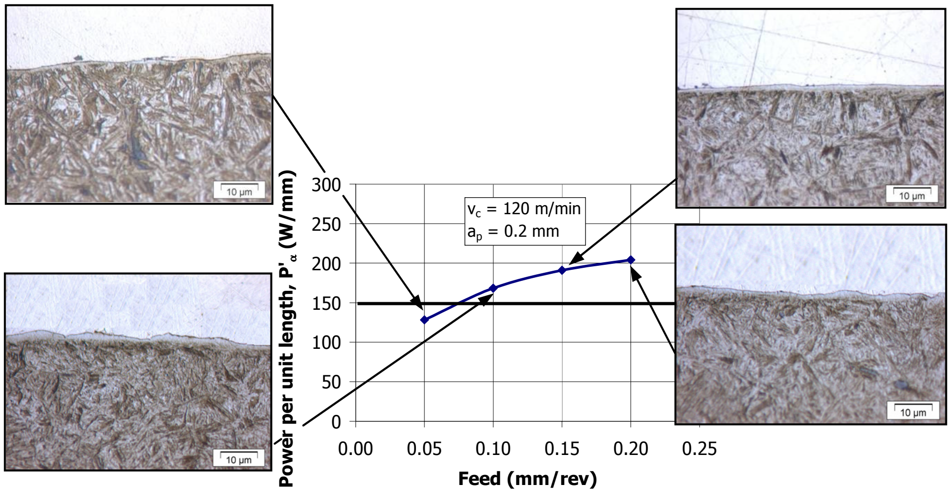

Workpiece:	20MnCr5	Cutting tool:	PCBN (coated) CNGA 120408 S01020 A7020
Diameter of the bore:	48 mm		
Length to diameter ratio:	0.57	Tool geometry:	γ_n = -6°, α_n = 6°, κ_r = 95°, ε_r = 80°, r_ε = 0.8 mm chamfer 0.1x20º
Machine tool:	EEN 400 turning lathe	Tool wear:	VB = 0.1 mm

Figure 7.28: White layer investigation, v_c = 120 m/min, a_p = 0.2 mm

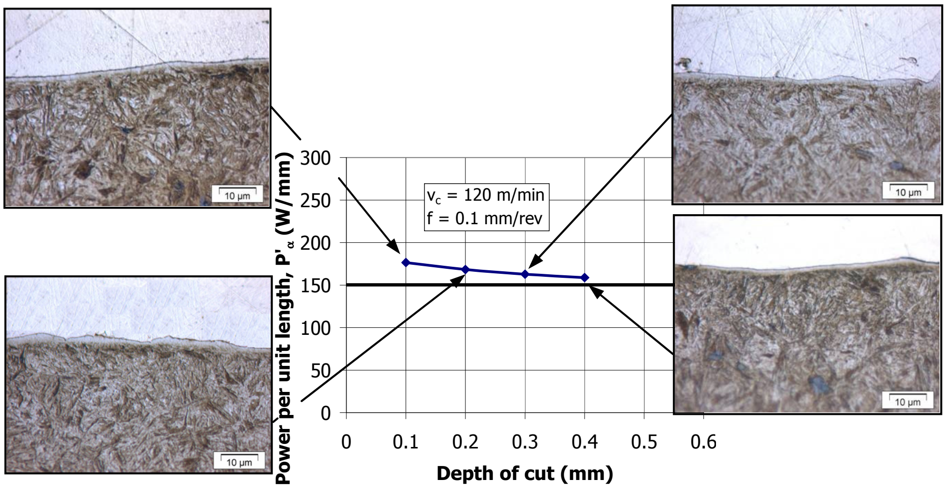

Workpiece:	20MnCr5
Diameter of the bore:	48 mm
Length to diameter ratio:	0.57
Machine tool:	EEN 400 turning lathe
Cutting tool:	PCBN (coated) CNGA 120408 S01020 A7020
Tool geometry:	γ_n = -6°, α_n = 6°, κ_r = 95°, ε_r = 80°, r_ε = 0.8 mm chamfer 0.1x20º
Tool wear:	VB = 0.1 mm

Figure 7.29: White layer investigation, v_c = 120 m/min, f = 0.1 mm/rev

The combined presence of the deformed lattice structure and the retained austenite means that the austenitic temperature (830°) of the steel was achieved during turning, and the surface cooled down very quickly [KUN06]. Besides martensite, retained austenite has developped.

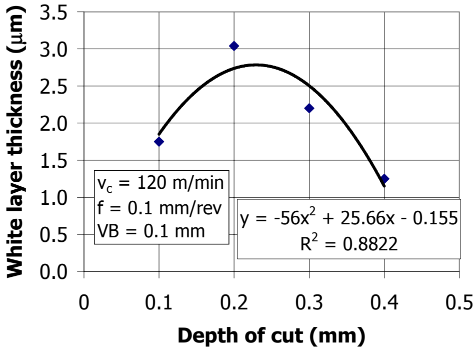

Workpiece:	20MnCr5
Diameter of the bore:	48 mm
Length to diameter ratio:	0.57
Machine tool:	EEN 400 turning lathe
Cutting tool:	PCBN (coated) CNGA 120408 S01020 A7020
Tool geometry:	γ_n = -6°, α_n = 6°, κ_r = 95°, ε_r = 80°, r_ε = 0.8 mm chamfer 0.1x20º

Figure 7.30: Relationship between the white layer thickness and the depth of cut

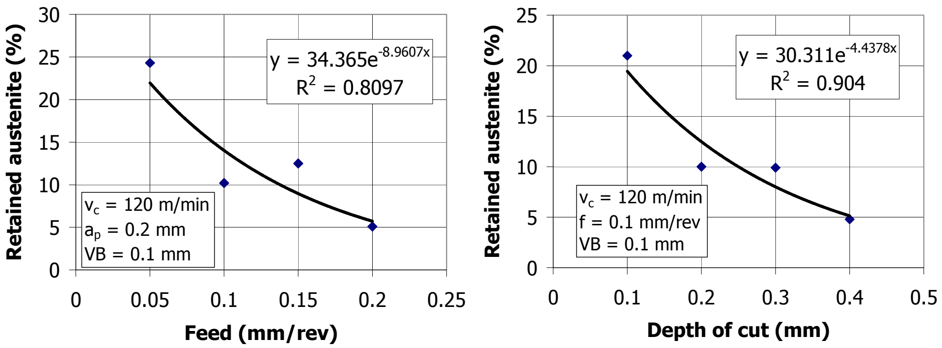

a) retained austenite versus feed

b) retained austenite versus depth of cut

Workpiece: 20MnCr5
Diameter of the bore: 48 mm
Length to diameter ratio: 0.57
Machine tool: EEN 400 turning lathe

Cutting tool: PCBN (coated) CNGA 120408 S01020 A7020
Tool geometry: $\gamma_n = -6°$, $\alpha_n = 6°$, $\kappa_r = 95°$, $\varepsilon_r = 80°$, $r_\varepsilon = 0.8$ mm chamfer 0.1x20°

Figure 7.31: Measured retained austenite content of the white layer

7.2 Models to predict the performance of hard turning

7.2.1 Model for determination of cutting forces

On the basis of the performed experiments, the empirical model of cutting forces can be defined. In this modelling, the common effect of the varied cutting data can be clearly seen. These are presented with Equations 7.1-7.3. The coefficient of determination (R-squared value) changes between 0.94 and 0.99. This means a proper approximation of the empirical models for the prediction of the cutting forces.

$$F_p = 1229.69 \cdot v_c^{-0.150} \cdot f^{0.319} \cdot a_p^{0.300} \tag{7.1}$$

R^2=0.9430

$$F_c = 935.45 \cdot v_c^{-0.011} \cdot f^{0.419} \cdot a_p^{0.649} \tag{7.2}$$

R^2=0.9561

$$F_f = 559.50 \cdot v_c^{-0.001} \cdot f^{0.172} \cdot a_p^{1.104} \tag{7.3}$$

R^2=0.9884

The cutting speed mainly influences the passive force, while the feed mostly affects the main cutting force, and the depth of cut notably increases the feed force. Figure 7.32 indicates the common effect of the variables on the cutting forces.

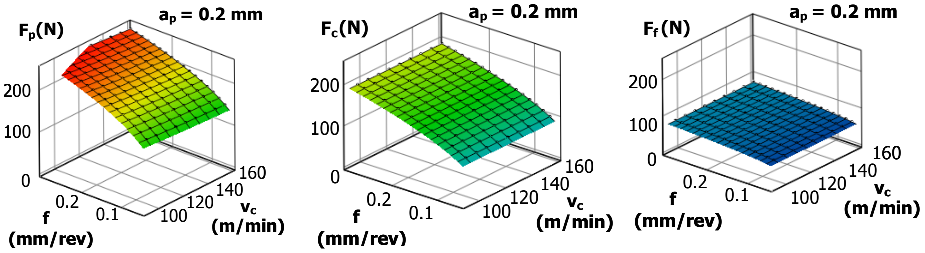

a) passive force b) main cutting force c) feed force

Figure 7.32: Relationship between cutting forces and data according to the empirical modelling

7.2.2 Prediction of cutting temperature

The measurement of the cutting temperature in turning of hardened steels makes it possible to determine the coefficient and exponent of Shaw's relation for PCBN tools, and predict the cutting temperature with empirical models. Furthermore, the establishment of the relationship between the FEM modelled temperature values and the measured data can be realized. The determination of the correction factor between the modelled and measured values improves the efficiency of the results achieved by FEM modelling.

According to Shaw [SHA84], the cutting temperature can be described as a function of the cutting speed with Equation 7.4:

$$\Theta = C_{\vartheta} \cdot v_c^{z\vartheta} \qquad (7.4).$$

The coefficient (C_{ϑ}) and exponent (z_{ϑ}) depend on the workpiece and tool material, and the tool geometry. It is defined for the cutting of hardened steel performed with a PCBN tool as:

$$\Theta = 279 \cdot v_c^{0.224} \qquad (7.5).$$

In the technical literature [PÁL80] the exponent of Equation 7.4 has already been given for HSS and hard metal tool materials, and could be determined for a PCBN cutting tool material, according to the performed experiments (Table 7.1).

Tool material	HSS	Hard metal	**PCBN**
z_{ϑ} value	0.400	0.270	**0.224**

Table 7.1: Values of z_{ϑ} exponent of the temperature relation, depending on the tool material

In metal cutting, it is a general observation that the cutting speed has the most significant effect on the temperature. Moreover, the other technological data also influences this. Therefore, it is necessary to extend Shaw's relation (Equation 7.4), with the other cutting characteristics such as feed and width of flank wear land. The common effect of these factors can be formulated with Equation 7.6:

$$\Theta = 126.38 \cdot v_c^{0.284} \cdot f^{-0.412} \cdot VB^{0.127} \qquad (7.6).$$

The coefficient of determination is R^2 = 0.9157, which indicates proper correlation. Figure 7.33 presents the influence of the cutting speed and width of flank wear land on the cutting temperature.

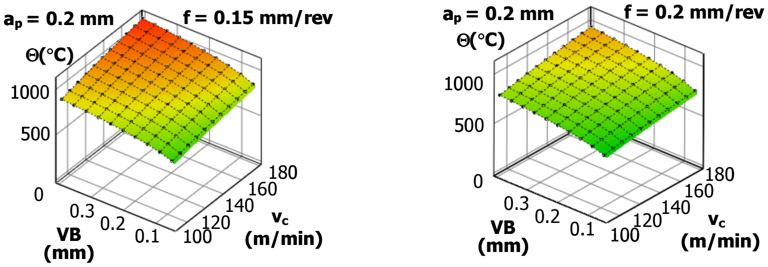

a) f = 0.15 mm/rev

b) f = 0.2 mm/rev

Figure 7.33: Relationship between cutting temperatures and data, according to the empirical modelling

In order to compare the measured cutting temperature values with the calculated data, the same cutting parameters, tool properties and workpiece material were applied in both cases. The simulation was performed with FEM software, as described in Chapter 6.3.2. Figure 7.34 indicates the modelled cutting temperature results. The model also proved that both the cutting speed and the tool wear enhance the cutting temperature.

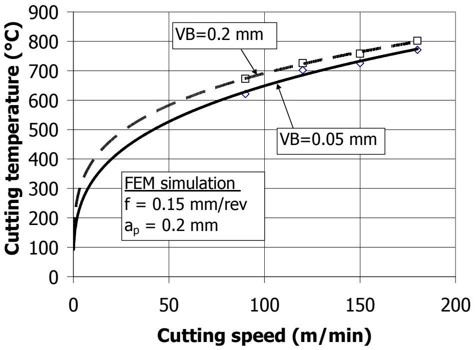

Workpiece:	20MnCr5
Cutting tool:	PCBN (coated) CNMA 120408
Tool geometry:	γ_n = -6°, α_n = 6°, κ_r = 95°, ε_r = 80°, r_ε = 0.8 mm chamfer 0.2x20°

Figure 7.34: Modelled cutting temperature performed with the FEM

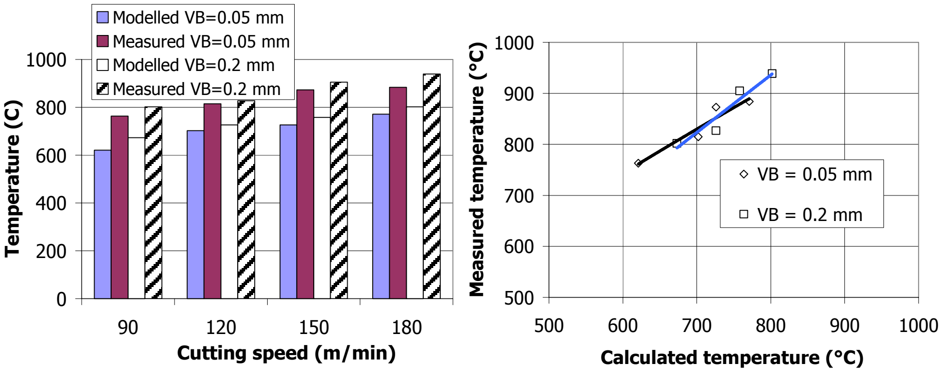

Workpiece: 20MnCr5
Cutting tool: PCBN (coated) CNMA 120408
Tool geometry: γ_n = -6°, α_n = 6°, κ_r = 95°, ε_r = 80°, r_ε = 0.8 mm, chamfer 0.2x20º

Figure 7.35: Relationship between the measured and modelled cutting temperature

With regard to the relationship between the modelled and measured cutting temperature, the model underestimated the magnitude of the cutting temperature (Figure 7.35). The deviation varies between 15 and 20 %, but the trends in both cases are similar. For a sharp tool, the relation can be formulated as:

$$\Theta_{real} = 7.52 \cdot \Theta_{calc}^{0.7181} \tag{7.7}$$.

And for a worn tool (VB = 0.2 mm), it can be given with Equation 7.8:

$$\Theta_{real} = 1.53 \cdot \Theta_{calc}^{0.9599} \tag{7.8}$$.

7.2.3 Modelling of surface roughness

In empirical modelling of the surface roughness, depending on the cutting data, regression analysis was applied. The regression analysis was performed with linear, power, logarithmic, exponential, and power functions, where the power function provided the best fit for each case. The prediction of surface roughness with empirical models can be given with Equation 7.9-7.12 as:

$$Ra_1 = 14.26 \cdot v_c^{-0.569} \cdot f^{0.280} \cdot a_p^{0.127} \tag{7.9}$$

R^2=0.9416

$$Rq_1 = 18.72 \cdot v_c^{-0.573} \cdot f^{0.319} \cdot a_p^{0.054} \tag{7.10}$$

R^2=0.9351

$$Rz_1 = 29.47 \cdot v_c^{-0.270} \cdot f^{0.395} \cdot a_p^{0.066} \tag{7.11}$$

R^2=0.9350

$$Rt_1 = 20.89 \cdot v_c^{-0.189} \cdot f^{0.316} \cdot a_p^{0.027} \tag{7.12}$$

R^2=0.9362

The coefficient of determination is above 0.93 in each case. The cutting speed mainly modifies the arithmetical mean deviation, and the root-mean-square deviation of the profile, while the feed has a similar effect on all roughness parameters. Figure 7.36 presents the common effect of the cutting speed and the feed on the surface roughness.

Taking into account the width of flank wear land, the surface roughness Rz can be predicted with the Equation 7.13:

$$Rz_2 = 193.75 \cdot v_c^{-0.235} \cdot f^{0.404} \cdot a_p^{0.067} \cdot VB^{0.922}$$

$$R^2 = 0.8979 \tag{7.13}$$

With regard to the four variables (v_c, a_p, f, VB), the multiplied power function also gives a good approach.

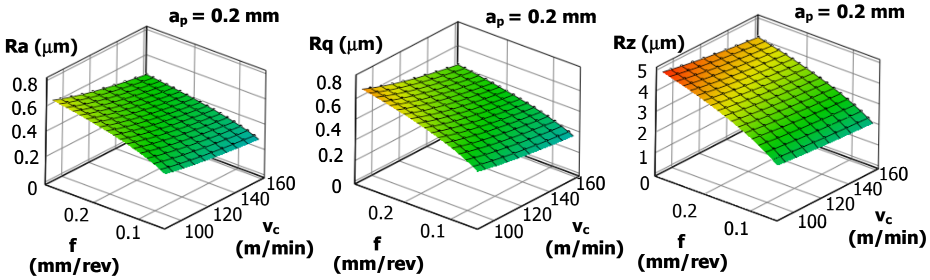

a) Ra b) Rq c) Rz

Figure 7.36: Relationship between the surface roughness and the cutting data (VB = 0.1 mm)

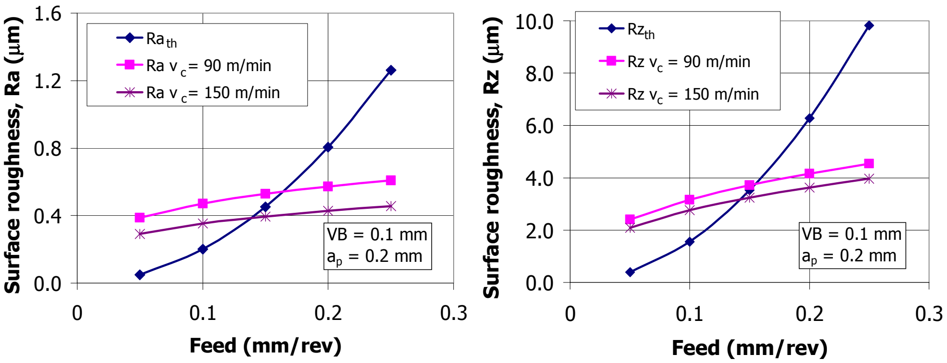

a) Ra b) Rz

Figure 7.37: Comparison of the theoretical roughness and real roughness (r_ε = 0.8 mm)

According to the description of the theoretical calculation of the surface roughness, as described in Chapter 6.4.1, the comparison between theoretical and real roughness values are defined (Figure 7.37). The values are calculated for a cutting tool with a tool corner radius of 0.8 mm.

The deviation between the theoretical and the real roughness values are dominant therefore the theoretical roughness values must be built into the empirical model. As the theoretical values already include the feed and the tool corner radius, the effect of the cutting speed and the depth of cut are the other variables (Equations 7.14-7.16).

$$Ra_3 = 13.11 \cdot v_c^{-0.652} \cdot a_p^{0.106} \cdot Ra_{th}^{0.125} \qquad (7.14)$$

R^2=0.9725

$$Rq_3 = 15.2 \cdot v_c^{-0.601} \cdot a_p^{0.052} \cdot Rq_{th}^{0.320} \qquad (7.15)$$

R^2=0.9312

$$Rz_3 = 19.3 \cdot v_c^{-0.388} \cdot a_p^{0.080} \cdot Rz_{th}^{0.204} \qquad (7.16)$$

R^2=0.9535

The theoretical roughness, namely the feed and the tool corner radius, has a more significant effect on the real values than the depth of cut, but the cutting speed still mainly influences the formation of the surface roughness, during the cutting of hardened bores.

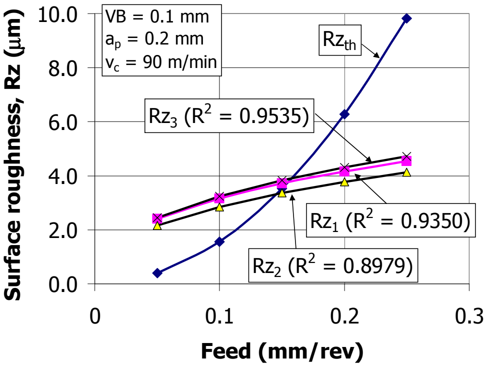

Figure 7.38: Comparison of the theoretical and modeled surface roughness, Rz

Among the roughness parameters as an example, Figure 7.38 presents the comparison of the theoretical and modelled values of the ten-point height of the profile. Among the empirical models the Rz_3 provides the best approach as the coefficient of determination is 0.9535. This empirical model (Rz_3) including the effect of v_c, a_p, Rz_{th} (f, r_ε) the most suitable for predicting of the ten-point height of the profile.

7.2.4 Modelling of macro geometrical accuracy

On the basis of the performed investigations, the empirical model concerning the macro geometrical accuracy is established. Equations 7.17-7.19 express the out-of-roundness, the cylindricity error, and the parallelism error. Compared to the other variables, such as the cutting speed and length of cut, it is obvious that there is a strong effect of the workpiece "rigidity" (WT) on the geometrical accuracy. The cutting speed decreases while the length of cut increases the macro geometrical errors. The increase of the wall thickness ratio mainly influences the cylindricity error and the parallelism error.

$$\mathrm{RONt} = 4.1 \cdot v_c^{-0.240} \cdot \mathrm{WT}^{-0.630} \cdot L^{0.230} \tag{7.17}$$

$R^2 = 0.9850$

$$\mathrm{CYLt} = 9.5 \cdot v_c^{-0.149} \cdot \mathrm{WT}^{-1.860} \cdot L^{0.220} \tag{7.18}$$

$R^2 = 0.9250$

$$\mathrm{CYLpar} = 5.4 \cdot v_c^{-0.609} \cdot \mathrm{WT}^{-1.600} \cdot L^{0.310} \tag{7.19}$$

$R^2 = 0.9591$

Figure 7.39 presents the geometrical accuracy with a cutting speed of 180 m/min, as a function of the length of cut and wall thickness ratio. Furthermore, the diagrams point out the effect of the wall thickness ratio, and the length of cut on the form and positional accuracy.

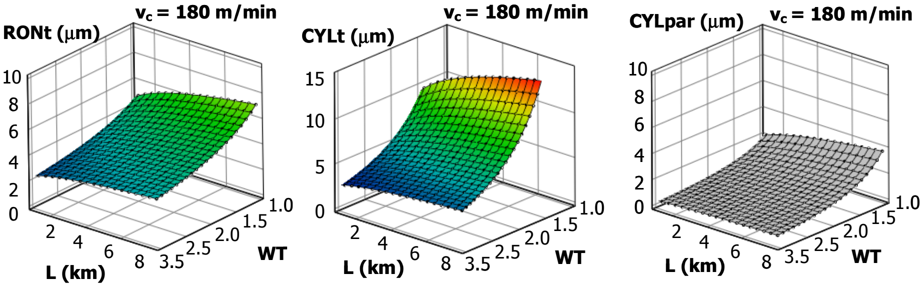

a) out-of-roundness b) cylindricity error c) parallelism error

Figure 7.39: Macro geometrical accuracy, as a function of the length of cut and wall thickness ratio

7.2.5 Computer-based modelling of thermal distortion

The applied FEM model for determining the thermal distortion of the bore has been described in Chapter 6.4.2. Among the simulation results, examples of roughing and finishing are presented, taking into account the effect of the width of flank wear land on the geometrical accuracy.

In roughing, with VB = 0.1 mm, the maximum workpiece temperature is 48.5 °C at the end of the last pass, and the workpiece temperature exists at a low level in the hard turning process (Figure 7.40a). This is because the PCBN tool possesses high thermal conductivity, and therefore a significant amount of heat generated during cutting is removed by the tool and chip. The extension of the width of flank wear land results in a higher workpiece temperature, exceeding 63 °C. The thermal errors caused by the heat are plotted as a function of the length of the workpiece, and the expansion in the workpiece's diameter (Figure 7.40b). Even if a cutting tool with VB = 0.4 mm is applied, the deviation remains below 4 μm.

In finishing, the workpiece's temperature still remains at a low level, but it increases slightly, as in the last pass, its maximum value is 74.3 °C for VB = 0.4 mm (Figure 7.41a). During machining, the workpiece's temperature is continuously rising. This is because in front of the moving heat source, a warm material part can be found. At the end of the workpiece, it is evident that the workpiece temperature suddenly increases, due to the reduction of the material volume. Thus, the progressive temperature rises localised to the partially limited place of the workpiece. Compared to roughing, the thermal distortion is higher in finishing, and the deviation exceeds 6 μm (Figure 7.41b).

In both roughing and finishing, the same characteristics can be observed with regard to the form of deviation. As the cutting tool begins to work, the workpiece expands to direction of +r, while after 5.5 mm in axis z, the material particles move to the direction of –r (Figure 6.6). This is due to the clamping of the workpiece (Figure 6.6). At the section where the gear is clamped, the material can only expand to the direction of –r. At first, the cutting tool removes less material, and it cuts more material getting on with the feed. Due to this, after the material cooled down, at the beginning of the bore, the diameter is smaller, whereas at the end of the bore, a diameter increase takes place. This phenomenon was also proved with the measurement of geometrical accuracy of the machined gear's bore (Figure 7.42).

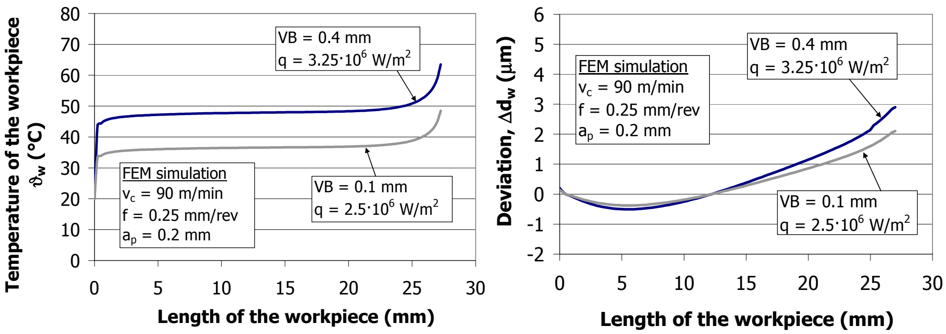

a) workpiece temperature

b) thermal distortion of the bore

Figure 7.40: FEM simulation in rough hard turning

The FEM modelling of thermal distortion indicates that heat has a significant influence on the machining result, especially in higher tool wear. Therefore, the technological data must be chosen properly, regarding the size, form, and positional accuracy prescribed for the bore. In the industrial application, the implementation of the presented simulation method can help in the design of the hard turning process, and the selection of the proper cutting parameters. Furthermore, the tool path correction during hard turning can be determined with greater ease and accuracy.

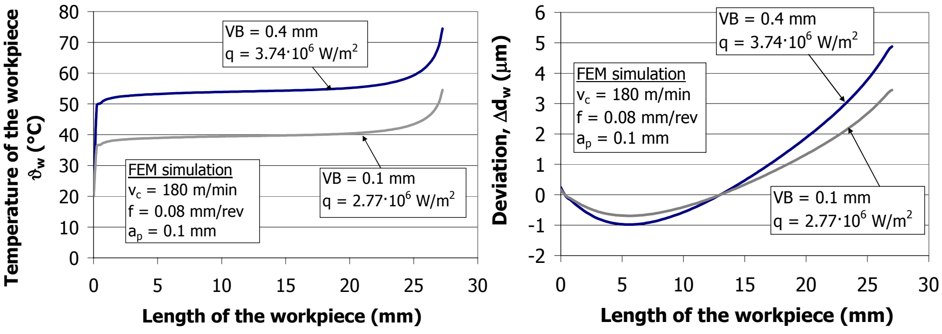

a) workpiece temperature

b) thermal distortion of the bore

Figure 7.41: FEM simulation in finish hard turning

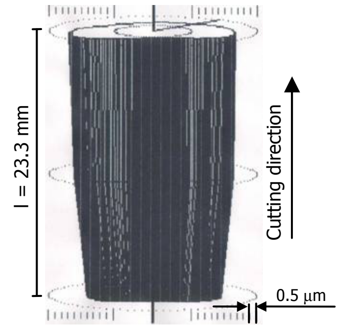

Workpiece:	20MnCr5
Diameter of the bore:	48 mm
Length to diameter ratio:	0.57
Machine tool:	EEN 400 turning lathe
Cutting tool:	PCBN (coated) CNGA 120408 S01020 A7020
Tool geometry:	γ_n = -6°, α_n = 6°, κ_r = 95°, ε_r = 80°, r_ε = 0.8 mm chamfer 0.1x20º
Cutting data:	vc = 200 m/min a_p = 0.1 mm f = 0.08 mm/rev

Figure 7.42: Measured cylindricity form after finishing

7.2.6 Modelling of the appearance of white layer

According to the performed experimental investigations (see Chapter 7.1.5), the empirical model for prediction of the white layer can be established. The power per unit length as a physical parameter can be given as a function of the cutting speed, depth of cut and feed (Equation 7.20).

$$P'_\alpha = 100.0 \cdot v_c^{0.410} \cdot f^{0.651} \cdot a_p^{0.236} \qquad (7.20)$$

R^2 = 0.9248

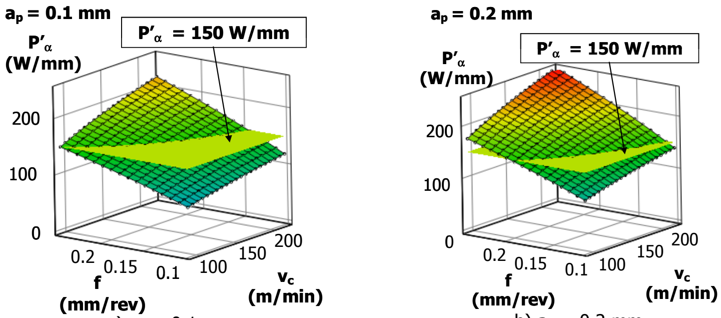

a) a_p = 0.1 mm b) a_p = 0.2 mm

Figure 7.43: Prediction of the white layer

This makes the selection of the cutting data to avoid the appearance of white layer possible, and means that the power per unit length must be lower than 150 W/mm. All cutting parameters enhance the cutting power, but the feed has the most significant effect. Figure 7.43 clearly represents the relationships between the appearance of the white layer and the feed, and the cutting speed and the depth of cut.

7.3 Cycle time and material removal rate

In addition to the surface quality, the economical points of view must be considered. The material removal rate and the surface rate are the most important factors to evaluate the productivity of the cutting process [TÖN00]. Moreover, due to the high flexibility of hard turning, different shapes and surfaces can be machined in one set-up. The number of applied machine tools is reduced, and thus, the production steps decrease noticeably. Owing to these advantages, the manufacturing time becomes shorter.

In bore manufacturing, the cycle time is compared, which can be formulated

for turning as

$$t_{c,HT} = \frac{(l + l_1) \cdot i}{n \cdot f} + t_{cs} \tag{7.21}$$

and for traverse grinding as

$$t_{c,GR} = \frac{(l + l_1) \cdot i}{n \cdot f} + t_{sp} + t_{cs} \tag{7.22}$$

where l is the length of the workpiece, l_1 the additional length for approach and overtravel, i the number of strokes, n the revolution, f the feed, t_{cs} the time of tool change and t_{sp} the spark-out time.

Figure 7.44 presents the cycle times calculated for roughing and finishing, after hard turning and grinding. For example, it is clear that hard turning is 2.5–4 times quicker than grinding, with respect to bores with diameters of 48 mm and 83 mm.

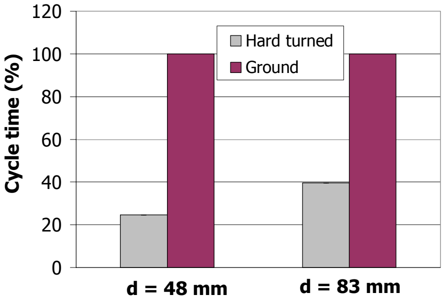

Workpiece:
Material: 20MnCr5
Diameter of the bore: 48 mm
83 mm
Allowance: 0.3 mm

Hard turning:
Machine tool: PITTLER PVSL-2 hard turning lathe
Cutting tool: PCBN (coated)
CNGA 120408 S01020 A7020
Tool geometry: $\gamma_n = -6°$, $\alpha_n = 6°$, $\kappa_r = 95°$, $\varepsilon_r = 80°$, $r_\varepsilon = 0.8$ mm
Depth of cut: $a_p = 0.1\text{-}0.2$ mm
Feed: f = 0.08-0.15 mm/rev
Cutting speed: $v_c = 120\text{-}200$ m/min

Internal traverse grinding:
Machine tool: SI-4/A internal grinder
Grinding wheel: CBN wheel
Wheel speed: $v_c = 25\text{-}43$ m/s
Speed ratio: q = 60-80
Workpiece speed: $v_w = 18\text{-}33$ m/min
Depth of cut: $a_e = 0.02\text{-}0.03$ mm/double stroke
Traverse speed: $v_f = 2.2$ m/min
Spark-out: 8-16 double stroke

Figure 7.44: Comparison of cycle time

The material removal rate (Q_w) means the volume of material removed per unit time, while surface rate (A_w) is the area of material removed per unit time. These factors can be calculated from the cutting data called theoretical indexes (Table 7.2). Typical values for Q_w and A_w are also presented, which vary in a wide range. The material removal rate is higher in hard turning, while the surface rates are more beneficial in grinding. It indicates that the grinding time is shorter, which is calculated only for one stroke. In reality, grinding is done in more steps (roughing, finishing and spark-out). The real indexes (Table 7.3) are more closely related to the certain machining process, as its definition considers the workpiece geometry (diameter and length), the material allowance, and the time required for metal removal [TÓT04]. Therefore, real indexes are applied for the comparison of economical aspects between grinding and turning.

	Grinding	**Hard turning**	**Unit**
Material removal rate	$Q_w = a_e \cdot f \cdot v_w$	$Q_w = a_p \cdot v_c \cdot f$	mm³/s
Surface rate	$A_w = v_f \cdot v_w$	$A_w = v_c \cdot f$	mm²/s
Characteristic parameter	$a_e = 0.01\text{-}0.03$ mm $v_w = 20$ m/min $v_c = 30$ m/s	$a_p = 0.05\text{-}0.3$ mm f = 0.05-0.2 mm/rev $v_c = 150$ m/min	
Typical values	$Q_w = 1.7\text{-}20$ mm³/s $A_w = 1670\text{-}6667$ mm²/s	$Q_w = 6\text{-}150$ mm³/s $A_w = 125\text{-}500$ mm²/s	

Table 7.2: Calculation of the theoretical indexes of the material removal rate and surface rate [KÖN80], [TÖN00]

	Grinding, Hard turning	Unit
Material removal rate	$Q_w = \frac{d \cdot \pi \cdot l \cdot 0.3}{t_c \cdot 60}$ 0.3 – allowance in mm (roughing and finishing)	mm^3/s
Surface rate	$A_w = \frac{d \cdot \pi \cdot l}{t_c \cdot 60}$	mm^2/s

Table 7.3: Calculation of the real indexes of the material removal rate and surface rate

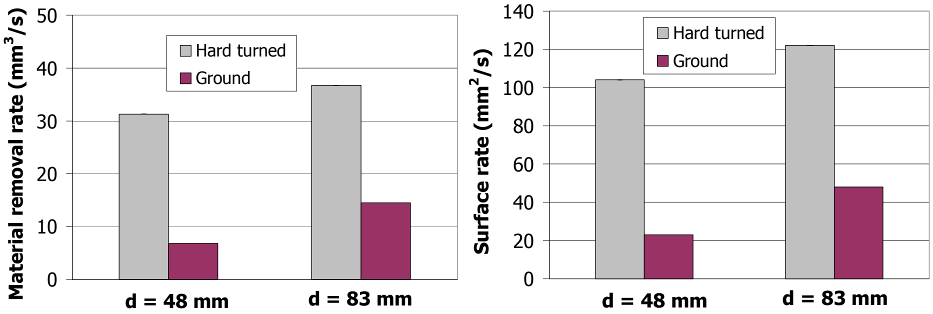

a) Workpiece: 20MnCr5 b)

Hard turning:
Machine tool: PITTLER PVSL-2 hard turning lathe
Cutting tool: PCBN (coated) CNGA 120408 S01020 A7020
Tool geometry: γ_n = -6°, α_n = 6°, κ_r = 95°, ε_r = 80°, r_ε = 0.8 mm
Depth of cut: a_p = 0.1-0.2 mm
Feed: f = 0.08-0.15 mm/rev
Cutting speed: v_c = 120-200 m/min

Internal traverse grinding:
Machine tool: SI-4/A internal grinder
Grinding wheel: CBN wheel
Wheel speed: v_c = 25-43 m/s
Speed ratio: q = 60-80
Workpiece speed: v_w = 18-33 m/min
Depth of cut: a_e = 0.02-0.03 mm/double stroke
Traverse speed: v_f = 2.2 m/min
Spark-out: 8-16 double stroke

Figure 7.45: a) Material removal rate, $Q_{w,}$ and b) surface rate, A_w

The calculated material removal rates and surface rates are presented in Figure 7.45. As an example, for bores with diameters of 48 and 83 mm, the material allowance to be removed is 0.3 mm. Hard turning shows a high potential to replace grinding in manufacturing of a gear's bore, as it provides remarkably higher material removal rates. Surface rates are higher in turning, when calculating on the basis of the real indexes, instead of on the theoretical one.

7.4 Optimal cutting data for machining of disc type parts

The optimisation model applied for the machining of disc type parts has been already described in Chapter 6.6. The objective function, which is the minimum production cost, and the constraints were also presented. To determine the optimal cutting data, the boundary conditions must be defined, which are summarized below:

Workpiece diameter:	$d = 48$ mm
Depth of cut:	$a_p = 0.1$ mm
Prescribed surface roughness:	$Rz = 3$ μm
Prescribed out-of-roundness:	$RONt = 6$ μm
Cutting tool:	Sandvik Coromant CNGA 120408 S0120 A7020
Cutting tool geometry:	$\gamma_n = -6°$, $\alpha_n = 6°$, $\kappa_r = 95°$, $r_\varepsilon = 0.8$ mm, $r_\beta = 0.075$ mm
Machine tool:	EEN-400 turning lathe
Effective power of the machine tool:	$P_c = 17$ kW
Revolution range:	$n = 0 - 4000$ 1/min
Feed range:	$v_f = 0 - 40$ m/min
Tool cost:	$K_e = 26.33$ €/edge
Machine tool cost:	$k_g = 0.24$ €/min
Time of tool change:	$t_{cs} = 1.5$ min

It is assumed that the optimisation is valid in the range of $v_c = 120 - 180$ m/min and $f = 0.05 - 0.125$ mm/rev. The maximum admissible tool wear was determined to be VB = 0.15 mm.

The constraints of the optimisation model are defined with Equations 7.23-7.34:

1. Adjustable maximum feed

$$f \leq 7.5 \text{ mm/rev} \tag{7.23}$$

2. Adjustable maximum revolution

$$n \leq 4000 \text{ 1/min} \tag{7.24}$$

3. Minimum chip thickness

$$\bar{h}_{min} = f \cdot \sqrt{\frac{a_p}{2 \cdot r_\varepsilon}} \rightarrow f \geq \frac{\bar{h}_{min}}{\sqrt{\frac{a_p}{2 \cdot r_\varepsilon}}} = 0.03 \text{ mm/rev} \tag{7.25}$$

where $h_{min} \geq 0.1 r_\beta$ [TÖN00]

4. Cutting power

$$P_c = \frac{F_c \cdot v_c}{60} \rightarrow$$

$$f^{y_{F_c}} \cdot n^{z_{F_c}+1} \leq \frac{60 \cdot P_c}{C_{F_c} \cdot \left(\frac{d\pi}{10^3}\right)^{z_{F_c}+1} \cdot a_p^{x_{F_c}}} \tag{7.26}$$

where

$$F_c = 935.45 \cdot v_c^{-0.011} \cdot f^{0.419} \cdot a_p^{0.649} \tag{7.27}$$

thus,

$$f^{0.988} \cdot n^{1.698} \leq 3.1 \cdot 10^5 \tag{7.28}$$

5. Surface roughness

$$Rz_3 = 19.3 \cdot v_c^{-0.388} \cdot a_p^{0.080} \cdot Rz_{th}^{0.204} \tag{7.29}$$

$$f^{0.408} \cdot n^{-0.388} \leq 0.03 \tag{7.30}$$

6. Geometrical accuracy

$$RONt = 4.1 \cdot v_c^{-0.240} \cdot WT^{-0.630} \cdot L^{0.230} \tag{7.31}$$

$$\left(\frac{1}{f}\right)^{0.230} \cdot n^{-0.240} \leq 0.247 \tag{7.32}$$

7. Prevention of the white layer

$$P_\alpha^{'} = 100.0 \cdot v_c^{0.410} \cdot f^{0.651} \cdot a_p^{0.236} \tag{7.33}$$

where $P_\alpha \leq 150$ W/mm [SCH99]

$$f^{0.651} \cdot n^{0.410} \leq 5.6 \tag{7.34}$$

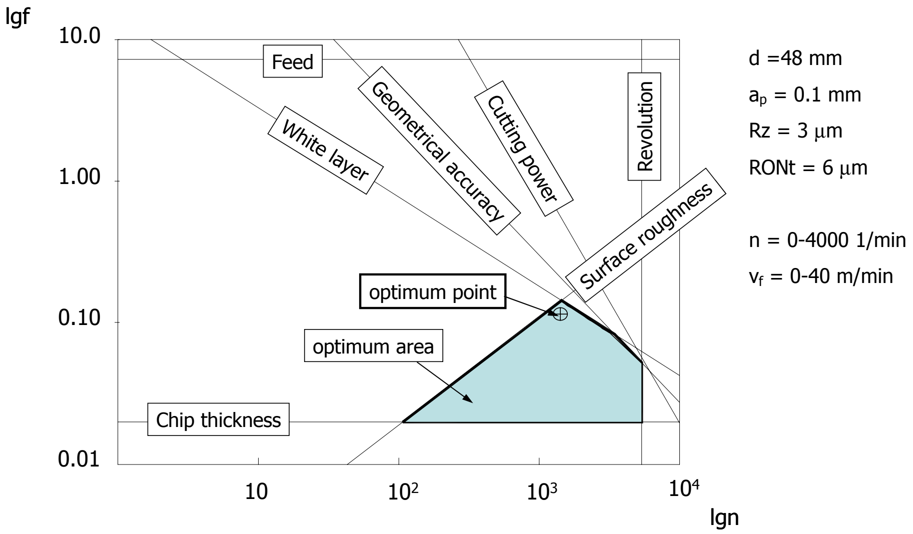

Figure 7.46: Optimisation result

After listing the constraints, the inequalities can be plotted in a log n-log f plane. These linear functions will define the area, where the optimal cutting data can be found, and indicate the optimum point (see Figure 7.46).

According to Figure 7.46, the intersection of line "surface roughness" and line "white layer" can be the optimum point, applying Equations 7.30 and 7.34:

$$f^{0.408} \cdot n^{-0.388} \leq 0.03$$

and

$$f^{0.651} \cdot n^{0.410} \leq 5.6$$

thus,

$$n = 1231 \text{ 1/min} \qquad (v_c = 185.6 \text{ m/min})$$

$$f = 0.16 \text{ mm/rev}$$

However, the tool life must be taken into account, which is formulated as:

$$v_c \cdot T^m = C \rightarrow v_c \cdot T^{0.66} = 2601.1 \tag{7.35}$$

At this possible optimum point, the tool life is:

$$T = \left(\frac{C}{v_c}\right)^{\frac{1}{m}} = \left(\frac{2601.1}{185.6}\right)^{\frac{1}{0.66}} = 53.9 \text{ min} \tag{7.36}$$

The optimal tool life regarding the minimum cost is:

$$T_{Kopt} = \left(\frac{1}{m} - 1\right)\left(t_{cs} + \frac{K_e}{k_g}\right) = \left(\frac{1}{0.66} - 1\right)\left(1 + \frac{26.33}{0.23}\right) = 61.2 \text{ min} \tag{7.37}$$

Considering the tool life, the minimum production cost can be realized, if:

$$v_{c,optK} = \frac{C}{T^m} = \frac{2601.1}{61.2^{0.66}} = 172.2 \text{ m/min} \rightarrow n = 1142.5 \text{ 1/min} \tag{7.38}$$

and

$$f_{optK} = \sqrt[0.408]{\frac{0.03}{n^{-0.388}}} = \sqrt[0.408]{\frac{0.03}{1142.5^{-0.388}}} = 0.14 \text{ mm/rev} \tag{7.39}$$

With regard to the constraints and boundary conditions, the optimum cutting speed is 172.2 m/min, and the optimum feed is 0.14 mm/rev.

Machining time per part is 0.18 min. Regarding the optimal tool life, cutting speed and feed, the tool change after 340 pieces is needed.

8 Machining of small bores

Small cylinders, like injection nozzles, have long bores, where the length to diameter ratio may reach 5. This means that tool bending is not negligible, and does cause geometrical error. The applied tools and tool holders must be chosen carefully. When reducing the bore diameter, the material removal process becomes more difficult. Due to the strong curvature of the machined bore (d = 3-4 mm), a turning tool with different edge geometry is required. It is necessary to set the rake angle to zero, while a secondary clearance face is formed, which makes metal removal possible and easier. In grinding, the tool clamping, grinding wheel, and quill materials have to be chosen properly. In tool mounting, the accurate thread clamping system ensures that ultimate rigidity, easy mounting, and high accuracy is possible (see Chapter 5).

It is the goal of this Chapter to determine and predict the performance of combined machining, and reveal the interconnection between the product and process characteristics in manufacturing of small bores. The experimental research work establishes the empirical models, which helps in the prediction of process performance. Measurement of the cutting forces is required to calculate tool bending, for both grinding and hard turning forecasting of the mechanical errors. Compared with the magnitude of mechanical errors to thermal errors, determination of thermal distortion with FEM method is performed. The economical points of view, namely the cycle time, material removal rate, and surface rate are also considered.

The research work carried out in machining of small bores defines the transition range between hard turning and grinding, and provides new alternatives for the manufacturing of diesel injection nozzles.

8.1 Experimental investigations

8.1.1 Cutting forces - machining a batch

Cutting forces were measured in both turning and grinding processes. The force measurement method and set-up has already been presented in Chapter 5.2.5. In turning, passive or back force, regarding its highest value among the force constituents was measured, as the pressure difference sensor can detect the pressure in one direction only. In grinding, tests for the measurement of the normal force were carried out.

Firstly, several experiments were done to study the effectiveness of different filters. A moving average filter and a low-pass filter (10 Hz) were used to filter the electrical disturbances, and other disturbances, which occurred occasionally. During the test, there was little difference between the results gained with these two filters.

The pressure difference sensor signal is influenced by several factors: 1) Unbalance of the main spindle, as an increased revolution generates higher disturbances in the signal. To avoid this, a notch filter was applied; 2) Pump of the hydraulic system: the oil pressure is kept at a constant value (55 bars), as the pressure regulation for the hydrostatic bearings is carried out with a pressure release valve, it cannot cause any significant disturbances; and 3) Angle of force measurement. The angle of the force measurement does not coincide with the passive force angle, as the difference is 15 degrees. The measured force is a resultant force, which consists of the main cutting force and the passive force. In Figure 8.1, the amount of passive force in the resultant force is presented. The measuring error is 7%, meaning that 93% of the measured force is the real back force.

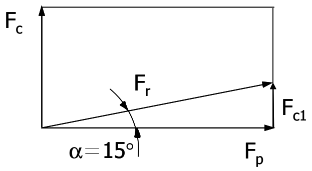

$$F_p = F_r \cdot \cos\alpha = 0.26 \cdot F_r$$

$$F_{c1} = F_r \cdot \sin\alpha = 0.97 \cdot F_r$$

$$F_r = \sqrt{F_p^2 + F_{c1}^2} = \sqrt{0.93 \cdot F_r^2 + 0.07 \cdot F_r^2}$$

Figure 8.1: Amount of cutting force in the resultant force

In the first instance, force measurement was tested and measured in turning. The cutting force was monitored when the cutting data were changed including the tool wear. Figure 8.2 presents the measured passive force besides modified cutting data.

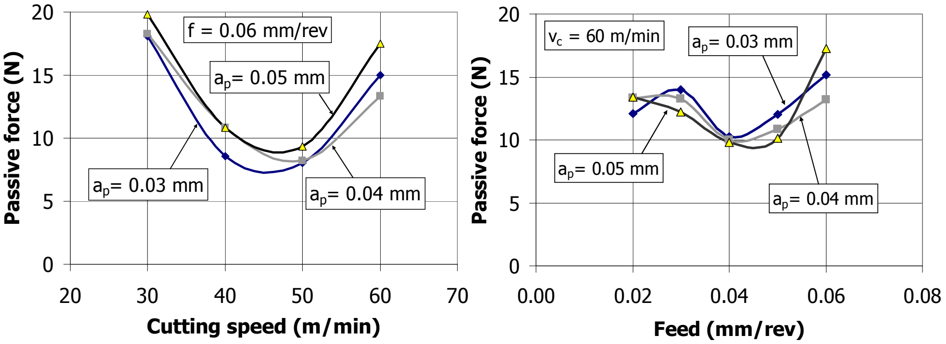

Workpiece:	100Cr6
Diameter of the bore:	4 mm
Length to diameter ratio:	4
Machine tool:	Slantbed Mikroturn 50CNC

Cutting tool:	Kennametal PCBN MKTB KB5625 MKTB31715R
Tool geometry:	γ_n = 0°, α_n = 10°, κ_r = 95°, $r\varepsilon$=0.2 mm
Tool wear:	VB < 0.06 mm

Figure 8.2: Passive force influenced by the cutting data

As seen in Figure 8.2 (left), it can be observed that the cutting speed significantly influences the passive force values, which do not exceed 20 N. The passive force is the highest at a cutting speed of 30 m/min, and is remarkably reduced at speeds of 40 and 50 m/min. Furthermore, an increase in the revolution also generates higher forces. At a higher revolution, the tool vibration increases that generates higher cutting forces. The depth of cut negligibly influences the present passive force. The effect of the feed on the force is also unclear. The force is lowest at a feed of 0.04 mm/rev, when varying the depth of cut (see Figure 8.2, right side).

Generally, the cutting speed reduces the cutting forces, while the feed and depth of cut increases them. The reason for the fluctuating values is most likely that the optimal cutting temperature is not achieved. In previous research work, it was found that the steadiness of the optimum cutting temperature is valid when cutting with superhard tools. In other words, the steady temperature of the cutting zone belongs to the optimum cutting speed, with different combinations of feed and depth of cut [KUN96].

The force measurement results of 160 machined workpieces are presented in Figure 8.3. When applying a sharp tool, the passive force is approximately 10 N, which doubles with a cutting of 160 workpiece. After 15 machined workpieces, the passive force remains constant. After 50 machined workpieces, the passive force starts to fluctuate mildly. When the tool has machined 85 workpieces, the passive force starts to increase slightly, and stays constant between 110 and 150 machined workpieces. From this point, the passive forces increase, until the 160 workpieces are machined. At that point, a bad surface finish was visible to the naked eye.

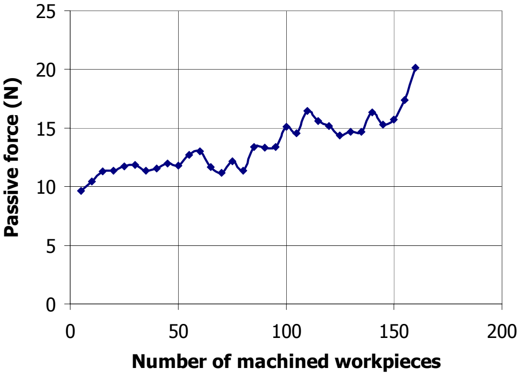

Workpiece:	100Cr6
Diameter of the bore:	4 mm
Length to diameter ratio:	4
Machine tool:	Slantbed Mikroturn 50CNC
Cutting tool:	Kennametal PCBN MKTB KB5625 MKTB31715R
Tool geometry:	$\gamma_n = 0°$, $\alpha_n = 10°$, $\kappa_r = 95°$, $r\varepsilon = 0.2$ mm
Cutting data:	$v_c = 50$ m/min f = 0.06 mm/rev $a_p = 0.03$ mm

Figure 8.3: Passive force measurement when machining a batch

During batch machining, the tool wear was continuously measured and analyzed with a digital microscope. The measured width of flank wear land (VB_{max}) hardly changes (see Figure 8.4). Therefore, the area of the flank wear land (A_{VB}) was also evaluated by means of the Keyence digital microscope. The interpretation of VB_{max} and A_{VB} on a real tool tip is shown in Figure 8.5.

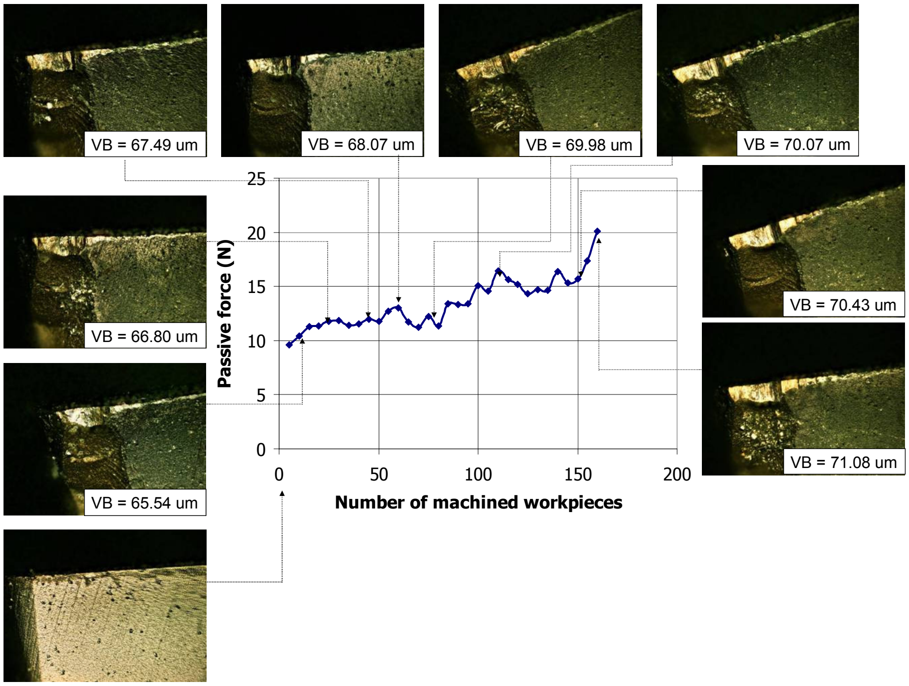

Figure 8.4: Results of VB_{max} measurement, including images from the tool-tip

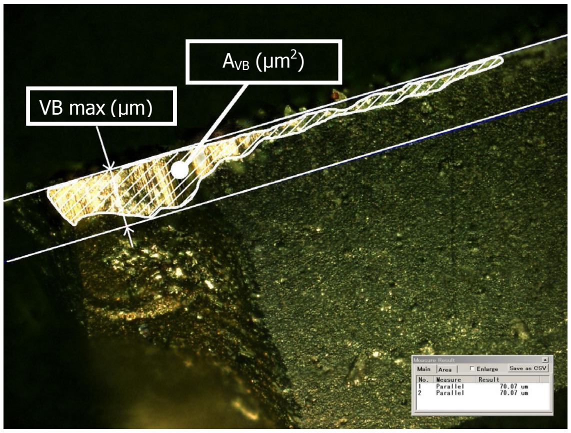
A_{VB} (μm^2)
VB max (μm)
Measure Result
Main
Area
☐ Enlarge
Save as CSV

No.	Measure	Result
1	Parallel	70.07 um
2	Parallel	70.07 um

Figure 8.5: Interpretation of VB_{max} and A_{VB}

The measured values of $A_{VB,}$ as plotted against the number of machined workpieces indicate the tool wear characteristic, which is well known from the cutting theory (see Figure 8.6). The degressive wear, the linear wear, and the progressive wear can be clearly seen.

In the cutting of small bores, in addition to the flank face, the rake face was also analysed during the tool wear behaviour. The rake face of a sharp tool and a worn tool was compared (Figure 8.7). In Figure 8.7c, the worn and disappeared area is outlined with white, which indicates remarkable tool corner wear. As the bore diameter to be cut is only 4 mm, and the length to diameter ratio 4, due to the tool vibration, small particles bounce off from the tool-tip, which causes significant corner wear.

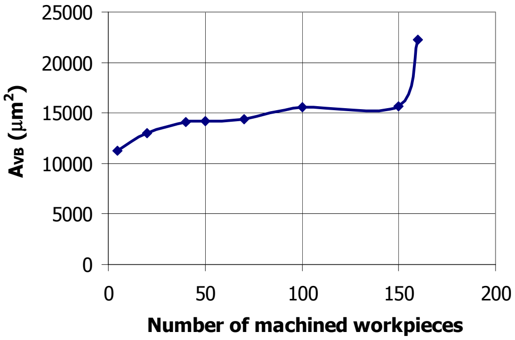

Workpiece: 100Cr6
Diameter of the bore: 4 mm
Length to diameter ratio: 4
Machine tool: Slantbed Mikroturn 50CNC
Cutting tool: Kennametal PCBN MKTB KB5625 MKTB31715R
Tool geometry: $\gamma_n = 0°$, $\alpha_n = 10°$, $\kappa_r = 95°$, $r\varepsilon = 0.2$ mm
Cutting data: $v_c = 50$ m/min
$f = 0.06$ mm/rev
$a_p = 0.03$ mm

Figure 8.6: Measured area of flank wear land plotted against the number of machined pieces

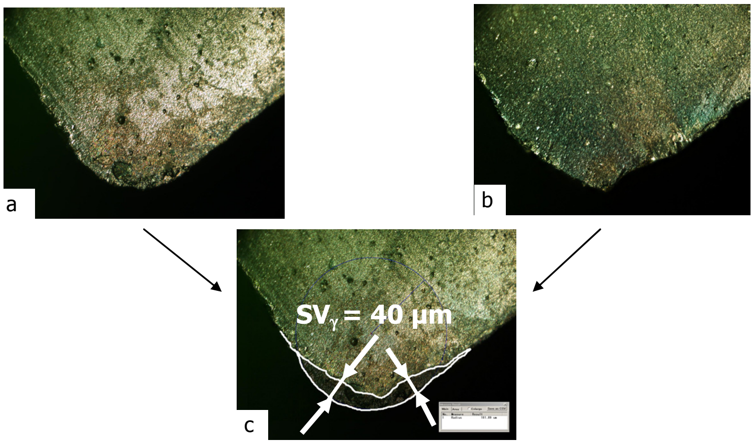

Figure 8.7: a) new cutting tool; b) worn tool; and c) tool corner wear

During batch machining, the formation of the cutting force and surface roughness indicates a correlation (see Figure 8.8). Namely, a higher passive force generates a higher ten-point height value of the profile.

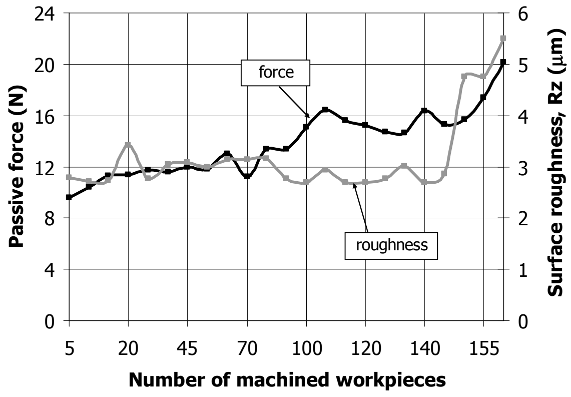

Workpiece:	100Cr6
Diameter of the bore:	4 mm
Length to diameter ratio:	4
Machine tool:	Slantbed Mikroturn 50CNC
Cutting tool:	Kennametal PCBN MKTB KB5625 MKTB31715R
Tool geometry:	$\gamma_n = 0°$, $\alpha_n = 10°$, $\kappa_r = 95°$, $r\varepsilon=0.2$ mm
Cutting data:	$v_c = 50$ m/min f = 0.06 mm/rev $a_p = 0.03$ mm

Figure 8.8: Passive force versus ten-point height of the profile

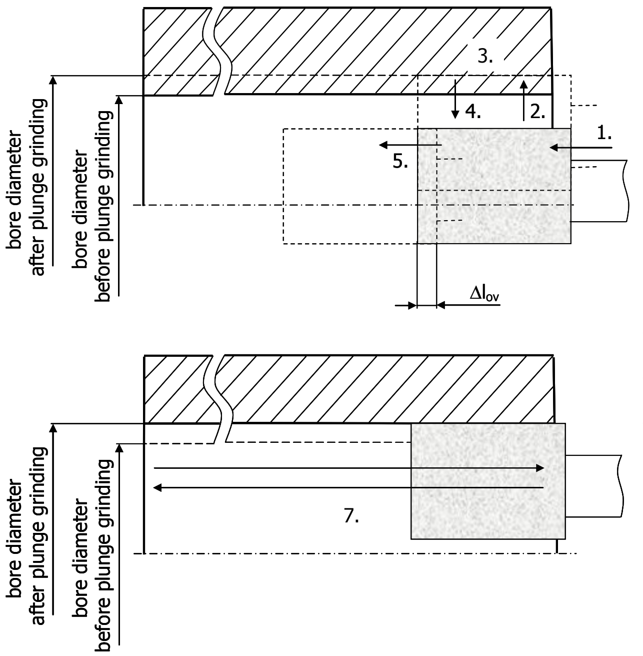
bore diameter after plunge grinding
bore diameter before plunge grinding
1.
2.
3.
4.
5.
Δl_{ov}
bore diameter after plunge grinding
bore diameter before plunge grinding
7.

Workpiece: 100Cr6
Diameter of the bore: 4 mm
Length to diameter ratio: 4
Machine tool:
Slantbed Mikroturn 50CNC
Grinding wheel: Meister Abrasives
CB5-500-Q-8-255-200-V55-31

Internal plunge grinding:
$n_s = 90000$ 1/min
$q_s = 60$
$d_s = 3.5$ mm
$v_w = 16.5$ m/min
$a_e = 0.004$ mm
$v_{frad} = 5$ mm/min
Spark-out time: 5 s
$v_{fax} = 400$ mm/min
number of strokes: 7

1. axial feed into the bore
2. plunge grinding
3. spark-out
4. retraction
5. axial displacement for next grinding cut
   (overlap of cuts: Δl_{ov})
6. continue at 2.
   total number of cuts depending on the workpiece length
7. traverse oscillation, spark-out on full bore length

Figure 8.9: Schematic figure and data of internal grinding strategy

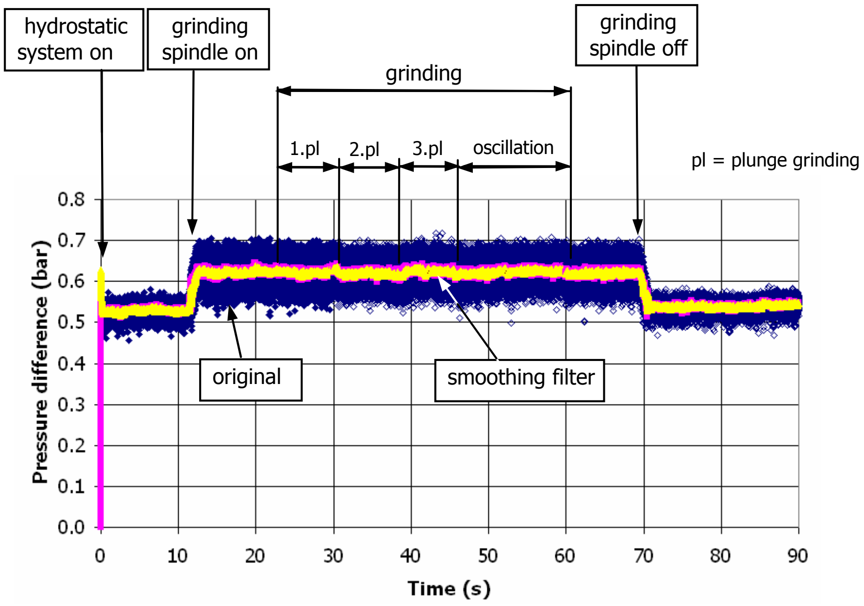

Figure 8.10: Sensor output from the grinding experiment

The cutting force measurement in internal plunge grinding was also carried out to investigate whether or not the normal force can be detected. The internal plunge grinding strategy, and the applied grinding data, is summarized in Figure 8.9. According to the estimations, the grinding force is very low in the grinding of small bores. As shown in Figure 8.10, the sensor signal shows no clear difference during grinding. Force monitoring was initiated with the running of the grinding spindle, and stopped with the completion of the grinding cycle. The noise appearing in the signal is higher than the grinding force. It can be influenced by the amount and pressure of coolant used in internal grinding.

8.1.2 Surface roughness

In both grinding and hard turning of small bores, investigations were carried out to reveal and define the effect of cutting data, grinding wheel wear, and cutting tool wear on the attainable surface roughness. Three-dimensional surface roughness topographies and parameters were compared and evaluated.

In the grinding experiments, the effects of wheel speed, depth of cut, oscillation speed, number of oscillations, and the spark-out time on the surface roughness were studied. The plunge grinding method was performed, which has already been presented in Figure 8.9. Among the investigated grinding parameters, grinding wheel speed (v_c), depth of cut (a_e) and oscillation speed (v_{fax}), the increase of the wheel speed enhances the surface roughness, while the depth of cut hardly affects it, and a higher oscillation speed generates a higher surface roughness (see Figure 8.11). Among the input parameters, the wheel speed and the oscillation speed have the highest influence on the surface roughness values. In applying higher cutting and oscillation speeds, the vibration increases, resulting in higher Ra and Rz values. The grinding parameters mainly affect the ten-point height of the profile.

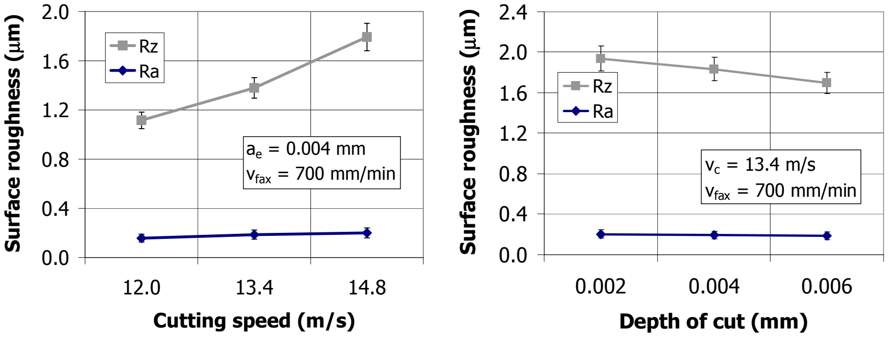

a) effect of the cutting speed

b) effect of the depth of cut

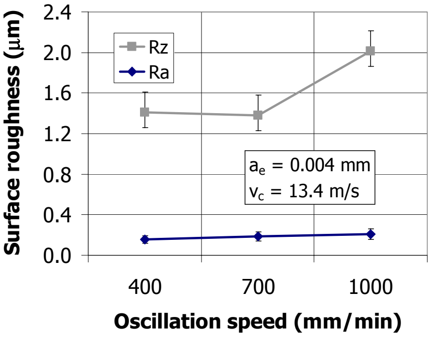

c) effect of the oscillation speed

Workpiece: 100Cr6
Diameter of the bore: 3 mm
Length to diameter ratio: 3
Machine tool: Slantbed Mikroturn 50CNC
Grinding wheel: Meister Abrasives CB111-325-P-7-260-150-V55-32

Internal plunge grinding:
q_s = 60
d_s = 2.7 mm
v_{frad} = 4.5 mm/min

Dressing:
n_s = 90000 1/min, v_c = 12.7 m/s
n_{dr} = 1830 1/min, q_d = 80, d_{dr} = 106 mm
a_d = 0.002 mm, v_{fd} = 100 mm/min

Figure 8.11: Effect of the grinding data on the surface roughness

With the increase of the number of oscillation movements, the surface roughness significantly reduces (see Figure 8.12). Without spark-out, and with using a spark-out time of 15 sec, the value of the arithmetical mean deviation of the profile is almost two times higher, compared to a spark-out time of 5 or 10 sec (see Figure 8.12a). However, the roughness values are approximately the same when applying either 5 or 10 seconds. The same trend can be observed with regard to the ten-point height of the profile (see Figure 8.12b). During spark-out and oscillation, the grinding forces decrease, which generate lower surface roughness.

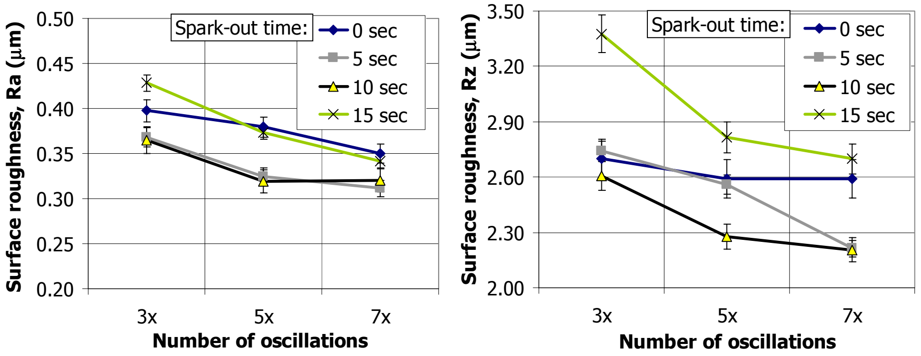

a) arithmetical mean deviation of the profile

b) ten-point height of the profile

Workpiece:	16MnCr5
Diameter of the bore:	4 mm
Length to diameter ratio:	2
Machine tool:	Slantbed Mikroturn 50CNC
Grinding wheel:	Meister Abrasives CB111-230-P-7-260-150-V55-32

Internal plunge grinding:
n_s = 90000 1/min, q_s = 60, v_w = 15.5 m/min
d_s = 3.5 mm, a_e = 0.004 mm
v_{frad} = 5 mm/min, v_{fax} = 400 mm/min

Dressing:
n_s = 90000 1/min, v_c = 16.5 m/s
n_{dr} = 2380 1/min, q_d = 80, d_{dr} = 106 mm
a_d = 0.002 mm, v_{fd} = 100 mm/min

Figure 8.12: Relationship between surface roughness, number of oscillations, and spark-out time

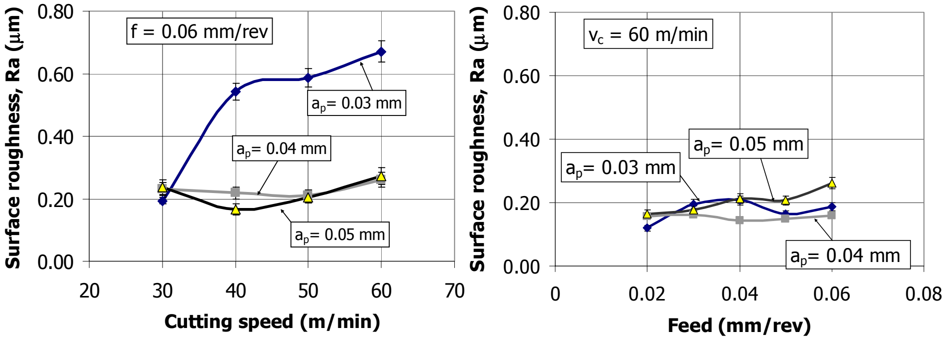

Workpiece:	100Cr6
Diameter of the bore:	4 mm
Length to diameter ratio:	4
Machine tool:	Slantbed Mikroturn 50CNC

Cutting tool:	Kennametal PCBN MKTB KB5625 MKTB31715R
Tool geometry:	γ_n = 0°, α_n = 10°, κ_r = 95°, rε=0.2 mm
Tool wear:	VB < 0.06 mm

Figure 8.13: Effect of cutting data on the average surface roughness, Ra, in turning

Figures 8.13 and 8.14 indicate the measured Ra and Rz roughness values in turning of bores with diameters of 4 mm. In hard turning, no clear trend can be found regarding the effect of the cutting data on the machining result. The depth of cut slightly influences the surface roughness except for a_p = 0.03 mm. With both the feed and the cutting speed, the roughness values fluctuate. This may be due to thermal and mechanical effects. The l/d ratio of the bore is 4. Depending on the applied cutting data, the tool bending generates fluctuating cutting forces, which generate a higher surface roughness. The thermal effect of the irregular values is that the optimal cutting temperature may not be achieved. This phenomenon has been already explained in detail in the force measurement summary.

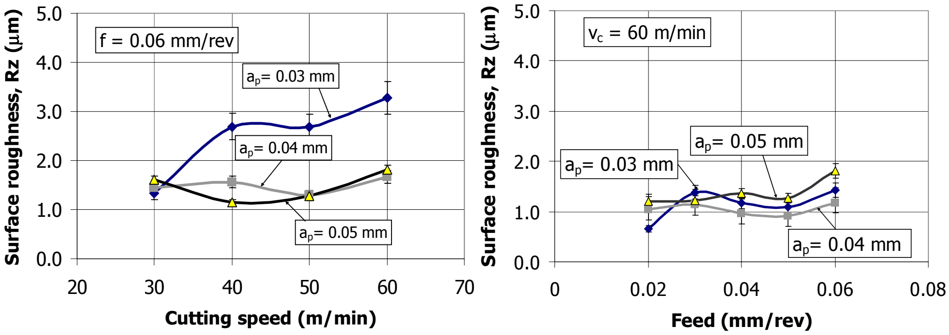

Workpiece: 100Cr6
Diameter of the bore: 4 mm
Length to diameter ratio: 4
Machine tool: Slantbed Mikroturn 50CNC

Cutting tool: Kennametal PCBN MKTB KB5625 MKTB31715R
Tool geometry: $\gamma_n = 0°$, $\alpha_n = 10°$, $\kappa_r = 95°$, $r\varepsilon$=0.2 mm
Tool wear: VB < 0.06 mm

Figure 8.14: Effect of cutting data on the ten-point height of the profile, Rz, in turning

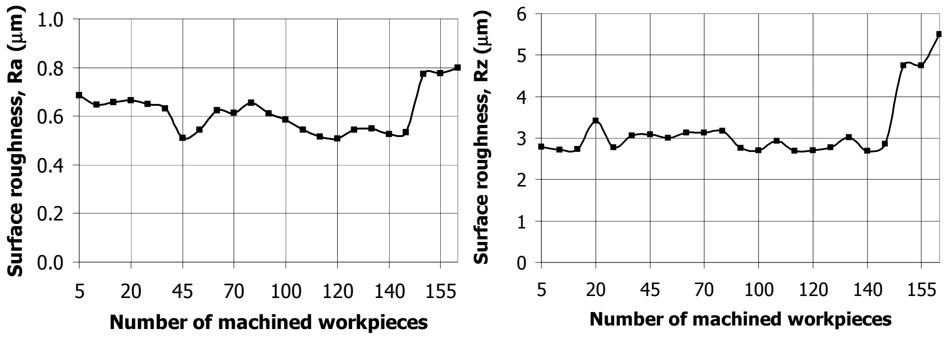

a) arithmetical mean deviation of the profile

b) ten-point height of the profile

Workpiece: 100Cr6
Diameter of the bore: 4 mm
Length to diameter ratio: 4
Machine tool: Slantbed Mikroturn 50CNC

Cutting tool: Kennametal PCBN MKTB KB5625 MKTB31715R
Tool geometry: $\gamma_n = 0°$, $\alpha_n = 10°$, $\kappa_r = 95°$, $r\varepsilon$=0.2 mm
Cutting data: v_c = 50 m/min, f = 0.06 mm/rev a_p= 0.03 mm

Figure 8.15: Surface roughness versus number of machined workpieces in turning

The surface roughness was analyzed in batch machining. The expected trend, that higher tool wear causes higher roughness values, is visible (Figure 8.15). The formation of surface roughness indicates a close connection to the cutting force arising in hard turning (Figure 8.8). The Rz values present more regularity, compared to the measured Ra surface roughness values.

Attainable surface roughness values were measured in the combination of grinding (finishing) and hard turning (roughing) in machining a small batch (45 pieces). Investigations were performed on case hardened steel, 16MnCr5. The bore diameter was 4 mm, while the length to diameter ratio was 2. As can be seen in Figure 8.16, the surface roughness increases with the increase of the width of flank wear land. The experiment proved that after the degressive wear of the cutting tool, the surface roughness is relatively constant for VB = 0.07-0.1 mm. With the extension of the width of flank wear land, the surface roughness deteriorates, and cutting tool change was necessary. After roughing, grinding was performed as a finishing process. The achieved Ra values varied between 0.08 and 0.12 μm. The grinding wheel was dressed only at the beginning of the test. No further dressing was done for the investigated 45 workpieces.

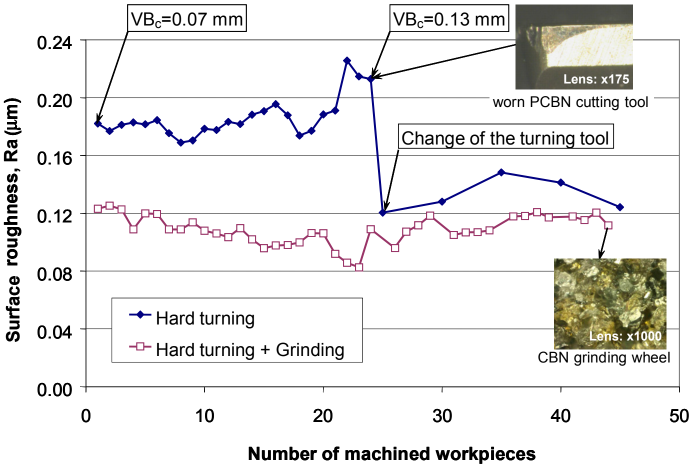

Workpiece:	16MnCr5
Diameter of the bore:	4 mm
Length to diameter ratio:	2
Machine tool:	Slantbed Mikroturn 50CNC

Hard turning:

Cutting tool:	PCBN BNBB04R
Tool geometry:	$\gamma_n = 0°$, $\alpha_n = 10°$, $\kappa_r = 95°$, $r\varepsilon$=0.2 mm
Cutting data:	v_c = 65 m/min, f = 0.03 mm/rev a_p= 0.035 mm

Internal plunge grinding:

Grinding wheel: Meister Abrasives
CB111-325-P-7-260-150-V55-32

Cutting data:
n_s = 90000 1/min, q_s = 60, v_w = 14.1 m/min
d_s = 3 mm, a_e = 0.004 mm
v_{frad} = 4.5 mm/min, v_{fax} = 400 mm/min
Spark-out time: 5 s

Dressing:
n_s = 90000 1/min, v_c = 14.1 m/s
n_{dr} = 2040 1/min, q_d = 80, d_{dr} = 106 mm
a_d = 0.002 mm, v_{fd} = 100 mm/min

Figure 8.16: Arithmetical mean deviation of the profile in combined machining

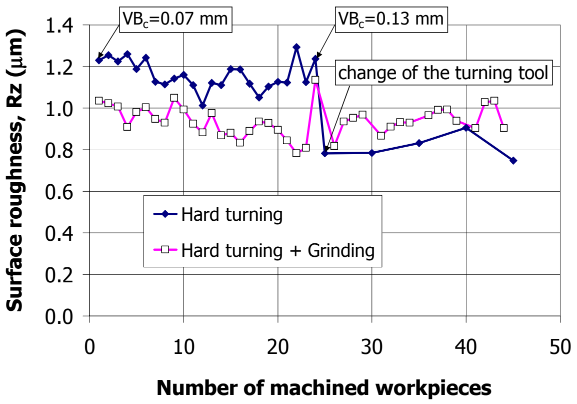

Internal plunge grinding:
Grinding wheel: Meister Abrasives
CB111-325-P-7-260-150-V55-32
Cutting data:
n_s = 90000 1/min, q_s = 60,
v_w = 14.1 m/min
d_s = 3 mm, a_e = 0.004 mm
v_{frad} = 4.5 mm/min,
v_{fax} = 400 mm/min
Spark-out time: 5 s

Dressing:
n_s = 90000 1/min, v_c = 14.1 m/s
n_{dr} = 2040 1/min, q_d = 80
d_{dr} = 106 mm
a_d = 0.002 mm, v_{fd} = 100 mm/min

Workpiece: 16MnCr5
Diameter of the bore: 4 mm
Length to diameter ratio: 2
Machine tool: Slantbed Mikroturn 50CNC

Hard turning:
Cutting tool: PCBN BNBB04R
Tool geometry: $\gamma_n = 0°$, $\alpha_n = 10°$, $\kappa_r = 95°$, $r\varepsilon$=0.2 mm
Cutting data: v_c = 65 m/min, f = 0.03 mm/rev
a_p= 0.035 mm

Figure 8.17: Ten-point height of the profile in combined machining

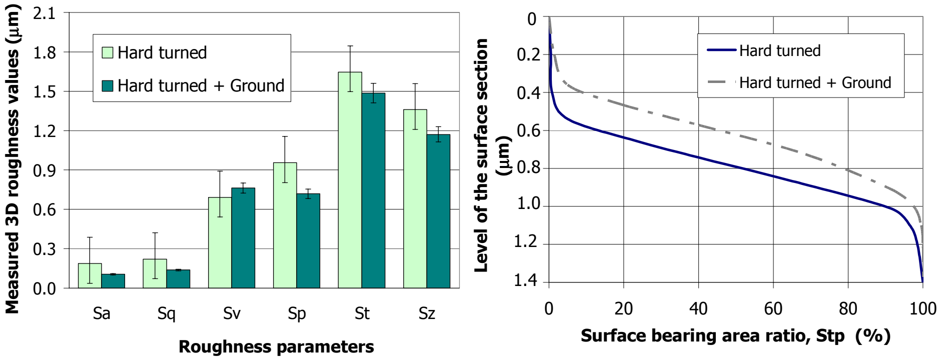

a) 3D roughness parameters

b) surface bearing area ratio

Workpiece: 16MnCr5
Diameter of the bore: 4 mm
Length to diameter ratio: 2
Machine tool: Slantbed Mikroturn 50CNC

Hard turning:
Cutting tool: PCBN BNBB04R
Tool geometry: $\gamma_n = 0°$, $\alpha_n = 10°$, $\kappa_r = 95°$, $r\varepsilon$=0.2 mm
Cutting data: v_c = 65 m/min, f = 0.03 mm/rev
a_p= 0.035 mm
Tool wear: VB < 0.06 mm

Internal plunge grinding:
Grinding wheel: Meister Abrasives
CB111-325-P-7-260-150-V55-32
Cutting data:
n_s = 90000 1/min, q_s = 60, v_w = 14.1 m/min
d_s = 3 mm, a_e = 0.004 mm
v_{frad} = 4.5 mm/min, v_{fax} = 400 mm/min
Spark-out time: 5 s

Dressing:
n_s = 90000 1/min, v_c = 14.1 m/s
n_{dr} = 2040 1/min, q_d = 80, d_{dr} = 106 mm
a_d = 0.002 mm, v_{fd} = 100 mm/min

Figure 8.18: Three-dimensional roughness parameters

In studying the ten-point height of the profile, the differences between the roughness values of hard turned and hard turned plus ground workpieces is less (Figure 8.17). When VB = 0.07-0.13 mm, the Rz values vary between 1.0 and 1.3 μm. When using a sharp tool, the values are approximately the same for both cases, or lower for the hard turned surface.

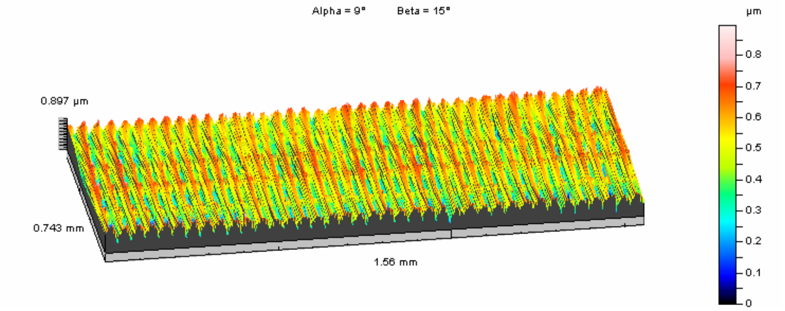

a) hard turned surface

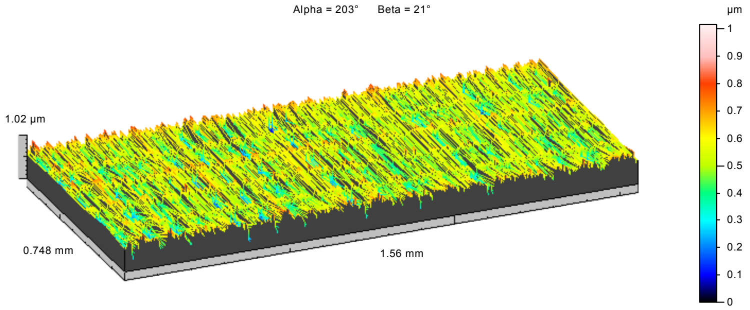

b) ground surface

Figure 8.19: Comparison of the surface topography

Besides the two-dimensional roughness parameters, three-dimensional values and surface topographies were also studied. The properties of the spatial texture can be determined more precisely by 3D parameters. The tribological and sealing factors are related to the three-dimensional nature of the surface [HUM01]. The two dimensional profile can easily miss the predominant peaks and valleys which exist. Among the three-dimensional characteristics, the amplitude and functional (Stp) parameters were investigated. The amplitude, or height distribution parameters, indicate more advantageous values after combined machining (see Figure 8.18). The arithmetic mean deviation of the surface (Sa) is 0.19 μm after hard turning, which can be reduced with application of grinding. Similarly to the Sa, the root-mean-square deviation of surface topography (Sq), measures the deviation of the surface points from the root-mean-square of the surface, but is more sensitive to the high surface peak heights and/or deep valley depths. In comparing the other spatial roughness parameters, it can be stated that the application of grinding as a finishing process is beneficial for the machining of small bores. The surface bearing area ratio also indicates different characteristics in the machining of small bores (Figure 8.18b), than in machining of bores with bigger diameters, as presented in Chapter 7. The surface bearing area ratio defines the bearing properties of the surface. A larger surface bearing area ratio indicates a better bearing property. When comparing it after hard turning and combined machining, it is evident that the hard turned and ground surface has a higher surface bearing area ratio. Typical hard turned and ground surfaces are presented in Figure 8.19. In the hard turned bore, the surface is smooth and regular, while the surface of the ground topography has a random characteristic.

8.1.3 Macro geometrical accuracy

As well as in the case of surface roughness, similar investigations were carried out to explore the effect of cutting data, grinding wheel wear, and cutting tool wear on the attainable macro geometrical accuracy. In the grinding experiments, the effects of wheel speed, depth of cut, oscillation speed, number of oscillations, and the spark-out time on the macro geometrical accuracy were studied. The plunge grinding method was performed, as previously presented in Figure 8.9.

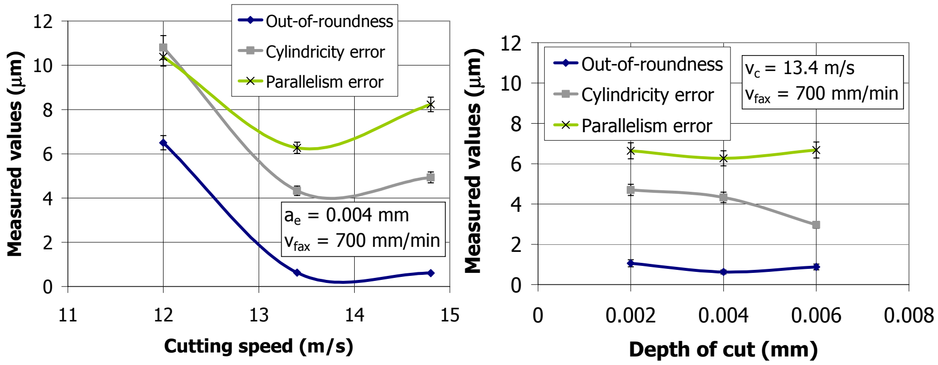

a) effect of the revolution

b) effect of the depth of cut

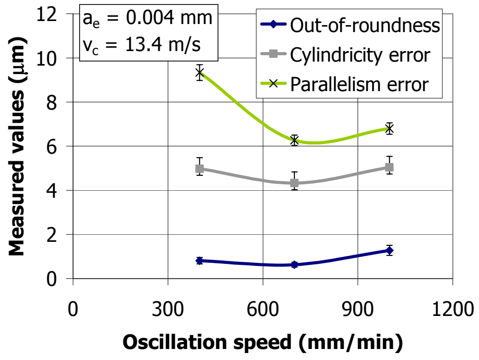

c) effect of the oscillation speed

Workpiece: 100Cr6
Diameter of the bore: 3 mm
Length to diameter ratio: 3
Machine tool: Slantbed Mikroturn 50CNC
Grinding wheel: Meister Abrasives CB111-230-P-7-260-150-V55-32

Internal plunge grinding:
$q_s = 60$, $d_s = 2.7$ mm
$v_{frad} = 4.5$ mm/min
Spark-out time: 5 s

Dressing:
$n_s = 90000$ 1/min, $v_c = 12.7$ m/s
$n_{dr} = 1830$ 1/min, $v_{dr} = 10.2$ m/s
$q_d = 80$, $d_{dr} = 106$ mm
$a_d = 0.002$ mm, $v_{fd} = 100$ mm/min

Figure 8.20: Effect of grinding data on the macro geometrical accuracy

Among the studied grinding parameters, the increase of the grinding wheel speed decreases all geometrical accuracy values, but increases the surface roughness (Figure 8.20). A grinding wheel revolution of 90000 rpm is suitable for the machining of small bores, as vibrations will occur with any higher value. The variation of depth of cut in plunge grinding negligibly influences the macro geometrical errors (Figure 8.20b). From the process point of view, a higher depth of cut would be more beneficial. However, it would increase the grinding forces and temperature, which deteriorate the surface quality. The most beneficial option may be to use a higher depth of cut in the first grinding cut, and to reduce it in finishing.

With the increase of the oscillation speed, the parallelism error decreases, while the out-of-roundness and the cylindricity errors only slightly change (Figure 8.20c). The usage of a higher oscillation speed is not necessary, as it would cause higher surface roughness. In finishing, the oscillation speed must be decreased.

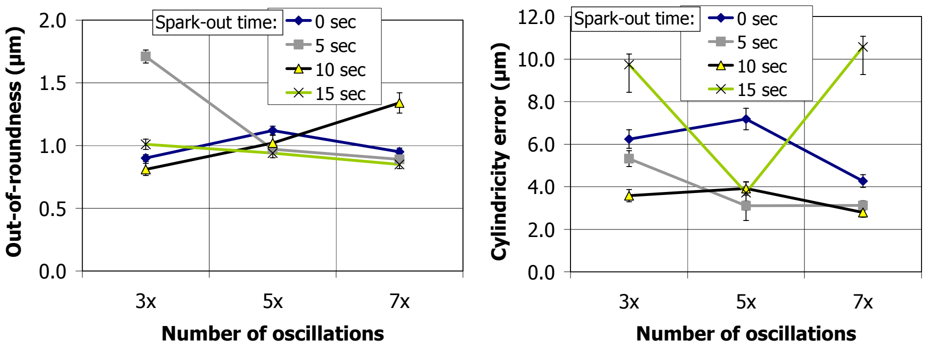

a) out-of-roundness

b) cylindricity error

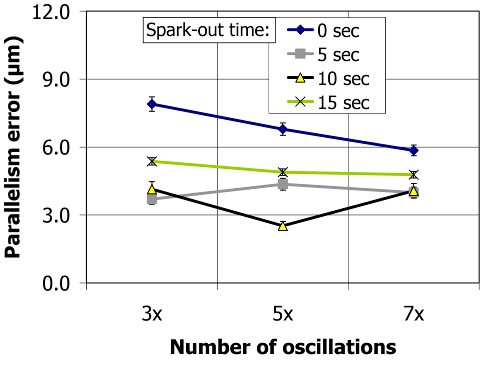

c) parallelism error

Workpiece:	16MnCr5
Diameter of the bore:	4 mm
Length to diameter ratio:	2
Machine tool:	Slantbed Mikroturn 50CNC
Grinding wheel:	Meister Abrasives CB111-230-P-7-260-150-V55-32

Internal plunge grinding:
n_s = 90000 1/min, q_s = 60, v_w = 15.5 m/min
d_s = 3.5 mm, a_e = 0.004 mm
v_{frad} = 5 mm/min, v_{fax} = 400 mm/min

Dressing:
n_s = 90000 1/min, v_c = 16.5 m/s
n_{dr} = 2380 1/min, v_{dr} = 13.2 m/s
q_d = 80, d_{dr} = 106 mm
a_d = 0.002 mm, v_{fd} = 100 mm/min

Figure 8.21: Relationship between macro geometrical accuracy, number of oscillations, and spark-out time

The number of oscillation movements has no significant influence on the geometrical accuracy (Figure 8.21). However, it does have a significant effect on the surface roughness, and therefore, the increase in the number of oscillation movements is necessary. The effects of spark-out time and the number of oscillations are the same. Without spark-out, and with long spark-out time (15 s), the surface roughness deteriorates. A spark-out time of 5 s is enough to reduce the grinding force.

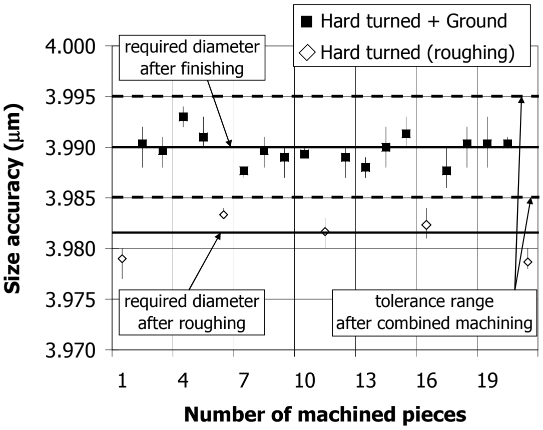

Internal plunge grinding:

Grinding wheel: Meister Abrasives CB111-325-P-7-260-150-V55-32

Cutting data:

n_s = 90000 1/min, q_s = 60,
v_w = 14.1 m/min
d_s = 3 mm, a_e = 0.004 mm
v_{frad} = 4.5 mm/min,
v_{fax} = 400 mm/min
Spark-out time: 5 s

Dressing:

n_s = 90000 1/min, v_c = 14.1 m/s
n_{dr} = 2040 1/min, q_d = 80
d_{dr} = 106 mm
a_d = 0.002 mm, v_{fd} = 100 mm/min

Workpiece:	16MnCr5
Diameter of the bore:	4 mm
Length to diameter ratio:	2
Machine tool:	Slantbed Mikroturn 50CNC

Hard turning:

Cutting tool:	PCBN BNBB04R
Tool geometry:	γ_n = 0°, α_n = 10°, κ_r = 95°, $r\varepsilon$=0.2 mm
Cutting data:	v_c = 65 m/min, f = 0.03 mm/rev a_p= 0.035 mm

Figure 8.22: Achieved size accuracy in combined machining

In studying the size accuracy in combined machining, the obtained results can be given a good rating. After hard turning, the required diameter was 3.982 mm, and 3.990 mm for grinding (Figure 8.22). In the investigated range, according to the number of machined workpieces, the size accuracy fulfils the tolerance, which is ±0.005 mm. Moreover, the scattering of the measured values is quite small. The out-of-roundness was measured, with regard to the form accuracy. In Figure 8.23, the obtained out-of-roundness values are plotted. After hard turning, the out-of-roundness values varied between 0.0004 and 0.0015 mm, which decreased when the finish grinding operation was accomplished. The average value of the out-of-roundness for the finished bore is 0.0004-0.0007 mm, which is below the prescribed tolerance.

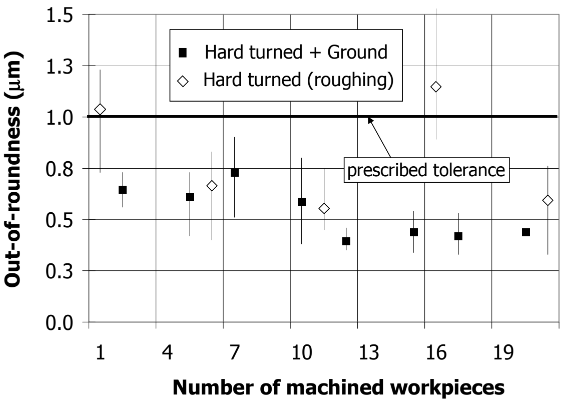

Internal plunge grinding:
Grinding wheel: Meister Abrasives CB111-325-P-7-260-150-V55-32
Cutting data:
n_s = 90000 1/min, q_s = 60,
v_w = 14.1 m/min
d_s = 3 mm, a_e = 0.004 mm
v_{frad} = 4.5 mm/min,
v_{fax} = 400 mm/min
Spark-out time: 5 s

Dressing:
n_s = 90000 1/min, v_c = 14.1 m/s
n_{dr} = 2040 1/min, q_d = 80
d_{dr} = 106 mm
a_d = 0.002 mm, v_{fd} = 100 mm/min

Workpiece: 16MnCr5
Diameter of the bore: 4 mm
Length to diameter ratio: 2
Machine tool: Slantbed Mikroturn 50CNC

Hard turning:
Cutting tool: PCBN BNBB04R
Tool geometry: $\gamma_n = 0°$, $\alpha_n = 10°$, $\kappa_r = 95°$, $r\varepsilon$=0.2 mm
Cutting data: v_c = 65 m/min, f = 0.03 mm/rev
a_p= 0.035 mm

Figure 8.23: Achieved form accuracy in combined machining

8.1.4 Effect of l/d ratio on the machining result

As a new alternative in the machining of injection nozzles, hard turning and grinding can be combined. The bore to be machined is small and long. The tools used in the machining bend, which generate geometrical errors. In grinding, the errors caused by tool bending can be reduced with spark-out, which diminishes the forces, and results in better surface quality. In addition to this, in turning, it is not possible to cut under a certain value of chip thickness. Therefore, cutting forces cannot be reduced to near zero. The aim of combined machining is to remove as much material as possible with roughing. In this case, hard turning is applied as a roughing process, and must ensure proper accuracy for finishing. The grinding allowance must cover the machining errors caused by turning. The question then becomes, how much allowance is required in grinding to remove the machining errors issuing from turning? This investigation aims to reveal the machining errors generated in the combination of hard turning and grinding, with respect to different l/d ratios and diameters of the machined bore. The length to diameter ratios vary between 2 and 4, while the bore diameters are 3 and 4 mm.

The measurements performed with an l/d = 3 indicate a remarkably reduced surface roughness in grinding (Figure 8.24). The Ra and Rz values are 3-5 times higher in turning, compared to grinding. After finishing, the attainable Ra is 0.070 µm for d = 3 mm, and 0.123 µm for d = 4 mm. A better surface roughness was accomplished with the diameter of 3 mm. At l/d = 4, the roughness values increase, as Ra is 0.13 µm after grinding of d = 3 mm. It is 0.17 µm, for a d = 4 mm (Figure 8.25). In this case, the roughness values are also lower when a diameter of 3 mm is machined.

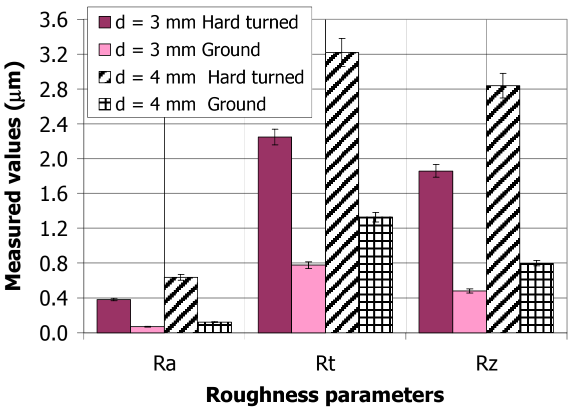

Internal plunge grinding:
Grinding wheel:
Meister Abrasives
CB111-325-P-7-260-150-V55-32

Cutting data:
V_c = 12.7, 16.5 m/s, q_s = 60
v_w = 12.7, 16.5 m/min,
d_s = 2.7, 3.5 mm
a_e = 0.004 mm, v_{frad} = 5 mm/min
v_{fax} = 400 mm/min
Spark-out time: 5 s

Dressing:
v_c = 12.7, 16.5 m/s
n_{dr} = 1830, 2380 1/min, q_d = 80
d_{dr} = 106 mm, a_d = 0.002 mm
v_{fd} = 100 mm/min

Workpiece: 100Cr6
Diameter of the bore: 3, 4 mm
Length to diameter ratio: 3
Machine tool: Slantbed Mikroturn 50CNC

Hard turning:
Cutting tool: Kennametal PCBN MKTB KB5625
Tool geometry: $\gamma_n = 0°$, $\alpha_n = 10°$, $\kappa_r = 95°$, $r\varepsilon$=0.2 mm
Cutting data: v_c = 50 m/min, f = 0.03 mm/rev
a_p= 0.03 mm
Tool wear: VB_c = 0.1 mm

Figure 8.24: Surface roughness, l/d = 3

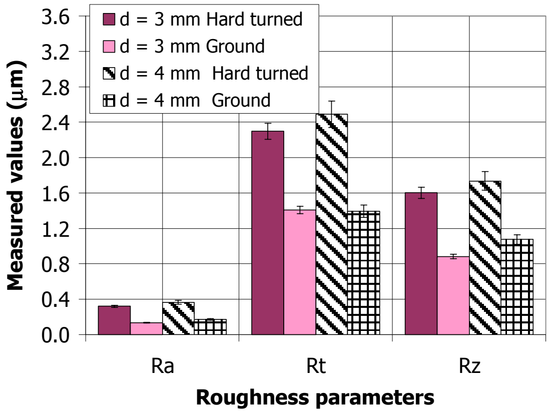

Internal plunge grinding:
Grinding wheel:
Meister Abrasives
CB111-325-P-7-260-150-V55-32

Cutting data:
V_c = 12.7, 16.5 m/s, q_s = 60
v_w = 12.7, 16.5 m/min,
d_s = 2.7, 3.5 mm
a_e = 0.004 mm, v_{frad} = 5 mm/min
v_{fax} = 400 mm/min
Spark-out time: 5 s

Dressing:
v_c = 12.7, 16.5 m/s
n_{dr} = 1830, 2380 1/min, q_d = 80
d_{dr} = 106 mm, a_d = 0.002 mm
v_{fd} = 100 mm/min

Workpiece: 100Cr6
Diameter of the bore: 3, 4 mm
Length to diameter ratio: 4
Machine tool: Slantbed Mikroturn 50CNC

Hard turning:
Cutting tool: Kennametal PCBN MKTB KB5625
Tool geometry: $\gamma_n = 0°$, $\alpha_n = 10°$, $\kappa_r = 95°$, $r\varepsilon$=0.2 mm
Cutting data: v_c = 50 m/min, f = 0.03 mm/rev
a_p= 0.03 mm
Tool wear: VB = 0.1 mm

Figure 8.25: Surface roughness, l/d = 4

With regard to the macro geometrical accuracy, the out-of-roundness, cylindricity error, and parallelism error were measured. Macro geometrical accuracy achieved by turning is shown in Figure 8.26.

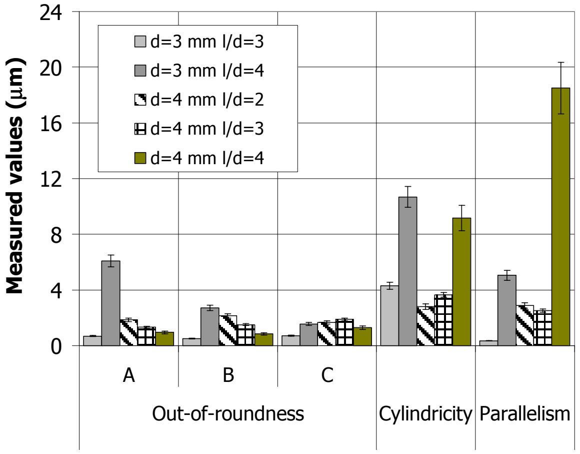

Workpiece: 100Cr6
Diameter of the bore: 3, 4 mm
Length to diameter ratio: 2-4
Machine tool:
Slantbed Mikroturn 50CNC

Hard turning:
Cutting tool: Kennametal PCBN MKTB KB5625
Tool geometry: $\gamma_n = 0°$, $\alpha_n = 10°$
$\kappa_r = 95°$
$r\varepsilon = 0.2$ mm
Cutting data: $v_c = 50$ m/min
f = 0.03 mm/rev
$a_p = 0.03$ mm
Tool wear: $VB_c = 0.1$ mm

Figure 8.26: Macro geometrical accuracy achieved after hard turning

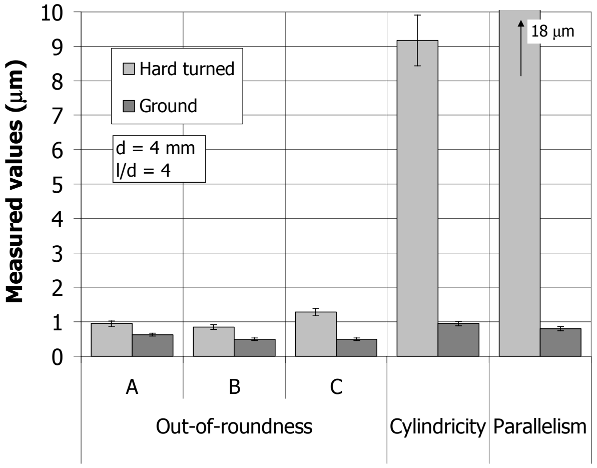

Internal plunge grinding:
Grinding wheel:
Meister Abrasives
CB5-500-Q-10-195-200-V55-31

Cutting data:
$V_c = 16.5$ m/s, $q_s = 60$
$v_w = 16.5$ m/min
$d_s = 3.5$ mm
$a_e = 0.004$ mm, $v_{frad} = 5$ mm/min
$v_{fax} = 400$ mm/min
Spark-out time: 5 s

Dressing:
$v_c = 16.5$ m/s
$n_{dr} = 2380$ 1/min, $q_d = 80$
$d_{dr} = 106$ mm, $a_d = 0.002$ mm
$v_{fd} = 100$ mm/min

Workpiece: 100Cr6
Diameter of the bore: 4 mm
Length to diameter ratio: 4
Machine tool: Slantbed Mikroturn 50CNC

Hard turning:
Cutting tool: Kennametal PCBN MKTB KB5625
Tool geometry: $\gamma_n = 0°$, $\alpha_n = 10°$, $\kappa_r = 95°$, $r\varepsilon = 0.2$ mm
Cutting data: $v_c = 50$ m/min, f = 0.03 mm/rev
$a_p = 0.03$ mm
Tool wear: $VB_c = 0.1$ mm

Figure 8.27: Comparison of macro geometrical accuracy, d= 4 mm, l/d = 4

The maximum value of the out-of-roundness is 6 μm, and its lowest value was 0.52 μm. It was measured in three planes in the bore. Higher l/d ratios generate higher macro geometrical errors. Due to the cutting temperature, cutting forces, and the bending of the cutting tool, the surface is conical. Both the cylindricity error and the parallelism error remain below 5 μm at l/d = 2 and 3. The cylindricity error exceeds 10 μm, when machining a bore with l/d = 4. Furthermore, high parallelism errors were also measured at d= 4 mm, and l/d = 4. This means that the grinding allowance should be between 10-20 μm, considering the length to diameter ratio. With the increase of the l/d ratio, more grinding cuts are needed to achieve a completely ground surface.

After grinding, the out-of-roundness decreased in comparison to hard turning, when the machining diameter of 4 mm and l/d = 4 was used (Figure 8.27). Grinding can significantly reduce the positional errors, if performed after hard turning.

8.1.5 Surface layer properties

With regard to the surface integrity in the machining of small bores with a diameter of 4 mm, and a length to diameter ratio of 2, microhardness measurements were performed and the appearance of the white layer was studied. The workpiece has a blind hole. The material of the test workpiece is case hardened steel, 16MnCr5. The microhardness measurement indicates different features after machining, related to the non-machined part (see Figure 8.28).

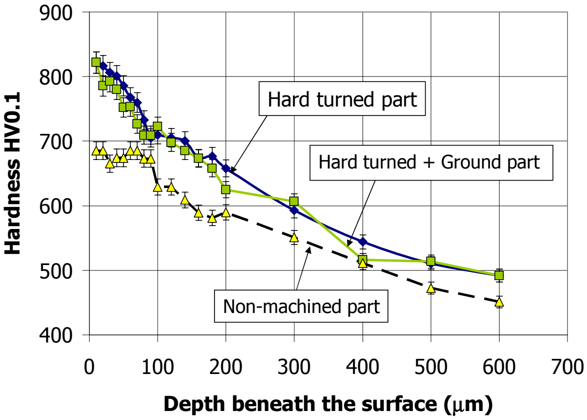

Internal plunge grinding:
Grinding wheel:
Meister Abrasives
CB111-325-P-7-260-150-V55-32

Cutting data:
n_s = 90000 1/min, q_s = 60
v_w = 14.1 m/min, d_s = 3 mm
a_e = 0.004 mm, v_{frad} = 4.5 mm/min
v_{fax} = 400 mm/min
Spark-out time: 5 s

Dressing:
n_s = 90000 1/min, v_c = 14.1 m/s
n_{dr} = 2040 1/min, q_d = 80
d_{dr} = 106 mm, a_d = 0.002 mm
v_{fd} = 120 mm/min

Workpiece: 16MnCr5
Diameter of the bore: 4 mm
Length to diameter ratio: 2
Machine tool: Slantbed Mikroturn 50CNC

Hard turning:
Cutting tool: PCBN BNBB04R
Tool geometry: $\gamma_n = 0°$, $\alpha_n = 10°$, $\kappa_r = 95°$, $r\varepsilon$=0.2 mm
Cutting data: v_c = 65 m/min, f = 0.03 mm/rev a_p= 0.035 mm
Tool wear: VB_c = 0.125 mm

Figure 8.28: Microhardness change in combined machining

The microhardness curves measured after heat treatments do not include the hardness values of the removed material. This means that the hardness values of the allowance (0.15 mm) was removed from the plotted curves. After hard turning applied as a roughing process, the surface layer presents higher microhardness close to the surface. The maximum value of the measured microhardness was 837 HV0.1. Grinding was employed as a finishing process, following hard turning. As the grinding allowance is small, the applied depth of cut is only 0.004 mm, and therefore the grinding process hardly influences the microhardness generated by hard turning.

The thermo-mechanical effect occurring in machining can cause changes in the surface integrity. The purpose of the microstructural investigation was to determine the possible change in the microstructure when applying combined machining.

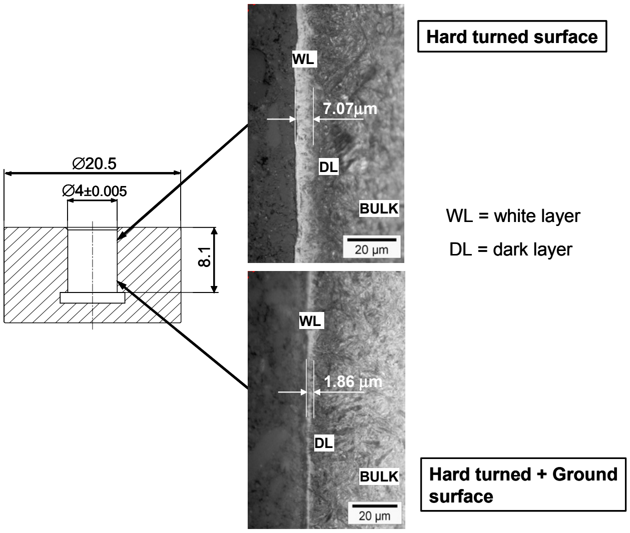

Internal plunge grinding:
Grinding wheel:
Meister Abrasives
CB111-325-P-7-260-150-V55-32

Cutting data:
n_s = 90000 1/min
q_s = 60
v_w = 14.1 m/min
d_s = 3 mm
a_e = 0.004 mm
v_{frad} = 4.5 mm/min
v_{fax} = 400 mm/min

Dressing:
n_s = 90000 1/min
v_c = 14.1 m/s
n_{dr} = 2040 1/min
q_d = 80
d_{dr} = 106 mm
a_d = 0.002 mm
v_{fd} = 120 mm/min

Workpiece:	16MnCr5
Diameter of the bore:	4 mm
Length to diameter ratio:	2
Machine tool:	Slantbed Mikroturn 50CNC

Hard turning:

Cutting tool:	PCBN BNBB04R
Tool geometry:	$\gamma_n = 0°$, $\alpha_n = 10°$, $\kappa_r = 95°$, $r\varepsilon$=0.2 mm
Cutting data:	v_c = 65 m/min, f = 0.03 mm/rev a_p= 0.035 mm
Tool wear:	VB_c = 0.125 mm

Figure 8.29: White layer in the machining of small bores

The thermo-mechanical effects are different in hard turning and grinding. In turning, the contact length between the tool and workpiece is much shorter than in grinding. Compared to grinding, the contact time is less, and the temperature gradient is higher for hard turning. Therefore, the conditions of the metallurgical transformations can be different [KAR03]. The specific cutting power

(P''_c) and the specific heat quantity (q''_w) are higher in hard turning [TÖN98], [BRI99], [KAR03], whereas the specific travelling energy (e''_w) is much lower due to the shorter contact time.

In the machining of small bores, the white layer generation was observed after hard turning (see Figure 8.29). The machined bore has a blind hole and a small diameter, and therefore the heat removal is less efficient. In the turning of small bores, the applicable cutting speed is much lower than the cutting speed generally applied in hard turning. For finishing, it is usually higher than 120 m/min. The contact time between tool and workpiece will increase due to this.

The common effect of the circumstances mentioned above may contribute to the generation of white layers after hard turning. The maximum thickness of the white layer is 7.07 μm, whereas after grinding, this thickness is reduced to 1.86 μm. Furthermore, along the length of the bore in some places, it disappeared altogether. Under the white layer, a so-called dark layer can also be observed. It is softer than the white layer, thus a Knoop hardness measurement was performed, to determine the hardness close to the surface (see Figure 8.30). It is clearly evident that the surface has a lower hardness at a depth of 10 μm.

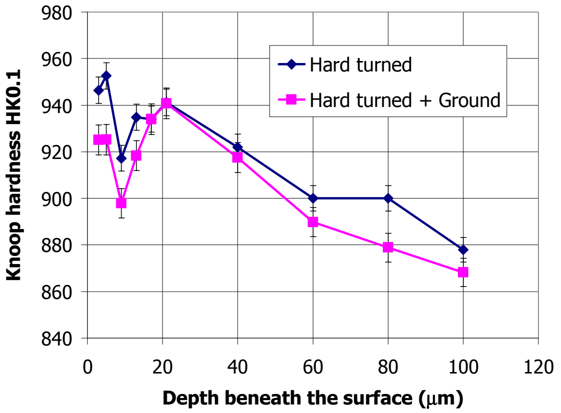

Internal plunge grinding:
Grinding wheel:
Meister Abrasives
CB111-325-P-7-260-150-V55-32

Cutting data:
n_s = 90000 1/min, q_s = 60
v_w = 14.1 m/min, d_s = 3 mm
a_e = 0.004 mm, v_{frad} = 4.5 mm/min
v_{fax} = 400 mm/min
Spark-out time: 5 s

Dressing:
n_s = 90000 1/min, v_c = 14.1 m/s
n_{dr} = 2040 1/min, q_d = 80
d_{dr} = 106 mm, a_d = 0.002 mm
v_{fd} = 120 mm/min

Workpiece:	16MnCr5
Diameter of the bore:	4 mm
Length to diameter ratio:	2
Machine tool:	Slantbed Mikroturn 50CNC

Hard turning:

Cutting tool:	PCBN BNBB04R
Tool geometry:	$\gamma_n = 0°$, $\alpha_n = 10°$, $\kappa_r = 95°$, $r\varepsilon$=0.2 mm
Cutting data:	v_c = 65 m/min, f = 0.03 mm/rev a_p= 0.035 mm
Tool wear:	VB_c = 0.125 mm

Figure 8.30: Knoop hardness measurement

With regard to the results due to the small grinding allowance, the finish grinding process does not modify the microstructure features. Moreover, it can reduce the thickness of the white layer generated by hard turning, or can remove it completely. When studying the surface quality in combined machining, it was found that combination of hard turning and grinding provided more benefits. Grinding lowers the surface roughness values and macro geometrical errors, and ensures such surface integrity. This is advantageous with respect to the functional behaviour of the components.

8.2 Models to predict the performance of combined machining

8.2.1 Empirical model for determination of cutting forces

On the basis of the performed investigations, the empirical model of the cutting force in the machining of small bores can be determined. Taking into account the cutting data, and the area of flank wear land, the passive force, F_p can be predicted as:

$$F_p = 4.7951 \cdot 10^3 \cdot v_c^{-1.24} + 1.1501 \cdot v_c \cdot a_p^{0.01} - 198.9669 \cdot f^{0.20} + 11.1466 \cdot f^{1.25} \cdot A_{VB}^{0.48} \qquad (8.1)$$

R^2=0.9070.

The coefficient of determination is 0.9070, which means a proper approximation of the empirical model for the prediction of passive force. Mainly, it is the cutting speed and the feed that affect the passive force.

Figure 8.31 indicates the common effect of the variables on the passive force. Figure 8.31a presents the effect of the feed and cutting speed on the cutting force. The influence of tool wear and cutting speed is given in Figure 8.31b.

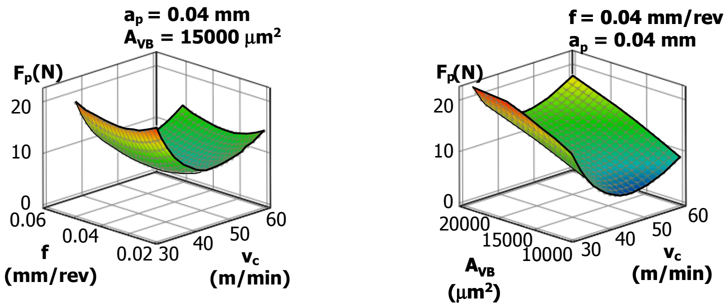

a) effect of the feed and cutting speed

b) effect of the cutting peed and the tool wear

Figure 8.31: Relationship between cutting data and passive force according to the empirical modelling

8.2.2 Modelling of surface roughness

In qualifying the workpieces after finishing, the surface roughness is significantly important. There are several empirical models, which predict the roughness values with respect to the cutting speed, speed ratio, equivalent diameter, depth of cut, and specific material removal [TÖN92]. These models forecast the ten-point height of the profile, or the total height of the profile. In grinding of small bores, the arithmetical mean deviation of the profile was modelled, as it was prescribed for the bore of injection nozzles. With respect to the cutting data, the wheel speed, the working engagement, and the oscillation speed are taken into account.

With regard to the grinding parameters the arithmetical mean deviation of the profile can be formulated with Equation 8.2 as:

$$Ra = 0.03 \cdot v_c^{0.164} \cdot a_e^{-0.088} \cdot v_{fax}^{0.138} \qquad (8.2)$$

$R^2 = 0.9156$

Generally, a higher cutting speed reduces the surface roughness, however, this is not valid in small bores. In internal grinding of injection nozzles, a high revolution is applied ($n \geq 85000$ rpm), vibration develops, which causes higher force, and leads to higher roughness values. In addition to the wheel speed, the oscillation speed also significantly determines the machining results. Higher oscillation speeds enhance the Ra values. The working engagement applied in grinding is small, and therefore has no relevant influence on the roughness. In Figure 8.32, the common effect of these parameters is presented.

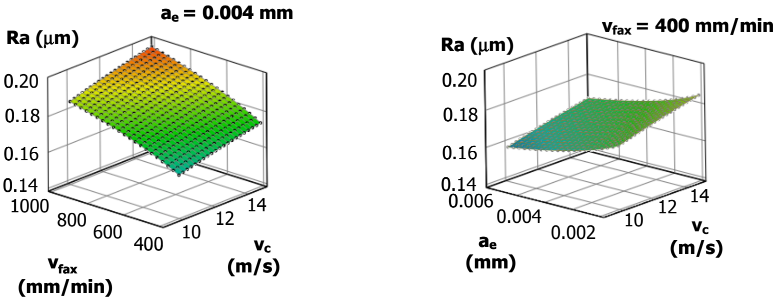

a) a_e = 0.004 mm b) v_{fax} = 400 mm/min

Figure 8.32: Relationship between cutting data and surface roughness, according to the empirical modelling

In the turning of small bores, it was observed that in addition to the cutting parameters, the area of flank wear land, rather than the width of flank wear land, is a determinant. With respect to the four variables (v_c, a_p, f, A_{VB}), the surface roughness (Ra, Rz), can be modelled as:

$$Ra = -0.8392 \cdot v_c^{0.4} + 7.0308 \cdot 10^{-4} \cdot f^{1.3} \cdot a_p^{-2.8} + 5.2928 - 9.7892 \cdot 10^{3} \cdot v_c^{-1.00} \cdot A_{VB}^{-0.55}$$

R^2=0.9091 (8.3)

$$Rz = -2.9424 \cdot 10^{-15} \cdot v_c^{7.8} + 8.29 \cdot 10^{-15} \cdot a_p^{-9.1} + 0.7487 \cdot f^{-0.1} + 0.5478 \cdot f^{7.9} \cdot A_{VB}^{2.4}$$

R^2=0.8956 (8.4).

In analysing the measured roughness values, the irregularity of the measured Ra and Rz values was found when changing the cutting data (see Chapter 8.1.2). They have no unambiguous increasing or decreasing trend on the surface roughness, which is clearly displayed in Figure 8.33.

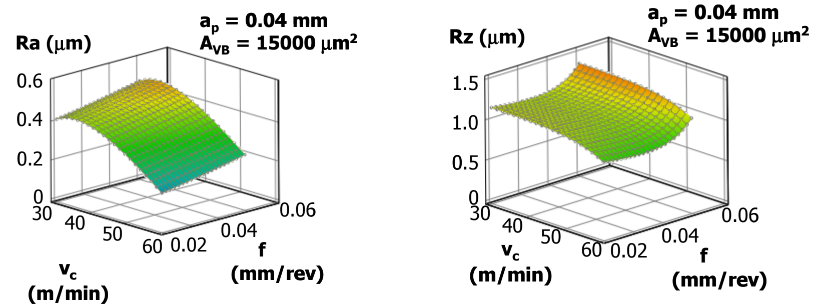

a) arithmetical mean deviation of the profile b) ten-point height of the profile

Figure 8.33: Relationship between the cutting data and surface roughness, according to the empirical modelling

8.2.3 Effect of l/d ratio on the machining accuracy

In turning and plunge grinding, the system can be regarded as rigid enough, if a tool with a short length and relatively large diameter is used. In manufacturing injection nozzles, the bore is long and small. Therefore, a turning tool and grinding quill with a small diameter and long shaft are applied. The geometrical errors, which arise in machining, depend on the cutting forces, mainly the passive force of turning and normal force of grinding. To determine the size, form, and positional errors in combined machining, the tool bending must be calculated. In the investigation of the effect of l/d ratio on the machining result, it was proved that the machining errors caused by hard turning are the determinants, which must be removed with grinding (see Chapter 8.1.4). Therefore, it is necessary to forecast the grinding allowance.

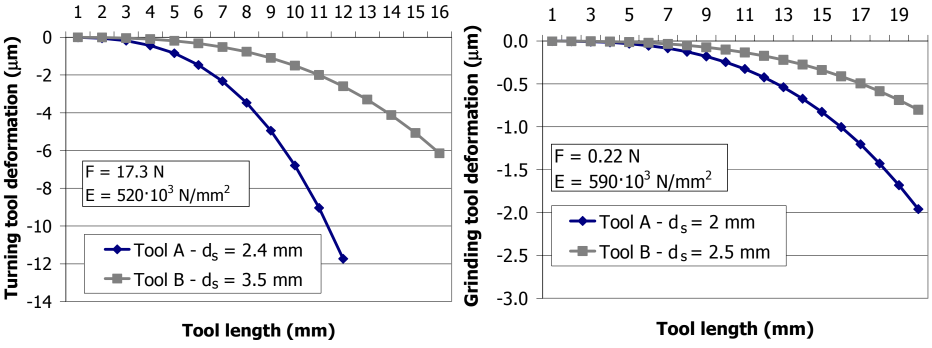

a) turning tool bending b) grinding tool bending

Figure 8.34: Tool deflection

TURNING

Workpiece: d = 4 mm, R1 = 2 mm, l/d = 4

Cutting tool:

$l_s = 18$ mm, $d_t = 3.5$ mm

Young modulus of the cutting tool material:

E = 520 GPa

Cutting data:

$v_c = 60$ m/min, f= 0.06 mm/rev, $a_p = 0.04$ mm

Cutting forces according to the measurements:

$F_p = 17.24$ N

$F_p = 1.3 \cdot F_c$, $F_c = 13.26$ N

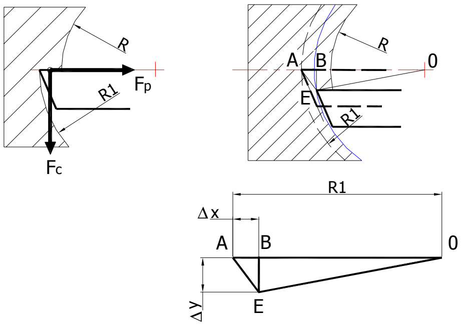

Mechanical distortion in turning:

$$\Delta d_w = 2(\overrightarrow{OA} - \overrightarrow{OE}) = 2(R1 - \overrightarrow{OE})$$

$$\overrightarrow{OE} = \sqrt{(R1 - \Delta x)^2 + \Delta y^2}$$

$$\Delta x = \frac{F_p \cdot l_s^3}{3EI} \qquad \Delta y = \frac{F_c \cdot l_s^3}{3EI}$$

$$I = \frac{\pi}{64} \cdot d_t^4$$

$\Delta d_w = 12.3\ \mu m$

GRINDING

Workpiece: d = 4 mm, R1 = 2 mm, l/d = 4

Grinding quill:

$l_s = 18$ mm, $d_t = 2$ mm, a = 15 mm

Grinding wheel: $b_s = 6$ mm, $d_s = 3.5$ mm

Young modulus of the cutting tool material:

E = 590 GPa

Grinding data:

$a_e = 0.005$ mm, q= 60,

$$d_{eq} = \frac{d_s}{1 - \frac{d_s}{d}} = 35$$

Normal force according to Equation 8.5:

$F'_n = 0.037$ N/mm

$F_n = 0.22$ N

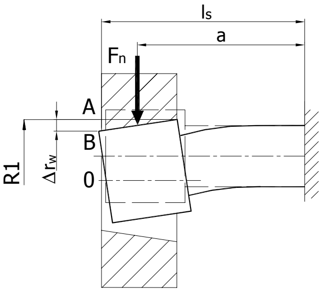

Mechanical distortion in grinding:

$$\Delta d_w = 2 \cdot \Delta r_w = 2(\overrightarrow{OA} - \overrightarrow{OB}) = 2(R1 - \overrightarrow{OB})$$

$$\overrightarrow{OB} = (R1 + \frac{F_n \cdot a^2}{6EI}(a - 3l_s))$$

$$I = \frac{\pi}{64} \cdot d_t^4$$

$\Delta d_w = 1.4\ \mu m$

Figure 8.35: Comparison of mechanical distortion

In Figure 8.34, the tool bending is compared in grinding and turning, for two different shaft diameters, when machining a bore with a diameter of 3 and 4 mm. The passive force applied for the calculation in turning was measured (see Chapter 8.1.1). As the force measurement was not successful in grinding, an existing empirical model was applied.

The specific normal force can be calculated according to [TÖN92], as:

$$F_n' = 10.34 \cdot \left(\frac{1}{q}\right)^{0.56} \cdot a_e^{0.78} \cdot d_{eq}^{0.22} \qquad (8.5)$$

where q is the speed ratio, a_e the depth of cut, and d_{eq} the equivalent wheel diameter. The product of specific normal force, and width of the grinding wheel determine the normal force:

$$F_n = F_n' \cdot b_s \qquad (8.6).$$

The exact value of the variables in Equations 8.5 and 8.6 can be found in Figure 8.35. The curves plotted in Figure 8.34 indicate a higher bending of the turning tool, which exceeds 12 μm. In grinding, it is only 2 μm, which can be further reduced with the application of spark-out.

Machining errors, caused by cutting forces, are compared between grinding and turning (see Figure 8.35). The diameter to be machined is 4 mm, and the length to diameter ratio is 4. The applied cutting and grinding parameters are also given in Figure 8.35. In turning, the mechanical distortion of the bore is 12.3 μm, and 1.4 μm for grinding, due to the passive force (F_p), and the normal force (F_n). This means that the grinding allowance must be higher than 0.012 mm to remove the machining errors caused by turning. The grinding tool bending can be reduced with spark-out, which will cause the calculated error (1.4 μm) to become lower.

8.2.4 Thermal distortion in machining of small bores

The thermal distortion of the small bore was defined with the FEM model. The model set-up has been described in Chapter 6.4.2. This modelling reveals the heat effect in turning of small bores. In the machining of diameters of 48 mm, it was observed that the thermal distortion is dominant. In turning of bores with a diameter of 4 mm, the question is whether the thermal distortion or the mechanical distortion was mainly responsible for the machining errors.

In the simulation, the heat flux as an input parameter had to be defined. It was carried out by calorimetric measurement. The measurement set-up and its explanation have been mentioned in Chapter 5.2.6. The heat flux of the moving heat source was determined for short (l/d = 2) and long (l/d = 4) workpieces, with a blind hole. The result is plotted in Figure 8.36. In the measurement, the cutting speed and the feed were varied, the depth of cut was constant, and the extension of width of flank wear land was taken into account. The increase of all three variables (v_c, f, VB) enhances the heat flux.

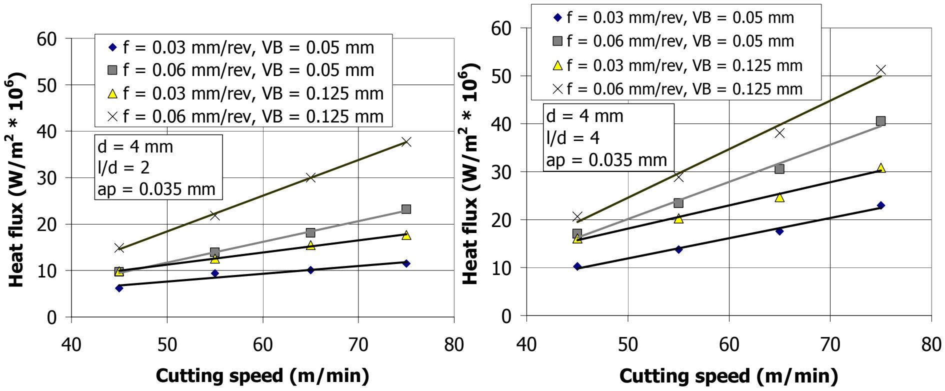

a) short workpiece, l/d = 2

b) long workpiece, l/d = 4

Figure 8.36: Heat flux on the basis of calorimetric measurement

In the machining of the short workpiece, the maximum workpiece temperature varies between 20 and 30 °C at the beginning. However, at the end of the last pass, it varies in the range of 40-90 °C (Figure 8.37a). The extension of the width of flank wear land and higher cutting speed result in a higher workpiece temperature. The thermal errors caused by the heat are plotted as a function of the length of the workpiece, and the expansion in the workpiece's diameter (Figure 8.37b). Even if a high cutting speed and a cutting tool with VB = 0.125 mm are applied, the deviation remains below 0.75 µm.

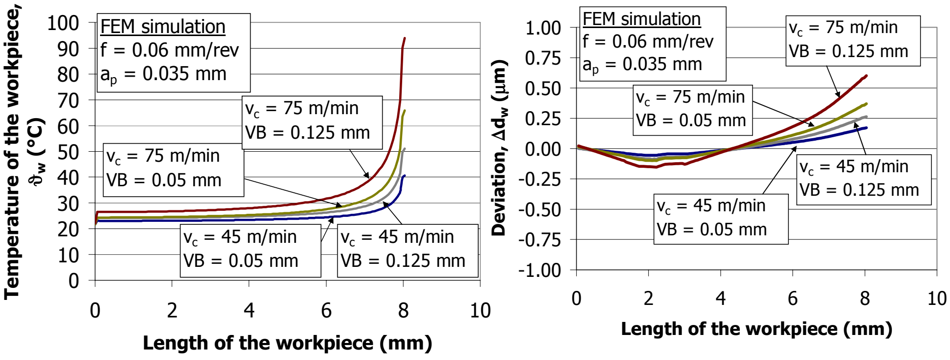

a) workpiece temperature

b) thermal distortion of the bore

Figure 8.37: FEM simulation in short workpiece

In the case of the longer workpiece, the workpiece's temperature still remains at a low level, but increases slightly, as in the last pass, its maximum value is 116 °C for VB = 0.125 mm (Figure 8.38a). During machining, the workpiece's temperature increases continuously. This is because in front of the moving heat source, a warm material part can be found. At the end of the workpiece, it is evident that the workpiece temperature suddenly increases, due to the reduction of the material volume. Thus, the progressive temperature rise is localised to the partially limited place of the workpiece. The thermal distortion is higher compared to a short workpiece, but the deviation remains below 1 µm (Figure 8.38b).

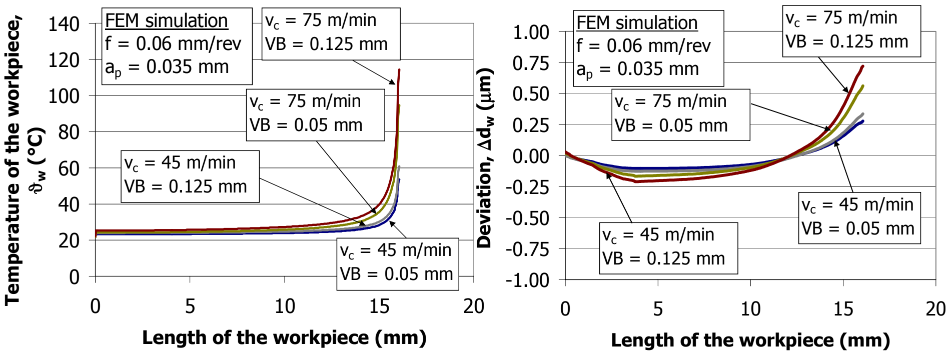

a) workpiece temperature

b) thermal distortion of the bore

Figure 8.38: FEM simulation in long workpiece

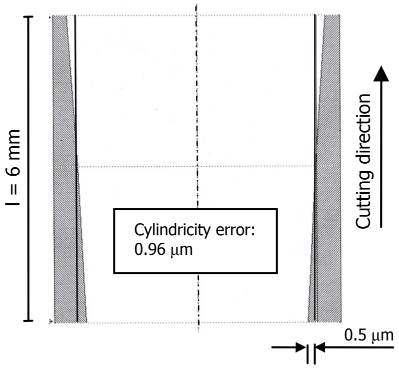

Workpiece:	100Cr6
Diameter of the bore:	4 mm
Length to diameter ratio:	2
Machine tool:	Slantbed Mikroturn 50 CNC
Cutting tool:	Kennametal PCBN MKTB KB5625
Tool geometry:	γ_n = 0°, α_n = 10°, κ_r = 95°, r_ε = 0.2 mm
Cutting data:	v_c = 50 m/min a_p = 0.035 mm f = 0.06 mm/rev
Tool wear:	VB_c = 0.1 mm

Figure 8.39: Measured cylindricity form

In the modelling of a small bore, the same characteristics can be observed as in the modelling of a gear's bore, with regard to the form of deviation. The phenomenon has been explained in Chapter 7.2.5. The modelling result was also proved with the measurement of geometrical accuracy of the machined bore (Figure 8.39). On the entry side, the bore diameter is smaller, while at the end of the bore the diameter is larger. The FEM modelling proved that the thermal distortion does not have a significant effect on the machining accuracy, as the diameter deviation caused by the heat remains below 0.001 mm.

8.3 Cycle time and material removal rate

In the machining of small bores, the economical points of view must be considered. As the combination of hard turning and grinding for the manufacturing of an injection nozzle is a new alternative, it is necessary to confirm its economical relevance. In this economical calculation, the cycle time, material removal rate, and surface rate are compared, with respect to the manufacturing of the bore.

In the manufacturing of small bores, the cycle time is compared, which can be formulated for turning as

$$t_{c,HT} = \frac{(l + l_1)\cdot i}{n \cdot f} + t_{cs} \tag{8.7}$$

and for plunge grinding as

$$t_{c,GR} = \frac{a_e}{v_{frad}} \cdot i + t_{sp} + t_{cs} \tag{8.8}$$

where l is the length of the workpiece, l_1 the additional length for approach and overtravel, i the number of plunge cuts, n the revolution, f the feed, t_{cs} the time of tool change, t_{sp} the spark-out time, a_e the depth of cut and v_{frad} the radial feed speed.

Figure 8.40 shows the cycle time calculated for roughing and finishing. In one case, both roughing and finishing are accomplished with grinding, and in the other case, the roughing is hard turning and the finishing is grinding. The machined bore diameter is 4 mm. When combined machining is used, the cycle time is 4.4 times quicker than applying the grinding process only.

In the determination of the material removal rate (Q_w) and surface rate (A_w), real indexes are applied, as they are more closely related to the certain machining process, compared with the theoretical values (see Table 8.1).

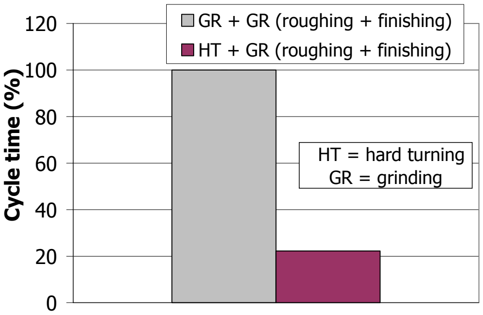

Workpiece
Material: 100Cr6
Diameter of the bore: 4 mm

Allowance: 0.15 mm
Machine tool: Slantbed Mikroturn 50 CNC

Hard turning (roughing):
Cutting tool: Kennametal PCBN MKTB KB5625
Tool geometry: $\gamma_n = 0°$, $\alpha_n = 10°$, $\kappa_r = 95°$, $r_\varepsilon = 0.8$ mm
Depth of cut: $a_p = 0.035$ mm
Feed: f = 0.06 mm/rev
Cutting speed: $v_c = 60$ m/min

Internal plunge grinding (roughing and finishing):
Grinding wheel: Meister Abrasives CBN wheel
Cutting data:
$v_c = 11\text{-}16.5$ m/s, $q_s = 60$
$v_w = 12.8\text{-}14.1$ m/min, $d_s = 3.5$ mm
$v_{frad} = 3.5\text{-}5$ mm/min
$v_{fax} = 400\text{-}600$ mm/min
Spark-out time: 5 s

Figure 8.40: Comparison of cycle time (roughing and finishing)

	Grinding, Hard turning	**Unit**
Material removal rate	$Q_w = \frac{d \cdot \pi \cdot l \cdot 0.15}{t_c \cdot 60}$ 0.15 – allowance in mm (roughing and finishing)	mm^3/s
Surface rate	$A_w = \frac{d \cdot \pi \cdot l}{t_c \cdot 60}$	mm^2/s

Table 8.1: Calculation of the real indexes of the material removal rate and surface rate

The calculated material removal rate and surface rate are presented in Figure 8.41 as an example of machining of a bore with $d = 4$ mm and $l/d = 2$. It is evident that the combined process provides a 4 times higher material removal rate than grinding. The application of hard turning and grinding processes offers a material removal rate of 0.48 mm^3/s, while it is 0.11 mm^3/s for grinding. The same phenomenon can be found with regard to the surface rate.

In analysing the economical points of view, it is obvious that combined machining is more advantageous for manufacturing of small bores, and provides proper surface quality for the components.

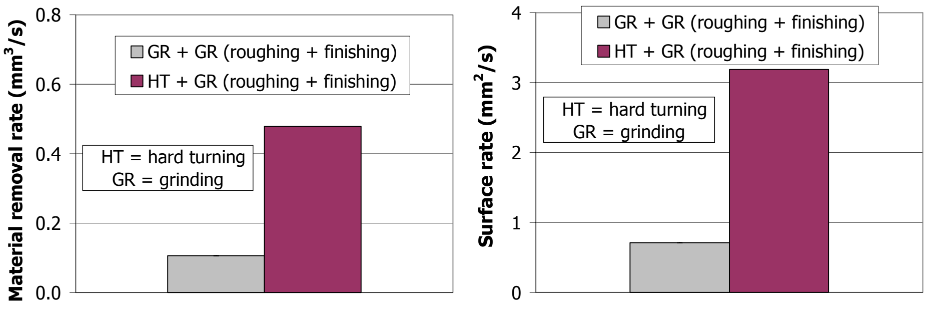

a)
b)

Workpiece
Material: 100Cr6
Diameter of the bore: 4 mm
Hard turning (roughing):
Cutting tool: Kennametal PCBN MKTB KB5625
Tool geometry: $\gamma_n = 0°$, $\alpha_n = 10°$, $\kappa_r = 95°$, $r_\varepsilon = 0.8$ mm
Depth of cut: $a_p = 0.035$ mm
Feed: $f = 0.06$ mm/rev
Cutting speed: $v_c = 60$ m/min

Allowance: 0.15 mm
Machine tool: Slantbed Mikroturn 50 CNC
Internal plunge grinding (roughing and finishing):
Grinding wheel: Meister Abrasives CBN wheel
Cutting data:
$v_c = 11\text{-}16.5$ m/s, $q_s = 60$
$v_w = 12.8\text{-}14.1$ m/min, $d_s = 3.5$ mm
$v_{frad} = 3.5\text{-}5$ mm/min
$v_{fax} = 400\text{-}600$ mm/min
Spark-out time: 5 s

Figure 8.41: a) Material removal rate, Q_w; and b) surface rate, A_w

9 Determination of the transition range between hard turning and grinding

This Chapter will discuss the limits of hard turning, and determine the transition range between hard turning and grinding. In addition to several advantages in hard turning, non-admissible machining errors may arise due to its disadvantages. The omission of a coolant is environmentally friendly, however, it may cause thermal distortion of the bore. Unlike grinding, hard turning cannot be performed under a minimum value of chip thickness, and the passive force may be a source of mechanical errors.

In disc type parts like gears, the effect of heat plays a significant role on the machining result, in comparison to cutting forces. In the injection nozzles, the bore is small and long. Undoubtedly, the heat distribution is less effective. Nevertheless, the thermal distortion is less relevant, in comparison to mechanical distortion.

GEAR	**INJECTION NOZZLE**
Workpiece: d = 48 mm, R1 = 24 mm, l/d = 0.57	Workpiece: d = 4 mm, R1 = 2 mm, l/d = 4
Cutting tool: l_s = 32 mm, d_t = 32 mm	Cutting tool: l_s = 18 mm, d_t = 3.5 mm
Young modulus of the cutting tool material:	Young modulus of the cutting tool material:
E = 500 GPa	E = 520 GPa
Cutting data:	Cutting data:
v_c = 180 m/min, f= 0.08 mm/rev, a_p = 0.1 mm	v_c = 60 m/min, f= 0.06 mm/rev, a_p = 0.04 mm
$I = \frac{\pi}{64} \cdot d_t^4$	$I = \frac{\pi}{64} \cdot d_t^4$
Cutting forces according to the measurements:	Cutting forces according to the measurements:
F_c = 49.6 N	F_p = 17.2 N
F_p = 99.23 N	F_c = 13.2 N
Δd_{mech} = 0.08 µm	**Δd_{mech} = 12.3 µm**
Δd_{ther} = 4.2 µm	**Δd_{ther} = 0.9 µm**

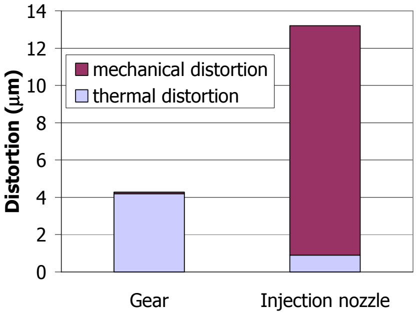

Figure 9.1: Mechanical and thermal distortions in hard turning

Figure 9.1 presents the comparison of mechanical and thermal distortions of the bore, when turning gears and injection nozzles. In the disc type part, the mechanical distortion is only 2%, in comparison with the thermal distortion. The high cutting speed results in high cutting temperature, and the chip cross sectional area of cut is also greater than in turning of small bores. Higher feed and depth of cut generate higher cutting temperatures. In the injection nozzle, the long tool bends, which causes the determinant mechanical distortion.

A "set of rules" is provided for the determination of the transition range between hard turning and grinding (see Figure 9.2). For the selection of the most suitable process, the workpiece properties must be considered. The "set of rules" for manufacturing high precision bores is determined with regard to the bore diameter. The machine tools and tooling are generally suited for diameters over 16 mm, however, in small bores, stricter tolerances are prescribed. This demands stiffer machine tools and a special clamping system.

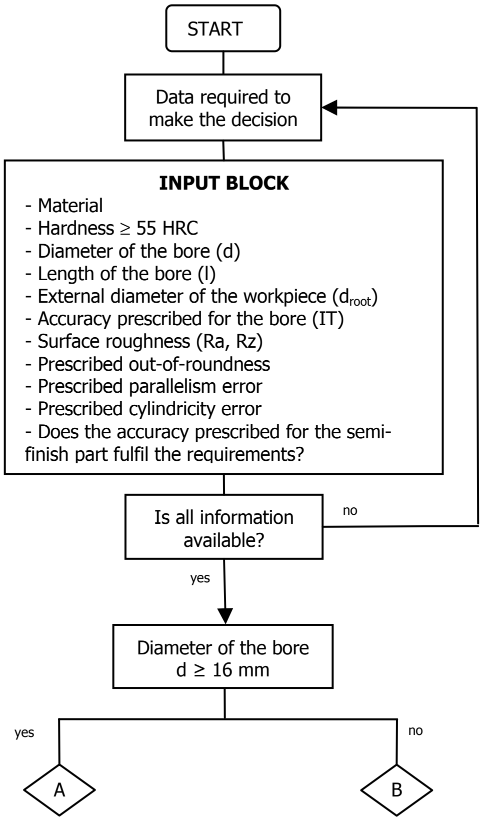
START
Data required to make the decision
INPUT BLOCK
- Material
- Hardness ≥ 55 HRC
- Diameter of the bore (d)
- Length of the bore (l)
- External diameter of the workpiece (d_{root})
- Accuracy prescribed for the bore (IT)
- Surface roughness (Ra, Rz)
- Prescribed out-of-roundness
- Prescribed parallelism error
- Prescribed cylindricity error
- Does the accuracy prescribed for the semi-finish part fulfil the requirements?
Is all information available?
no
yes
Diameter of the bore d ≥ 16 mm
yes
no
A
B

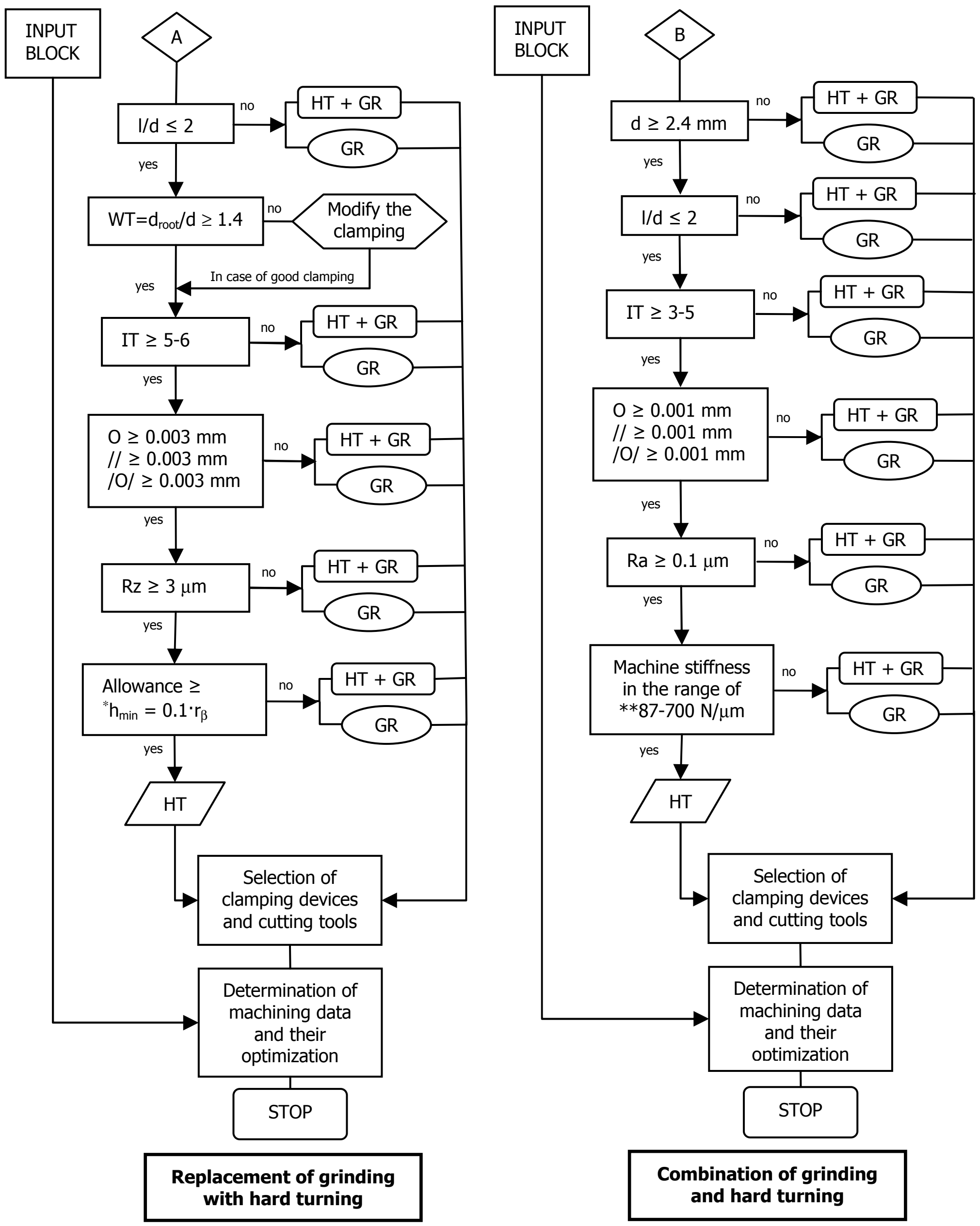
INPUT BLOCK
A
l/d ≤ 2
no
yes
HT + GR
GR
WT=d_root/d ≥ 1.4
Modify the clamping
In case of good clamping
IT ≥ 5-6
O ≥ 0.003 mm
// ≥ 0.003 mm
/O/ ≥ 0.003 mm
Rz ≥ 3 µm
Allowance ≥ *h_min = 0.1·r_β
HT
Selection of clamping devices and cutting tools
Determination of machining data and their optimization
STOP
Replacement of grinding with hard turning
INPUT BLOCK
B
d ≥ 2.4 mm
l/d ≤ 2
IT ≥ 3-5
O ≥ 0.001 mm
// ≥ 0.001 mm
/O/ ≥ 0.001 mm
Ra ≥ 0.1 µm
Machine stiffness in the range of **87-700 N/µm
HT
Selection of clamping devices and cutting tools
Determination of machining data and their optimization
STOP
Combination of grinding and hard turning

* source: [TÖN00]
** source: [HAN05]

GR – grinding
HT – hard turning

Figure 9.2: Selection criteria for bore manufacturing

To verify the selection guide, two typical application areas from the automotive industry were chosen - gears and injection nozzles. Generally, the gears built into transmissions are disc type parts. In this case, the length to diameter ratio of the bore is generally lower than 1. If the prescribed accuracy is not lower than IT5-6, hard turning can replace finish grinding, as described by Side "A" in Figure 9.2. In this case, it means that hard turning can guarantee the same accuracy as grinding. It is also more economically viable and environmentally friendly, due to the omission of coolant. As conclusively stated previously, the determination of optimal cutting data is necessary in order to ensure a better performance. The process optimisation is possible, if the cutting process characteristics and product characteristics are investigated. Therefore, in manufacturing high precision bores, cutting forces and temperatures were studied, and the surface quality was investigated and predicted to optimize and control the process. The investigated bore's diameter varied between 35 and 80 mm, while the maximum length to diameter ratio was 1.1.

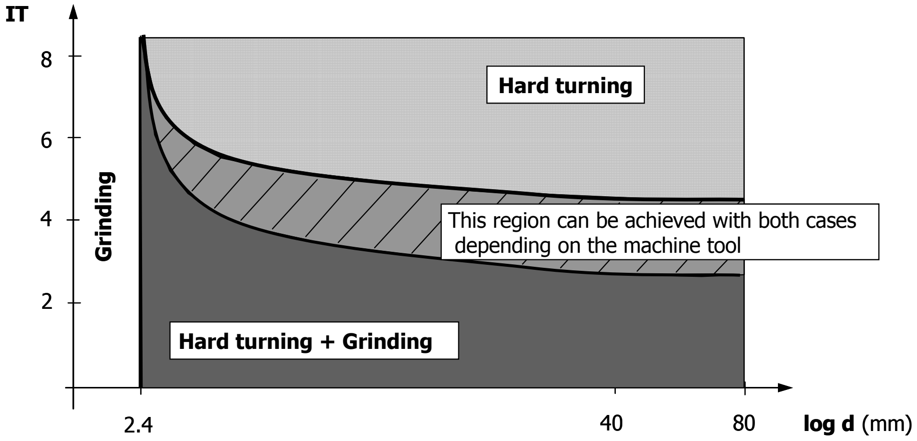

Figure 9.3: IT-d diagram in bore manufacturing

Injection nozzles possess small and long bores, as prescribed in Side "B" in Figure 9.2. The bore diameter is less than 10 mm, while the length to diameter ratio can reach 5. Due to this, hard turning itself cannot fulfil the prescribed tolerances. The application of the grinding process is still needed. One possible solution is to combine hard turning and grinding technologies in the most favourable way. Pre-machining is accomplished by hard turning, while grinding is applied as a finishing operation. To avoid non-productive times and clamping errors, the two processes must be performed in the same machine tool. A combined technology for machining small bores with high quality was developed. In this technology, the advantages of grinding and hard turning are combinable. The significant amount of allowance can be removed with hard turning, and the quality improvement can be done with grinding. Due to the high value of l/d ratio, the occurring cutting forces play a significant role. Compared to hard turning, grinding can be performed with near zero depth of cut (application of spark-out), leading to reduced grinding forces. The effect of process characteristics (forces and heat) on the product characteristics was studied. The investigated bore's diameter was 3-4 mm, while the length to diameter ratio was 2-4.

On the basis of this comprehensive work, the definition of the attainable tolerance as plotted against the bore diameter in manufacturing high precision bores has been attempted (see Figure 9.3). In the case of diameters below 2.4 mm, only the grinding process can be applied for bore manufacturing, as there is no turning tool available in this range. If the prescribed accuracy is not lower than tolerance IT5-6, hard turning must be chosen. If lower tolerances are required, a combined process is more beneficial than the application of grinding only. The transition range between hard turning and combined machining depends on the machine tool. Its static, dynamic and thermal stiffness determine this transitional boundary.

10 Conclusions and recommendations

In the automotive industry, the manufacturing technology has continuously shifted into the direction of micro- and nanomachining scales. Components with precision accuracy and surface quality are required. The surfaces of these parts are generally hardened to ensure accurate reliability and lifetime during function. Primarily, finishing processes must guarantee the macro and micro geometrical accuracy prescribed for the machined surfaces. However, economical factors and protection of the environment play a dominant role in the selection process as well.

Until now, the finishing process for bores with high hardness was accomplished with grinding only. With the development of PCBN tools, and machine tools with a higher accuracy and stiffness, the combination of grinding with turning, or the application of turning instead of grinding, has become possible.

The goal of this research work was to select the proper process and process conditions for the manufacturing of high precision bores. It attempted to define the limit of hard turning, and determine the transition range between hard turning and grinding. For the process selection, a "set of rules" was established with regard to two typical application areas from the automotive industry.

In manufacturing gears, it proved that hard turning can guarantee a tolerance of IT5-6, and can therefore replace the finish grinding operation. It is environmentally friendly, as well as beneficial from an economical point of view. The hard turning process was optimised to maximize its economical benefit. In the optimisation model, the process and product characteristics were implemented as constraints. The cutting forces, cutting temperatures, and surface quality properties were studied and measured in the machining of disc type parts, and were predicted with empirical models.

As a new alternative, a combined technology for manufacturing of injection nozzles was developed. If the bore is small and long, and the required tolerance is lower than IT3-5, hard turning cannot guarantee the prescribed tolerances. Grinding as a finishing application must be applied. Hard turning removes the significant part of the material allowance, and grinding improves the macro and micro geometrical accuracy. Cutting forces and surface quality were explored in a combination of hard turning and grinding and predicted with empirical models. The calculated cycle time, material removal rate, and surface rate definitively proved the advantages of the combined technology in comparison to grinding.

In both gears and injection nozzles, the effect of the cutting forces and cutting temperatures on the machining result was compared in hard turning. The thermal distortion was dominant, where disc type parts are machined, but is negligible in small bores. In this case, the mechanical distortion is significant. With regard to the machining error caused by turning, the grinding allowance was determined.

A set of models was developed to describe the entire process, which interconnects the input and output models via the process models. The performed investigations and the sub-parts of the process models together, have created the "set of rules", and made it possible to define the attainable tolerance with regard to the diameter in bore manufacturing.

During the development of a combined technology for machining small bores, a few problems were raised, which point out possible directions for further research work:

1) The depth of cut applied in both grinding and dressing is only a few micrometers. The detection of the first contact between grinding wheel and dressing wheel is required. This can be accomplished with the application of an acoustic emission system. In this case, the process time can be reduced, which would result in higher productivity.

2) In the grinding of small bores, the coolant and its supply must be chosen carefully, to improve the surface roughness and reach a longer tool life. The bore is long and small, which leads to difficulties in the coolant supply. During the research work, coolant was lead from the front side of the bore. Via the grinding quill, it is not possible to transfer the liquid, as the quill diameter is only 2 mm. The probable best solution is to lead it from the backside, but it is only feasible if an open-ended bore is ground. In the case of a blind hole, it cannot be accomplished. Rather than using emulsion, the application of neat oil may extend the tool life of the grinding wheel.

3) Optimisation of the grinding process is necessary for the further improvement of the performance of a combined technology. The application of another grinding method, (e.g. traverse grinding), may also reduce the cycle time hence improve the productivity.

4) In turning, the height of the cutting tool edge has great importance. A turning tool with a different length and diameter, results in a diverse cutting edge height. The adjustment of tool tip height should be solved. The surface roughness may be improved by modification of the tool edge geometry. The machining errors caused by turning must be reduced as much as possible. This leads to a lower grinding allowance, which results in higher productivity.

References

ABR96a Abrao A. M., Aspinwall D. K.: The surface integrity of turned and ground hardened bearing steel. Wear 196/1996 pp.: 279-284.

ABR96b Abrao A. M., Aspinwall D. K., Ng E.-G.: Temperature evaluation when machining hardened hot work die steel using PCBN tooling. IDR Vol. 2/1996 pp.: 40-44.

ABR97 Abrao A. M., Aspinwall D. K.: Temperature evaluation of cutting tools during machining of hardened bearing steel using polycrystalline cubic boron nitride and ceramic cutting tools. Material Science and Technology, Vol.13/1997, pp.: 445-450.

AGH00 Agha S. R., Liu C. R.: Experimental study on the performance of superfinish hard turned surfaces in rolling contact. Wear 244/2000 pp.: 52-59.

AKC99 Akcan S., Shah S., Moylan S. P., Chabra P. N., Chandrasekar S., Farris T. N.: Characteristics of white layers formed in steels by machining. Manufacturing Science and Engineering, Vol. 10/1999, pp.: 789-795.

ANK99 Anker A., Wernz C.: Hard turning and finish grinding on one machine. IDR 1/99, pp.: 38-40.

BÄH98 Bähre D., Dollmeier R., Warnecke G.: Modelling of thermo-elastic workpiece deformation for compensation of dimensional errors in turning of hard metals. Transactions of NAMRI/SME VolXXVI/1998, pp.: 123-128.

BAI02 Bailey M. W., Juchem H. O., Cook M. W., Collins J. L., Butler-Smith P.: The increasing importance of PCD/diamond/CVDD and PCBN/CBN tooling in the automotive industry. IDR 1/2002, pp.: 53-60.

BAL85 Bali J.: Cutting. Hungarian Handbook Publisher, Budapest, 1985, pp.: 109-122 (in Hungarian).

BAR89 Barnard J. M.: A definitive guide to problem assessment and solving when considering the grinding of automobile camshafts using vitrified cubic boron nitride wheels. The Winter Annual Meeting of the American Society of Mechanical Engineers, San Francisco, California, Dec. 10-15, 1989 pp.: 55-75.

BAR97 Barbacki A., Kawalec M.: Structural alterations in the surface layer during hard machining. Journal of Materials Processing Technology Vol. 64/1997, pp.: 33-39.

BAR02 Barry J., Byrne G.: Chip formation, acoustic emission and surface white layers in hard machining. Annals of the CIRP Vol.51/1/2002, pp.: 65-70.

BOR01 Borbe C.: Bauteilverhalten hartgedrehter Funkcionsflächen. Dr.-Ing. Dissertation Universität Hannover, 2001.

BRA95 Brandt D.: Randzonenbeeinflussung beim Hartdrehen. Dr.-Ing. Dissertation, Universität Hannover, 1995.

BRI82 Brinksmeier E., Cammett J. T., König W., Leskovar P., Peters J., Tönshoff H. K.: Residual stresses – measurement and causes in machining processes. Annals of the CIRP Vol.31/2/1982, pp.: 491-510.

BRI99 Brinksmeier E., Brockhoff T.: White layers in machining steels. High Speed Machining: 2nd International German and French Conference, Darmstadt 1999, pp.: 7-13.

CHE00a Chen W.: Cutting forces and surface finish when machining medium hardness steel using CBN tools. Int. Journal of Machine Tools and Manufacture Vol. 40/2000, pp: 455-466.

CHE02 Chen X., Rowe W. B., Cai R.: Precision grinding using CBN wheels. International Journal of Machine Tools & Manufacture 42 (2002) pp.: 585-593.

CHO97 Chou Y. K., Evans C. J.: White layers and thermal modelling of hard turned surfaces. MED-Vol.6-2, Manufacturing Science and Technology Vol2, ASME 1997, pp.:75-82.

CHO99a Chou Y. K., Evans C. J.: White layer and thermal modelling of hard turned surfaces. International Journal of Machine Tools & Manufacture 39/1999 pp.: 1863-1881.

CHO99b Chou Y. K., Evans C. J.: Cubic boron nitride tool wear in interrupted hard cutting. Wear 225-229 (1999) pp.: 234-245.

CHO03 Chou Y. K., Evans C. J., Barash M. M.: Experimental investigation on cubic boron nitride turning of hardened AISI 52100 steel. Journal of Materials Processing Technology Vol 134/2003, pp.: 1-9.

COL91 Colding B. N.: A tool temperature/tool life relationship covering a wide range of cutting data. Annals of the CIRP Vol40/1/1991, pp.: 35-40.

DON94a Dong W. P., Sullivan P. J., Stout K. J.: Comprehensive study of parameters for characterizing three-dimensional surface topography III: Parameters for characterising amplitude and some functional properties. Wear 178 (1994) 29-43, pp.: 29-43.

DON94b Dong W. P., Sullivan P. J., Stout K. J.: Comprehensive study of parameters for characterizing three-dimensional surface topography III: Parameters for characterising spatial and hybrid properties. Wear 178 (1994) 29-43, pp.: 45-60.

EGA95 Egawa T.: Material Characteristics and Cutting performance of TiN-Al_2O_3 ceramic tool. Int. J. Japan Soc. Prec. Eng., 1995/Vol 29/No3 pp.: 222-228.

ELB96 Elbestawi M. A., Srivastava A. K., El-Wardany T.: A model for chip formation during machining of hardened steel. Annals of the CIRP Vol45/1/1996, pp.: 71-76.

ELW00a El-Wardany T. I., Kishawy H. A., Elbestawi M. A.: Surface integrity of die material in high speed hard machining, Part 1: Micrographical analysis. Transaction of the ASME, Journal of Manufacturing Science and Engineering. 2000/Vol122, pp: 620-631.

ELW00b El-Wardany T. I., Kishawy H. A., Elbestawi M. A.: Surface integrity of die material in high speed hard machining, Part 2: Microhardness variations and residual stresses. Transactions of the ASME, Journal of Manufacturing Science and Engineering, 2000/Vol122 pp.: 632-641.

FLE98 Fleming M. A., Sweeney C., Valentine T. J., Simpkin R.: PCBN hard turning and workpiece surface integrity. IDR 1998/4, Vol58/No579 pp.: 128-133.

FLE00 Fleming M. A., Bossom P. K.: PCBN – performance goals for the 21st century. IDR 2000/4, Vol 60/No 587, pp.: 259-268.

FRO02 Frohmüller R.: Entwicklung, Aufbau und Funktionserprobung von Strahlungsmesstechnik zur Messung der Temperaturen in der Wirkzone bei hochdynamischen Zerspanvorgängen. Dr.-Ing. Dissertation TU Magdeburg 2002.

GRO99 Gróf Gy.: Heat transfer, Budapest University of Technology and Economics Publisher, 1999, p. 143, (in Hungarian).

GUO02 Guo Y. B., Liu C. R.: 3D FEA modelling of hard turning. ASME, Journal of Manufacturing Science and Engineering. Vol124/2002 pp.: 189-199.

GUO04 Guo Y. B. Sahni J.: A comparative study of hard turned and cylindrically ground white layers. International Journal of Machine Tools & Manufacture Vol44/2004, pp.: 135-145.

GYA93 Gyáni K.: Cutting fundamentals. National Textbook Publisher, Miskolc, 1993 (in Hungarian).

HAN05 Hanson S.: Cutting the hard stuff right. Manufacturing Engineeering, Vol. 134/No. 5/2005, p: 5.

HOF98 Hoffmeister H.-W., Michel S., Wenda A.: Selection of tool material for turning tungsten. IDR, Vol 58/No576/1998 pp.: 28-31.

HOR79 Horváth M., Somló J.: Optimisation and adaptive control of machining processes. Engineering Book Publisher, Miskolc, 1979 (in Hungarian).

HOU04 Hou Z. B., Komanduri R.: On the mechanics of the grinding process, Part II – thermal analysis of fine grinding. International Journal of Machine Tools & Manufacture 44 (2004), pp.: 247-270.

HUM01 Humienny Z., Bialas S., Osanna P. H., Tamre M., Weckenmann A., Blunt L., Jakubiec W.: Geometrical product specifications. Warsaw University of Technology Printing House, 2001, Warsaw, Poland.

JAC02 Jacobson M.: Surface integrity of hard turned M50 steel. ImechE, Journal of Engineering Manufacture, Vol 216/No B1/2002, pp.: 47-54.

JOC01 Jochmann S.: Untersuchung zur Prozess- und Werkzeugauslegung beim Hochpräzisionshartdrehen. Dissertation RWTH Aachen, Shaker Verlag, 2001.

JOH03 Johlen G.: Prozessoptimierung für die Hartfeinbearbeitung durch Kombination von Hartdrehen und Schleifen. Dr.-Ing. Dissertation TU Dortmund 2003.

JOH04 Johlen G.: Kombinierte Bearbeitung von Futterteilen durch Hartdrehen und Schleifen. IDR, Vol 38/1/2004, pp.: 37-44.

JUY98 Ju Y., Farris T. N., Chandrasekar S.: Theoretical analysis of heat partition and temperatures in grinding. Trans ASME, Journal of Tribology 120 (1998), pp.: 789-794.

JÜR80 Jürgenhake B.: Innenrundschleifen. Dr.-Ing. Dissertation TU Hannover 1979.

KAL95 Kalpakjian S.: Manufacturing Engineering and Technology. Addison-Wesley Publishing Co. USA 1995.

KAR01 Karpuschewski B.: Sensoren zur Prozeßüberwachung beim Spanen. Habilitationsschrift, TU Hannover 2001.

KAR03 Karpuschewski B.: Hard draaien en slijpen vergeleken. Mikroniek 2/2003, pp.:18-23.

KIN86 King R. I., Hahn R. S.: Handbook of modern grinding technology. New York: Chapman and Hall, 1986.

KIS99 Kishawy H. A.,. Elbestawi M. A.: Effects of process parameters on material side flow during hard turning. Int. J. of Machine Tools & Manufacture 39/1999 pp.: 1017-1030.

KIS01 Kishawy H. A., Elbestawi M. A.: Tool wear and surface integrity during high-speed turning of hardened steel with polycrystalline cubic boron nitride tools. Journal of Engineering Manufacture, Part B 2001/Vol215/NoB6 pp.: 755-767.

KLO05 Klocke F., Brinksmeier E., Weinert K.: Capability profile of hard cutting and grinding processes. Annals of the CIRP Vol. 54/2/2005 p. 24.

KOC96 Koch K. F.: Technologie des Hochpräzisions-Hartdrehens. Dr.-Ing. Dissertation RWTH Aachen, 1996.

KOM95 Komócsin M.: Material science in engineering. Cokom Kft, 1995. p. 120 (in Hungarian)

KNU00 Knuefermann M. M. W., Read R. F. J., Nunn R., Clark I. E., Fleming M. A.: Ultra-precision turning of hardened steel with AMBORITE DBN 45 on the DeltaTurn40 lathe. IDR 2000/2, Vol60/No585 pp.: 107-114.

KÖN80 König W.: Schleifen, Honen, Läppen. VDI-Verlag GmbH, Düsseldorf, 1980.

KÖN90 König W., Klinger M., Link R.: Machining hard materials with geometrically defined cutting edges – Field of applications and limitations. Annals of the CIRP Vol. 39/1/1990 pp.: 61-64.

KÖN93a König W., Berktold A., Koch K.-F.: Turning versus grinding - A comparison of surface integrity aspects and attainable accuracies. Annals of the CIRP Vol.42/1/1993 pp.: 39-43.

KÖN93b König W., Neises A.: Wear mechanism of ultrahard, non-metallic cutting materials. Wear 162-164/1993 pp.: 12-21.

KÖN94 König W., Berktold A., Liermann J., Winands N.: Top quality components not only by grinding. IDR 1994/3, Vol54/No562, pp.: 127-132.

KUN79 Kundrák J.: Cutting of hardened steels with defined edge superhard tools. PhD dissertation, Heavy Industrial University in Miskolc, Hungary, 1979 (in Hungarian).

KUN82 Kundrák, J.: Roughness characteristics of surfaces cut with policrystalline superhard tools. Scientifical forum for young researchers and teachers II, Section of Industrial Technology, University of Budapest, 1982, pp.: 340-347 (in Hungarian).

KUN85 Kundrák, J.: Surface quality of internal cylindrical surfaces cut by cubic boron nitride tools. Production Technology, Vol10/XXV,1985 pp.: 463-466 (in Hungarian).

KUN96 Kundrák, J.: The Scientific Principles of Increasing the Effectiveness of Inner Surfaces' Cutting with CBN Tools, Academic Doctoral Dissertacion. Harkov, 1996.

KUN00 Kundrák J.: The quality of the machined surface in hard turning. Proc. on the microCAD´2000 International Computer Science Conference, Miskolc, Hungary, February 23-24, 2000, pp.: 47-52.

KUN06 Kundrák J., Tomolya K., Sólyom J., Gácsi Z., Bana V.: Investigation of surface integrity of gears machined with hard turning. Proceeding on the microCAD06 International Computer Science Conference, Miskolc, Hungary, March 16-17, 2006 pp.: 61-68.

LEE99	Lee W.-S., Su T.-T.: Mechanical properties and microstructural features of AISI4340 high-strength alloy steel under quenched and tempered conditions. Journal of Materials Processing Technology 87 (1999), pp.: 198-206.
LES78	Leskó B., Pap J.-né: Determination of theoretical values of some microgeometrical characteristics in turning and planing. Mechanical Engineering, 24/2, Heavy Industrial University in Miskolc, Hungary, 1978 pp.: 97-122 (in Hungarian).
LES97	Leshock C. E., Shin Y. C.: Investigation on cutting temperature in turning by a tool-work thermocouple technique. Journal of Manufacturing Science and Engineering, Vol.119/1997, pp.: 502-508.
LIN73	Lindsay R. P.: On the surface finish - metal removal relationship in precision grinding. Transaction of ASME, Journal of Engineers for Industry, Vol95/1973, p.: 815.
LIU95	Liu Z-C., Chen D-Y.: A study of cutting with a CBN tool. Journal of Materials Processing Technology 49/1995 pp.: 149-164.
LIU96	Liu C. R., Mittal S.: Single-step superfinish hard machining feasibility and feasible cutting conditions. Robotics&Computer Integrated Manufacturing, Vol12/No1, 1996. pp.: 15-27.
LUT98	Luttervelt van C. A., et al.: Present situation and future trends in modelling of machining operations. Annals of the CIRP Vol. 47/2/1998 pp.: 587-626.
MAL89	Malkin S.: Grinding Technology; theory and applications on machining with abrasives. Chichester: Horwood, 1989.
MAT86	Matsumoto Y., Barash M. M., Liu C. R.: Effect of hardness on the surface integrity of AISI 4340 steel. Journal of Engineering for Industry, 1986/Vol. 108 pp.: 169-175.
MAT99	Matsumoto Y., Hashimoto F., Lahoti G.: Surface integrity generated by precision hard turning. Annals of the CIRP Vol48/1/1999 pp.: 59-62.
MEI05	Meister Abrasives AG. http://www.meister-abrasives.ch/ 2005.
MES05	Mészáros I., Szepesi D.: Hochpräzisions-Hartdrehen als optimierter Prozess. Werkstatt und Betrieb Vol138/11/2005 pp.: 58-62.
MON06	Monici R. D., Bianchi E. C., Catai R. E., de Aguiar P. R.: Analysis of the different forms of application and types of cutting fluid used in plunge cylindrical grinding using conventional and superabrasive CBN grinding wheels. International Journal of Machine Tools & Manufacture, Vol 46/2, February 2006, pp.: 122-131.

MÜL03	Müller N.: Combination-/simultaneous-machining: Hard turning, grinding and hard roller burnishing. Proc. on the 1st European Conference on Grinding, Aachen, 6-7 Nov. 2003. pp.: 2/1-16.
NAK88	Nakayama K., Arai M., Kanda T.: Machining characteristics of hard materials. Annals of the CIRP, Vol37/1/1988, pp.: 89-92.
NGE99a	Ng E-G., Aspinwall D. K.: The effect of workpiece hardness and cutting speed on the machinability of AISI H13 hot work die steel when using PCBN tooling. MED-Vol 10, Manufacturing Science and Engineering, 1999, pp.: 773-780.
NGE99b	Ng E-G., Aspinwall D. K.: Evaluation of cutting force and temperature when turning hardened die steel with AMBORITE AMB90 and DBC50 tooling. IDR 1999/3, Vol59/No582 pp.: 183-195.
NIC80	Nicolai M., Hegler R. P.: Werkstücktemperatureinflüsse beim Drehen. VDI-Z 122 Nr.6-March (II), 1980, pp.: 225-228.
OSA92	Osanna P. H., Totewa P.: Workpiece accuracy – The critical path to economical production. Int. Journal of Machine Tools & Manufacture. Vol32/No1/2/1992 pp.: 45-49.
PAL92	Palásti Kovács B.: Investigation of surface microgeometry. GEP, Vol XLIV/5, 1992. pp.: 30-36 (in Hungarian).
PÁL80	Pálmai Z.: Cutting ability of metals, Hungarian Book Publisher, Budapest, 1980 (in Hungarian).
PAT00	Patz M., Dittmar H., Hess A., Wagner W.: Better hard turning with optimised cooling. IDR 2000/4, Vol60/No587, pp.: 277-282.
PAW97	Pawlus P.: Change of cylinder surface topography in the initial stage of engine life. Wear 209 (1997), pp.: 69-83.
PET04	Petit-Grostabussiat S., Taleb L., Jullien J.-F.: Experimental results on classical plasticity of steels subjected to structural transformations. International Journal of Plasticity 20 (2004), pp.: 1371-1386.
POU01	Poulachon G., Moisan A., Jawahir I. S.: Tool-wear mechanism in hard turning with polycrystalline cubic boron nitride tools. Wear 250/2001, pp.: 576-586.
RAM99	Ramesh A., Thiele J. D., Melkote S. N.: Residual stress and sub-surface flow in finish hard turned AISI 4340 and 52100 steels: a comparative study. Manufacturing Science and Engineering MED-Vol. 10/1999, pp.: 831-837.

RAM05 Ramesh A., Melkote S. N., Allard L. F., Reister L., Watkins T. R.: Analysis of white layers formed in hard turning of AISI 52100 steel. Material Science and Engineering A, Vol390/1-2/2005, pp.: 88-97.

REC03 Rech J., Moisan A.: Surface integrity in finish hard turning of case-hardened steels. International Journal of Machine Tools & Manufacture 43 (2003), pp.: 543-550.

REZ81 Reznikov A. N.: Thermal processes in machining of materials. Masinostroenie, Moskva, 1981 (in Russian).

SAL80 Salje E., Riefenstahl J.: Probleme und Zusammenhänge beim Innenrundschleifen. Industrie Anzeiger 19/1980 pp.: 34-37.

SCH99 Schmidt J.: Mechanische und thermische Wirkungen beim Drehen gehärteter Stähle. Dr.-Ing. Dissertation, Universität Hannover, 1999.

SHA84 Shaw M. C.: Metal cutting principles. Oxford: Clarendon, 1984.

SHA93 Shaw M. C., Vyas A.: Chip formation in the machining of hardened steel. Annals of the CIRP Vol42/1/1993 pp.: 29-33.

SHA98 Shaw M. C., Vyas A.: The mechanism of chip formation with hard turning steel. Annals of the CIRP Vol 47/1/1998, pp.: 77-82.

SHI86 Shigley J. E.: Mechanical Engineering design. McGraw-Hill Book Company, Singapore, 1986.

SOO00 Sood R., Guo C., Malkin S.: Turning of hardened steels. Journal of Manufacturing Processes 2000/Vol2/No3 pp.: 187-193.

STE97 Stephenson D. A., Agapiou J. S.: Metal cutting theory and practice. Marcel Dekker INC, New York, USA, 1997, pp.: 491-527.

STO83 Stout K. J., Spedding T. A.: The characterisation of internal combustion engine bores. Wear 43 (1983), pp.: 311-327.

STO84 Stout K. J., Davis E. J.: Surface topography of cylinder bores – the relationship between manufacture, characterisation and function. Wear 95 (1984), pp.: 111-125.

SUB88 Subramanian K.: Vitrified bonded CBN wheels – current applications and future directions. Proceedings of the Industrial Diamond Association – Japan Symposium, 10/1988.

SUK03 Sukaylo V.: Numerische Simulation der thermisch bedingten Werkstück-Abweichungen beim Drehen mit unterschiedlichen Kühlschmiermethoden. Dr.-Ing. Dissertation, Universität Magdeburg, 2003.

SUK04 Sukaylo V. A., Kaldos A., Krukovsky G., Lierath F., Emmer T., Pieper H. J., Kundrák J. and Bana V.: Development and verification of a computer model for thermal distortions in hard turning. J. of Materials Processing Technology 155-156, 2004 pp.: 1821-1827.

TAY07 Taylor F. W.: On the art of cutting metals. ASME 1907/Vol 28, p. 31.

THI99 Thiele J. D., Melkote S. N.: Effect of cutting edge geometry and workpiece hardness on surface generation in the finish hard turning of AISI 52100 steel. Journal of Materials Processing Technology 94, 1999 pp.: 216-226.

THI01 Third Wave Systems, Inc., "AdvantEdge v3.6 Machining Simulation Software", Minneapolis, MN (2001).

TIS00 Tisza M.: Metallography. University of Miskolc Publisher, 2000 (in Hungarian).

TOR78 Torrance A. A.: Metallurgical effects associated with grinding. Proceedings of the 12th Int. Machine Tool Design and Research Conference, Manchester, England, 15-17 September 1978, p.: 637.

TÓT04 Tóth T., Kundrák J., Gyáni K.: The material removal rate and the surface rate as two new parameters of qualification for hard turning and grinding, Fifth International Symposium on Tools and Methods of Competitive Engineering (TMCE 2004) Switzerland, Lausanne, 2004. pp: 629-639.

TÖN89 Tönshoff H. K., Heuer W.: Wear behaviour of small vitreous bonded CBN wheels during internal and external grinding. The Winter Annual meeting of the American Society of Mechanical Engineers, San Francisco, California, Dec. 10-15, 1989 pp.: 1-15.

TÖN92 Tönshoff H. K., Peters J., Inasaki I., Paul T.: Modelling and simulation of grinding processes. Annals of the CIRP Vol. 41/2/1992 pp.: 677-688.

TÖN93 Tönshoff H. K., Wobker H.-G., Brandt D.: Hartbearbeitung aus der Sicht der Forschung. VDI-Berichte 988 (1993), pp.: 189-209.

TÖN95a Tönshoff H. K., Wobker H.-G., Brandt D.: Tribological aspects of hard turning with ceramic tools. Journal of the Society of Tribologists and Lubrication Engineers, 1995 pp.: 163-168.

TÖN95b Tönshoff H. K., Wobker H. – G., Brandt D.: Hard turning – influences on the workpiece properties. Transactions of NAMRI/SME 1995 Vol. XXIII pp.: 215-220.

TÖN98 Tönshoff H. K., Karpuschewski B., Mandrysch T.: Grinding Process Achievements and their consequencies on machine tools - challenges and opportunities. Annals of the CIRP Vol. 47/2/1998 pp.: 651-668.

TÖN00 Tönshoff H. K., Arendt C., Ben Amor R.: Cutting of hardened steel. Annals of the CIRP Vol. 49/2/2000 pp.: 547-566.

UED99 Ueda T., Al Huda M., Yamada K., Nakayama K.: Temperature measurement of CBN tool in turning of high hardness steel. Annals of the CIRP Vol. 48/1/1999 pp.: 63-66.

UES99 Uesaka S., Sumiya H.: Mechanical properties and cutting performances of high purity polycrystalline CBN compact. MED-Vol 10, Manufacturing Science and Engineering, 1999, pp.: 759-766.

VAL96 Valasek I.: Handbook of tribology. Tribotechnik Kft., Budapest 1996, pp.:72-73 (in Hungarian).

VYA99 Vyas A., Shaw M. C.: Mechanics of saw-tooth chip formation in metal cutting. Journal of Manufacturing Science and Engineering, Vol. 121/1999, pp.: 163-172.

WAN99 Wang J. Y., Liu C. R.: The effect of tool flank wear on the heat transfer, thermal damage and cutting mechanics in finish hard turning. Annals of the CIRP Vol. 48/1/1999 pp 53-58.

WAR90 Warren C.: Infrared thermometers, out of the lab and into the factory. Machine Design No 4/1990, pp.: 85-88.

WEI98 Weinert K., Appelt H., Schneider M.: Gedreht oder geschliffen – gehupft wie gesprungen? Technika 5/98, pp.: 18-21.

YOK77 Yokoyama K., Ichimiya R.: Thermal deformation of workpiece in surface grinding. International Journal Japan Soc. Prec. Eng. Vol 11/No4/1977, p.: 195.

ZIM97 Zimmermann M., Lahres M., Viens D. V., Laube B. L.: Investigation of the wear of cubic boron nitride cutting tools using Auger electron spectroscopy and X-ray analysis by EPMA. Wear 209/1997 pp.: 241-246.

ZHO03 Zhou J. M., Walter H., Andersson M., Stahl J. E.: Effect of chamfer angle on wear of PCBN cutting tool. Int. Journal of Machine Tools & Manufacture Vol. 43/2003, pp.: 301-305.

About the author

Personal data:

Name:	BANA, Ivett Viktória
Date of birth:	23 January 1976
Place of birth:	Miskolc (Hungary)
Nationality:	Hungarian

Work experience:

2003-	TUDelft, Faculty of 3ME, Laboratory for Precision Manufacturing and Assembly PhD researcher Main research field: micromachining (combination of hard turning and grinding in machining of small bores)
2000-2003.	University of Miskolc, Miskolc, Hungary Department of Production Engineering PhD student Main research field: precision machining, hard turning, surface quality
2000. February	Machine-tool Factory of Diósgyőr, Miskolc, Hungary industrial training (as a student)
1999. June	Machine-tool Factory of Diósgyőr, Miskolc, Hungary industrial training (as a student)
1998. July	Hungarian State Railways, Repairing works of Coach, Miskolc, Hungary industrial training (as a student)

Education:

1994-2000.	University of Miskolc, Hungary Faculty of Mechanical Engineering, Dept. of Production Engineering MSc degree
1990-1994.	Földes Ferenc Grammar School, Miskolc, Hungary

Foreign scholarships:

2002. Dec 2001. Oct-Dec	Otto-von-Guericke Universität Magdeburg Fakultät für Machinenbau Institute für Fertigungstechnik und Qualitatssicherung, Magdeburg, Germany
2002. May-June	Technische Universität Wien, Abt. Austauschbau und Messtechnik, Wien, Austria
2001. Apr-July	Institut National Polytechnique de Lorraine Études et Recherche en Mécanique et Énergétique des Surfaces, Nancy, France
2000. March-April	Technische Universität Wien, Abt. Austauschbau und Messtechnik, Wien, Austria

Language knowledge:

English (good)
German (intermediate)
Dutch (fair)
Hungarian (mother tongue)